3D modelling of the interactions between the atmosphere-ocean system and the marine biogeochemistry in the coastal zone (focussing on the Bay of Marseille): Influence of anthropogenic contributions by a large coastal city on the marine ecosystem

Christel Pinazo, Lucille Barré, Frédéric Diaz, Andrea M. Doglioli, Vincent Martin Faure, Marion Fraysse, Katixa Lajaunie-Salla, Camille Mazoyer, Ivane Pairaud, Oliver N. Ross, et al.

3D modelling of the interactions between the atmosphere-ocean system and the marine biogeochemistry in the coastal zone (focussing on the Bay of Marseille): Influence of anthropogenic contributions by a large coastal city on the marine ecosystem

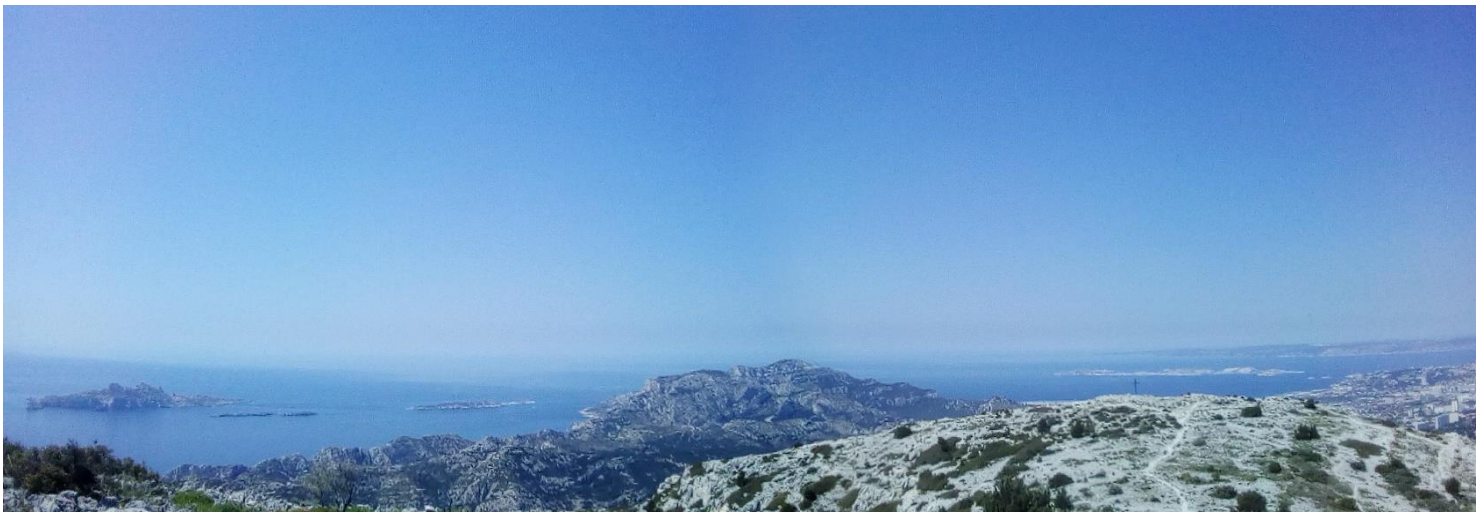

Pinazo C., L. Barré, F. Diaz, A. Doglioli, V. Faure, M. Fraysse, K. Lajaunie-Salla, C. Mazoyer, I. Pairaud, O. Ross, B. Thouvenin, R. Verney, T. Wagener, C. Yohia

2022

Summary

ACKNOWLEDGEMENTS

The authors particularly thank:

- the Marseille Provence Métropole Urban Community and SERAM (Société d'Exploitation du Réseau d'Assainissement de Marseille) for providing data on urban river flow and discharge data from the Marseille waste water treatment plant from 2007 to 2014;

- the team of the National SOMLIT coastal observation network (INSU 767 CNRS), the National MOOSE program (Mediterranean oceanic Observing System on Environment) and the Observation Service of the Mediterranean Institute of Oceanography (MIO) in particular P. Raimbault, N. Garcia, V. Lagadec, M. Lafont, and M. Fornier for providing the concentrations of riverine inputs from the Rhone, atmospheric inputs, and *in-situ data* collected at SOLEMIO station in the Bay of Marseille as well as their analytical and field assistance. We are also grateful to the crew of the RV Antedon II, the DT-INSU, and the SAM platform (Service Atmosphere Sea) of the MIO for assisting with the sample collection;

- the HPC Intensive Computing Cluster of the OSU Institut Pythéas (Christophe Yohia, Julien Lecubin) for access to computing facilities;

- Camille Mazoyer for her modelling support;

- the IFREMER team, and in particular Francis Gohin, for providing the MERIS and MODIS water colour satellite images processed with the OC5 algorithm;

- the Compagnie Nationale du Rhône for river flow data;

- Météo-France for meteorological data;

- SNAPO-CO2 at LOCEAN, CNRS-INSU, and OSU Ecce-Terra, Paris;

- Irène Xueref-Rémy for providing the atmospheric pCO2 data measured at the Observatoire de Haute Provence (OHP) and Alexandre Armengaud ATMOSUD for data measured at Cinq Avenues.

The authors also acknowledge financial support by:

- the AERMC Water Agency for Lucille Barré's thesis grant;
- the PACA Region and IFREMER for Marion Fraysse's BDO thesis grant;
- the EC2CO PNEC program;
- the FUI GIRAC program;
- the FP7 PERSEUS project;
- the company ACRI-ST;
- the Labex OT-MED (ANR-11-LABEX-0061, “Investment for the Future” A*MIDEX project ANR-11-IDEX-0001-02);
- The ERDF (European ERDF Fund under project 1166-39417);
- European Union’s Caroline Herschel Framework Partnership Agreement on Copernicus User Uptake under grant agreement No FPA 275/G/GRO/COPE/17/10042, project FPCUP (Framework Partnership Agreement on Copernicus User Uptake), Action 2018-1-88 “Translation of Master courses using Copernicus data” for the Translation.

Many thanks to Pierre Garreau, Cassandre Jany, and Cedric Garnier for fruitful discussions and exchanges.

To Fred...

1 INTRODUCTION

1.1 CONTEXT

From a sustainable development perspective, it is necessary to determine public policies and management methods that are based on basic scientific research to help identify and assess the influence of humans on their environment. The study of the anthropogenic impact of large coastal cities on the functioning of marine ecosystems is one of the priorities to achieve sustainable development.

Several scientific projects (EC2CO MASSILIA, OT-Med AMC, AERMC: METROC, GIRAC, IAMM) have studied the influence of the greater Marseille area on the coastal marine environment using numerical modelling approaches. The objective is to better understand the particular functioning of this ecosystem which is subject to multiple anthropogenic influences: land run-off, coastal rivers, the Rhône, and atmospheric CO_2 by using a large database of available *in situ* observations and integrating it into numerical tools. We will use this case study to understand the influence that a large coastal city can have on the coastal environment.

1.2 STUDY OBJECTIVES

The main objective of this study is to understand the functioning of the ecosystem in the Bay of Marseille which is subject to strong anthropogenic inputs of CO_2 , nutrients, POM, DOM, and its role in the partial restoration of water quality in this coastal area.

This work is all divided into two areas of study:

- Study the impacts of various inputs on the ecosystem and identifying individual contributions by source (atmosphere, run-off, coastal rivers, Rhône).

This involves studying the impact of CO_2, nutrients, POM, and DOM inputs based on their very different origins.

- Study how physical forcings can modulate these impacts (wind, stratification, upwelling, eddies).

The aim is to understand how the hydrodynamic processes due to general circulation and/or atmospheric processes (wind mixing, upwelling, downwelling; stratification; eddies; intrusions of the Rhône, or the Northern Current into the Bay of Marseille) will modulate the impact of the above inputs.

By using the Bay of Marseille ecosystem as a case study, we will try to answer the following more general questions:

- What are the respective roles played by physical and biogeochemical forcings (inputs of nutrients, POM, DOM) in the processes of degradation or relative restoration of coastal ecosystems subjected to strong anthropogenic inputs?

- How do extreme physical events (floods, storms, heat waves), whose frequency is likely to increase with climate change, affect the marine ecosystem?

1.3 APPROACH USED

Using satellite and atmospheric data, flow rates of the Rhône and other coastal rivers, as well as precipitation data we establish:

- a typology of the physical and climatic forcings for the study area
- a typology of the biogeochemical forcings (CO_2, nutrient, and OM inputs)

By analysis all available data (new data and reanalysis of historical data) we can learn how the system functions and these data also allow us to calibrate and validate the different numerical models.

The models provide distribution maps of relevant indicators such as current fields, temperature, salinity, alkalinity, *p*H, *p*CO2, turbidity, chlorophyll, as well as the inorganic (as total inorganic carbon and nutrients) and dissolved and particulate organic carbon content. These distribution maps result from a range of realistic scenarios driven by certain forcing conditions (wind regimes, mixing, stratification, upwelling, eddies, floods, storms) that include both typical and extreme events.

We can then apply a wavelet analysis to the model results to detect eddies and vortices. Models represent diagnostic tools to explore different scenarios. By simulating realistic scenarios, they allow us to understand the different forcings and determine their impact on the functioning of the ecosystem.

Table 1

Typical and extreme events considered in this study:

Forcing	Typical situation	Extreme situation
Wind	**Mistral (upwelling) : September 2007** **South-East : November 2007**	**Mistral storm (e.g.: Dec 2004, Nov 2007 - Dec 2007; one full month: Feb-Mar 2009)** **Strong South-Westerlies (Jan 2008 and Dec 2008)**
Air Temp	**West : March 2008** **Weak wind + summer heat in 2009 and 2010 (stratification)**	**Strong Westerlies (Apr 2008)** **Heat wave (e.g.: summer 2003)**
Marseille Eddy	**May 2011**	**Eddy breaks through the surface: Jun 2008, Jun 2017**
Northern Current	**May – Jun 2008**	**Intrusion of the Northern Current: Oct 2011**
Rhône	**Significant eastward extension or intrusion of the plume: 1 Oct 2007; May 2008; May 2011; Mar 2017**	**Significant eastward extension or intrusion of the plume: Dec 2003; Jun 2008**
Rain	**Spring/Autumn thunderstorms: Oct 2007, Oct-Nov 2008, Apr 2008**	**Exceptional thunderstorms: Nov 2011, Sep 2009**

We ran realistic simulations of both typical (occurring several times a year) and extreme situations (recorded between 2001-2021) to answer the questions summarized above. The events to simulate were chosen after a careful study of satellite images, wind and air temperature data, Rhône flow data, and rainfall over the larger Marseille area, etc, extracting the necessary data to create the model forcing and parameterizations and to perform subsequent model validation. After a detailed study of meteorological data, in particular from 2008, we were able to identify events of interest. For instance, the strong South-Easterlies observed during the months of January and December 2008 yielded the strongest wind velocities on record for the period 2001-2009. We therefore addressed these research

questions using simulations that represent typical and extreme situations of these processes from among the various realistic situations listed in recent years (Table 1).

2 STUDY AREA

The study area is located on the continental shelf in the Gulf of Lion and is subject to forcings associated with the atmosphere, freshwater input from the Rhône (Pont et al., 1996), and the general circulation. Although the Bay of Marseille is a key area as it sits at the Northern Current's entry point to the Gulf of Lion, it has been much less investigated than the Gulf as a whole.

The city of Marseille is located in the southeast of France, bounded to the north by a mountain range with peak altitudes ranging from about 600-1000m (Sainte-Victoire 1011m, Sainte-Baume 1042m, Massif de l'Etoile 779m, Garlaban 731m) and to the south by the Mediterranean Sea (Figure 1).

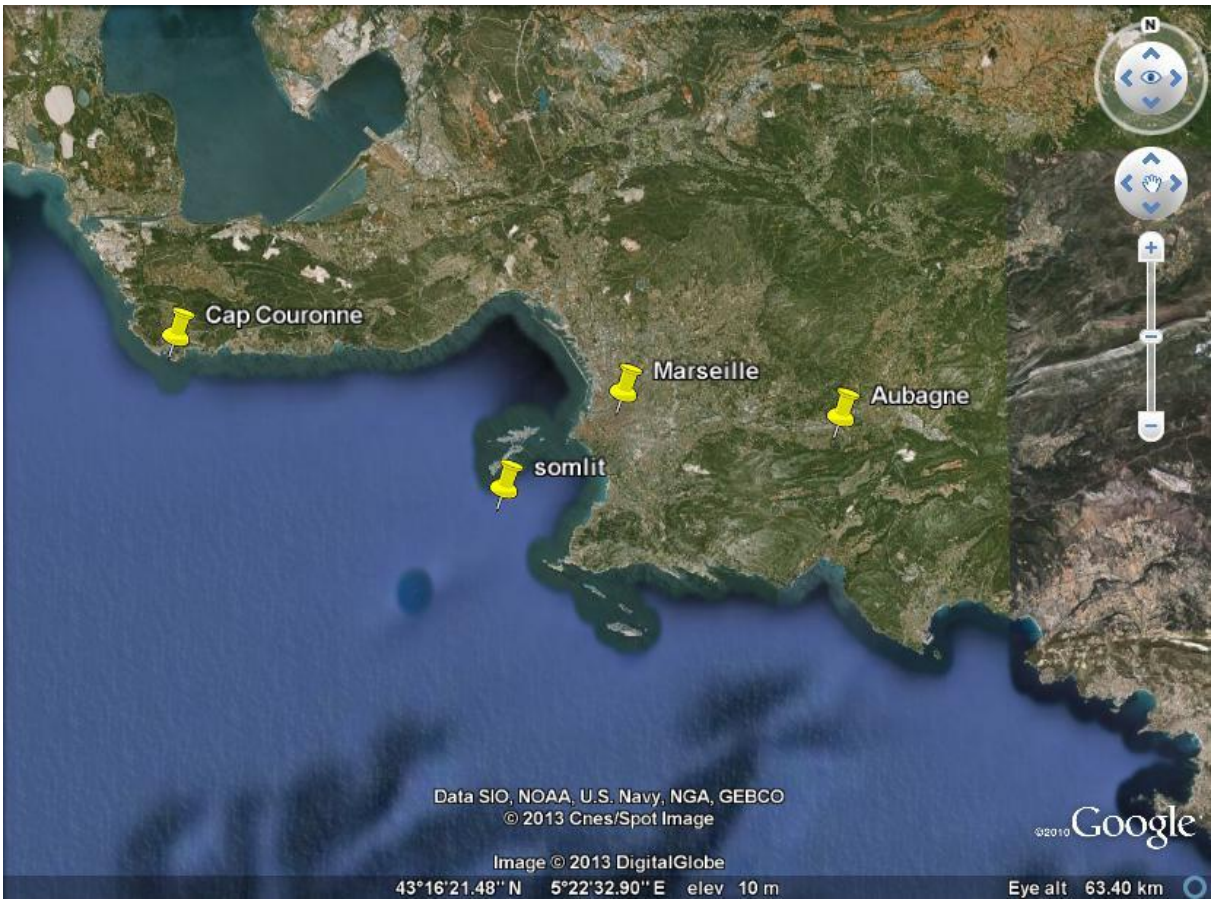

Figure 1: Satellite image of the study area showing Marseille and its surroundings.

This gives the city a highly rugged topography which has led to a dense, highly complex, interconnected network of fresh- and wastewater channels. Two rivers converge onto the city: the Aygalades in the northern Aygalades area, from which the suburb takes its name, and the Huveaune in the south of the city with the Jarret as a tributary. Within the city limits both rivers run fully underground.

Particularly the Huveaune will be of interest to this study as its source is located in the Sainte-Baume mountains. It has a length of 49 km and runs between Sainte-Baume, via Aubagne to Marseille along the lower part of the valley. While this river has very low average flow rates, it can grow significantly as a result of strong rainfall (as in January 1978). Apart from flooding events, the Huveaune and its

tributary, the Jarret, are screened at Pugette station before being diverted to Channel 2 (Emissiare 2) of the Marseille wastewater treatment plant (STEP) and entering the sea near Cortiou (Figure 2). Until 2008, the effluent would leave the treatment plant through Channel 1, while the Huveaune was taken back after deviation to Channel 2. Since 2009, the treatment plant releases its effluents through Channel 2 where they get mixed with Huveaune river water before entering the sea in the Calanque de Cortiou. The mean annual discharge by the treatment plant reaches about 100 $\times 10^6$ m^3.
During heavy rains, planned overflows occur, allowing part of the effluent to be discharged into the sea without passing through the treatment plant. This occurs whenever the treatment plant reaches its capacity to prevent pipe blockages and flooding of the surrounding areas. There are several intermittent watercourses that represent additional routes for untreated land run-off to enter the sea, including the Pelouque and Bonneveine streams for which automated monitoring stations show that the volume of water passing through these streams is below the volume passing through the Aygalades or Huveaune rivers. A detailed description of the different pathways and associated assessment has been published by Jany et al. (2012a).

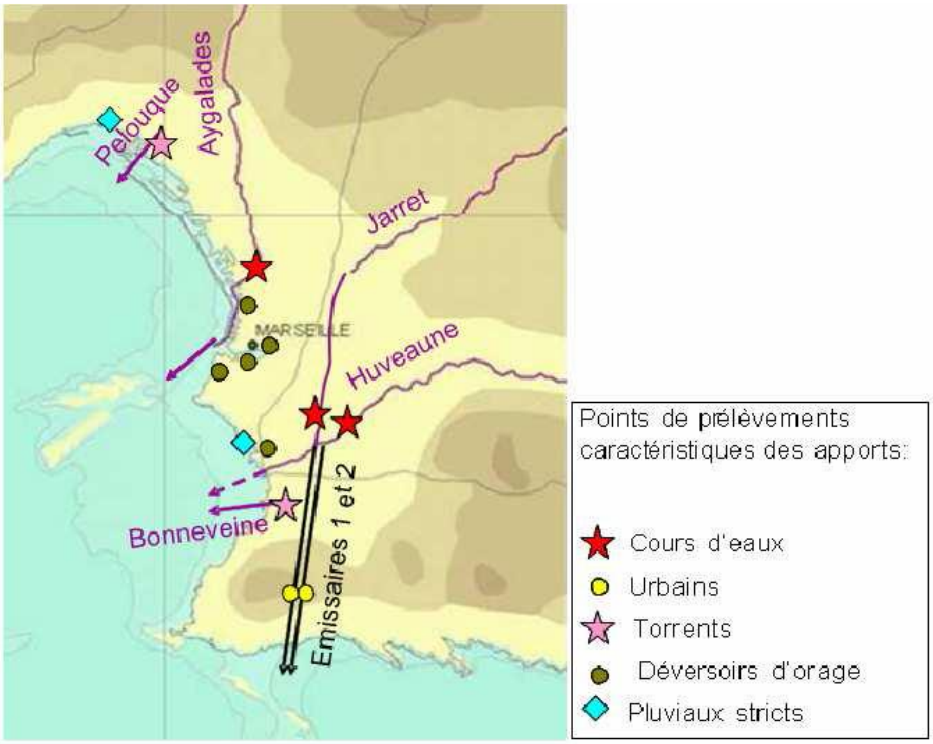

Figure 2: Map showing the most important water discharge routes for the larger Marseille area, based on samples taken as part of the METROC project (Figure 4 from Jany et al., 2012).

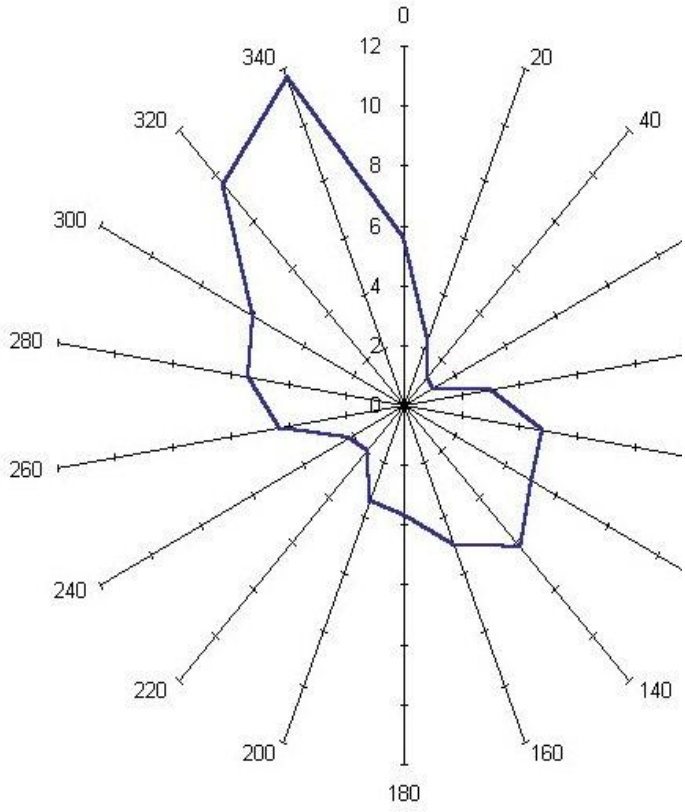

Figure 3: Wind rose for Marignane showing the climatological normal (1961-1991).

The weather in Marseille is highly variable with weather extremes that are typical of the Mediterranean climate. Thunderstorms at the end of summer can be fierce and bring large quantities of water: between 80-100 mm within a few hours (with extremes reaching up to 230 mm in a 4h period; Météo France, Bulletin Climatique Sud-Est n°9/2000) which is a significant fraction of the annual average of 545 mm.
During these thunderstorms and strong rains, water not only flows through the existing rivers but also finds its way through to the sea via storm drains and overflow channels (Figure 2).

The dominant wind directions are the southeasterlies and the Mistral which is a cold and dry north to northwesterly wind with strong gusts (Figure 3) that occurs about every 3 to 4 days (using wind direction as the sole definition of a Mistral event), but less frequently (every 12 days) if we use the definition put forward by Yohia (2017). It can be violent with gust speeds reaching 150 km/h (e.g., the storm on 27 October 2012 on the Frioul islands). Wind being the dominant dynamic forcing in this region, meteorological forcings have a strong impact on the sea temperature. We sometimes observe local cold patches where water surface temperatures are several degrees below the surrounding areas due to wind-driven upwelling events where cold bottom water rises to the surface. These upwellings are caused by northwesterly winds (Mistral) pushing surface water offshore, which then need to be replaced by water rising up from depth. In contrast, southerly and southeasterly winds push the surface water toward the coast where it can only sink thus creating a downwelling, through which warm surface waters are pushed to the bottom.

The climatological normal at Marignane meteorological station for the period 1960-1990:

Precipitation

Table 2

Average monthly rainfall (mm) at Marignane station for 1960-1990

	Jan	Feb	Mar	Apr	May	Jun	Jul	Aug	Sep	Oct	Nov	Dec
Mean	47.2	54	43.7	47.9	42.3	27.8	13.7	29.3	46.7	77.6	58.4	55.8

Table 3

Mean number of days with precipitation at Marignane station for 1960-1990

	Jan	Feb	Mar	Apr	May	Jun	Jul	Aug	Sep	Oct	Nov	Dec
>1mm	6.5	6	5.5	5.3	4.9	3.5	1.6	3	3.6	5.8	5.1	6
>5mm	2.7	3.1	2.8	2.7	2.2	1.7	0.9	1.4	2.2	3.3	2.9	2.9
>10mm	1.5	1.7	1.4	1.3	1.3	1	0.4	1	1.4	1.9	2	1.6

Wind:

Table 4

Mean number of days with wind at Marignane station for 1960-1990

	Jan	Feb	Mar	Apr	May	Jun	Jul	Aug	Sep	Oct	Nov	Dec
>57.6 km/h	10.7	8.2	10.4	11.1	5.8	7	8.5	6.1	6.7	8	8.7	9.1
>100 km/h	1	0.9	1.3	0.9	0	0.3	0.3	0	0.1	0.3	0.8	0.7

In addition to the hydrodynamic processes generated by wind blowing toward or away from the cost (down- and upwelling), the Bay of Marseille is subject to various hydrodynamic processes. Eddies, and in particular the so-called Marseille Eddy (Schaeffer et al, 2011), also play a key role in transporting water parcels from the Rhône river mouth eastward into the Bay of Marseille or by interacting with upwelling plumes or the Northern Current (NC). Moreover, as pointed out by Albérola and Millot (2003), the NC can intrude from the south into the Bay of Marseille and significantly alter the coastal dynamics in the area by generating a strong westward flow. Such a NC intrusion onto the shelf was observed in June 2000 by Petrenko et al. (2005). Similar intrusions were also observed using the Tethys2 hull-mounted ADCP in October 2007 by Pairaud et al. (2011) and in October 2011 with a significant impact on the local biogeochemistry (Ross et al., 2016). Figure 4 presents all of these processes as well as. Figure 4 provides a summary of these processes and the main fluxes.

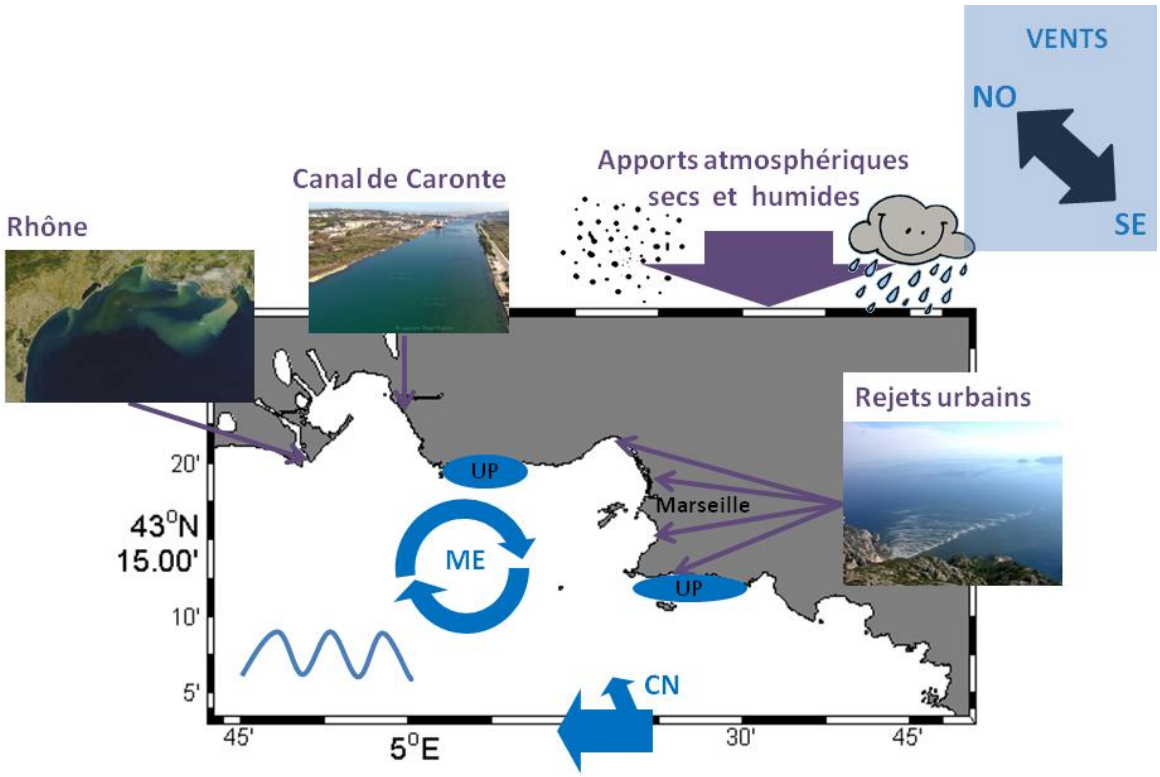

Figure 4: Map of the study area showing the different sources of freshwater input and the main physical forcings and processes (UP : upwelling, ME : Marseille Eddy, CN : Northern Current) after Fraysse (2014).

The Bay of Marseille constitutes a very special ecosystem, since it oscillates between a base level corresponding to a rather oligotrophic environment with typical chlorophyll concentrations of < 0.1 µg/L (measured at SOLEMIO station of the SOMLIT Observation network, Anse des Cuivres in Endoume) and a level corresponding to an environment receiving multiple anthropogenic inputs from the Cortiou runoff (urea: 51 µmol/L, NH4: 34 µmol/L, NO3: 17 µmol/L, PO4 : 13 µmol/L; annual averages according to Arfi et al., 2000), via coastal rivers (Aygalades and Huveaune), during heavy rainfall events, and when the Rhône river plume is pushed eastward and intrudes into the bay. These different inputs regularly lead to chlorophyll measurements ranging from 1 to 3 µg/L (SOLEMIO March 6, 2007). For each of these input sources, the amounts and composition of nutrient, POM, and DOM can vary significantly.

The influence of the Rhône can be felt as far as the Bay of Marseille, where low salinity water (mixed at the river mouth) can be detected for several days in a row (Para et al., 2010). After a flood event in December 2003, Gatti et al., (2006) detected an extension of the plume at a site further south (SOFI/GOLTS). Model results for the years 2007-2008 indicate that intrusions were most frequent between June and October (Pairaud et al., 2011) with over 10 events per year. During such intrusion events, the Rhône plume creates the most important and persistent biogeochemical input into the Bay of Marseille (eastward push of the plume due to wind and eddies) (Fraysse et al., 2014).

The discharges at Cortiou provide relatively constant nutrient inputs with a marked daily cycle. The discharge plume can enter the Bay of Marseille under weak or southeasterly winds, including isolated pockets of polluted water (possibly created and maintained via eddies), and can persist for a long time (Arfi et al., 2000). The input of nutrients by coastal rivers fluctuates strongly depending on the amount of rainfall, the length and severity of a preceding drought period, and on the season.

A chemical contaminant discharged into the Bay of Marseille is dispersed in the marine environment with the currents; the pollutant type usually determines its fate, i.e., it may enter the atmosphere, be deposited in the sediment, be dispersed toward the open sea, or enter the trophic chain. Of particular interest is atmospheric CO_2, found in very large quantities in Marseille, which is exchanged with the ocean (absorption – degassing) which can act as either a sink or source of CO_2. CO_2 is found in dissolved form in seawater and dissociates into the different carbonates affecting ocean acidity levels, with higher CO_2 leading to a decrease in *pH* which is causing ocean acidification.

3 AVAILABLE MODELS

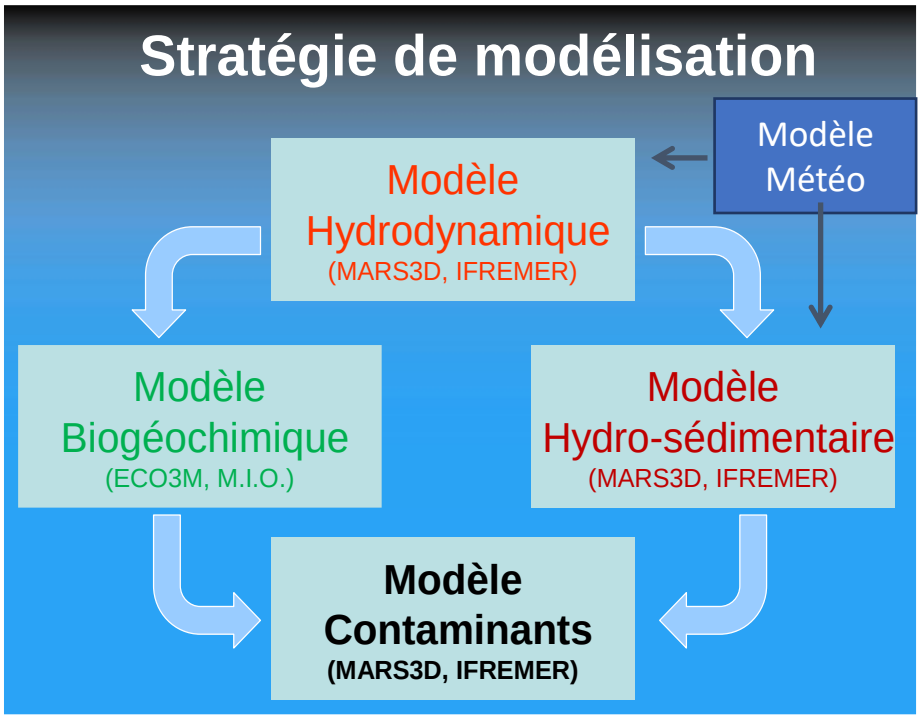

Figure 5 : Coupling of models within the framework of the MASSILIA-GIRAC-METROC projects.

In order to understand the impact of the different physical forcings (both typical and extreme wind, storm, thunderstorm, and flood events) on our study area it is necessary to employ a hydrodynamic model. This model was developed, calibrated and validated specifically for use in the Gulf of Lion. A smaller-scale grid extended between the RHOne River and MArseille (RHOMA, Pairaud et al., 2011)) was embedded in the NORth MEditerranean Sea model (MENOR, Lazure & Dumas, 2008). Due to the importance of water-sediment exchanges (deposition, resuspension, chemical interactions) in the coastal zone, we also need a sediment model that can simulate the dispersion and deposition of particles and their effect on the local biogeochemistry and turbidity (METROC). The coupling with a mechanistic ecological model makes it possible to simulate the functioning of the ecosystem subjected to physical and anthropogenic forcings and, in particular, to isolate the response to anthropogenic disturbances. In order to study a contaminant more precisely, specific models can be developed that use the results of the more general models to explore, for example, the PCB speciation in relation to the natural ecological variations of the system (POC, DOC, and phytoplankton contents) (Figure 5), or to include the carbonate system with the air-sea fluxes of CO_2 in the biogeochemical model ECO3M-Carbox (Figure 6).

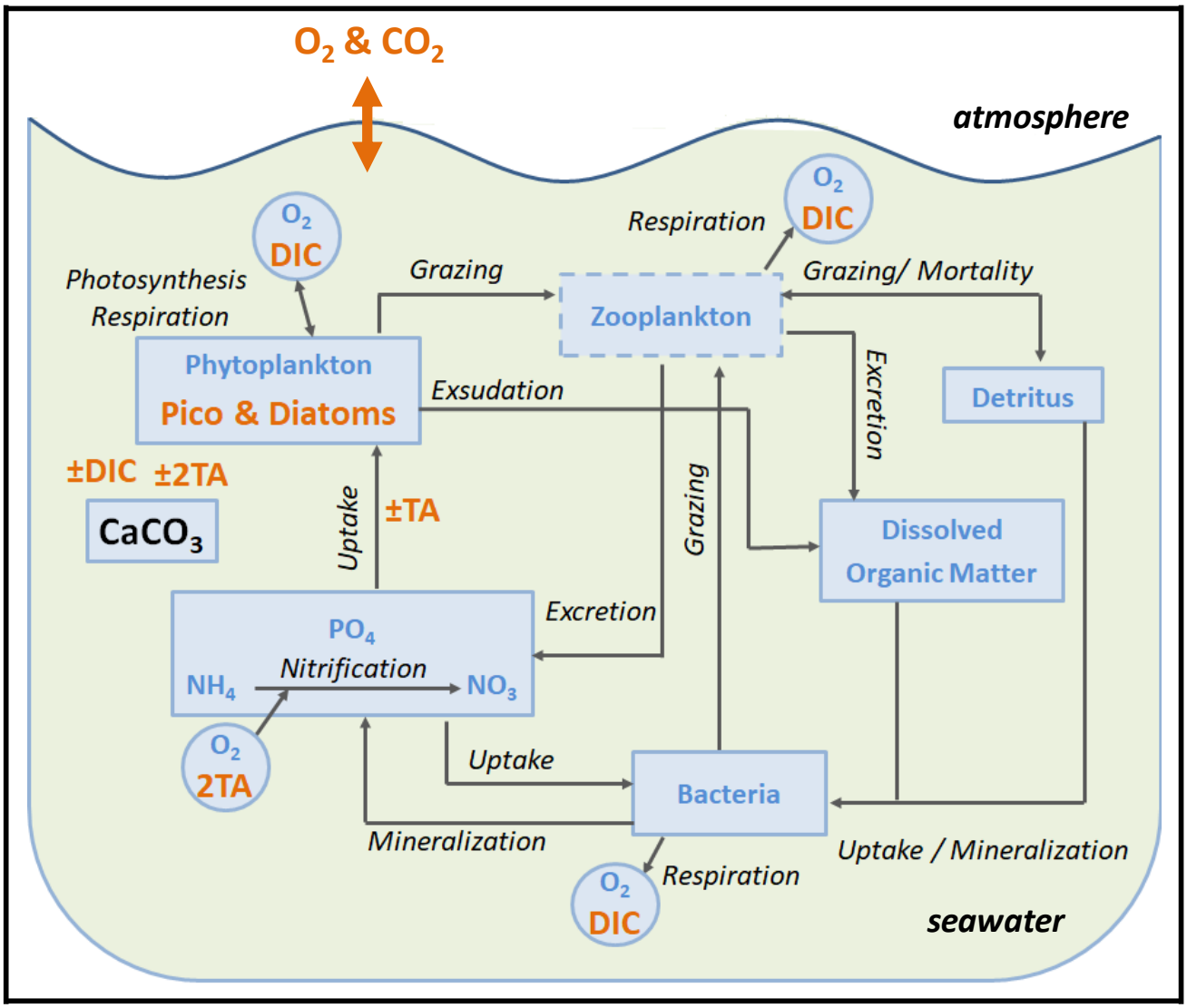

Figure 6 : Flow chart of the biogeochemical model including a compartment to simulate the carbonate system (CarbOx) as used projects OT-Med AMC and AERMC IAMM.

3.1 ATMOSPHERE MODELLING

Atmospheric modelling using the MM5 model (ACRI-ST) was carried out for the years 2007 to 2012 to provide the atmospheric forcings used by the models show in Figure 5. For the years from 2012 to 2016, the AMICO projects also used the AROME model. The WRF model has also been used to create some of the results presented here and for use with projects AMC and IAMM (from 2017 onward).

The WRF model has been developed by the US National Center for Atmospheric Research (NCAR), the US National Centers for Environmental Prediction (NCEP), and the US-AIR Force (AFWA). It is currently used by NOAA (National Oceanic and Atmospheric Administration) as an operational forecast model.

There are two dynamic solvers in the WRF model:
-The ARW (Advanced Research WRF) and
-the NMM (Non-Hydrostatic Mesoscale Model).

The ARW dynamic solver has been developed for research purposes by providing a vast array of physics and dynamics options and a data assimilation system.
The NMM dynamic solver has been developed for operational purposes to simulate mesoscale dynamics and weather phenomena such as single-cell storms or topographic waves. From a computational point of view, both dynamic solvers have been optimized to be run in highly parallelized computing architectures.

In the MASSILIA project we used the NMM solver, configuring the model to use three nested grids with 38 vertical levels, centred on the city of Marseille.
The first grid consists of 60×90 grid points (x×y) to yield a spatial resolution of 0.096°×0.096°. The second grid has 62×110 points and a resolution of 0.032°×0.032°. Finally, the third grid has 100×200 points and a resolution of 0.016°×0.016°.
The atmospheric fields are represented in pressure coordinates, a proxy for altitude based on the following correspondence between altitude and pressure in a standard atmosphere:
1000 hPa =200 m
850 hPa=1450 m
700 hPa=3010 m
500 hPa=5570 m
300 hPa=9160 m.

In the following, any reference to an altitude will be made using pressure coordinates. The model output variables used for the analysis were:
- temperature (in °C) at different altitudes.
- wind speed (m/s) at different altitudes.
- the geopotential (using geopotential height with units of geopotential meters where 1 gpm corresponds to a geopotential of 9.81 J/Kg)
- specific humidity (ratio of the mass of contained water vapor to the total mass of the air parcel); a conserved quantity during changes of altitude and/or temperature as long as there is no condensation or evaporation.
- potential vorticity (in potential vorticity units: 1 PVU=10^{-6} m^2 K s^{-1} kg^{-1}) of an air particle increases as its static stability decreases. In other words, it is a conservative parameter that can be used to track individual air particles over time and know its altitude dynamics.
- CAPE (convective available potential energy in units of J/Kg) is the amount of energy available for convection. Positive CAPE will cause an air parcel to rise, while negative CAPE will cause the air parcel to sink. Nonzero CAPE is an indicator of atmospheric instability.
- θ_w: pseudo wet-bulb potential temperature, is the temperature that a parcel of air at any level would have if, starting at the wet-bulb temperature, it was brought at the saturated adiabatic lapse rate to the standard pressure of 1000 hPa.

3.2 COMPARING THE WRF AND MM5 ATMOSPHERIC MODELS

The purpose of developing a Marseille's configuration of the WRF model was to increase the spatio-temporal resolution of the atmospheric forcing and thus be able to model smaller-scale processes.

Figure 7 shows the simulation results of a weak northerly wind by both models in the RHOMA area. MM5 is used to force the hydrodynamic model in the MASSILIA-GIRAC-METROC projects. There is a change in the intensity and direction of the winds in the Bay of Marseille and in the Calanques area when accounting for the topography at a higher spatial resolution in the WRF configuration. These differences are likely affect the spatial extent of freshwater plumes at the different rivers mouths and coastal streams.

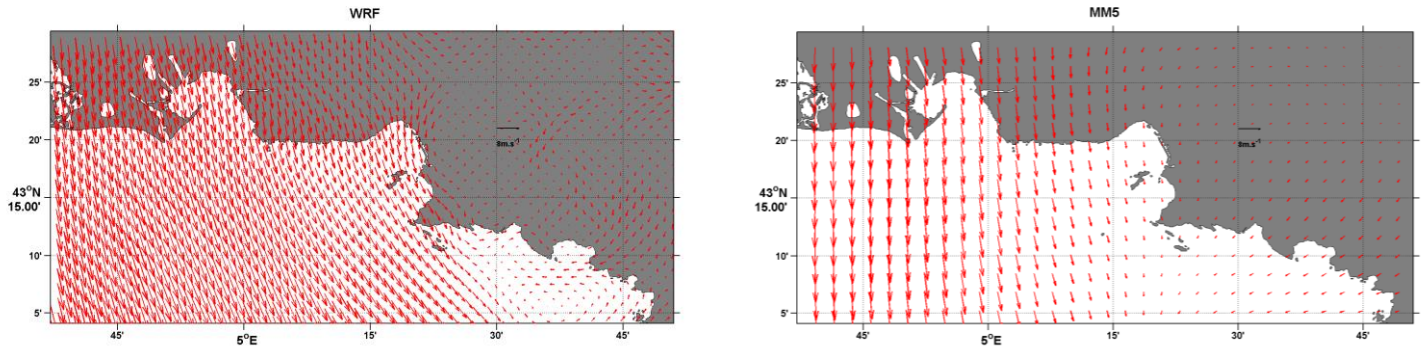

Figure 7: Northerly winds as simulated by WRF (left) and MM5 (right) for 21 July 2007 at 0h.

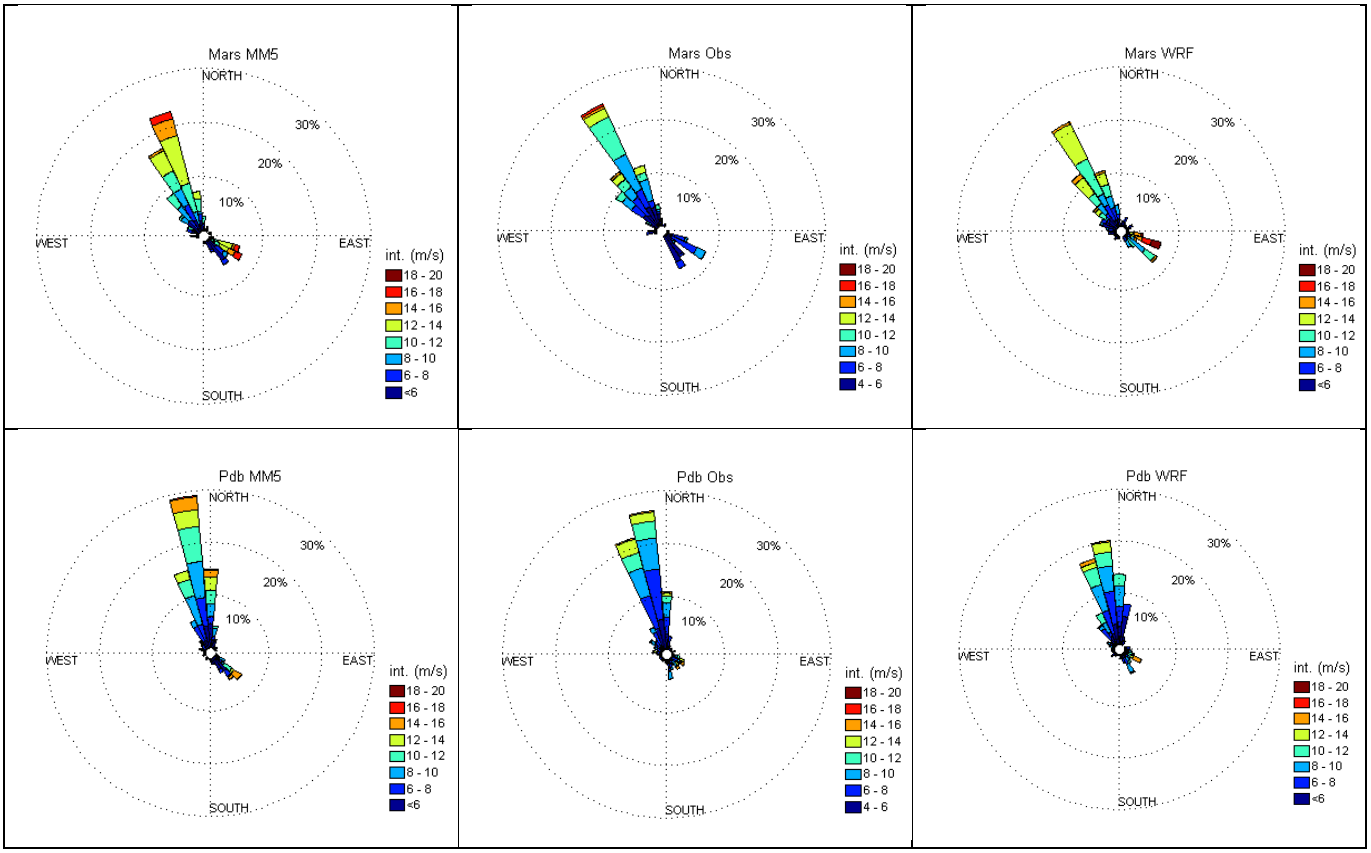

Figure 8: Wind roses of modelled and observed wind velocities and directions for Marseille (top row) and Port-De-Bouc (bottom), from MM5 (left), observations (centre), and WRF (right).

As part of the GIRAC project, observations at the Port-De-Bouc and Marseille-Hippodrome meteorological stations were used to validate the winds modelled by MM5 and the air temperature used to force the RHOMA model (Pairaud et al., 2011). For technical reasons, the comparison of WRF and MM5 with observations is limited to the period September-November 2007 (Figure 8) from which we can draw some first conclusions as to the validity of the two wind forcings for this period. While the main directions are well reproduced by both models, they tend to overestimate the wind speeds, particularly WRF for easterlies and MM5 for northerlies at the Marseille station. We also note a greater directional spread in the WRF winds compared to MM5, although from such a visual inspection it is unclear which model provides the best representation of observations at these two

stations. For reasons of consistency with the forcing model used in the larger MENOR model region, the MM5 model was chosen to provide the forcing within the framework of the MASSILIA-GIRAC-METROC projects.

Subsequently, the outputs from the WRF model were adapted to provide the forcing for the MARS3D hydrodynamic model for use with the AMC and IAMM projects.

3.3 HYDRODYNAMIC MODELLING

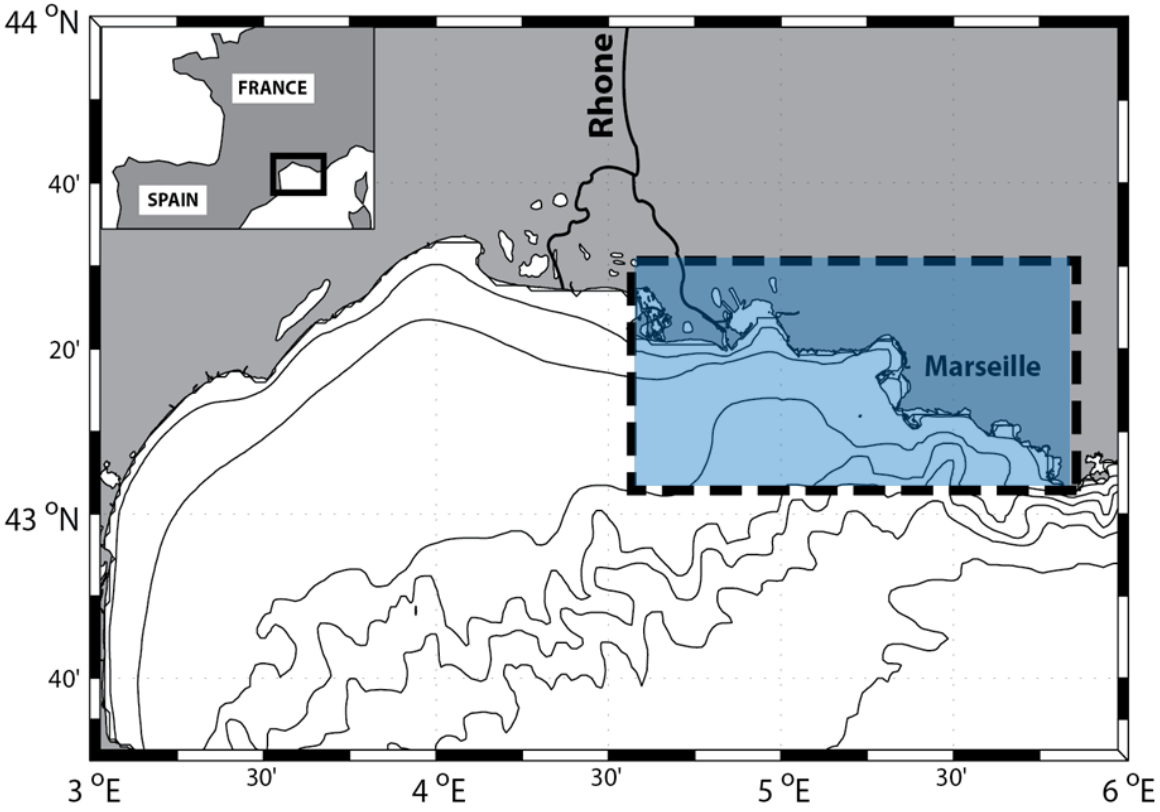

Figure 9: Map of the study area showing the RHOMA model domain (shaded box)

A hydrodynamic model of the Bay of Marseille, extending from the Rhône to Cap Sicié has been set up (Figure 9) by creating the RHOMA (Rhône-Marseille) configuration of the MARS3D model (3D hydrodynamic Model for Applications at Regional Scale, IFREMER). It aims to be as realistic as possible and takes into account the interactions of processes at different scales. The model was validated using different data sets (*in situ* and remote sensing of temperature, salinity, and currents) acquired in 2007-2008. This work is described in detail in Pairaud et al. (2011). Improving the model and gaining an understanding of the processes that govern the physics of the zone constitute the essential prerequisites to correctly model the sedimentary and biogeochemical processes as they are forced by the advective movements and the mixing of the water masses, i.e., by the hydrodynamic model.

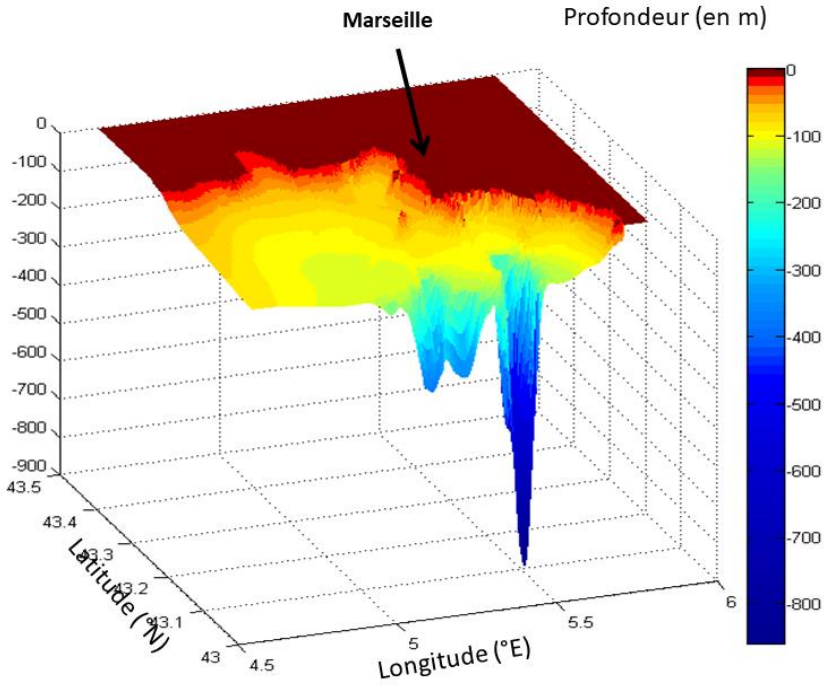

Figure 10: Bathymetry of the RHOMA model domain.

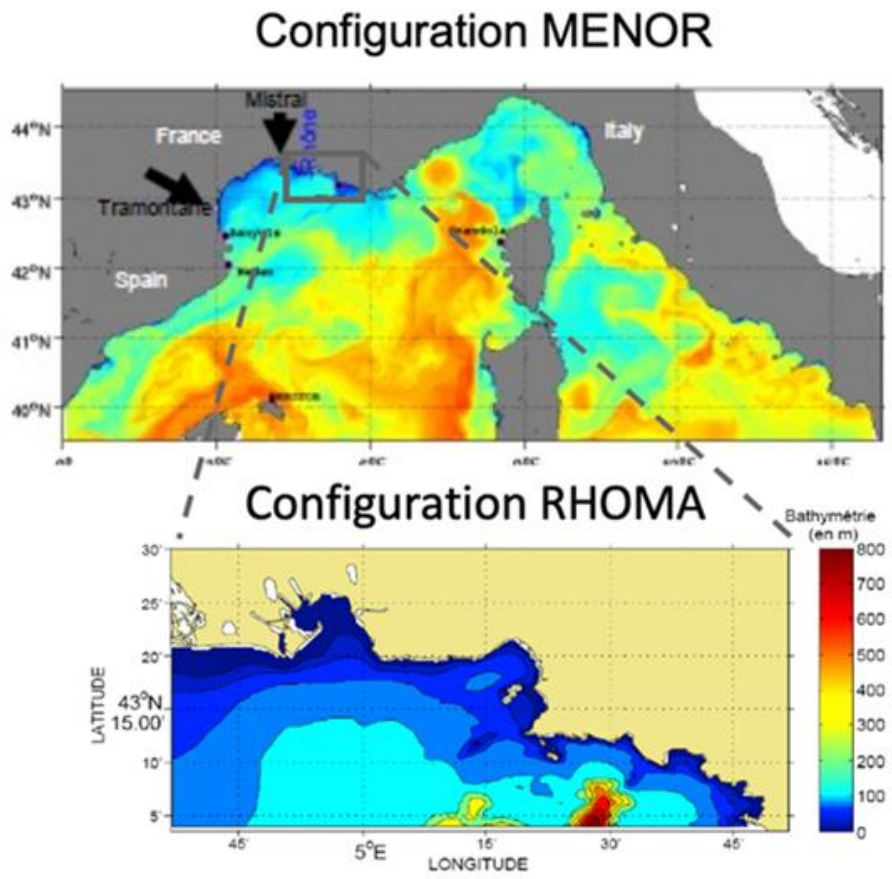

Figure 11: Nesting strategy for the MARS3D model configurations. The MENOR configuration provides the open boundary conditions (OBC) that drive the RHOMA configuration.

Within the framework of this study, we use the three-dimensional MARS3D model (Lazure and Dumas, 2008). In its RHOMA configuration there are 503×240 grid points in the horizontal ('C' grid), corresponding to a spatial resolution of about 200m, and 30 vertical sigma levels (with a finer vertical resolution near the surface and bottom). The time step is fixed at 30s. Apart from a realistic bathymetry (Figure 10), the model is forced by the Rhône (daily flow volumes provided by CNR), the atmosphere (wind, rain, and heat flux provided by the MM5 model) and the general circulation (by nesting the smaller RHOMA domain in the larger MARS3D-MENOR configuration, Figure 11).

During the development of the coupled models, a version with a grid of 400 m of horizontal resolution was also set up and validated for the period 2007-2008. This version was subsequently used for all couplings with other models.

The flow rates of run-off coming from the city of Marseille are defined using flow data provided by the local administration. These run-offs include storm overflows and rain-fed torrents. Discharges at Cortiou are divided into three parts: (i) an estimate of the flows from the WWTP (treated water), (ii) discharge through Channel 1 excluding WWTP water (thus mostly residual and overflow water), (iii) discharge through Channel 2 excluding WWTP water (mostly Huveaune and Jarret river and overflow water) (Le Masson, 1995;1997;1998). Figure 12shows time series of each part during two rain events (October 24-30, 2007 and December 12-18, 2008). It should be noted that these figures do not represented the run-off due to rain in its entirety as diffuse water discharges are unmeasured and cannot be accounted for. Furthermore, some measuring devices are disconnected when the flow rates are too high.

The model estimates the nutrient and contaminant inputs during such rain events by assigning each input constant or variable concentrations based on measurements or estimates from published data (Jany & Thouvenin, 2012).

(a)

Emissaire 1: overflow (red line)
Emissaire 2: Huveaune, Jarret + overflow (blue line)
STEP: treated water passing through the WWTP (green line)
Huveaune: water from the Huveaune and Jarret discharged into Prado (pink line)

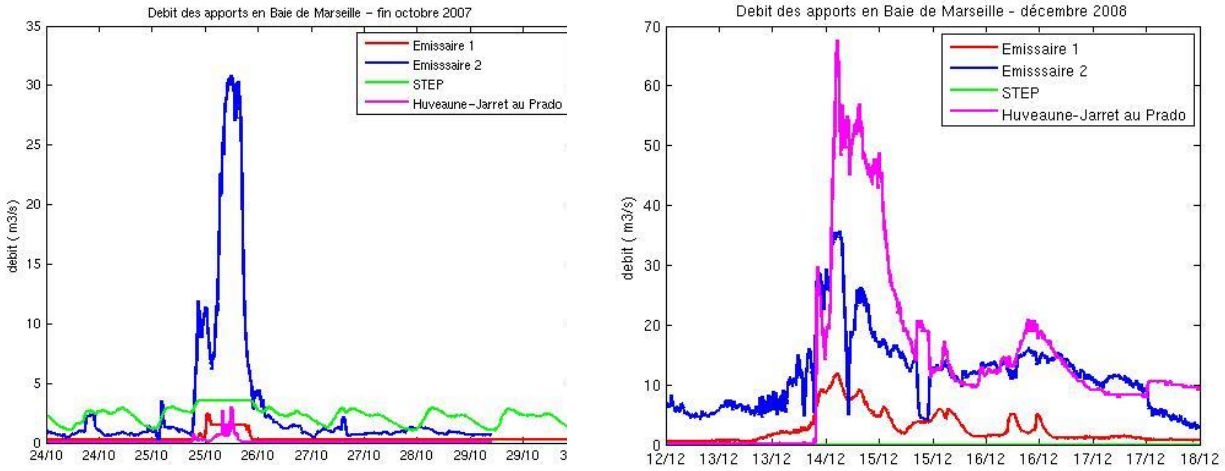

(b)

Aygalades: Aygalades stream
Littoral Nord: streams and torrents on the northern coast
Littoral Sud: streams and torrents on the southern coast

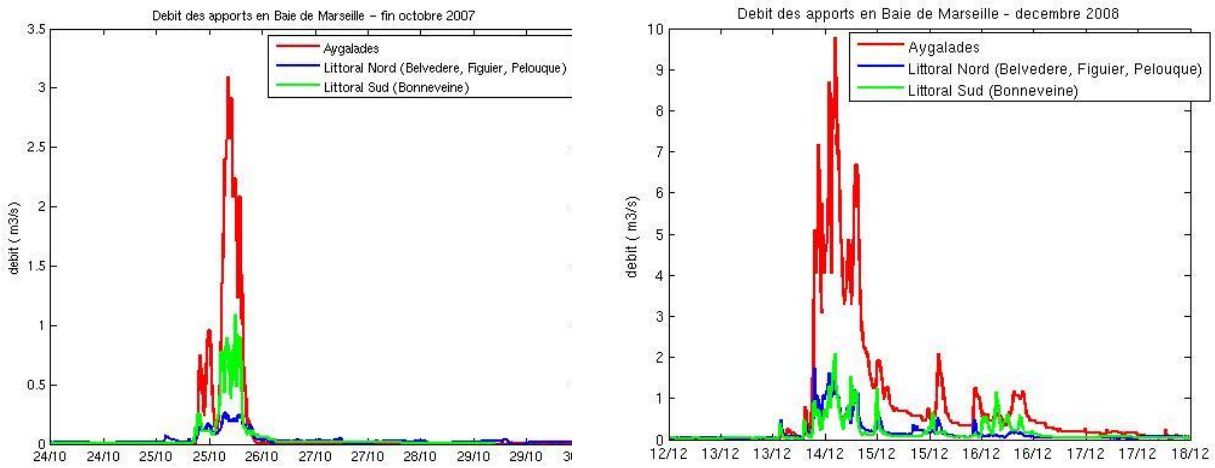

(c)

Storm overflows: grouped into 4 discharge points

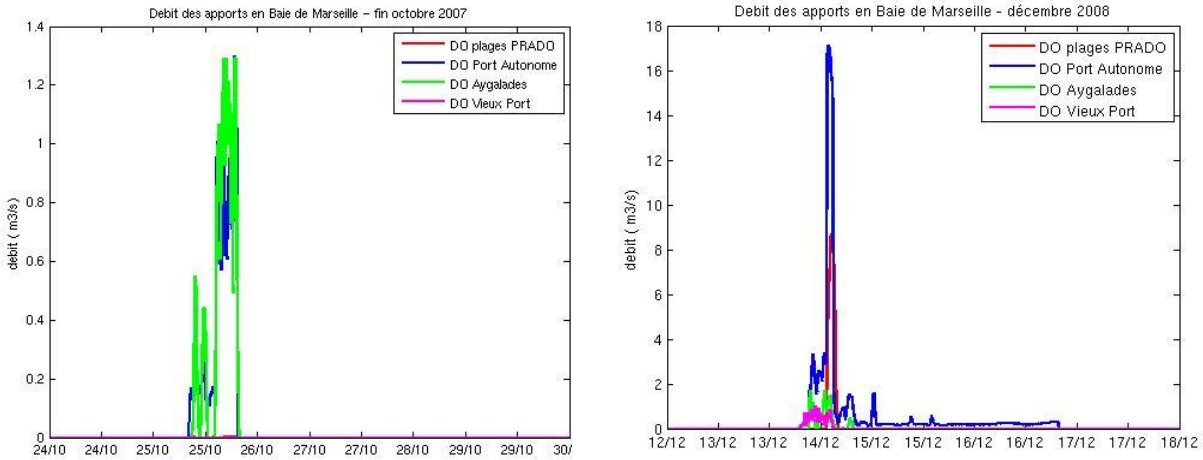

Figure 12: Discharge flow data for the Bay of Marseille during two extended rain events in October 2007 (left) and December 2008 (right): contributions by (a) WWTP (STEP) at Cortiou and by the Huveaune and Jarret at Cortiou and Prado, (b) streams, and (c) storm drains.

3.4 BIOGEOCHEMICAL MODELLING AND COUPLING

The biogeochemical model presented in Faure et al. (2010a and b), was modified by Marion Fraysse, Katixa Lajaunie, and Lucille Barré to yield successive versions of ECO3M configurations: MASSILIA (Figure 13), CarbOx (
Figure 6), and MixCarbOx, respectively.

In the first modification, a 0D study introduced a new parameterization making zooplankton grazing temperature sensitive and included the phosphorus cycle (Fraysse, 2010). This resulted in the so-called ECO3M-MASSILIA configuration which contains 17 state variables divided into 5 compartments: phytoplankton, bacteria, dissolved and particulate organic matter, and dissolved inorganic matter (Figure 13).
The biogeochemical model was coupled online and in 3D with the MARS3D hydrodynamic model using the RHOMA 400m configuration. Several studies assessed the capabilities of the coupled model to reproduce the key processes and seasonal variations of the coastal ecosystem (Fraysse et al., 2013; 2014; Ross et al., 2016).

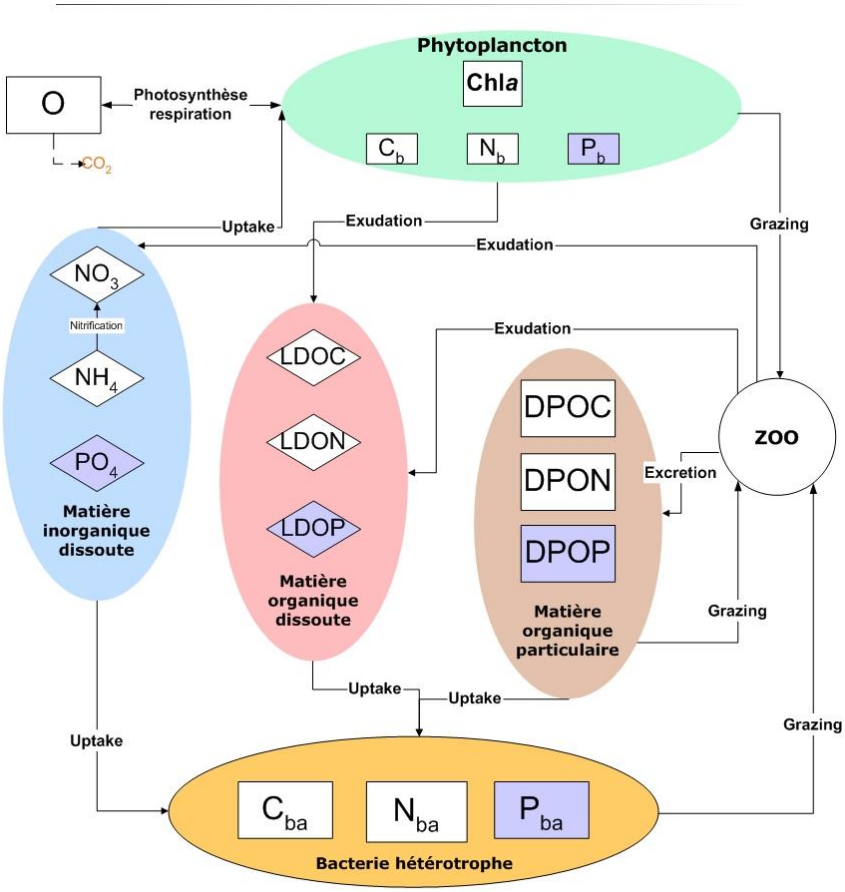

Figure 13: Schematic illustrating the different compartments and interactions in the ECO3M-MASSILIA biogeochemical model.

The Eco3M-MASSILIA biogeochemical model (Fraysse et al., 2013) was extended by splitting the existing phytoplankton compartment into two phytoplankton groups and a carbonate compartment resulting in the so-called Eco3M-CarbOx version (Lajaunie-Salla et al., 2021). This model contains 26 variables divided into 5 compartments: phytoplankton, bacteria heterotrophs, particulate organic matter (POM), dissolved organic matter (DOM), and dissolved inorganic matter (DIM). Eco3M-CarbOx can account for certain variables associated with the carbonate system: DIC (in its three main forms), calcium carbonates (CaCO3), pCO2, pH, and total alkalinity (TA). The phytoplankton compartment is divided into two sub-compartments, namely picophytoplankton and diatoms, each using carbon (C), nitrogen (N), phosphorous (P) and Chl as state variables. The POM and DOM compartments use C, N and P as state variables. The DIM compartment comprises NH4, NO3, PO4, and O2, and also contains the aforementioned variables associated with the carbonate system (
Figure 6).
From the total of 26 variables, 22 are prognostic variables (derived from a state equation: advection-diffusion-reaction) and 4 are diagnostic (Chl of both phytoplankton groups, pCO2, and pH; calculated from prognostic variables). pCO2 and pH are calculated from other conserved variables associated with the carbonate system (DIC and TA). Phytoplankton Chl is obtained from the nutrient state of phytoplankton (N/C ratio) using the formulation from Tett (1990) as presented in Fraysse (2014) and Lajaunie-Salla et al. (2021).
While zooplankton is not represented by a state variable, the associated physiological functions (grazing, production and excretion of faecal pellets) are described explicitly in the model.

Subsequently, Lucille Barré added the functional trait of mixotrophy using variable stoichiometry and state variables of C, N, P, and Chl to produce the so-called Eco3m-MIX-CarbOx model (Barré et al., 2023a). The mixotrophs, as well as the properties characterizing the mixotrophic organisms are represented there. The model was modified further to add interactions between oxygen and other variables (e.g., zooplankton respiration), carbonate system variables (TA, pH, pCO2, and CaCO3) (Barré et al., 2023b) from the Eco3M-CarbOx model (Lajaunie et al., 2021), and to improve the representation of heterotrophic bacteria. After these modifications, the correct representation by the model of the properties of mixotrophic organisms was verified.

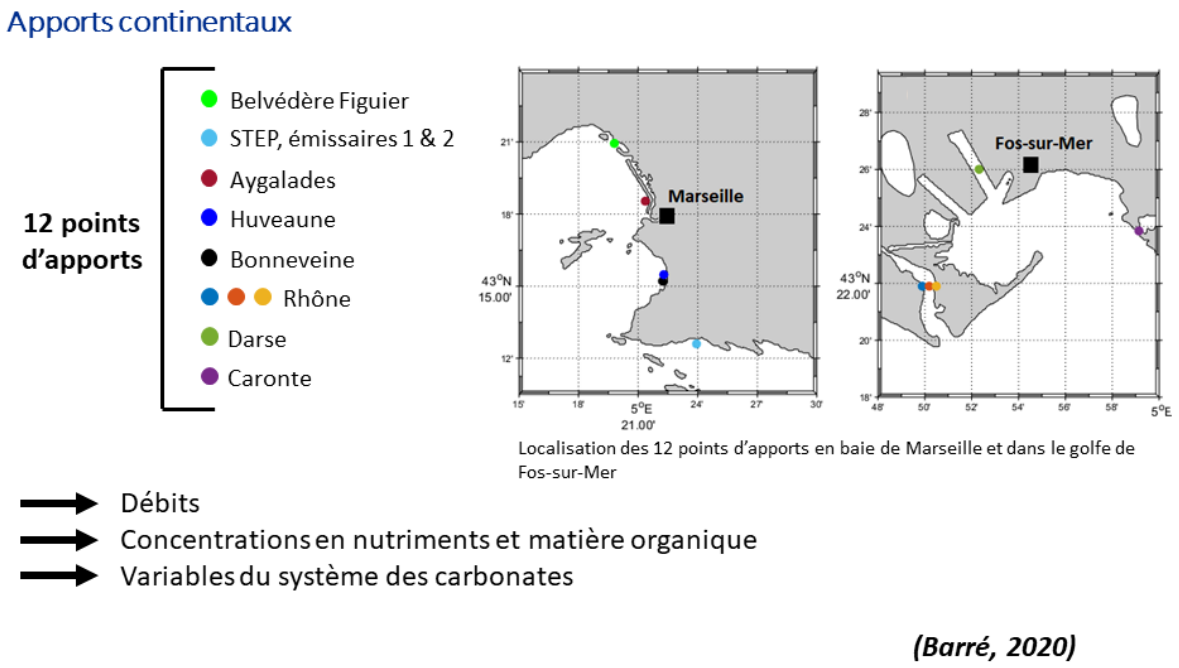

Localisation des 12 points d'apports en baie de Marseille et dans le golfe de Fos-sur-Mer

Figure 14: Location of freshwater inputs included in the RHOMA model configuration.

Particular attention had to be paid to the open boundary conditions (OBC) which play an important role in our model simulations: the western boundary is very close to the Rhône River mouth and the southern boundary is important during Northern Current intrusion events. The same biogeochemical model was therefore deployed within a larger configuration that covers the entire Gulf of Lion geographical area and which forms part of the larger MENOR domain (configuration of the MARS3D model that covers the North Western Mediterranean) (Figure 11). This coupled model of the Gulf of Lion is forced at its OBC by a zero gradient condition and the outputs of interannual simulations using the BFM operational model (Lazzari et al., 2010), developed by OGS (Trieste). The CarbOx biogeochemical model is forced by temperature, irradiance, flow volume and concentration levels of the Rhône, other land-based discharges (urban rivers, outlets, etc.), dry and wet atmospheric inputs, and atmospheric pCO_2.

The biogeochemistry of the Rhône River water is based on daily observations by OSU Institut Pythéas. The biogeochemical data of other discharges are either provided by the Marseille Provence Métropole Urban Community/Seram for nitrates and ammonium up to 2014, or estimated from the literature (Figure 14).

3.5 HYDROSEDIMENTARY MODELLING

The sediment model used in MARS3D is based on the S*i*AM3D model (Le Hir et al., 2001; Waeles et al., 2007, 2008; Dufois, 2008) which simulates the processes of erosion, deposition, consolidation, and flocculation of mixed mud/sand/gravel sediments. The process of sediment advection occurs in the hydrodynamic model. Sediment is modelled as thin millimetric layers that are created/destroyed following erosion/deposition processes. The sand/mud model that was set up for the Bay of Marseille uses some modifications to save computing time: sand is not transported in the water column but remains in the sediment compartment and the consolidation processes are not simulated. The erosion parameters governing the behaviour of the sediments were calibrated from erodimetry tests conducted on about fifteen cores extracted from the Bay of Marseille and representing different facies present in the study area. The simulated suspended solids (SS) are divided into three categories: heavy SS corresponding to the densest bottom sediment, light SS representing organic aggregates, and very light SS associated with the residual turbidity of surface waters. Considering the variability of SS fluxes and the lack of detailed observational data for the various tributaries and coastal rivers, we tested different scenarios and compared them to the limited observational data in order to identify the most likely contribution scenario. Given the scarcity of observational data on aggregation processes in the Bay of Marseille, we will address this point here.
The WW3 unstructured high-resolution wave model has also been set up for the Bay of Marseille area (www.marc.ifremer.fr), making it possible to simulate sea states and associated resuspension. It was validated using ADCP-based wave measurements collected at FRAME station in 2007 and 2008 (Vousdoukas et al., 2011).
Instead of using directly the sediment layer from *in situ* observations, we ran the model for 1 year (so-called spin-up, in aim to prescind from the initial conditions) to generate the initial conditions for the actual model runs.

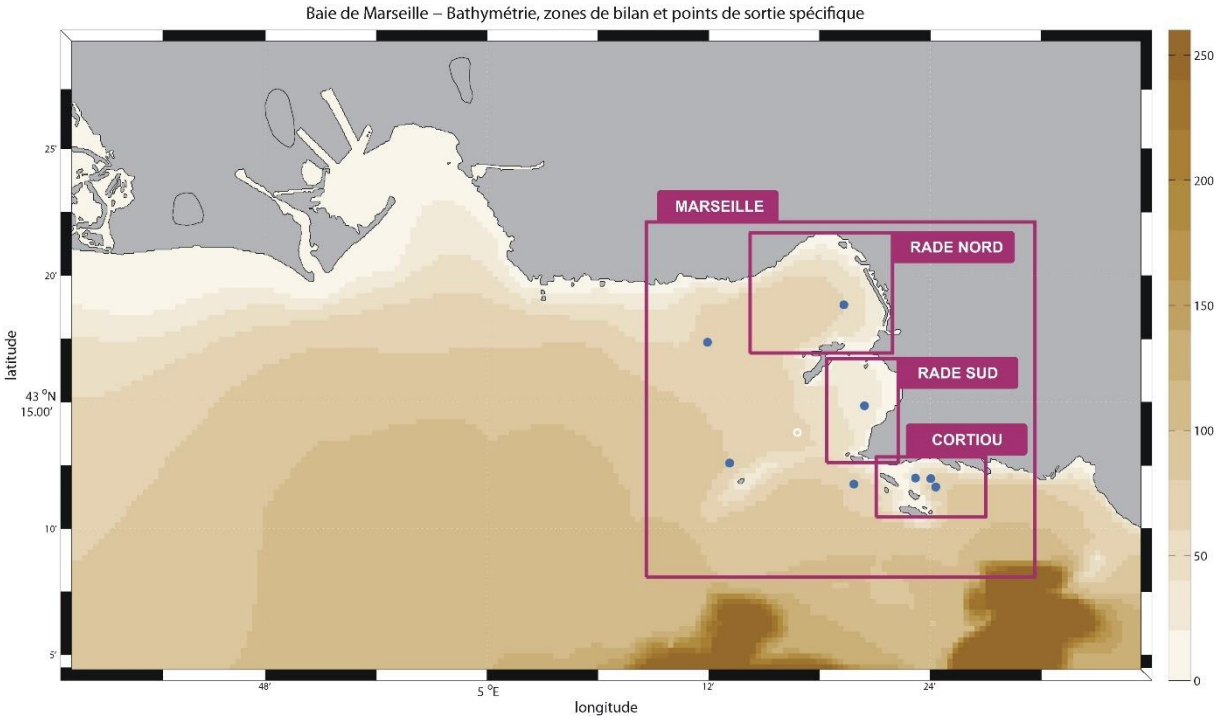

Figure 15 : RHOMA model domain and specific areas (boxes) and points of interest (blue dots) for which the global sediment flux is calculated.

In the next chapters, we will calculate the mass budgets of particulate and dissolved matter for different areas of the Bay of Marseille and certain reference points (Figure 15).

3.6 CONTAMINANT MODELLING

Modelling PolyChloroBiphenyls (PCBs) in the Bay of Marseille is based on (i) the hydrosedimentary MARS3D model presented above, (ii) knowledge of the ambient biogeochemical conditions as derived from the coupled biogeochemical MARS3D-ECO3M-MASSILIA model described below, (iii) an assessment of the biogeochemical inputs by land-based run-off (work by Ifremer/Protée within the framework of the METROC/GIRAC project; Zebracki, 2011; Jany et al, 2012a), (iv) modelling speciation and dynamics of PCBs, i.e. their adsorption-desorption on particles, their volatilization and their degradation, and (v) determining PCB speciation from *in situ* observations at a station in Marseille harbour. Both the estimation of forcings and the particular parametrizations used to represent certain processes in the model are based on a number of assumptions and on a choice of appropriate parameters. These have been tested and a sensitivity analysis has been carried out within the framework of the METROC project. While there are insufficient measurements to conduct a proper model validation, but ChloroBiphenyl 153 (CB153) concentrations measured in the area have been compared with available knowledge (Harmelin-Vivien et al., 2012).

3.7 WAVELET ANALYSIS

For the detection of eddies present in the circulation model outputs, we use a method based on a wavelet decomposition of horizontal fields of relative vorticity (Doglioli et al., 2007; WATERS - Wavelet package Analysis for Time Tracking Eddies in Regional modelS; for the Matlab version: http://www.mio.osupytheas.fr/~doglioli/waters.htm; for the Fortran version: http://stockage.univ-brest.fr/~grima/WASSCO).
Using 3D velocity fields as input, the software constructs 2D velocity fields by interpolating at a chosen depth (here this was set to -20 m). It then calculates the relative vorticity field, which is decomposed into wavelets based on an entropy calculation. Thresholding occurs by minimizing the entropy value. The retained signal can be considered representative of the eddies present in the vorticity field. In order to follow a particular eddy over time, an overlap criterion between two successive instants is applied, which makes it possible to identify the lifetime and the trajectory of the eddy.
For more details, see Doglioli et al. (2007), Rubio et al. (2009), Dencausse et al. (2010), and for a comparative study between this method and other automatic eddy identification and tracking methods, see Souza et al (2011).

4 MODEL RESULTS

4.1 ATMOSPHERIC MODELLING

We carried out a comparison between the WRF-NMM model outputs and observations at 5 stations in the Provence-Alpes-Côte d'Azur (PACA) region over a period of 5 months. The station locations were chosen to have the most heterogeneous spatial representation possible: two are located on the coast, two are inland, and one is in the mountains.
This approach made it possible to verify the behaviour of the model in different climatic zones:
- maritime zone
- sea/land transition zone
- in complex terrain.

We then created 2 configurations of the WRF model which were used in nesting mode. The first configuration, which we will refer to as the operational version, has two grids, the finer of which with a horizontal resolution of 3 km and 28 vertical levels.
The second configuration (referred to as the test version) has three grids, the finest of which with a horizontal resolution of 1.5 km and 38 vertical levels.

All data except for Orres station are from METAR (taken by planes at the airports) (of five months

Over the entire period of 5 months, the model behaves well in each climatic zones and remains close to observations (Table 5,
Table 6, and
Table 7). Compared to observations, the NMM model underestimates temperatures by about -0.6 to -2.5 °C, although they may briefly differ by up to -5 °C, especially during the early hours of the day before the model is rebalanced. The daily maximum temperatures differ by about -2°C.
Regarding the wind, the differences are of the order of 1 to 2 m/s. In the mountains, the model overestimates the wind speeds while the direction of the sea breeze is slightly off as well. This bias for weak winds has been noted by the developers of the NCAR model in regions with a more rugged topography (like the PACA region). In mountain areas, these weak winds are linked mainly to gravity flows (flowing down slopes with velocities < 4 m/s). Overall, the range of velocities predicted by the model is similar to the observed range.

Table 5

Mean temperatures, $\overline{T}$, and correlation coefficients, R, at different stations.

Station name	$\overline{T}$ (obs., °C)	$\overline{T}$ (operational, °C)	R (obs.-operational)	$\overline{T}$ (test config., °C)	R (obs.-test)
Istres	22.8	21.7	0.91	22.4	0.92
Hyères	23.1	20.7	0.62	21.1	0.55
Orange	23.1	22.1	0.92	23.9	0.94
Nice	23.2	20.6	0.68		
Orres	15.2	15.8	0.91		

Table 6

Mean wind speeds, $\overline{V}$, and correlation coefficients, R, at different stations.

Station name	$\overline{V}$ (obs., m/s)	$\overline{V}$ (operational, m/s)	R (obs.-operational)	$\overline{V}$ (test config., m/s)	R (obs.-test)
Istres	4.8	5.6	0.83	5.6	0.81
Hyères	3.7	4.6	0.59	4.5	0.63
Orange	4.8	5.5	0.84	5.3	0.86
Nice	2.9	2.8	0.38		
Orres	1.1	3.5	0.34		

Table 7

Mean absolute difference in temperature, $|\overline{\Delta T}|$, and wind speed, $|\overline{\Delta V}|$, between observations and model results for both model configurations.

Station name	$\lvert\overline{\Delta T}\rvert$ (operat. config.) (°C)	$\lvert\overline{\Delta T}\rvert$ (test config.) (°C)	$\lvert\overline{\Delta V}\rvert$ (operat. config.) (m/s)	$\lvert\overline{\Delta V}\rvert$ (test config.) (m/s)
Istres	-1.6	0.9	+0.2	+0.2
Hyères	-2.3	3.2	+0.9	+0.6
Orange	-0.9	0.4	+0.5	+0.7
Nice	-2.5		-0.1	

Orres	-0.6		+2.4	

4.2 HYDRODYNAMIC MODELLING

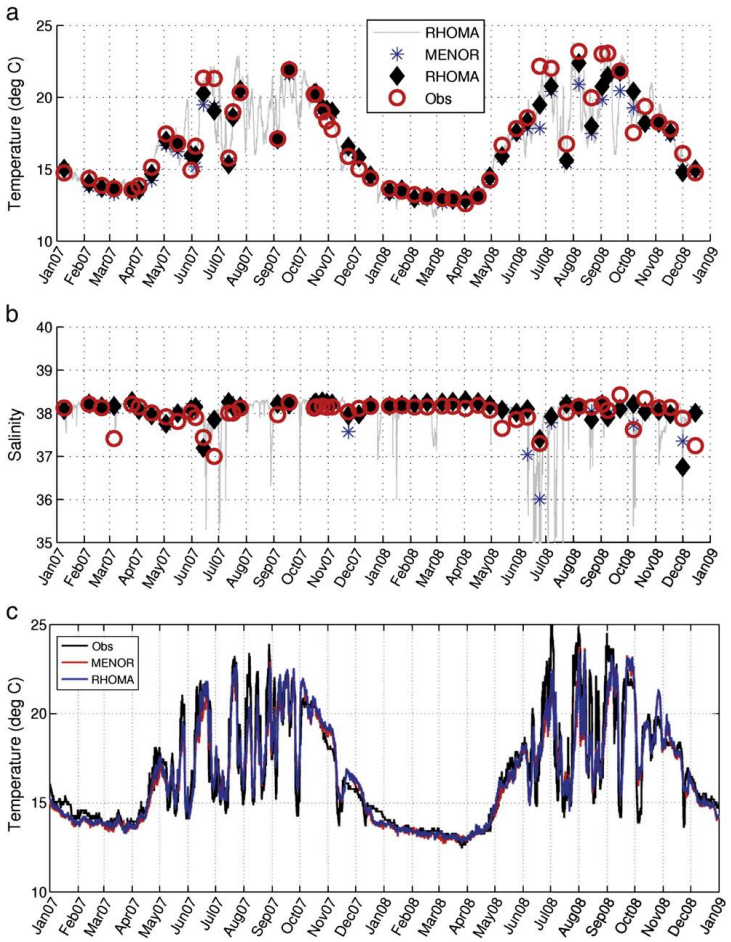

Figure 16: Comparing the (a) modelled temperature and (b) modelled salinity for the MENOR and RHOMA configurations to observations at SOMLIT station (from 0.75m depth) collected on the same date; (c) as in (a) but for Sud-Riou Station (observations collected at a depth of 5m) (from Pairaud et al. 2011, Journal of Marine Systems, Figure 4).

The hydrodynamic RHOMA model has been validated using *in situ* (temperature, salinity, currents) and remote sensing data (SST, ocean colour) collected from 2007-2008 (Pairaud et al., 2011). The comparison between modelling results and observations shows that all main processes that govern the dynamics in the Bay of Marseille (upwellings, cooling/warming events in summer, destratification in autumn followed by winter mixing, intrusions of low-salinity water from the Rhône, etc.) are well reproduced by the high-resolution RHOMA model (Figure Figure 16).

Other comparisons with observations including a statistical analysis of model errors (calculations of bias, correlations, RMS, etc.) are available in the publication. Overall, although the processes are well reproduced (e.g., temperature correlation R greater than 0.9 at the SOMLIT-Frioul station), the model tends to underestimate extreme summer temperature variations such as cooling associated with upwelling events under the presence of northerly winds, which then leads to a bias in the subsequent warming events (average bias reaching 0.5°C in the first ten meters at SOMLIT-Frioul station).

4.3 COUPLED BIOGEOCHEMICAL MODELLING

Initially, the realistic 3D simulations of the period 01/05/2007 to 31/12/2008 were compared to remote sensing data of ocean colour from the MODIS, MERIS, and GLOBCOLOUR satellites as well as to *in situ* data from SOLEMIO station (SOMLIT network) in order to calibrate the ECO3M-Massilia model (Figure 17-19).

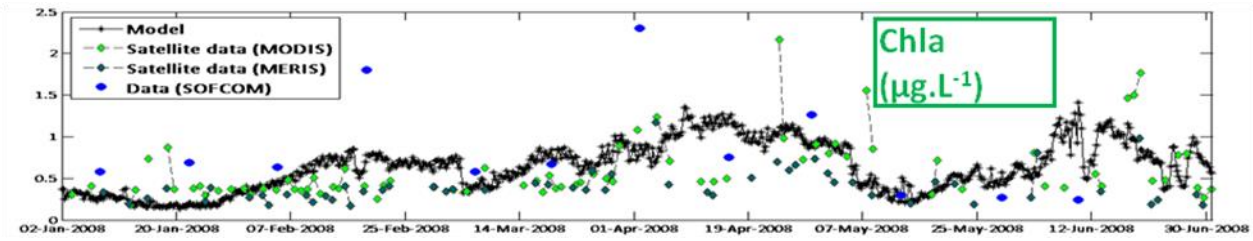

Figure 17: Comparing modelled surface Chla with ocean colour data from MODIS and MERIS and *in situ* observations at SOLEMIO station for Jan-Jun 2008.

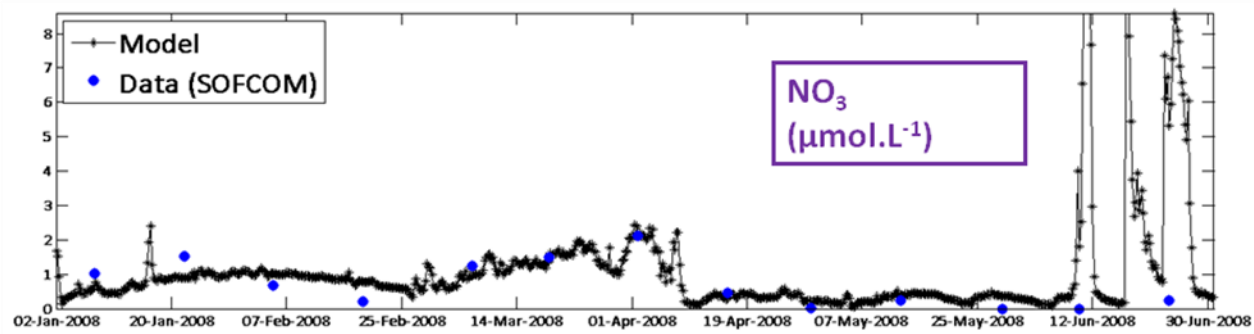

Figure 18: Comparing modelled surface nitrate concentrations with *in situ* observations at SOLEMIO station for Jan-Jun 2008.

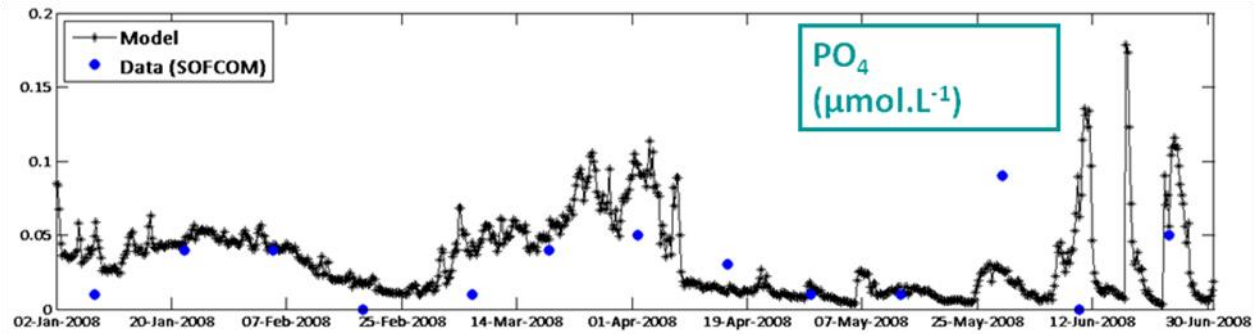

Figure 19: Comparing modelled surface phosphate concentrations with *in situ* observations at SOLEMIO station for Jan-Jun 2008.

Statistical criteria (cost function, bias) have been used to assess the model results using the approach from Allen et al., (2007) (Table 8). The cost function indicates that the variables included in Table 8 are very well represented (CF<1) except for salinity which is still well represented (CF<2). The bias analysis indicates that temperature and salinity are neither systematically over- nor underestimated by the model. In contrast, Chla is underestimated by the model by 17.9% at the surface and by 13.3% at the sea bed, and overestimated by MODIS by 5.5%. Nitrate is overestimated at the sea bed by 36%, while ammonium is underestimated (by 59.6% at the surface and 49.3% at the sea bed). Phosphate is overestimated at the surface (by 19%) and underestimated at the sea bed (by 17.5%).

Table 8

Statistical assessment of the results from the coupled biogeochemical model vis-a-vis observations from SOLEMIO station for Jan-Jun 2008. (a) Bias, (b) cost function, (c) performance criteria of statistical indicators used.

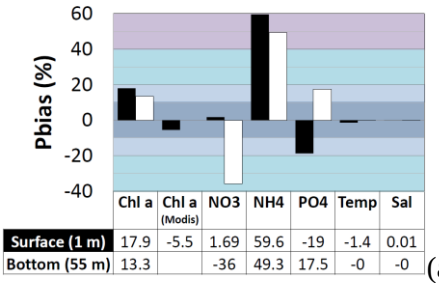

	Chl a	Chl a (Modis)	NO3	NH4	PO4	Temp	Sal
Surface (1 m)	17.9	-5.5	1.69	59.6	-19	-1.4	0.01
Bottom (55 m)	13.3		-36	49.3	17.5	-0	-0

(a)

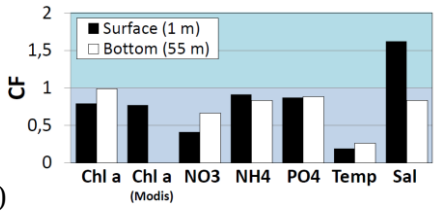

(b)

	excellent	very good	good	reasonable	poor	Reference
CF		CF<1	1-2	2-3	>3	Radach and Moll, 2006
|Pbias|	<10	10-20	20-40		>40	Maréchal, 2004

(c)

After completing the model calibration, we ran realistic simulations of other years (2009-2011) in order to compare the performance of the two Eco3M-Massilia configurations with (P) and without (noP) phosphorous cycle (Table 9, Figure 20, Figure 21, Figure 22, Figure 23) (to see the results for other variables see Fraysse et al., 2013). After this comparison, a decision was made to use the version that includes the P cycle for all subsequent simulations.

Table 9

Comparing the model results for the period 2009-2011 with observations at SOLEMIO station using statistical indicators (orange: poor, light green: good, dark green: very good).

2009-2011	CHL (µg L^{-1})		NO_3 (µmol L^{-1})		POC (µmol L^{-1})		PO4 (µmol L^{-1})
Model version	P	No P	P	No P	P	No P	P
Mean (*in situ*)	0.40		0.68		5.13		0.03
Cost function	1.01	1.16	0.80	0.81	1.20	1.19	1.39
Bias (%)	-28.75	-44.41	14.17	17.05	30.03	16.30	-15.35

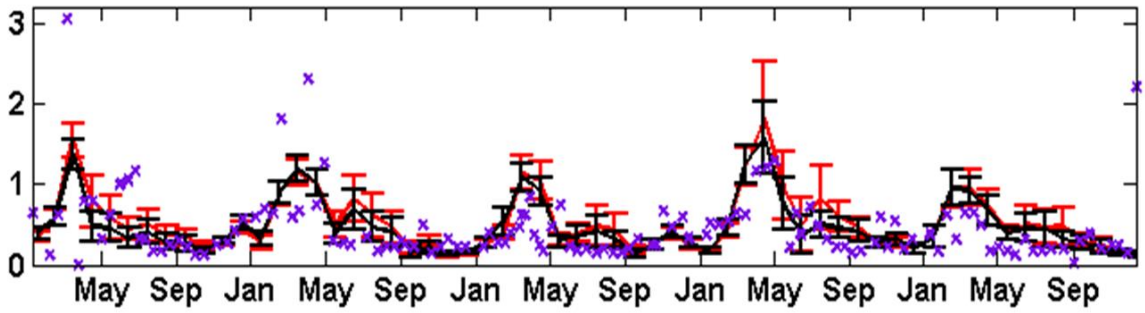

Figure 20: Comparing surface Chla obtained from the P (black) and noP (red) model configuration and averaged over a 10-day period (from 5 days before to 5 days after the date of the corresponding *in situ* measurement) to *in situ* observation at SOLEMIO station (markers) from 2007 to 2011.

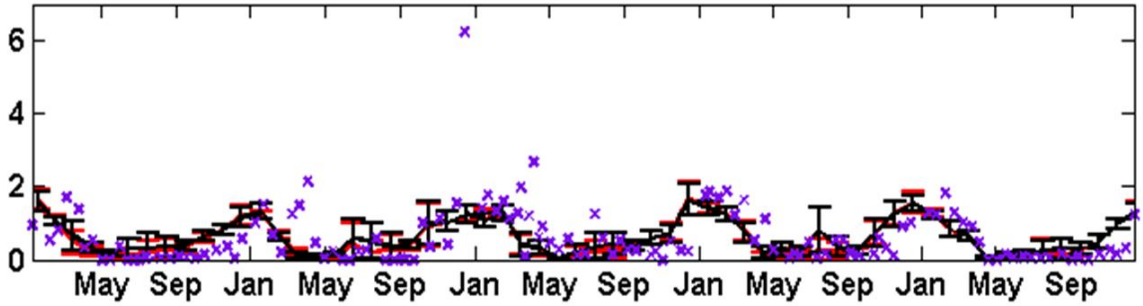

Figure 21: As in Figure 20 but for surface nitrate.

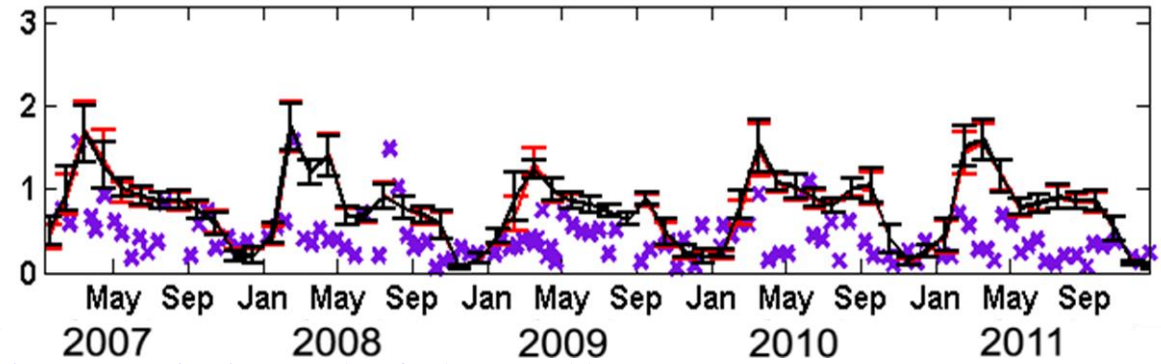

Figure 22: As in Figure 20 but for bottom Chla.

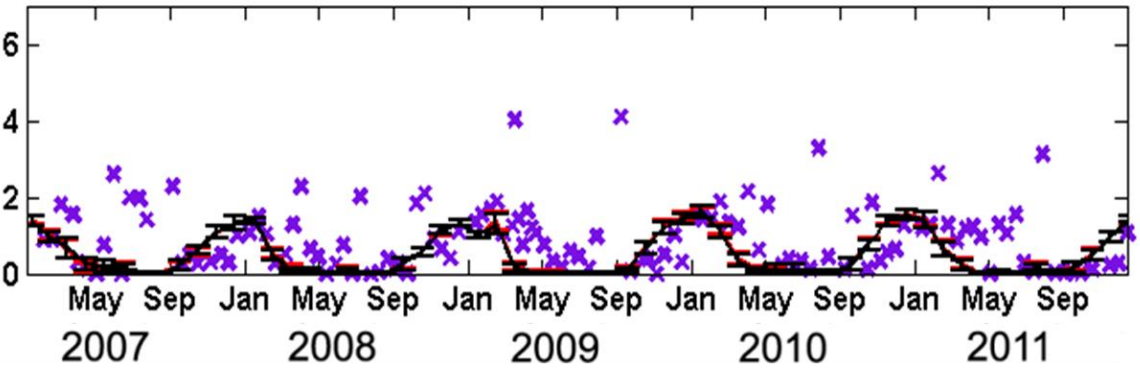

Figure 23: As in Figure 20 but for bottom nitrate.

4.4 HYDROSEDIMENTARY MODELLING

A simulation covering the years 2007 and 2008 (Figure 24) was carried out in order to evaluate the annual variability of suspended matter concentrations in the study area, focusing on 4 key stations: SOMLIT, and three stations in the Northern and Southern part of the harbour (Rade Nord/Sud) and near the Cortiou outlet (Figure 15).

The Rade Nord and SOMLIT stations are both deeper sites and show the same general behaviour with the lowest overall turbidity levels (maxima around 20 mg/L, except at the end of 2008). However, the Rhône intrusion in June 2008 has a clearly visible surface signature (concentrations reaching ~15 mg/L). Storm events are also visible as they produce bottom concentrations of 10 mg/L to 20 mg/L. However, these high-turbidity events are sporadic (less than ten events with turbidities exceeding 5 mg/L in over 2 years). Since the Rade Sud station lies closer to the coast and is shallower, it is very sensitive to meteorological events while high turbidities near the bottom are likely related to resuspension by swell. The observed SS concentrations are significantly elevated and model results suggest that values can exceed 100 mg/L. The station near the Cortiou outlet exhibits a completely different dynamic, with surface turbidity clearly being affected by the discharges through the outlet that generate SS concentrations of several mg/L, occasionally reaching between 5 and 10 mg/L. Episodes of heavy rain are also associated with very high levels of turbidity (>20 mg/L) as can be observed at the end of 2008. It should be noted that there is a significant change in the concentrations of suspended solids between before and after May 2008, directly linked to changes made to the freshwater inflow imposed at the model's terrestrial boundaries in response to *in situ* measurements having become available.

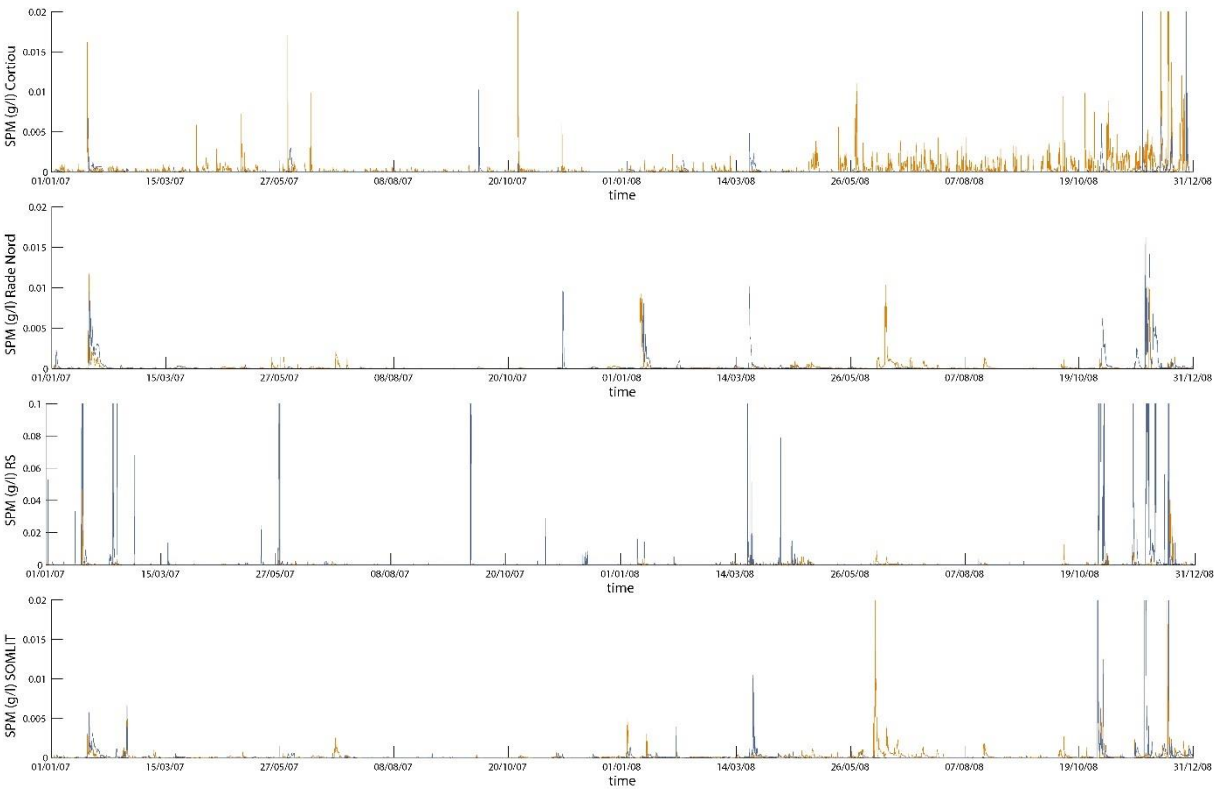

Figure 24: Variability in SS concentration (orange: surface, blue: bottom) at four key stations of the study area: Cortiou, Rade Nord, Rade Sud, and SOMLIT.

4.5 CONTAMINANT MODELLING

The example presented in Figure 25a shows that the dissolved PCB concentration varies mostly between 3 to 5 pg/L, with significant peaks in June and July 2008 when concentrations exceed 300 pg/L following a Rhône river intrusion event that occurred at the end of June. Particular PCB concentrations are lower and vary between 1 and 4 pg/L in winter with slightly higher values during other times, reaching between 2 and 10 pg/L in summer, and exceptionally high concentrations of over 100 pg/L in June 2008. Particulate CB153 content varies between about 1 and 12 ng/g (Figure 25b), depending on the depth and situation, but usually does not exceed this range.

While the uncertainties associated with the parameters used generates uncertainties regarding this speciation, the sensitivity tests have shown that the magnitudes remain of the same order and agree with observations (CB153 : 4 pg/L dissolved, 8.8 ng/g particulate content); these are insufficient in number and do not allow to specify the parameterization of the partition reactions.

The CB153 associated with algal POC is of the order of 5 to 20 ng/g (dry weight), corresponding to concentrations of between 0.1 and 2 pg/L, which corresponds to a total PCB (dissolved + particulate) between 0.2 and 8% (Figure 25c), which in turn depends on the on the bioconcentration coefficient used and on the modelled phytoplankton concentration (Figure 17).

The sensitivity tests were conducted by varying the parameter values and showed the results depend on the total concentration (sensitivity to the boundary conditions, to episodes of erosion, and to local input via urban run-off). The speciation of PCB depends on the partition coefficients chosen, especially with respect to the very light and light particles that dominate further offshore. In areas directly impacted by the urban run-off and discharges, the partition coefficient with respect to heavy solids plays an important role, as well as the kinetics of desorption, which will induce a more or less significant accumulation of contaminated particles in areas close to the coast. The dissolved PCB and the PCB associated with light and very light particles mostly disperse offshore and leave the Marseille harbour within a few days.

(a)

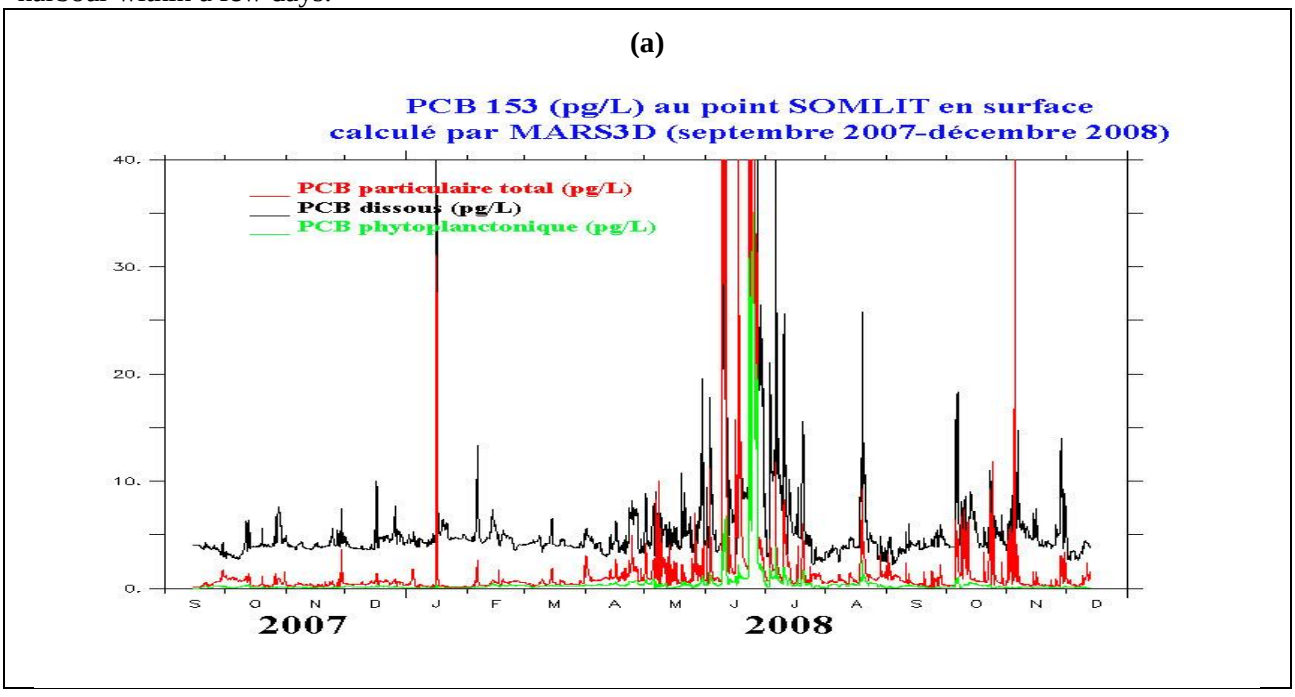

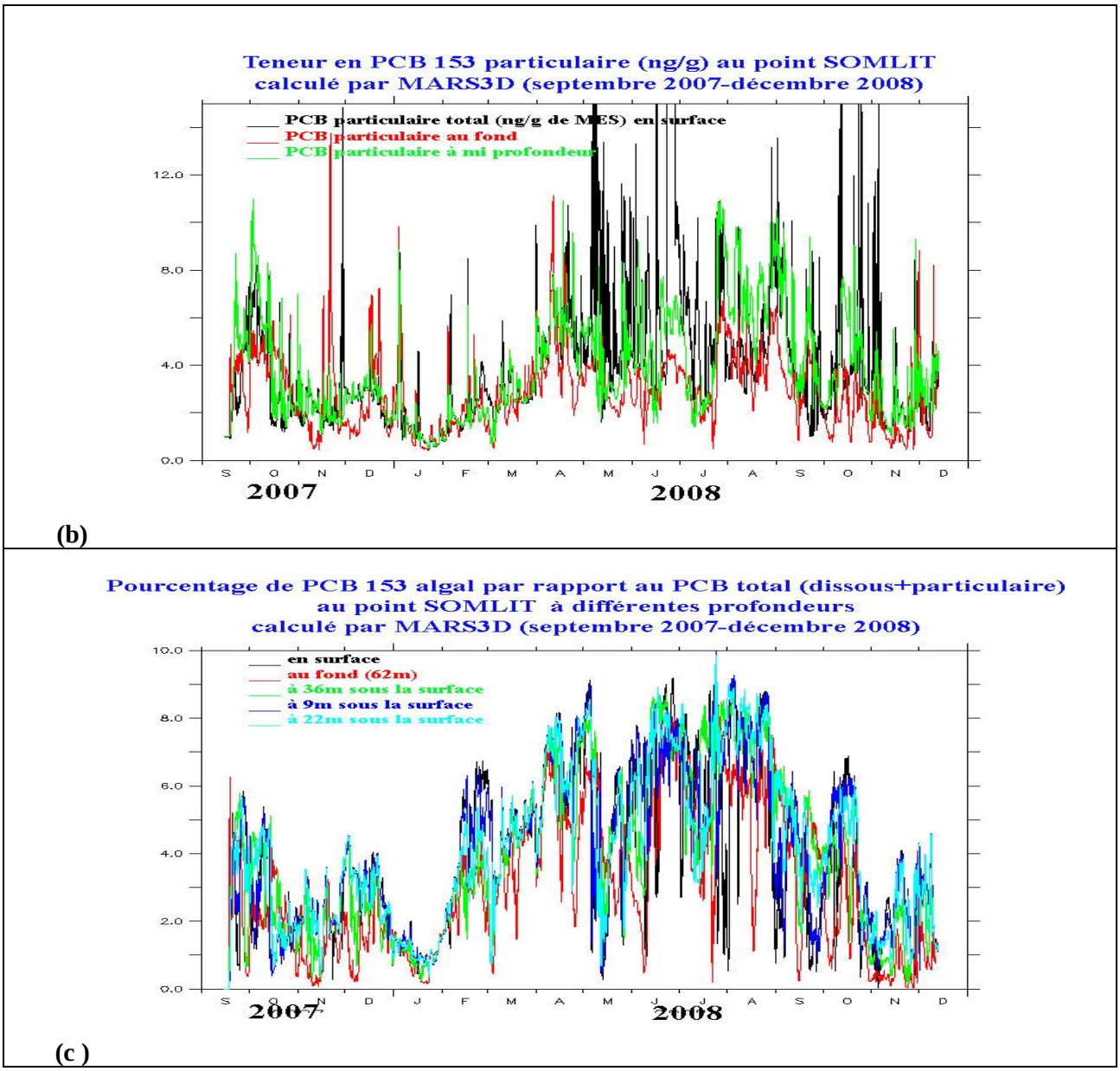

Figure 25: Modelled variability in CB153 in pg/L: dissolved PCB (black), particulate PCB (red), phytoplankton PCB (green) calculated for SOMLIT station for the period from September 2007 to December 2008.

Changes in the biogeochemical conditions over time that cause an increase in detrital organic particles or phytoplankton production lead to variations in particulate PCB concentrations, but there do not seem to be any particular differences between Marseille harbour and areas further offshore.

The results presented below correspond to the typical and extreme situations encountered in Marseille harbour; they are described using the following indicators:

- concentrations of total dissolved CB-153 in water (freely dissolved species plus dissolved species associated with dissolved organic matter); only the surface maxima will be plotted to visualize the areas impacted during the event.
- concentrations of total particulate CB153 (sum of all particulate species associated with the different types of detrital and living suspended matter), expressed either volumetrically (per litre) or as contents in suspended particles (expressed per gram of particles present in the

water). The surface maxima as well as the average values at the surface and at the bottom will be shown.

- the mass fluxes of CB153 into and out of the study area by the different transfer processes during the study period; these variations are examined for of the zones described in Figure 15. These fluxes make it possible to determine the origins of total contaminant variations in the area by visualizing the inputs/outflows at the domain boundaries, i.e., contributions due to discharges, erosion and deposition events, atmospheric inputs (dry deposition and rain), and from volatilization. These mass fluxes are represented as a function of time and a positive slope will indicate an overall input, a negative slope an overall decrease, and a zero slope indicating no change over time. The total quantity that was input/leaving the study area during the study period is represented by the value shown at the end of the period.

For instance, Figure 26 shows the influence of the different processes on the total amount of CB153 in the water column in the four study areas. At this annual scale, it becomes clear that the most important process is the input from the city of Marseille (red line) although it is mostly compensated by the flow across the domain boundaries further offshore (purple line). As a result, the overall variability in total CB remains low and barely visible in Figure 26 (cyan line) given the significant inputs. Some of the significant fluctuations are related to input from offshore areas (Rhône river intrusions) and to other erosion events, particularly in the northern and southern parts of the harbour (rades sud and nord).

Part of the PCB supplied evaporates and another fraction is deposited locally; overall, the balance between erosion/deposit after more than 15 months is negative (light green line), showing a more or less significant residual deposit depending on the area. Atmospheric input (dry deposition and deposition by rain) appears to be negligible. These results depend on the initial assumptions made in the preamble and in particular on the concentrations chosen to determine the inputs by the Rhône and urban run-off/discharge. The erosion and deposition fluxes depend on the chosen parameterization and the initial conditions. The comparison of fluxes induced by each process should therefore be taken with great caution, even if the orders of magnitude appear reasonable. These fluxes will be described in more detail below for both the typical and extreme scenarios.

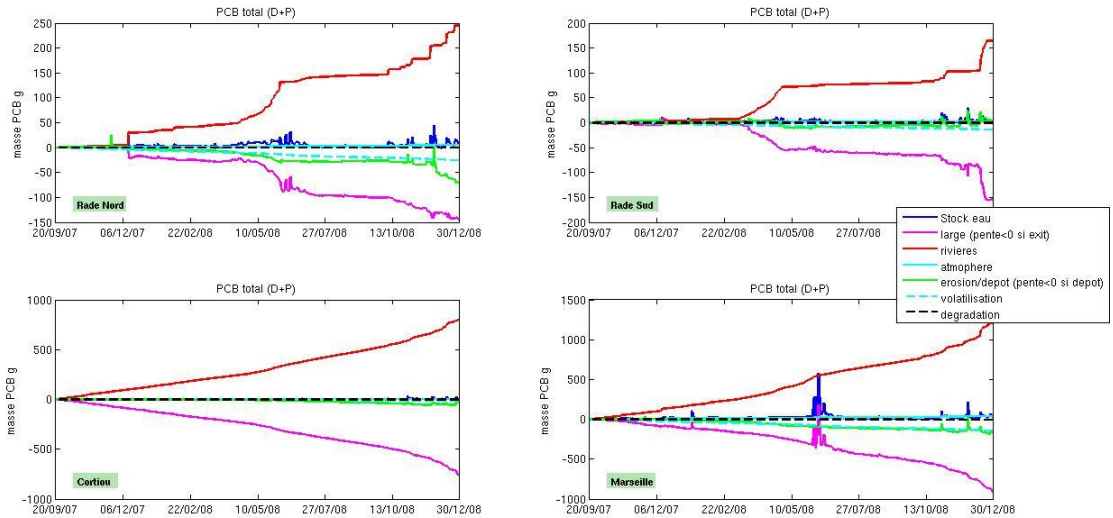

Figure 26 : Variation in total CB153 in the water column between Sep 2007 and Dec 2008 in each zone (see Figure 15), associated with variations in concentration due to the different processes: "large" : input/outflow at the boundaries ; "rivières": input at the coast; "atmosphère": dry deposits and from rain; "érosion/dépôt"; "volatilisation" and "dégradation" (if slope >0 = concentration increase = contaminant input, conversely if slope < 0 = net contaminant outflow).

5 RESULTS FOR INDIVIDUAL SCENARIOS

MISTRAL EVENT

5.1 MISTRAL EVENTS

5.1.1 Typical Mistral Situation (upwelling): 25 to 29 September 2007

5.1.1.1 Data from Météo France for the Marseille Hippodrome station

The month of September 2007 was characterized by three Mistral events of increasing intensity, of which the event from 25 to 27 September with wind speeds of 13 m/s represents a typical event (Table 10).

Table 10

Date, wind intensity (m/s) and direction (°)

25/09/2007	12.3	320
26/09/2007	13.2	320
27/09/2007	13	320
28/09/2007	13.2	300

5.1.1.2 Atmospheric modelling

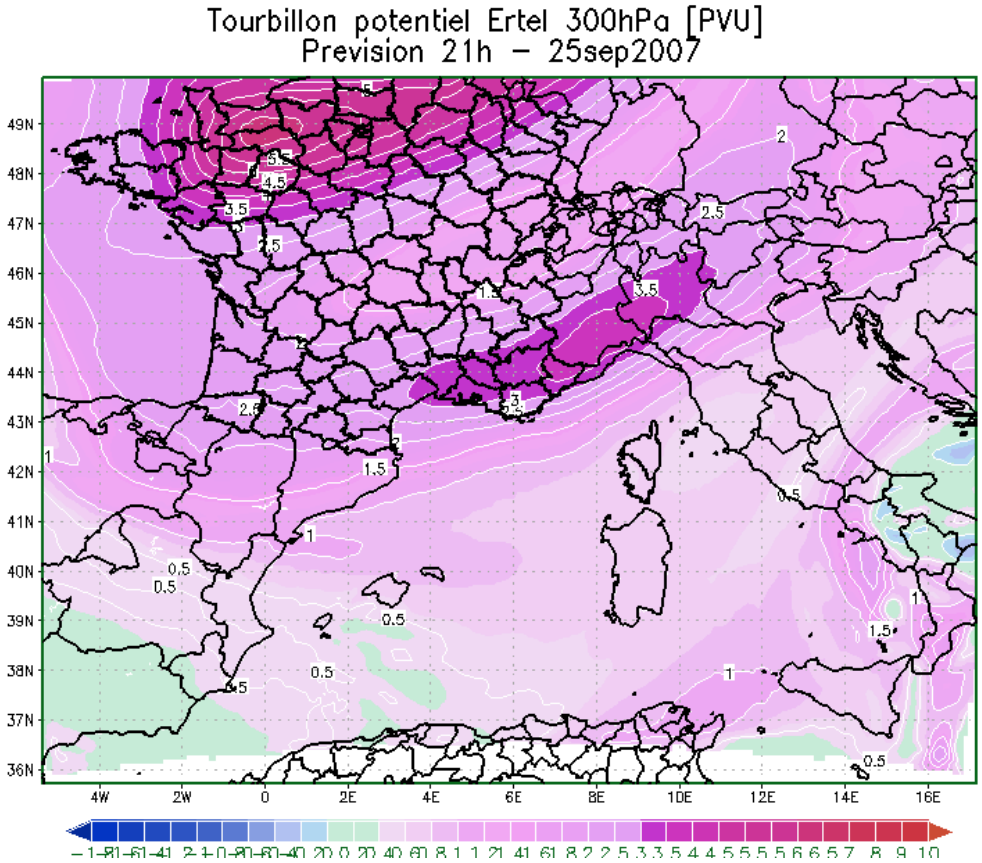

Figure 27: Potential eddy (colour scale in PVU=potential vorticity units, i.e., 10^{-6} m² K s^{-1} kg^{-1}) at 300 hPa forecast for 25 Sep 2007 at 21h.

A moderate mistral event is generated by the formation of a low pressure system (850hPa) to the south of the Alps. Due to the low pressure gradient, the mistral remains moderate.

On September 25, there is a small core of potential vorticity at 300hPa circulating in a north-westerly flow over the south of France. It becomes isolated over the Mediterranean Alps on the night from September 25 to 26 (Figure 27). Further north, a more pronounced tropopause anomaly moves across the entire country and reaches the South-East by midday on September 26. The country will remain under the influence of this potential vortex until September 28 when it switches to a West-East axis. Under the first core of potential vorticity, in the low layer, a minimum develops (low pressure zone) on the Var coast, generating a strong mistral over the west of the PACA region with gusts of the order of 30 to 35 m/s (Figure 28).

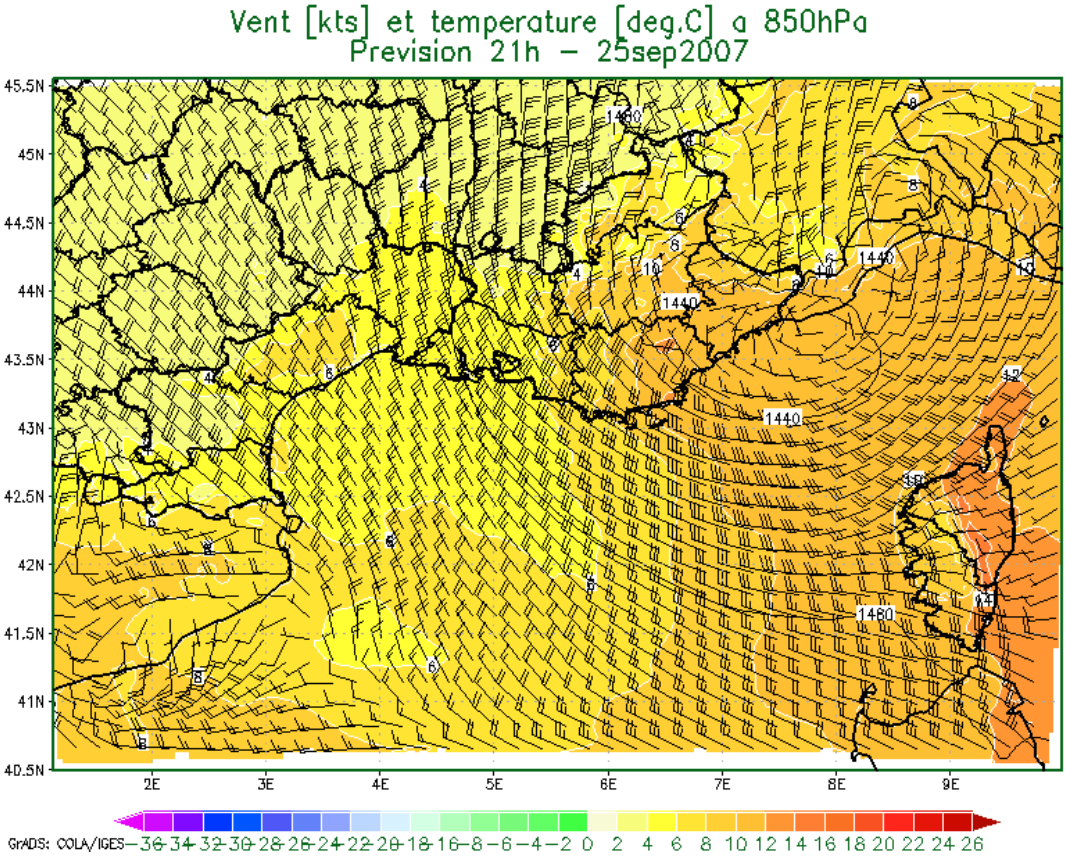

Figure 28: Wind (kts) and temperature (°C, colours) at 850hPa on 25 September 2007 at 21h.

As the cut-off moved to the east, the Mistral progressed as far as Saint-Tropez. Only on the evening of September 26, once the minimum surface was filled, did the Mistral abate. But the northerly wind remained and oscillations of the isohypse field on the 850 hPa surface contributed to a further strengthening of the Mistral during the following day (September 27) which lasted until the early morning on September 28 when the wind shifted to a westerly on the coast near the Rhone river moth after the disturbance has filled in on the Po plain (Figure 29).

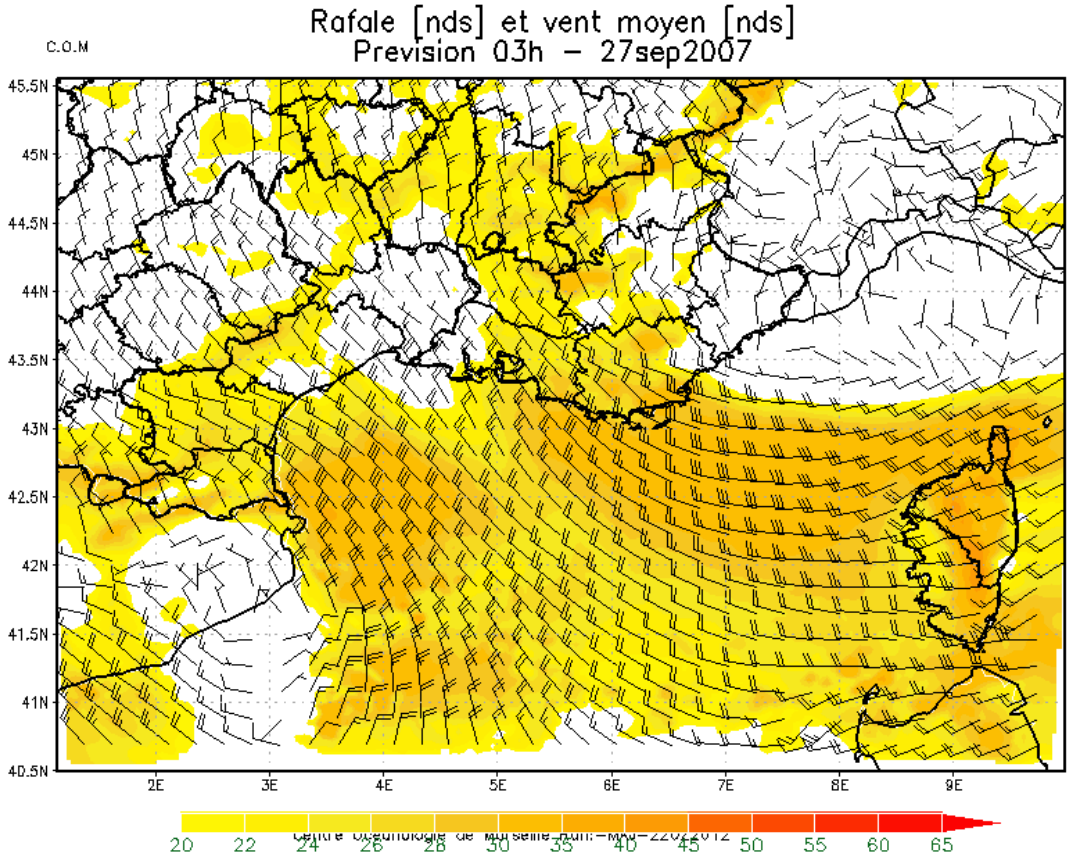

Figure 29 : Gust speeds (kts, colours) and mean velocities (kts) at 10m on 27 Sept 2007 at 03h.

5.1.1.3 Hydrodynamical situation (MARS3D-RHOMA):

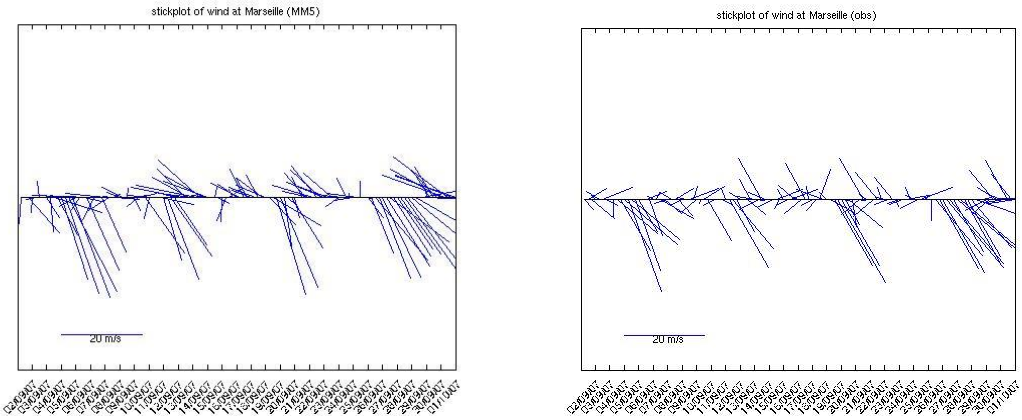

Figure 30: Modelled winds using the MM5 model (left) and measurements provided by Météo France (right) for Hippodrome station in Marseille in September 2007.

This typical situation is relatively well reproduced by the MM5 atmospheric model which provides the forcing for MARS3D-RHOMA (Figure 30).

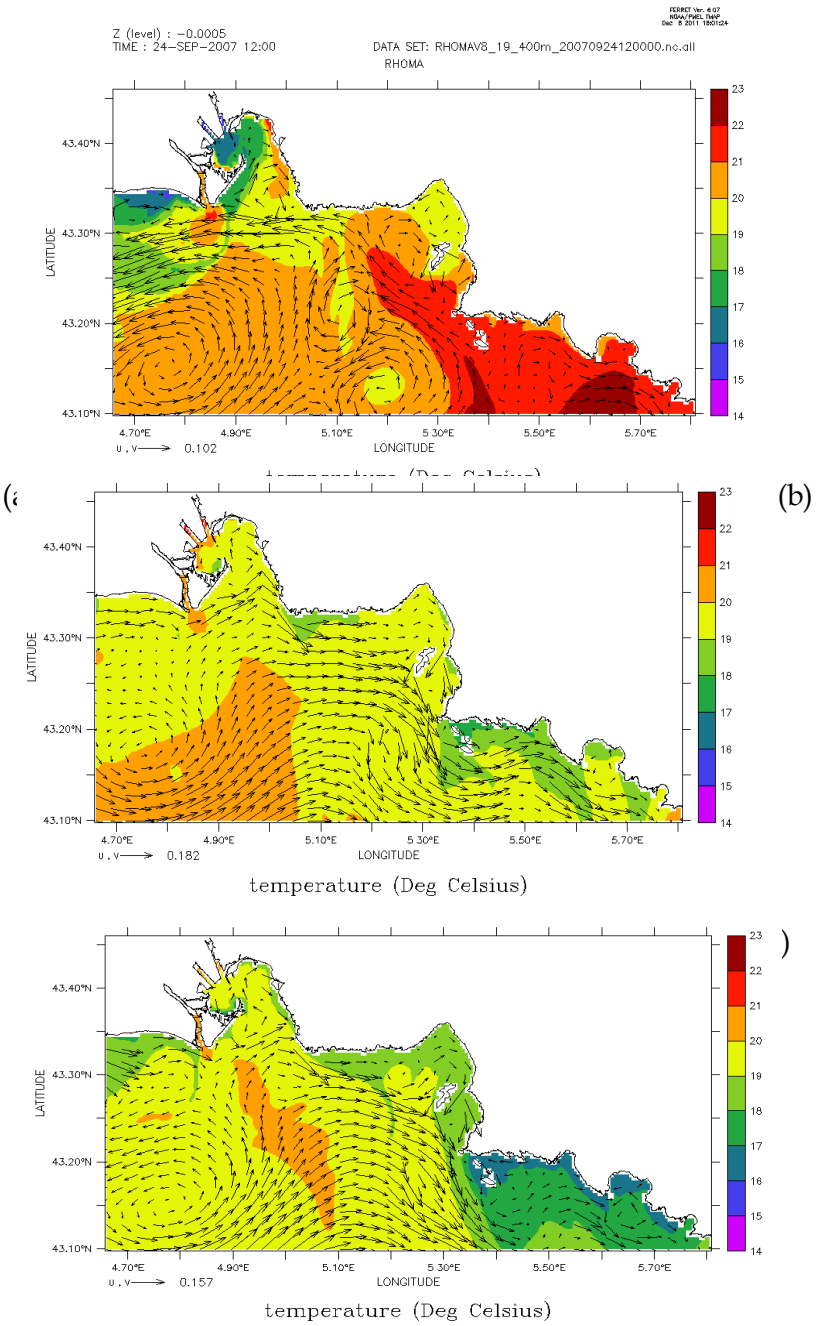

Figure 31 : Modelled SST (°C) and current velocities (m/s) on (a) 24, (b) 26, and (c) 27 Sept 2007 at 12h.

On 24 Sept 2007, there is a south-easterly wind pushing warm waters from the south into the Bay of Marseille (Figure 31a), before the wind turns into a Mistral. The response time between the start of the gale and the start of the SST cooling is about 12h, clearly visible on 09 Sept 2007 (Figure 31b). The upwelling induces a much greater cooling in the Calanques (4°C) than on the Côte Bleue (2-3°C). Temperatures dropped to 16°C in the Calanques and 18°C in the Côte Bleue on 9 Sept 2007 (Figure 31c). These differences in the SST decrease can be explained by differences in vertical speed and upwelling depth.

5.1.1.4 Biogeochemical situation (ECO3M-MASSILIA)

The differences between the Côte Bleue and Calanques areas are also visible on Figure 32a where we see an upwelling of nitrate to the surface is more pronounced along the Calanques (about 2 µmol/L) than at the Côte Bleue (1 µmol/L). As nitrate concentrations typically increase with depth, this difference in surface concentrations suggests upwellings from different depths. This difference in nitrate yields an equally different phytoplankton response with the bloom at the Côte Bleue occurring right inside the upwelling zone while in the Calanques the bloom seems to be located around the edges of the upwelling area (Figure 32b).

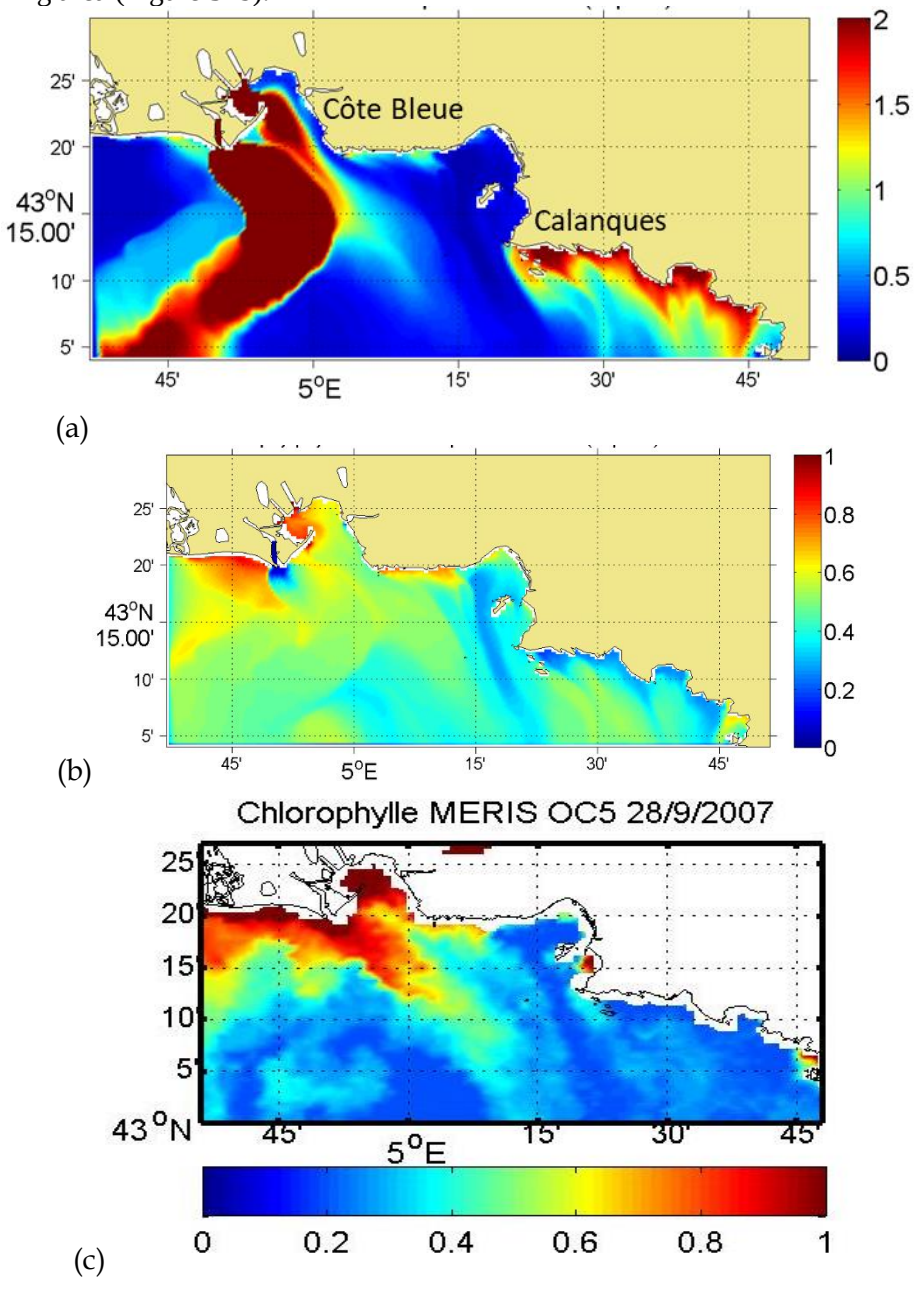

Figure 32 : Modelled surface (a) nitrate (µmol/L) and (b) chlorophyll (µg/L) for 28 Sept 2007 at 12 h; (c) calculated chlorophyll (µg/L) from the OC5 algorithm and MERIS images for 28 Sept 2007.

5.1.1.5 Sediments

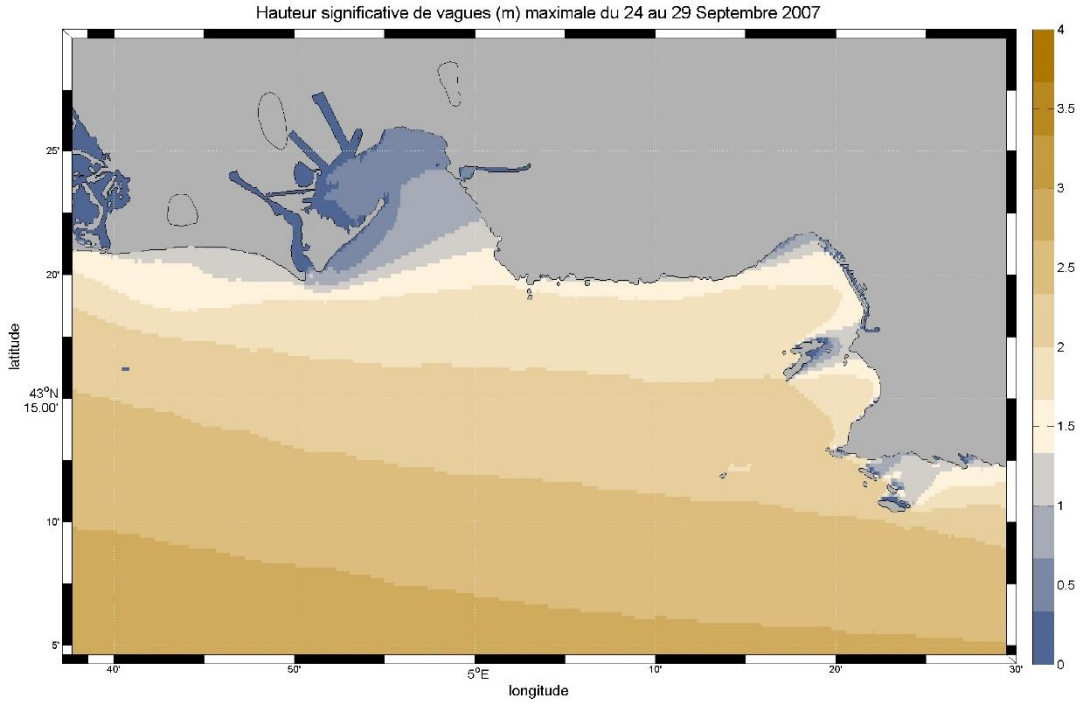

Figure 33: Maximum significant wave heights (m) between 24 and 29 Sept 2007

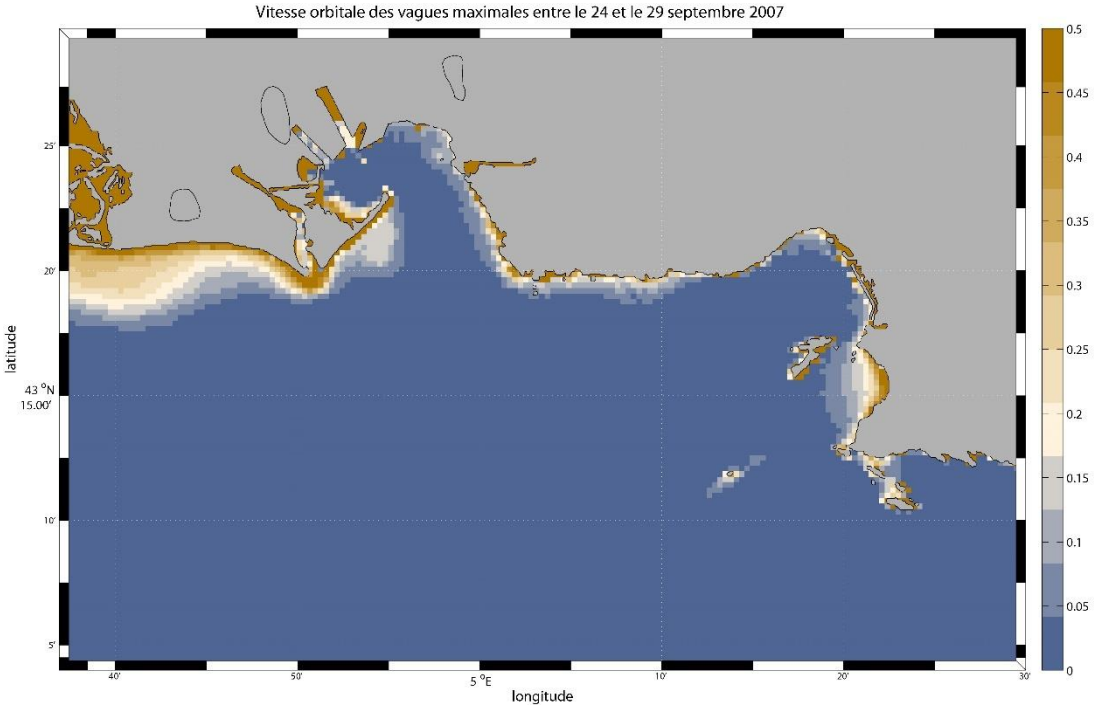

Figure 34: Maximum orbital wave velocities (m/s) between 24 and 29 Sept 2007

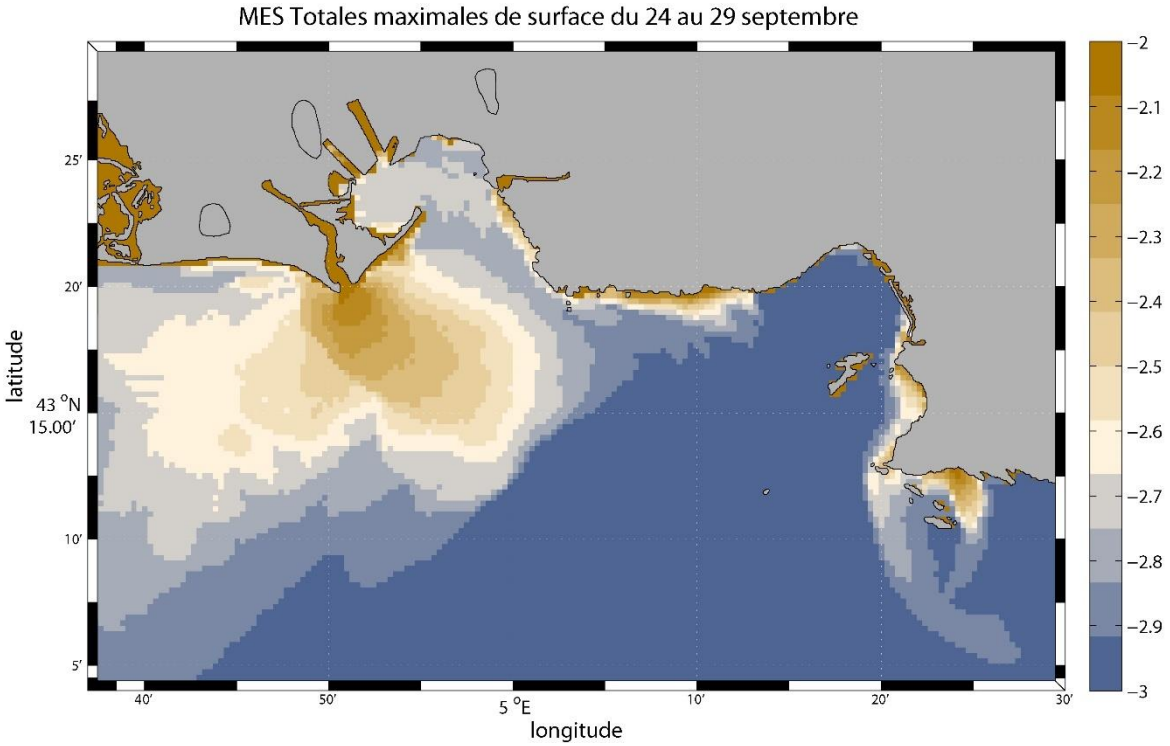

Figure 35: Maximum concentrations of suspended solids in surface waters between 24 and 29 Sept 2007 (logarithmic colour scale: -2 = 10mg/L, -3 = 1mg/L)

During this period of moderate Mistral, the waves only impact the southern harbour (Figure 34), where the cause erosion and a transfer of suspended solids towards the South. The Cortiou plume is clearly visible, with concentrations greater than 5mg/L far from the mouth, and a plume directed towards the south under the effect of the surface currents. A significant surface SS concentration is also observed along the Côte Bleue, without any obvious link to wave effects (Figure 35).

5.1.1.6 Contamination with CB153

Mistral events induce a southward movement of surface waters which causes a rapid dispersion of contaminants from the coast out to sea. The surface plumes extend southward and follow the coast along the southern and northern bays (Figure 36). Surface concentrations in the Cortiou plume are of the same order of magnitude as in the Rhône plume but much more localized. Dissolved concentrations are of the same order of magnitude as particulate concentrations, but they are lower in turbid plumes and higher offshore than particulate concentrations. CB153 contents in particles (ng /g) is linked to the inputs and the re-suspension of the sediments at the coast; in particular, fairly high levels are observed at the bottom near the coast (Figure 37). The variation in concentrations and flows (Figure 38) indeed shows several successive resuspension events in the southern bay, but also in the northern bay between 26 and 28 September (Figure 39). The resuspended PCB is partially redeposited in the same areas while the remaining part is carried away southward.

(a) Dissolved in surface layer (pg/L)

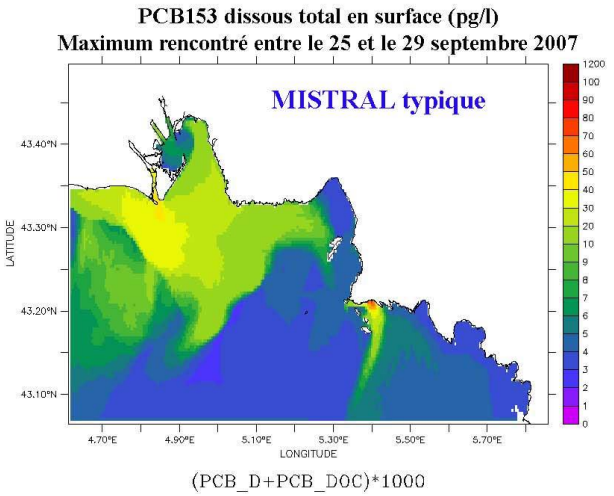

(b) Particulate in surface layer (pg/L)

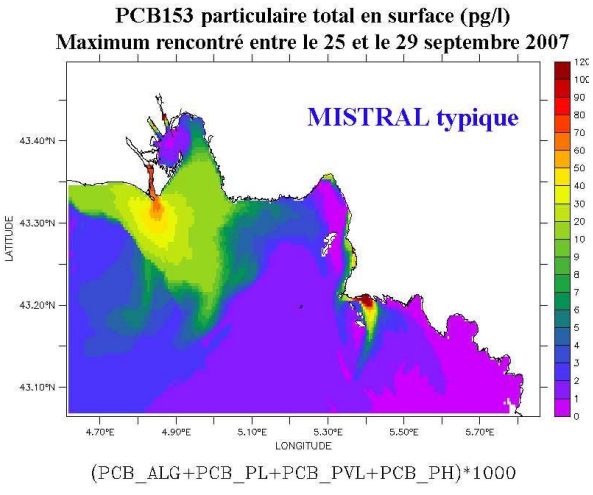

Figure 36: Maximum concentrations at the surface (pg/L) between 25 and 29 Sept 2007.

(a) Particulate in surface layer (ng/g)

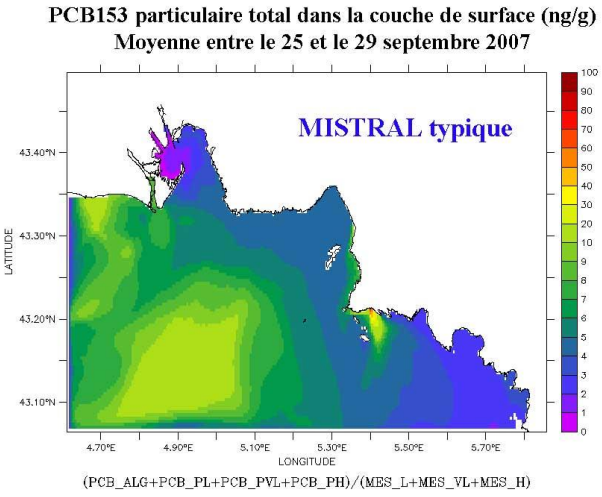

(b) Particulate in bottom layer (ng/g)

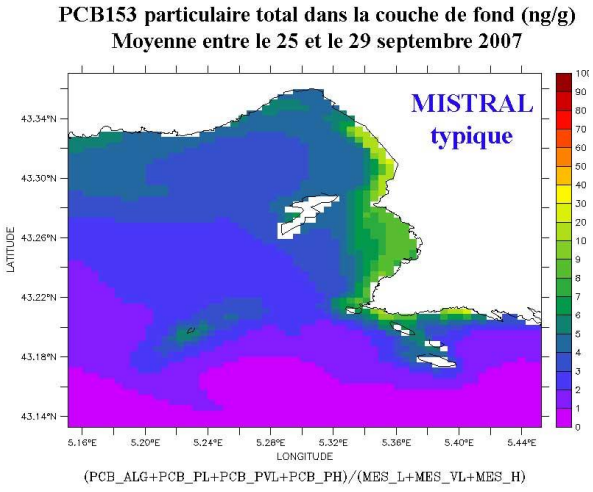

Figure 37: Mean concentrations of particulate CB153 (ng/g) in the surface and bottom layers between 25 and 29 Sept 2007.

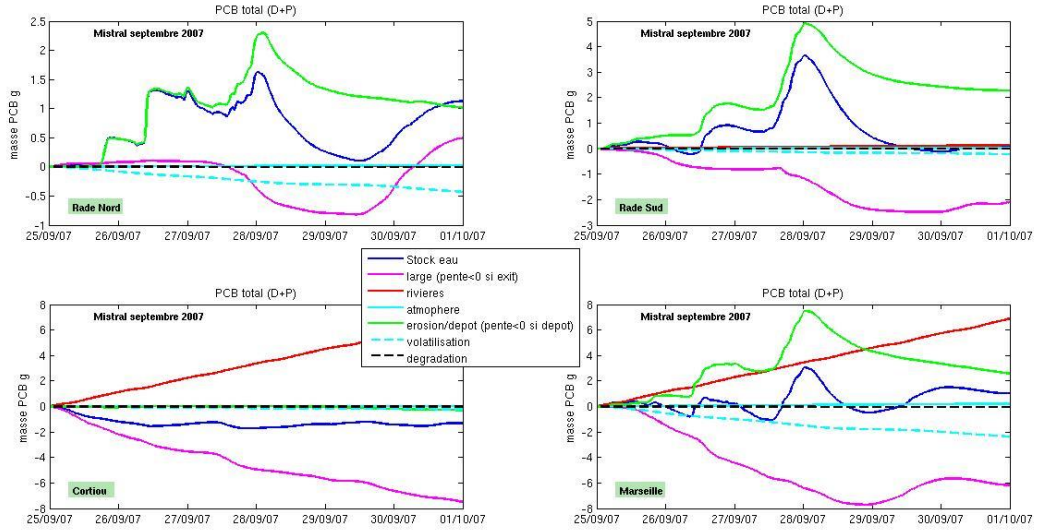

Figure 38: Variation in total CB153 in the water column in different geographic areas for the Sept 2007 Mistral event (cf., Figure 15), associated with concentration variations due to each process: "large": flux at model boundaries; "rivières": riverine inputs; "atmosphère": dry and wet depositions; "érosion/dépôt": erosion/deposition; "volatilisation" and "dégradation". (if the slope >0 = concentration increase = input of contaminant; inversely if the slop <0 = loss of contaminant).

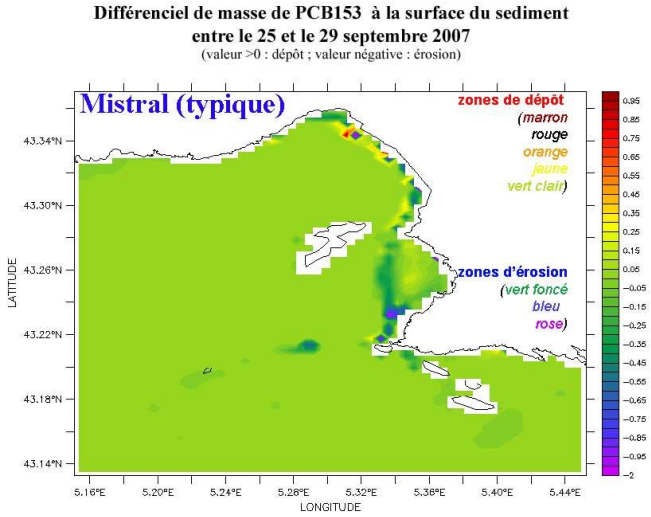

Figure 39: Zones of deposition/erosion during the typical Mistral in Sept 2007.

5.1.2 Extreme Mistral event on 9, 10, and 14 Nov 2007

5.1.2.1 Data from Météo France for Marseille Hippodrome station

Table 11

Date, wind speed (m/s) and direction (°)

Date	Speed	Direction
03/11/2007	3.1	290
04/11/2007	4.3	290
06/11/2007	15.6	330
07/11/2007	11.2	350
08/11/2007	9.1	320
09/11/2007	15.7	330
10/11/2007	17.4	330
11/11/2007	13.4	330
12/11/2007	14.9	330
13/11/2007	8.7	320
14/11/2007	14.7	320
15/11/2007	11.8	350
16/11/2007	7.4	320
17/11/2007	4.4	310
24/11/2007	4.1	330
25/11/2007	6.3	340
26/11/2007	6.3	330
27/11/2007	3.4	310
29/11/2007	7.8	340
30/11/2007	10.7	330
01/12/2007	5.1	290
02/12/2007	8.3	330
03/12/2007	13.5	320
04/12/2007	14.4	330
05/12/2007	5	340
06/12/2007	12.8	330
07/12/2007	13.4	290
08/12/2007	14.2	320
09/12/2007	13.4	300
10/12/2007	14.3	300
11/12/2007	12.2	340
12/12/2007	6.9	320
13/12/2007	3.1	290
14/12/2007	6.5	310
16/12/2007	4.3	320

The months of November/December 2007 were characterized by Mistral winds of >3 m/s almost throughout the entire period from 3 November till 16 December, with only a brief interlude of south-easterlies around 20 November (see typical SE situation in November 2007)
Table 11). Several high wind velocities were recorded during this period (
Table 11); they can be considered extreme even if they are below the maximum values ever recorded for the months of November and December, two months with typically strong Mistral winds (since 2001, the maximum mean daily wind speeds recorded for November and December are 19.0 m/s and 21.9 m/s, respectively).

5.1.2.2 Atmospheric modelling

On 9 November 2007, there is a marked anomaly in the tropopause above Northern Europe (maximum potential vorticity at 300hPa). Moving from the west to the east it becomes isolated over central Europe during 10 November (Figure 40).

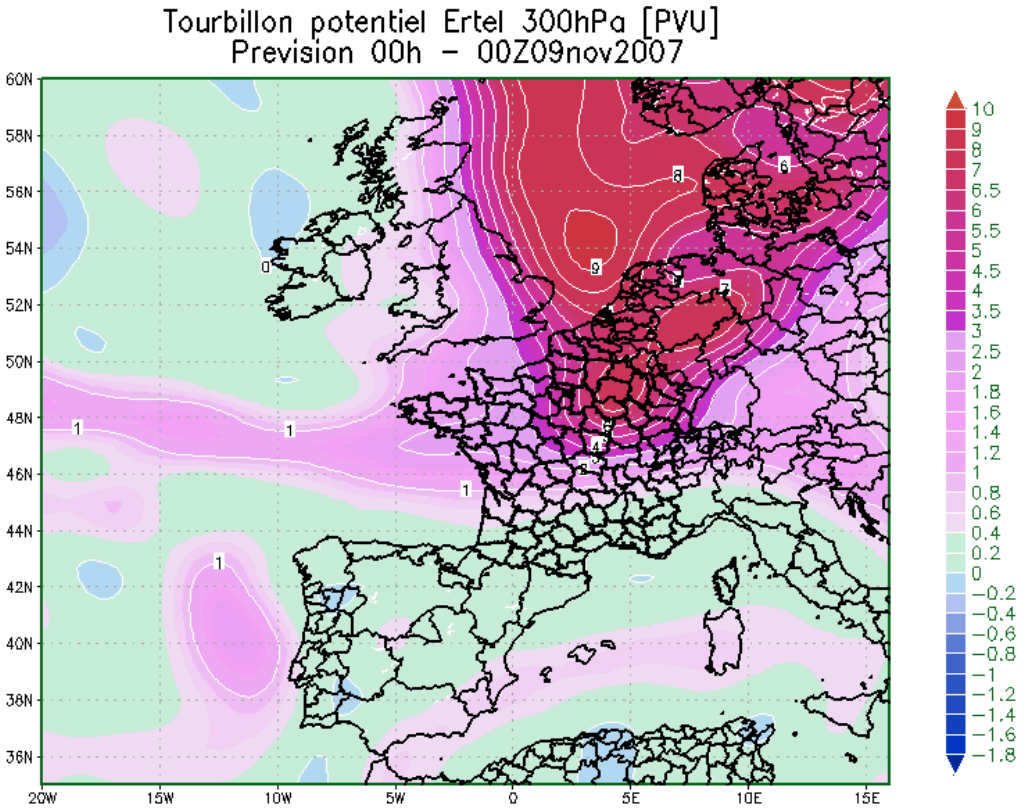

Figure 40: Potential vortex (PVU= potential vorticity units equivalent to 1 rad m² K kg⁻¹ s⁻¹) at 300hPa on 09 Nov 2007 at 00h.

On the western edge of this anomaly, there is a fairly rapid north-westerly flow along the Scotland-Sardinia axis. At the same time, a ridge over the Atlantic is moving over France on 10 November (Figure 41).

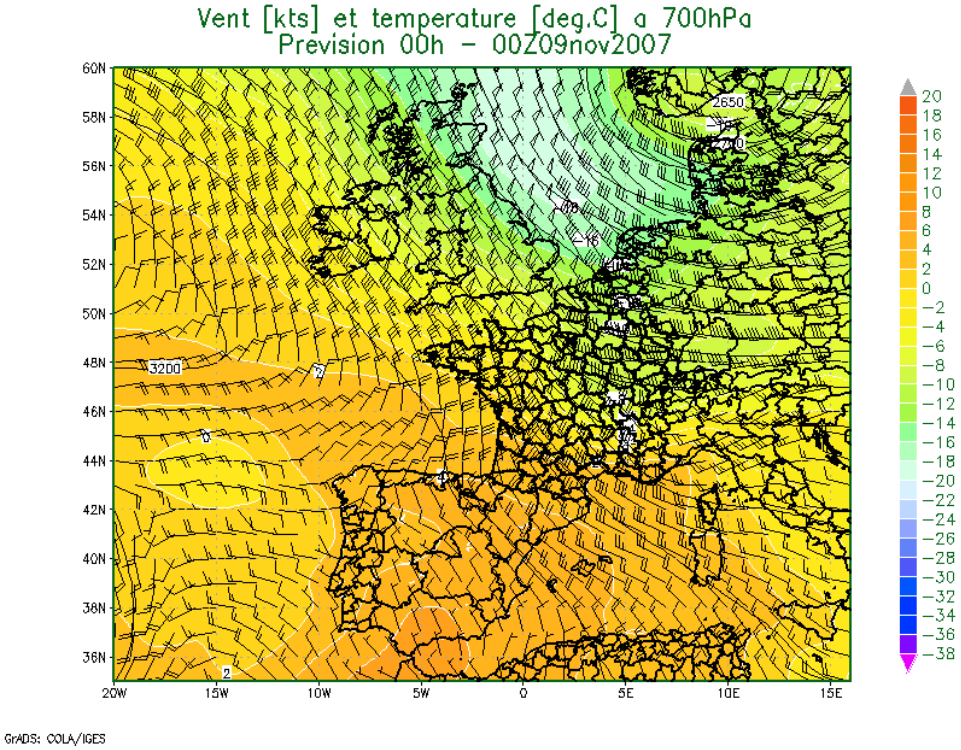

Figure 41: Wind (kts) and temperatures (°C - colour bar) at 700hPa on 9 Nov 2007 at 00h.

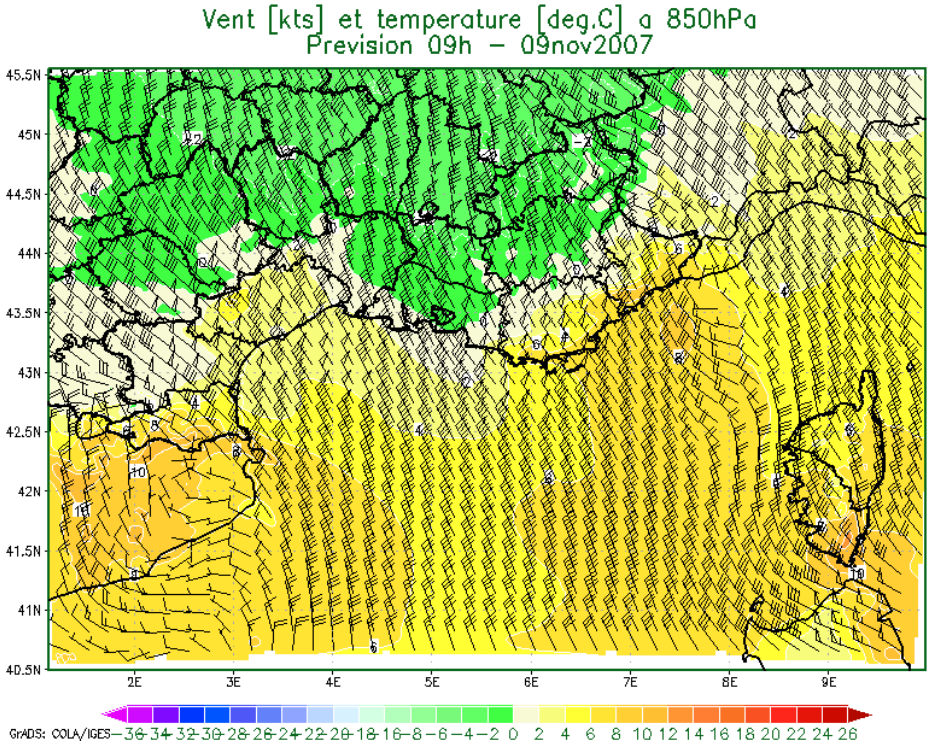

Figure 42: Wind (kts) and temperatures (°C - colour bar) at 850hPa on 9 Nov 2007 at 09h.

In the PACA region, in connection with the north-westerly flow at altitude, on the morning of November 9 the isohypses exhibit a stronger gradient at 850hPa toward the east of the Bouches du Rhône, the Alpes de Hautes Provence and the Var generates a strong wind zone (Figure 42).

It is under this low level jet that the Mistral blows strongly to the east of the Bouches du Rhône and the Var coasts. During the afternoon, the wind weakens at lower levels and it is in the second part of

the night from November 9 to 10 that a relative low develops near the Côte d'Azur and starts to move to the west (Figure 43).

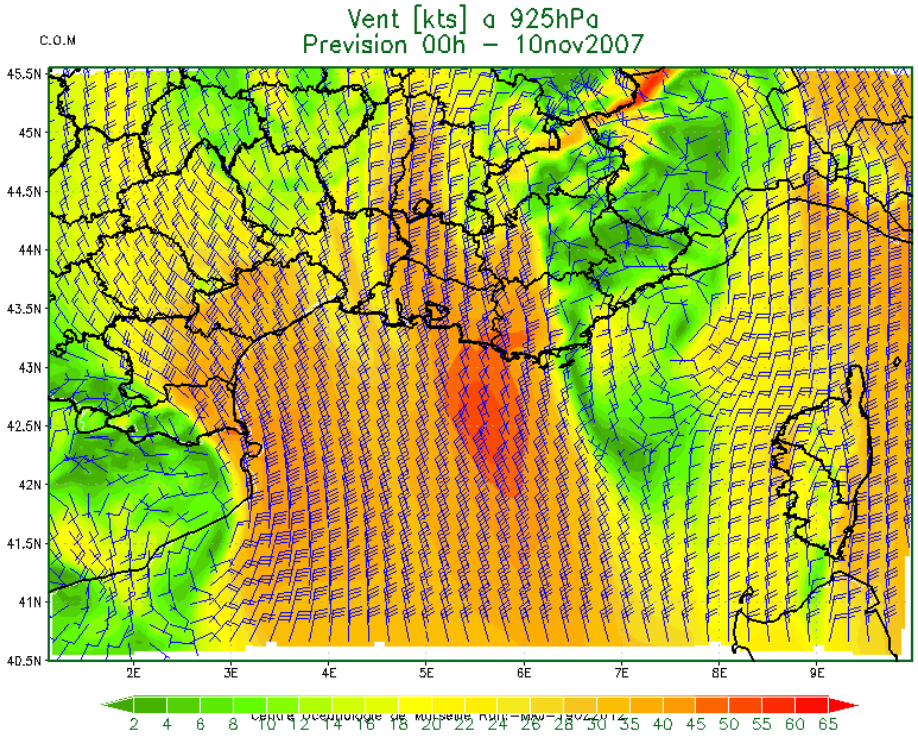

Figure 43: Wind (kts) at 925hPa on 10 Nov 2007 at 00h.

The low level jet moved along the Provençal coast during the night to reach Marseille where the Mistral was very strong on 10 November before moving further west to the Var region in the evening.

5.1.2.3 Hydrodynamic situation (MARS3D-RHOMA)

The winds strongly affected the circulation and hydrology on the shelf to the east of the Gulf of Lion. The drops in temperature linked to the upwelling episodes in autumn 2007 were recorded by thermographs as part of the MEDCHANGE program on the island of Riou (Figure 44), a station which is part of the TMedNet network (http://www.t-mednet.org). Upwellings create autumnal mixing of waters.

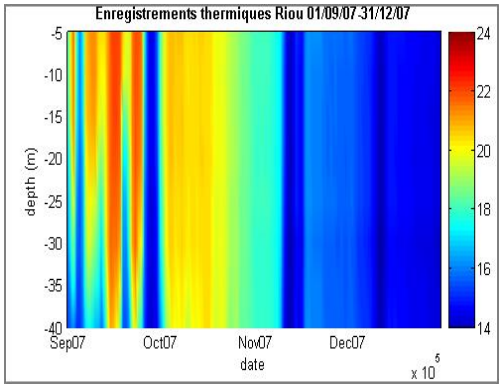

Figure 44: Temperature observations (N. Bensoussan, pers. comm.) at Riou island (43.17N,5.38E) between Sept and Dec 2007.

The surface water cooling as a result of the upwelling on 13 November, 2007 is shown in Figure 45and Figure 46. A comparison shows good agreement between the RHOMA-modelled and satellite-observed temperatures (Figure 45) at the upwelling locations to the east of the Gulf of Lion: the Côte Bleue, the Bay of Marseille, and especially the Calanques. Within a few hours, surface temperatures dropped by up to 4° near Riou island (Figure 46).

a)

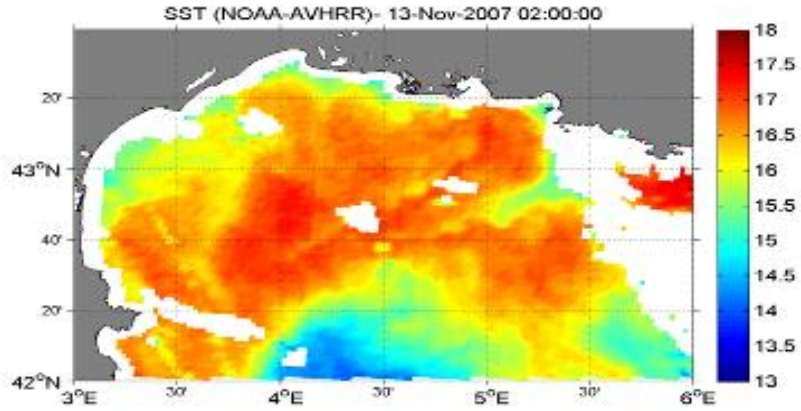

b)

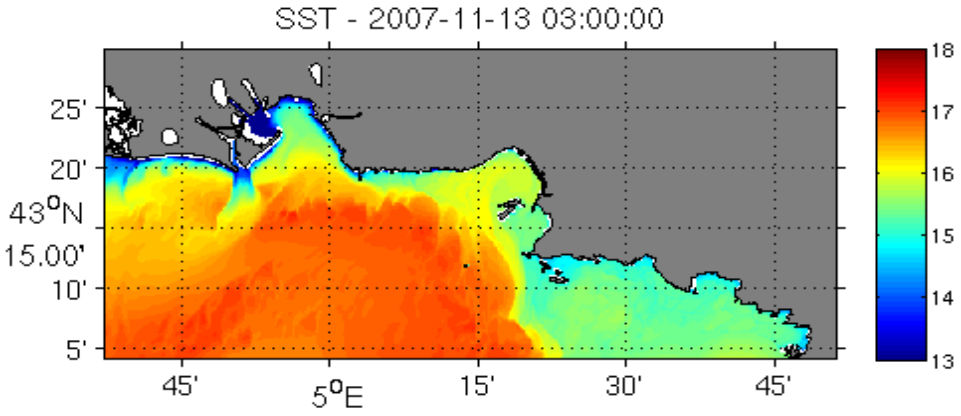

(c)

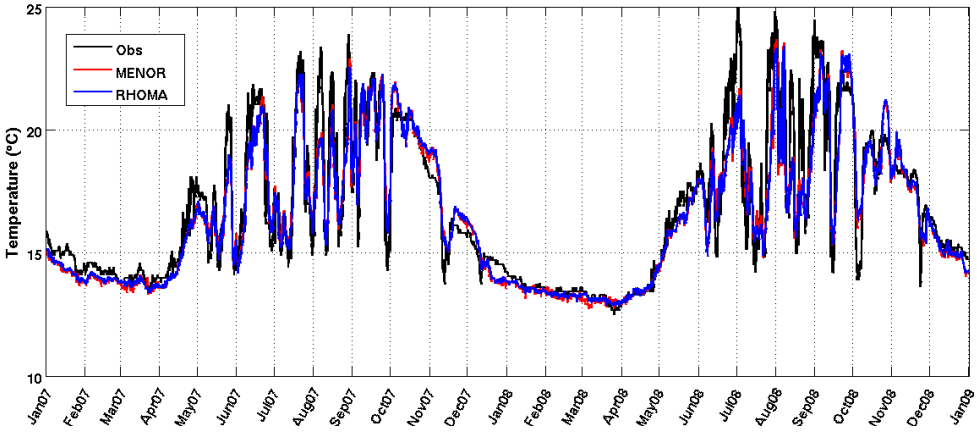

Figure 45: SST (°C) on 13 Nov 2007: a) satellite observations (SST NOA-AVHRR) of the Gulf of Lion, b) simulations using the RHOMA configuration, c) a comparison between RHOMA, the larger scale MENOR configuration, and observations at SOLEMIO station.

5.1.2.4 Biogeochemical situation (ECO3M-MASSILIA)

From mid-November till the end of December 2007, during the Mistral period, the entire water columns is well mixed with low temperatures throughout. This corresponds to the typical situation in winter as described by Conan (1996) which is characterized by strong mixing and therefore a homogeneous water column. Nitrate concentrations are high (>1 µmol L^{-1}) from the surface to the bottom while chlorophyll concentrations are low (Figure 46).

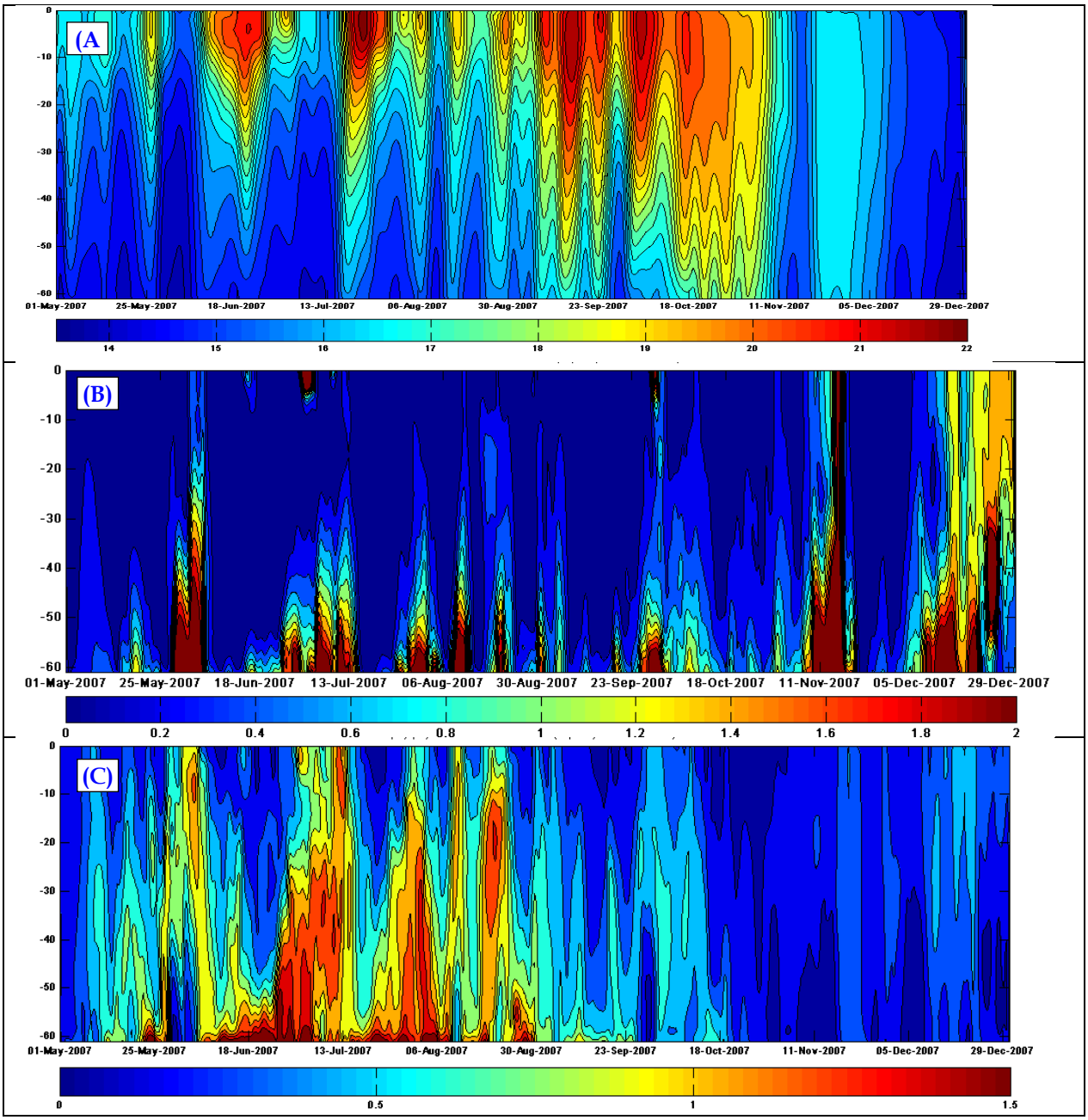

Figure 46: Modelled (A) temperature (°C), (B) nitrate (µmol L^{-1}), and (C) chlorophyll (µg L^{-1}) for SOMLIT station from 01/05/07 till 31/12/07. The model output has been smoothed using a 2-day (hence 7 values) Hanning filter.

The difference between the Côte Bleue and Calanques is also remarkable in Figure 47where nitrate concentrations at the surface in the Calanques (4 µmol/L) is twice the concentration at the Côte Bleue (2 µmol/L), which again suggests different upwelling depths. This trend was already observed for a typical Mistral event and is accentuated here, indicating that upwelled waters are rising from greater depths than in a typical Mistral situation. This also results in different phytoplankton responses (Figure

47). The extreme event which occurred in November, a month and a half later than the typical event (i.e., in conditions that are closer to winter conditions) which resulted in much lower chlorophyll concentrations (Figure 46). There is no bloom in the nutrient rich waters along the Côte Bleue nor in the Calanques.

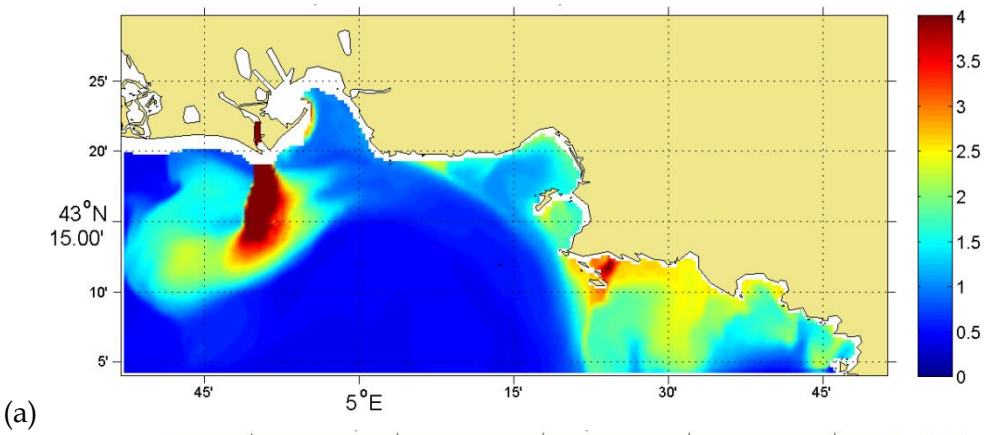

(a)

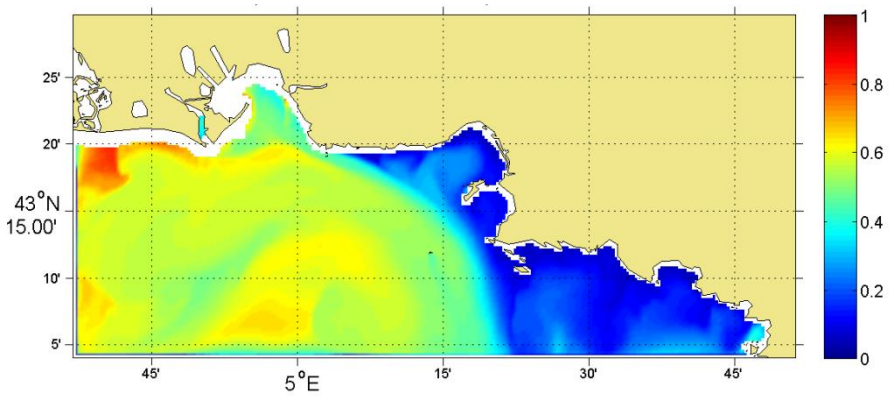

(b)

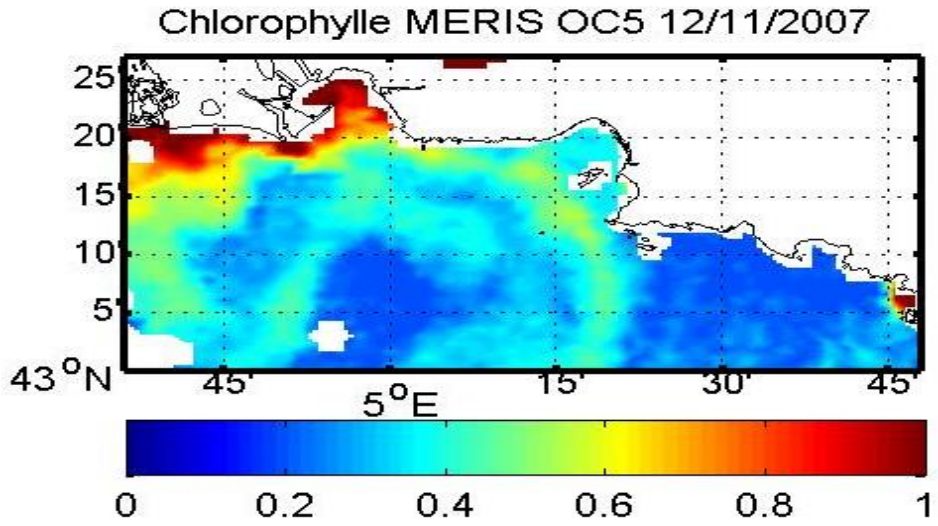

(c)

Figure 47: Modelled surface concentrations of (a) nitrate (µmol/L) and (b) chlorophyll (µg/L) for 12 Nov 2007 at 12 h. (c) Calculated chlorophyll a (µg/L) concentration obtained using the OC5 algorithm on a MERIS image from 12/11/2007.

The bloom seems to be located in a frontal zone at the edge of the upwelling zone. It merges with a filament generated by the front between the upwelling waters and the surrounding surface waters (Rhône plume). This filament is clearly visible in the ocean colour image for the same day (Figure

47c). It should be noted that the bloom in the more southern part is linked to a poor representation of the concentrations at the southern open boundary (Figure 47b).

5.1.2.5 Sedimentation

During Mistral events, the Bay of Marseille is mostly protected from the influence of waves and only has a limited fetch (Figure 48). Only the Rade Sud is impacted by waves (Figure 49and Figure 50), causing significant erosion, intense mixing (maximum surface concentrations of around 8mg/L) and a southward flux of sediments, mainly heavy suspended solids, by the Mistral-induced surface flow. A small part of the sediment is redistributed in the Rade Sud (Figure 51). Similarly, the Cortiou plume is pushed seaward. However, it is not very marked (concentrations of just a few mg/L) as the outflow is quickly diluted unless there is a major rain event.

This offshore transport is clearly visible by calculating the particle budgets: a majority of the resuspended sediments (Rade Sud, Figure 53) are transported offshore (Figure 52).

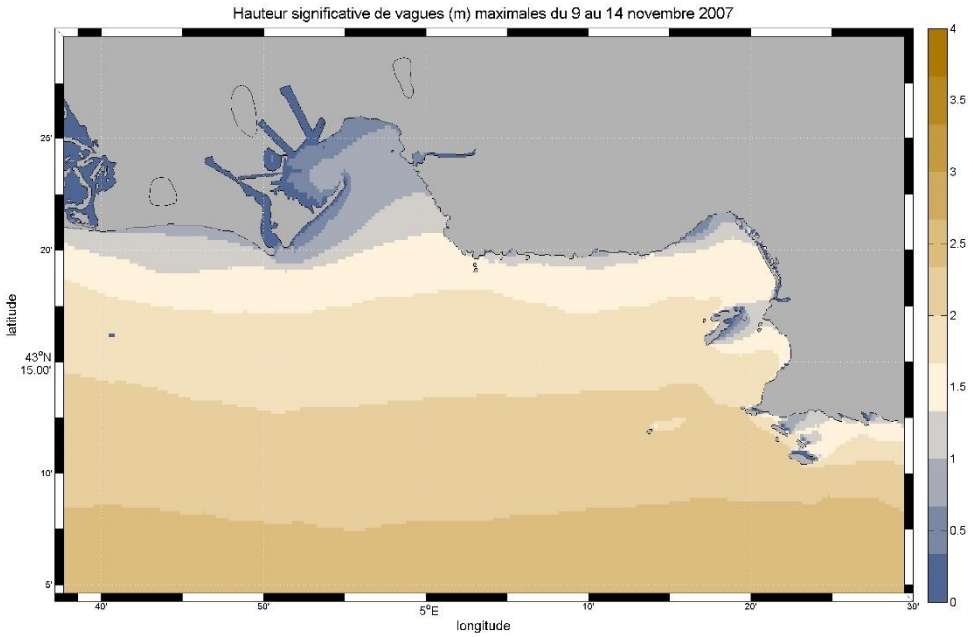

Figure 48: Maximum significant wave height (m) between 9 and 14 Nov 2007

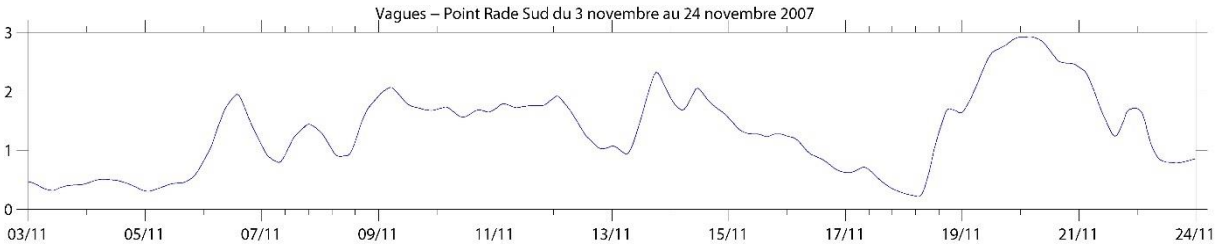

Figure 49: Maximum significant wave height (m) at the Rade Sud station between 3 and 24 Nov 2007.

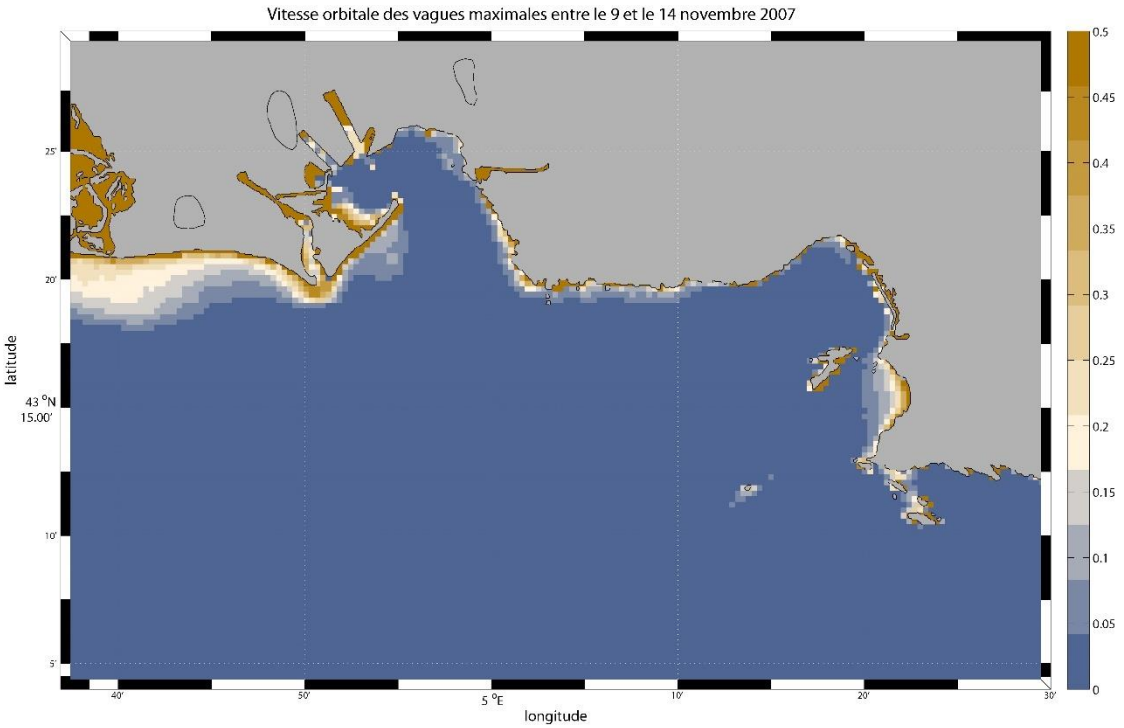

Figure 50: Maximum orbital wave velocities (m/s) from 9 to 14 Nov 2007

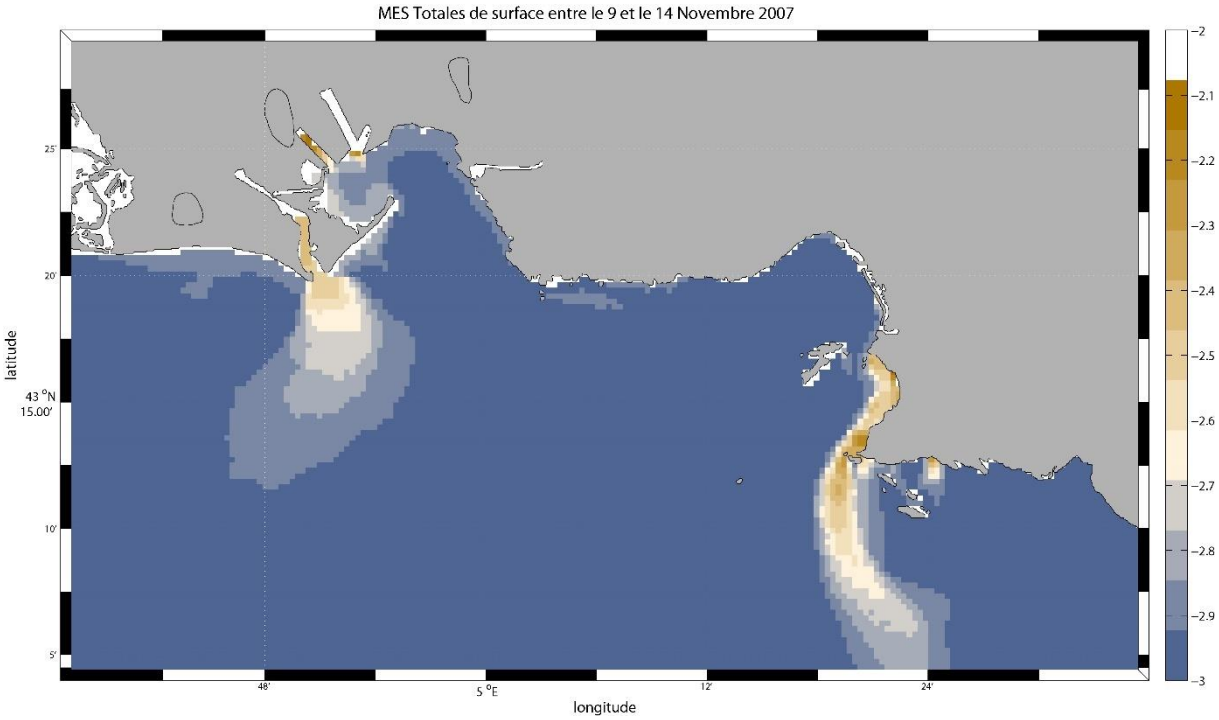

Figure 51: Total suspended matter concentration in the surface between 9 and 14 Nov 2007 (g/L, log scale).

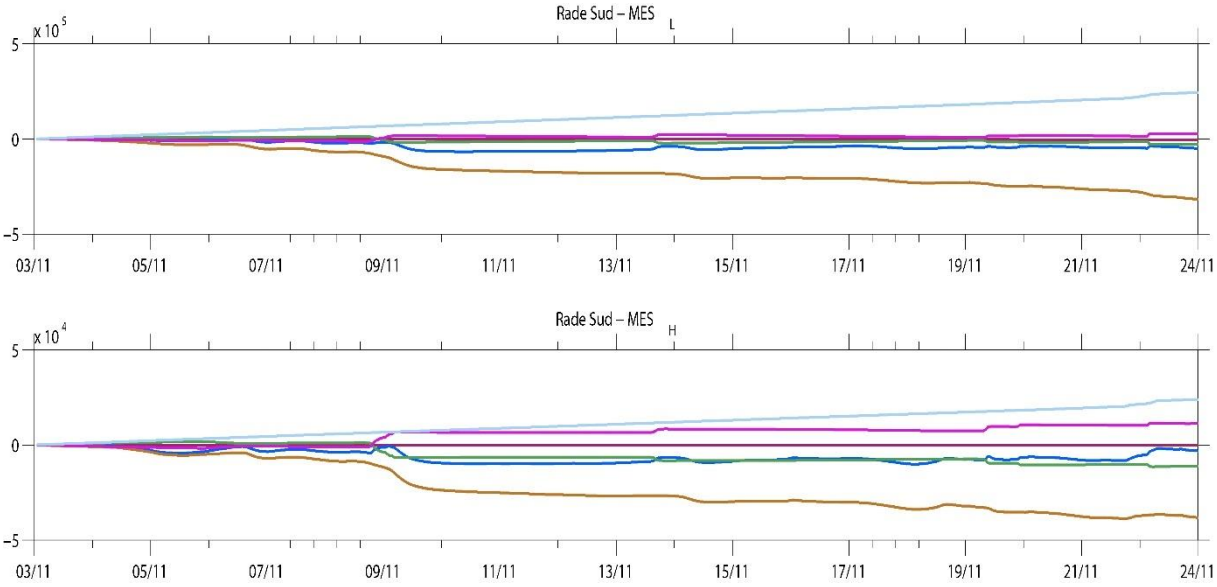

Figure 52: Sediment flux budgets in the southern harbour between 3 to 24 Nov 2007 for SS_L (light suspended solids, upper panel) and SS_H (heavy, lower panel). Overall balance (red), suspended mass (dark blue), mass in sediment (green), flux at boundaries (negative means exiting the domain) (brown), flux across the water/sediment interface (negative = sedimentation, positive = resuspension) (pink), from external sources (cyan).

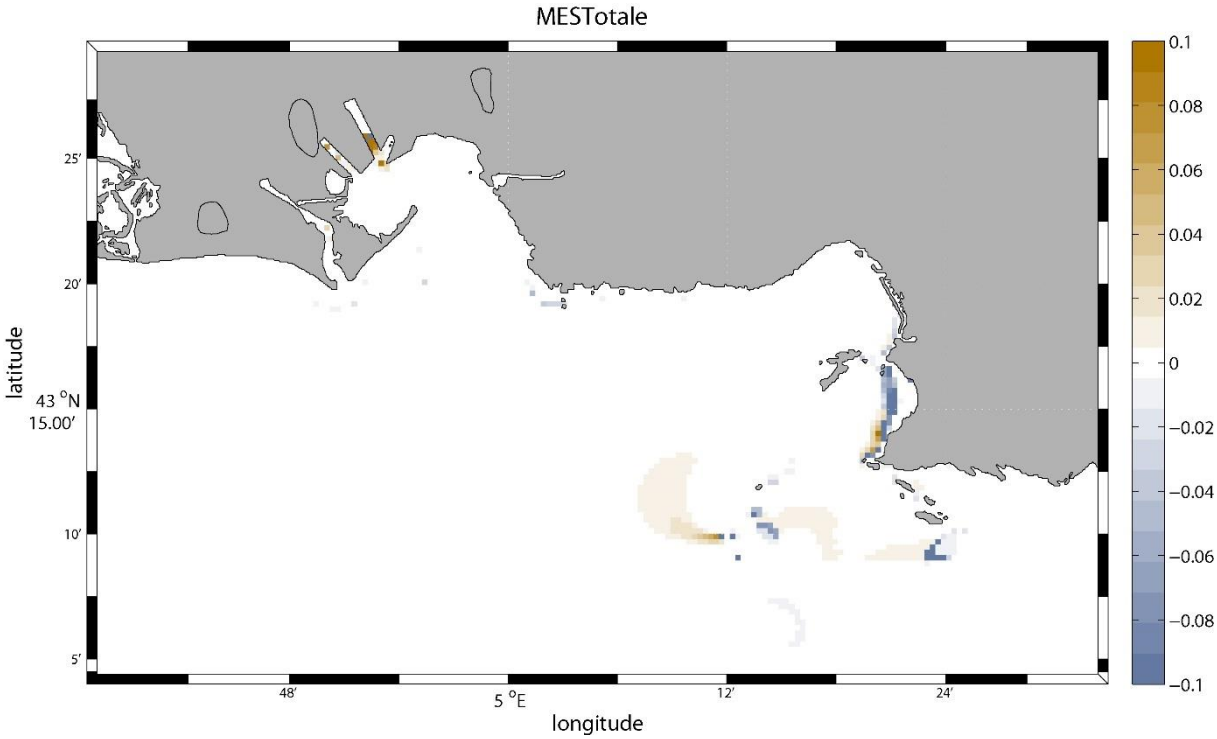

Figure 53: Sedimentation (beige) and resuspension zones (blue) for fine sediments (kg/m2) between 9 and 14 Nov 2007.

5.1.2.6 Contamination with CB153

The situation in November 2007 is quite similar to September 2007, except that the resuspension of PCBs on November 9 in the northern and southern bays (more marked in the southern bay) is less

severe than in the typical situation (Figure 54); the average concentrations are lower (Figure 55and Figure 56), partly due to reduced inflows compared to the situation in September. As in the typical situation, the Cortiou zone is not subject to much resuspension and the major source is the Cortiou plume which disperses rapidly. Most of the input, whether of coastal or sedimentary origin, is transported offshore (Figure 56); there is very little sedimentation. A non-negligible part becomes air-borne, although the importance of this process is probably overestimated. The total stock of CB153 decreases during the event in all areas Figure 56).

(a) Dissolved in surface layer (pg/L)

(b) Particulate in surface layer (pg/L)

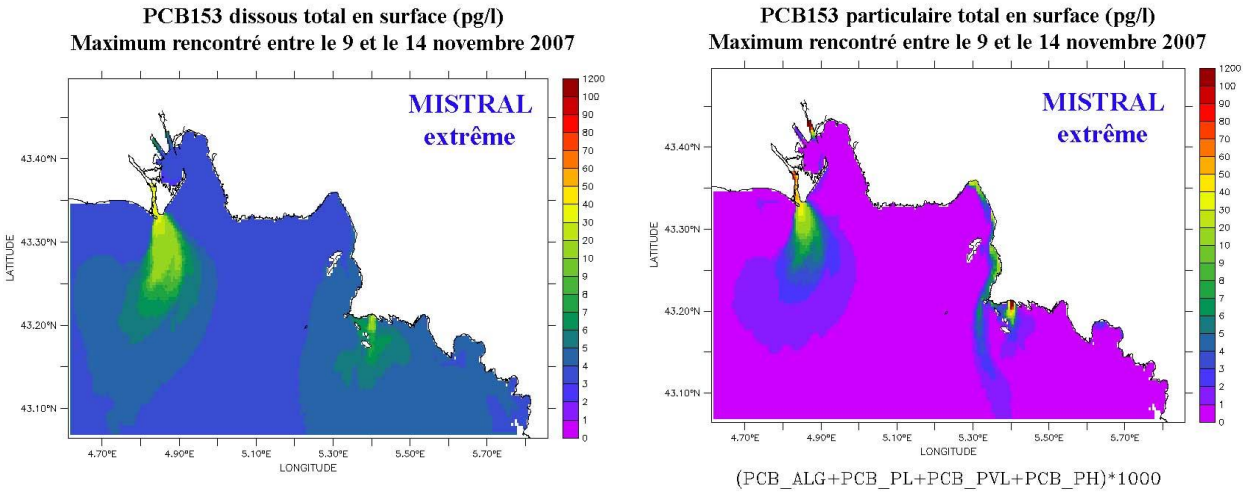

Figure 54: Maximum surface concentrations (pg/L) between 9 and 14 Nov 2007

(a) Particulate in surface layer (ng/g)

(b) Particulate in bottom layer (ng/g)

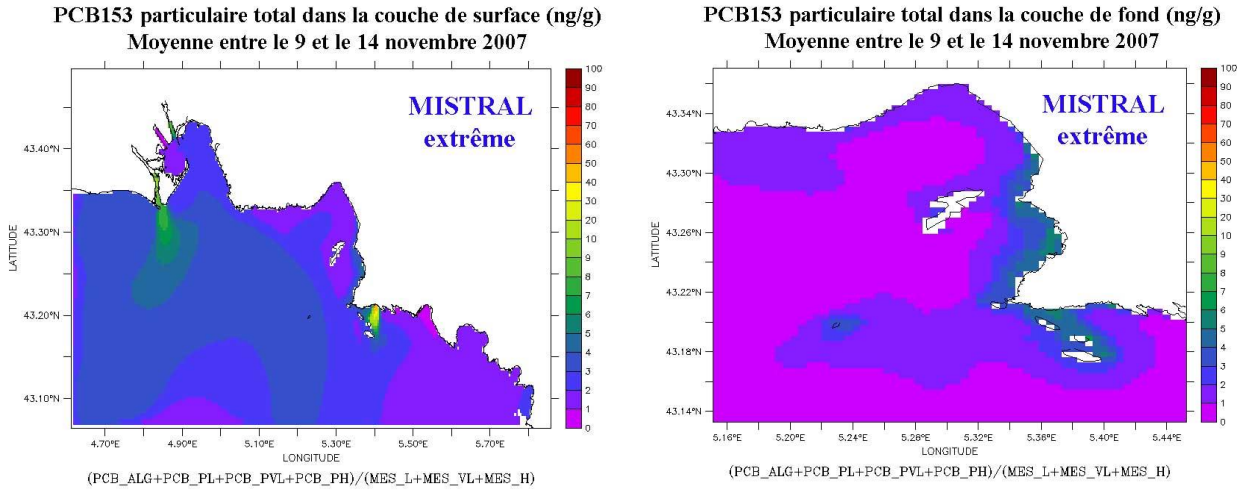

Figure 55: Mean CB153 particulate concentrations (ng/g) in the surface and bottom layers between 9 and 14 Nov 2007.

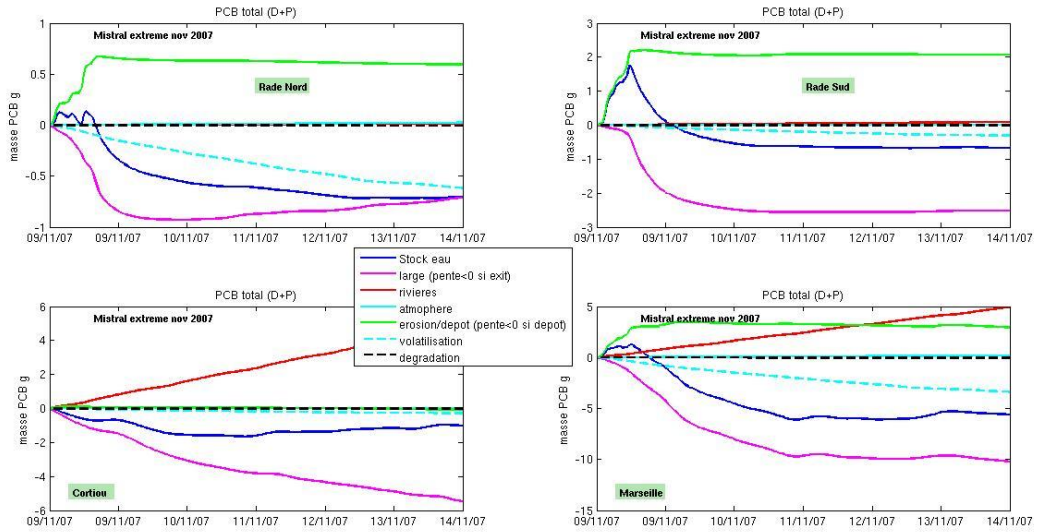

Figure 56 : Variation in total CB153 in the water column in different zones (see Figure 15), linked to changes in concentration due to each of the following processes: "large": flux across boundaries; "rivières": costal inputs; "atmosphère": dry and wet deposition; "érosion/dépôt": resuspension/sedimentation; "volatilisation" and "dégradation". (if slope >0 = concentration increase = influx of contaminant and vice versa).

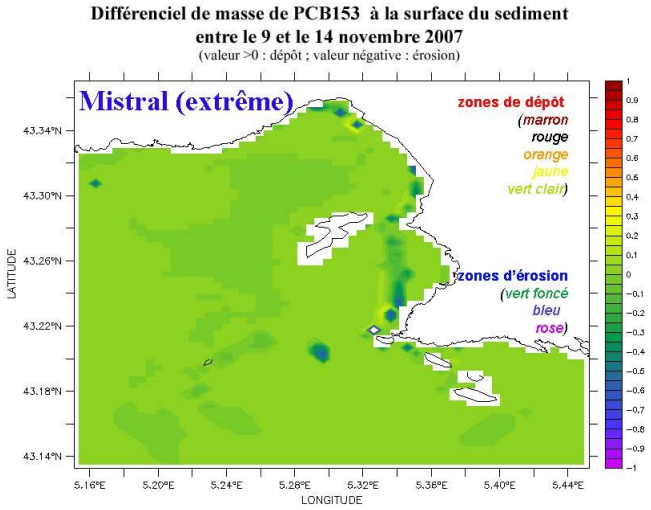

Figure 57: Zones of sedimentation and resuspension during the extreme Mistral event.

SOUTH-EASTERLY WINDS

5.2 SOUTH-EASTERLY WINDS :

5.2.1 Typical situation: 19 till 23 Nov 2007

5.2.1.1 Météo France data for Marseille Hippodrome station

According to Météo France data, easterly winds prevailed from November 19 to 23, 2007, with maximum velocities of 11.1 m/s reached on November 20, 2007 (the record since 2001 for the month of November is 11.6 m/s which was observed in 2008 and the maximum for south-easterly wind is 14.1 m/s, observed in January/December 2008; NB: the year 2008 saw particularly high wind velocities of south-easterlies).

5.2.1.2 Atmospheric modelling

A potential vorticity (PV) anomaly was present over the North Atlantic on 18 November, and reached England and France by the morning of November 19. This tropopause anomaly causes a temperature drop in lower layers that was centred over southern Ireland (Figure 58and Figure 59).

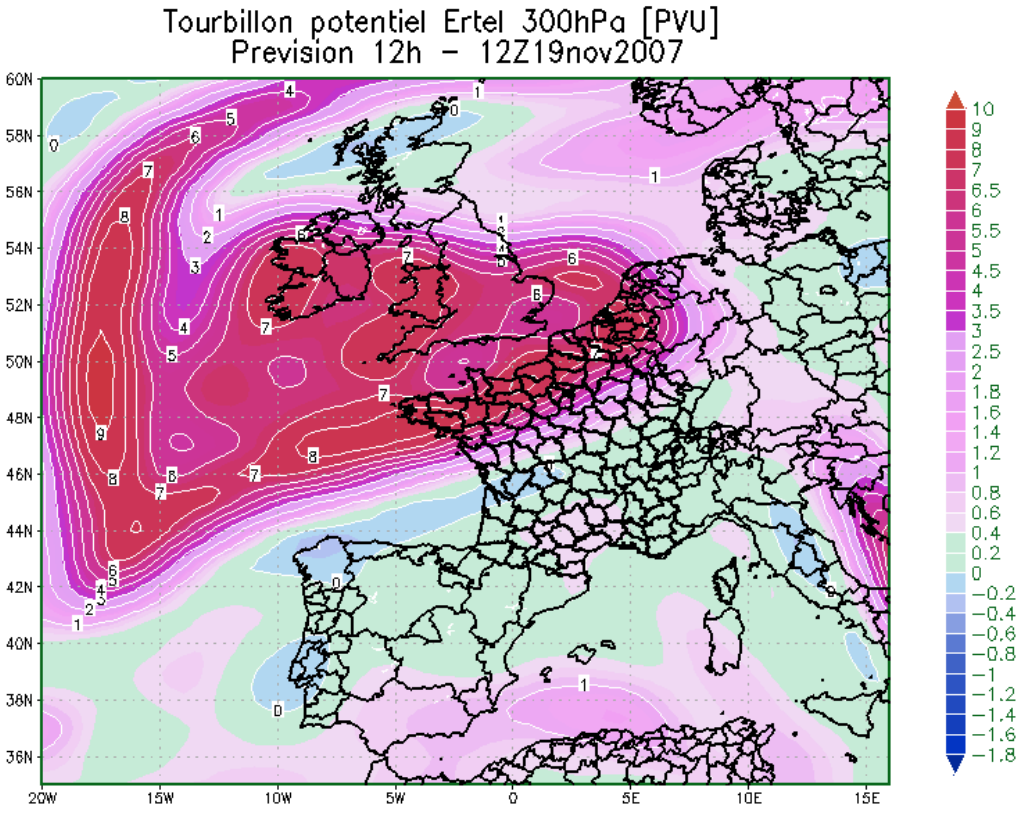

Figure 58: Potential vorticity (PVU= potential vorticity units, corresponding to 1 rad m^2 K kg^{-1} s^{-1}) at 300hPa on 19 Nov 2007 at 12h.

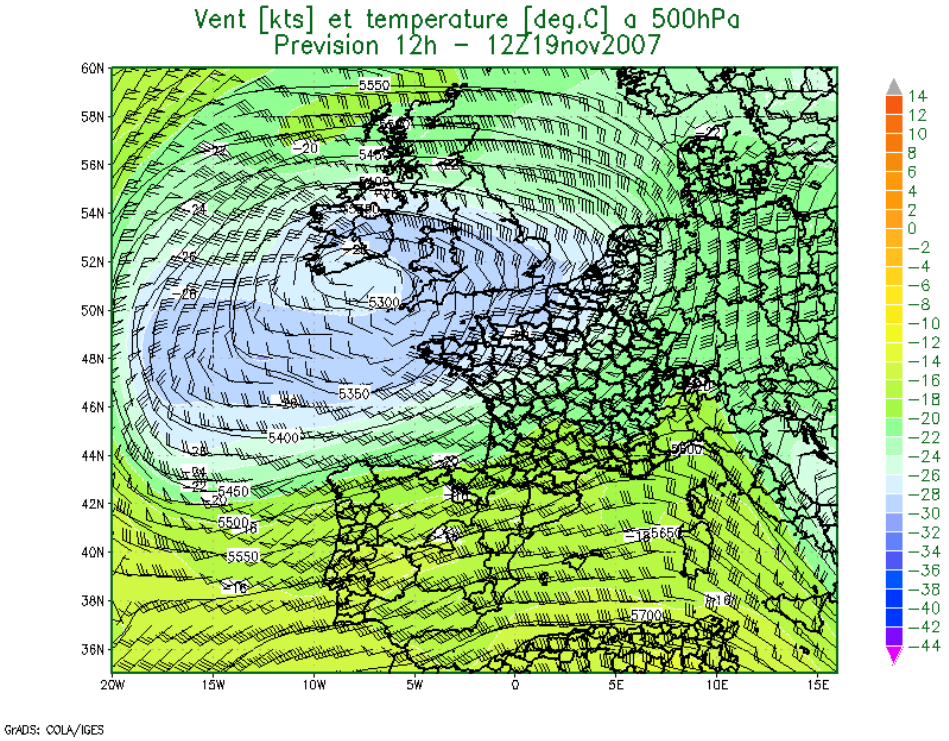

Figure 59: Winds (kts) and Temperature (°C, colour scale) at 500hPa on 19 Nov 2007 at 12h.

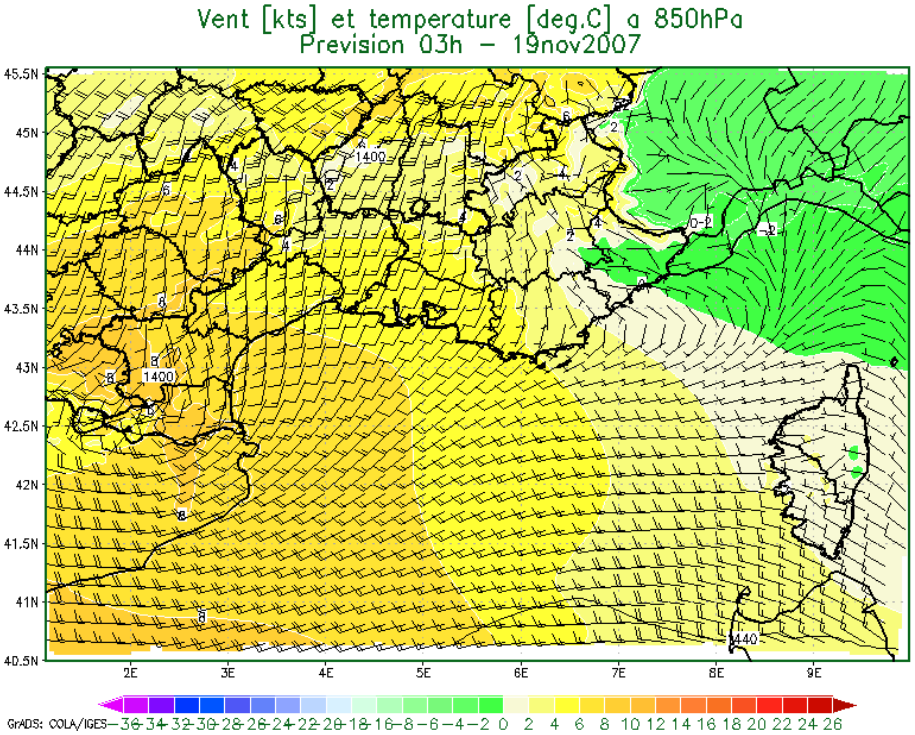

Figure 60: Winds (kts) and Temperature (°C, colour scale) at 850hPa on 19 Nov 2007 at 03h.

In the southern part of this cold air, there is a south-westerly wind blowing throughout southern France. However, advection of humidity remains limited to the northern part of the country and the Mediterranean basin is under relatively dry air. This zone is ahead of the axis of the thalweg, and as a result the flow at lower altitudes is oriented toward the southeast at the start of the day (Figure 60). During the day, a hot baroclinic zone develops over the Rhône and Var River mouths, strengthening the wind along this hot anomaly. On the surface, the south-easterly wind is blowing moderately and reaches 30/35 knots along the Provençal coasts (Figure 61).

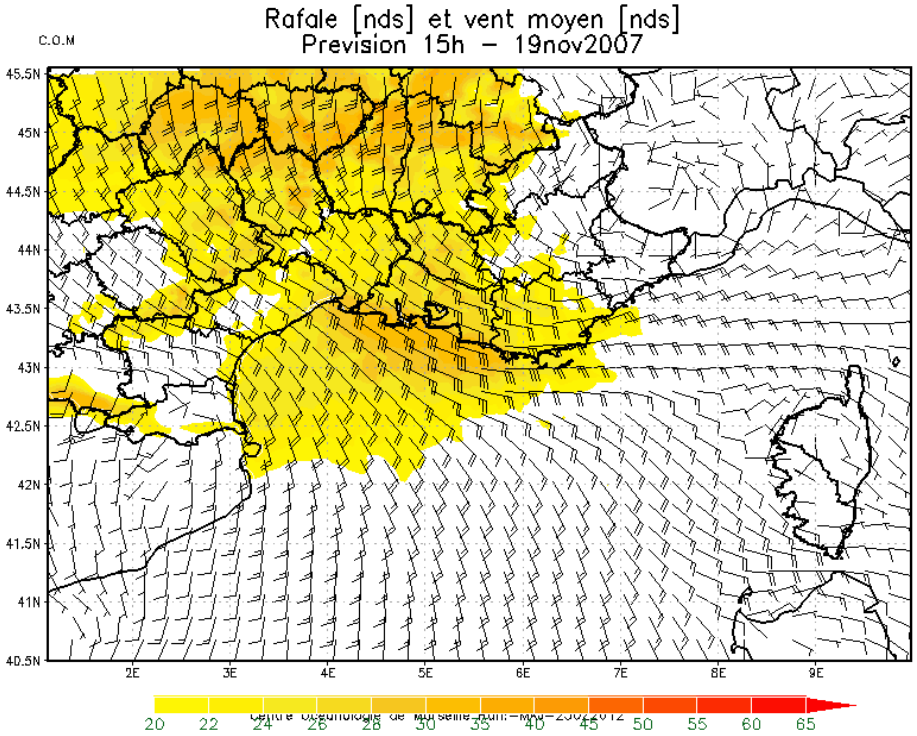

Figure 61: Mean wind (kts) and gust speeds (kts, colours) at 10m on 19 Nov 2007 at 15h.

As the low pressure over Spain moves toward the Gulf of Lion, the south-easterly wind gets stronger and the jet in the lower layer intensities over the Rhône River mouth (Figure 62). Rain starts to fall over the PACA region and intensity throughout the night from 19 to 20 Nov.

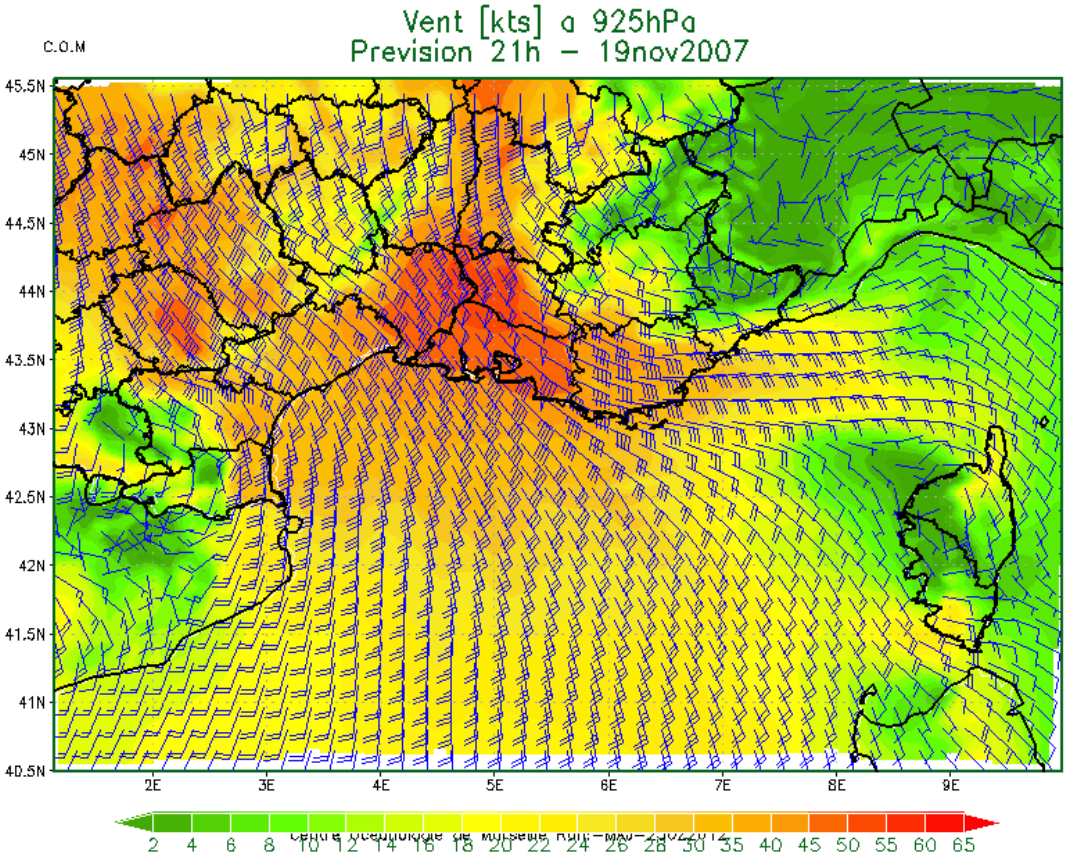

Figure 62 : Winds (kts) at 925hPa on 19 Nov 2007 at 21h.

5.2.1.3 Hydrodynamics and biogeochemistry

Due to the east/west orientation of the coastline around Marseille, the south-easterly winds push the warmer offshore waters towards the coast (Figure 63).

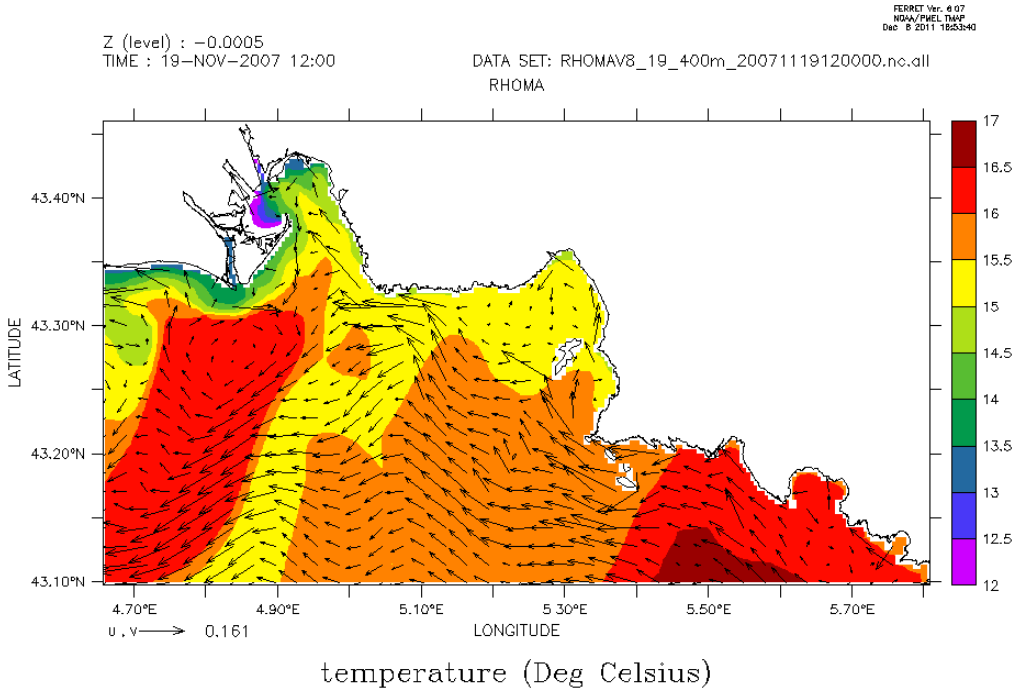

Figure 63: Modelled surface temperatures and currents on 19 Nov 2007 at 12h.

There is thus an accumulation of water along the coast which produces a downwelling (submergence of surface waters) (Figure 64). On 23 November, 2007, at the end of the south-easterly wind event, very small variations in temperature, salinity, fluorescence/chlorophyll were observed in vertical *in situ* profiles collected at SOLEMIO station, that were also visible in the model results. The water column seems homogeneous which suggests that the event is sufficiently strong to push surface water all the way to the bottom (about 100 m).

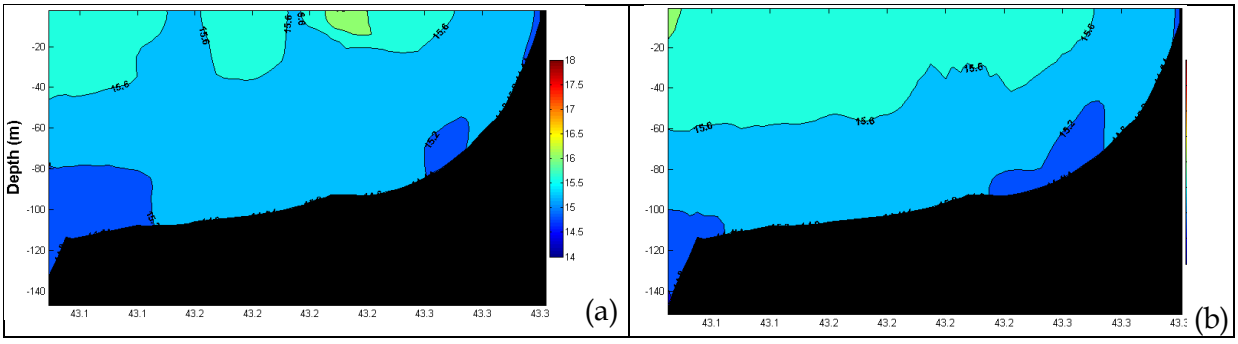

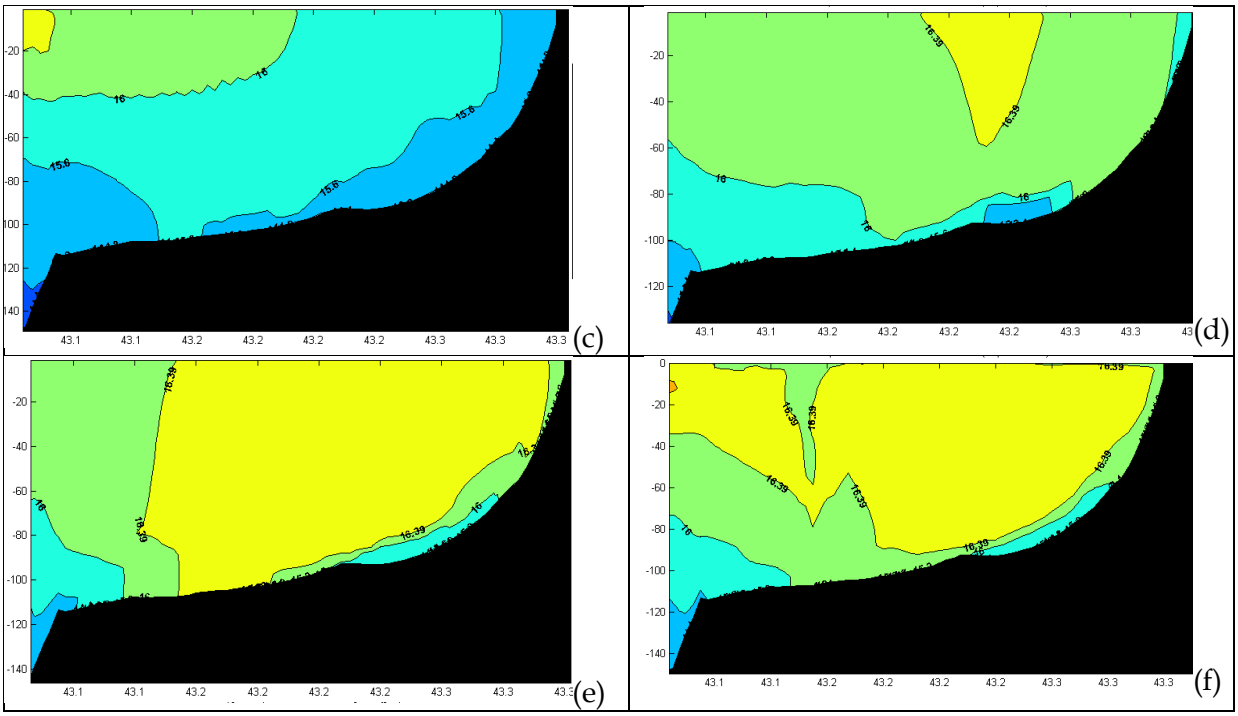

Figure 64: Vertical cross-section of temperature (°C) from 18 to 23 Nov (a to f, respectively) 2007 as output by the RHOMA 400m configuration along a line of longitude on the Côte Bleue.

This downwelling phenomenon is also visible in the nitrate concentration maps (Figure 65). On 18 November (before the onset of easterly winds), the coastal area around Marseille was relatively rich in nitrates with concentrations between 1 and 1.5 µmol/L (Figure 65a and c) while surface waters off Marseille were relatively low in nitrates. The vertical sections clearly show the arrival of low-nitrate water at the surface, moving toward the coast and descending to depth (Figure 65d-g). At the end of the event, the water column has been homogenised and shows low nitrate concentrations of 0.5–0.6 µmol/L throughout, corresponding to the nitrate concentrations present in offshore waters before the event. At this time of year, the surface waters off Marseille are warmer and more oligotrophic (low in nitrate), and these downwelling events, induced by south-easterly winds, lead to a further warming and decrease in nutrient and subsequently chlorophyll concentrations throughout the water column.

Generally, the surface waters off Marseille are typically poorer than other coastal areas and south-easterly winds therefore lead to a depletion of the entire water column (approximately 0 -100 m) in the coastal area around Marseille.

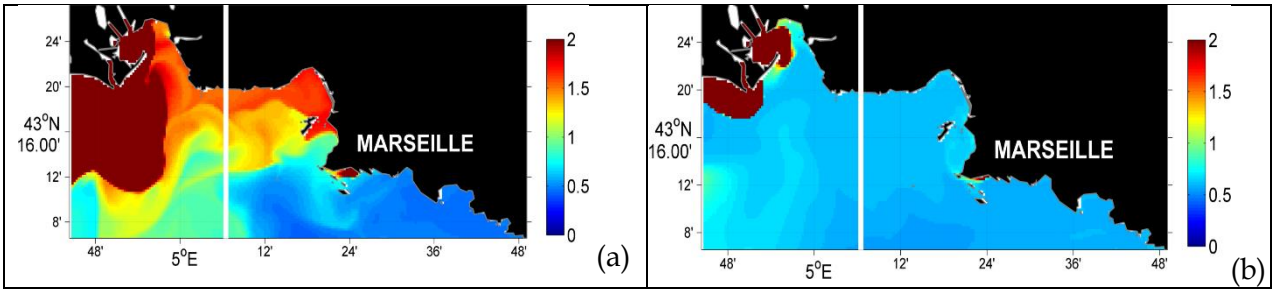

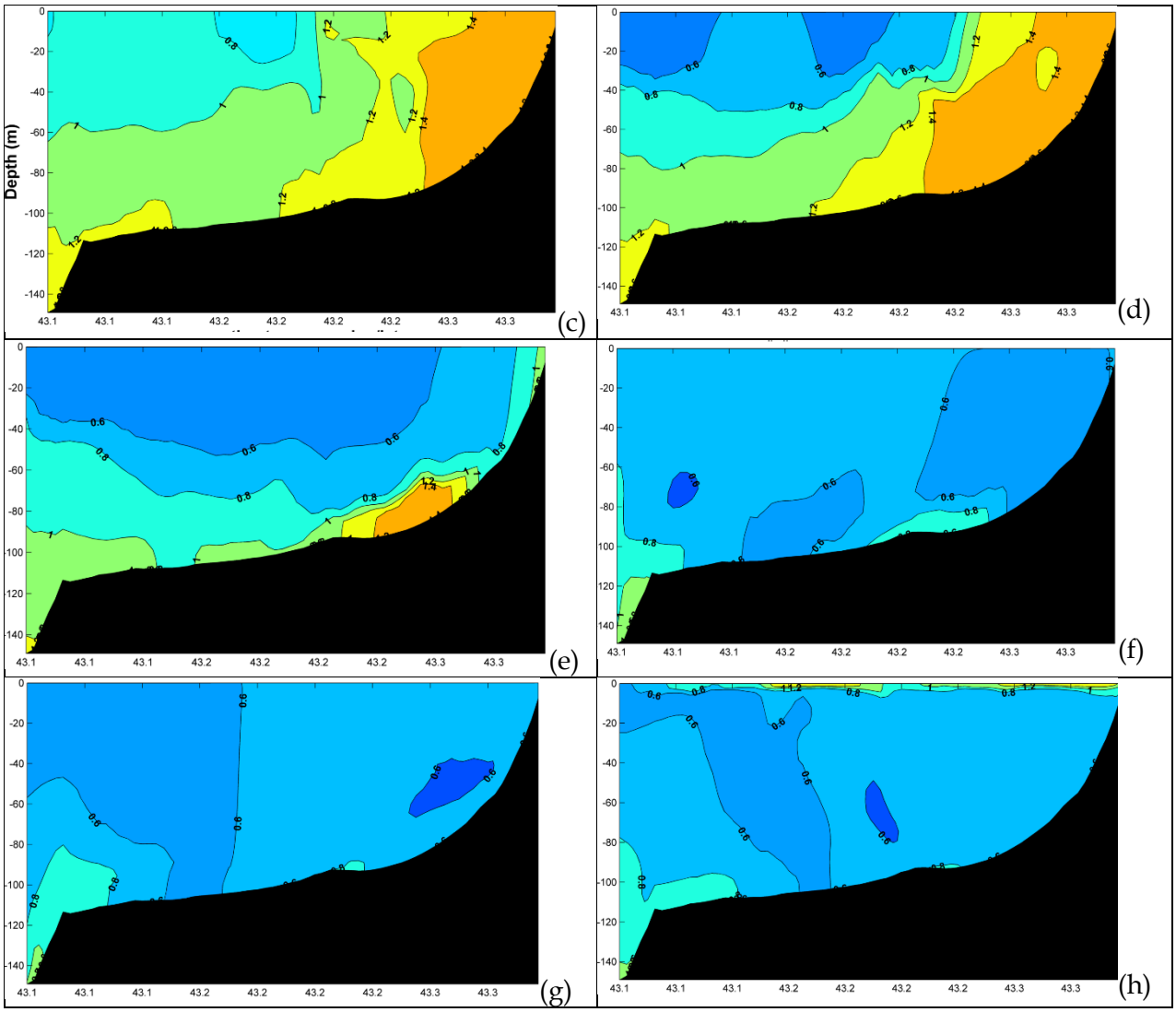

Figure 65: Maps showing surface nitrate concentrations (µmol/L) (a) on 18 Nov 2007 and (b) 22 Nov 2007. Vertical sections of nitrate concentrations along 5.1°E for (c) 18 Nov, (d) 19 Nov, (e) 20 Nov, (f) 21 Nov, (g) 22 Nov, and (h) 23 Nov.

5.2.1.4 Sedimentation

During a south-easterly wind event, the northern and southern parts of the harbour are protected from the influence of the waves, unlike the Calanques (SWH>2m), the islands, the Rhône delta (SWH>3m) and parts of the Côte Bleue (Figure 66).

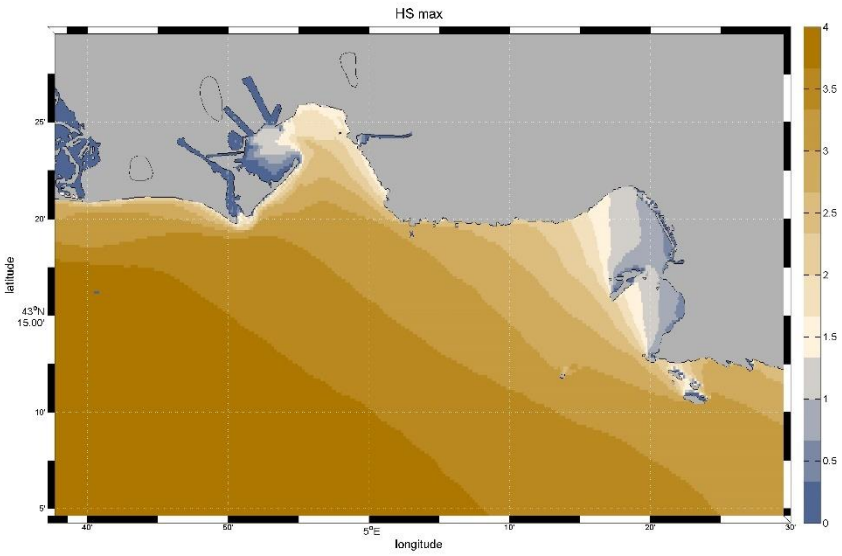

Figure 66: Maximum significant wave height (m) between 18-23 Nov.

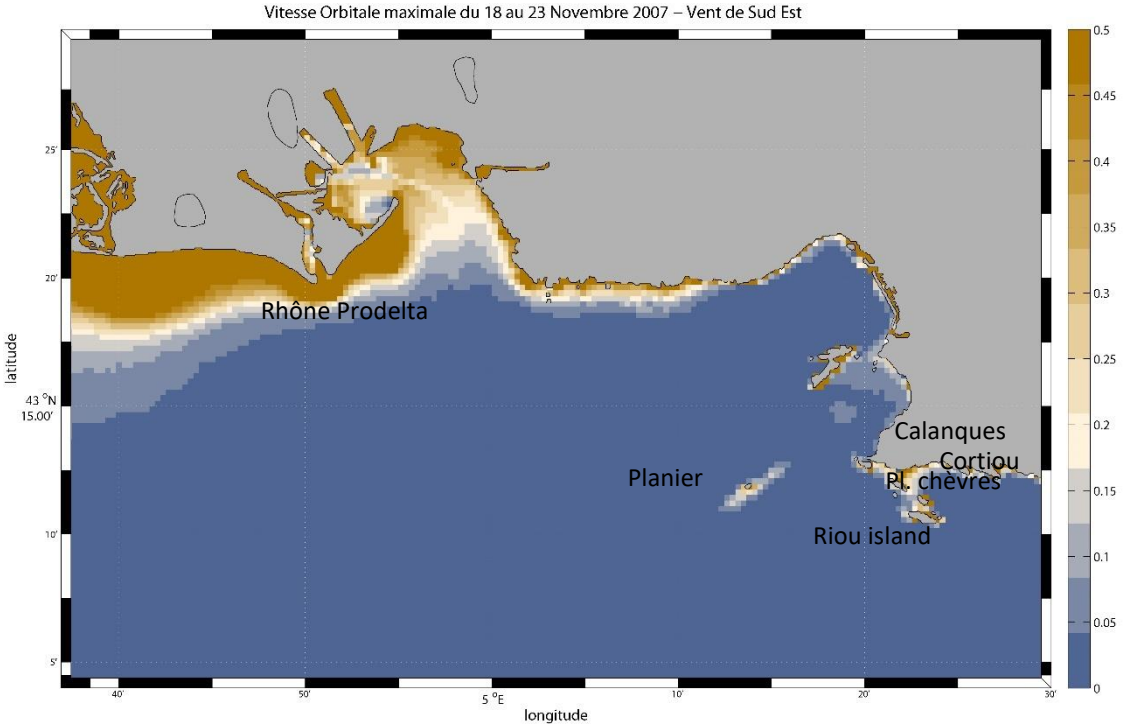

In this case, the areas most sensitive to south-easterly winds remain the coastal fringe around the Rhône prodelta and the Calanques and the plateau des chèvres (orbital speeds >0.5m/s) (Figure 67). In addition to strong erosion at the level of the prodelta, the waves induce erosion and strong re-suspension near the coast near Cortiou (Figure 68and Figure 69), near Riou island, and – to a lesser extent - near Planier (maximum concentrations of >10 mg/L at the surface and of >100 mg/L near the bottom).

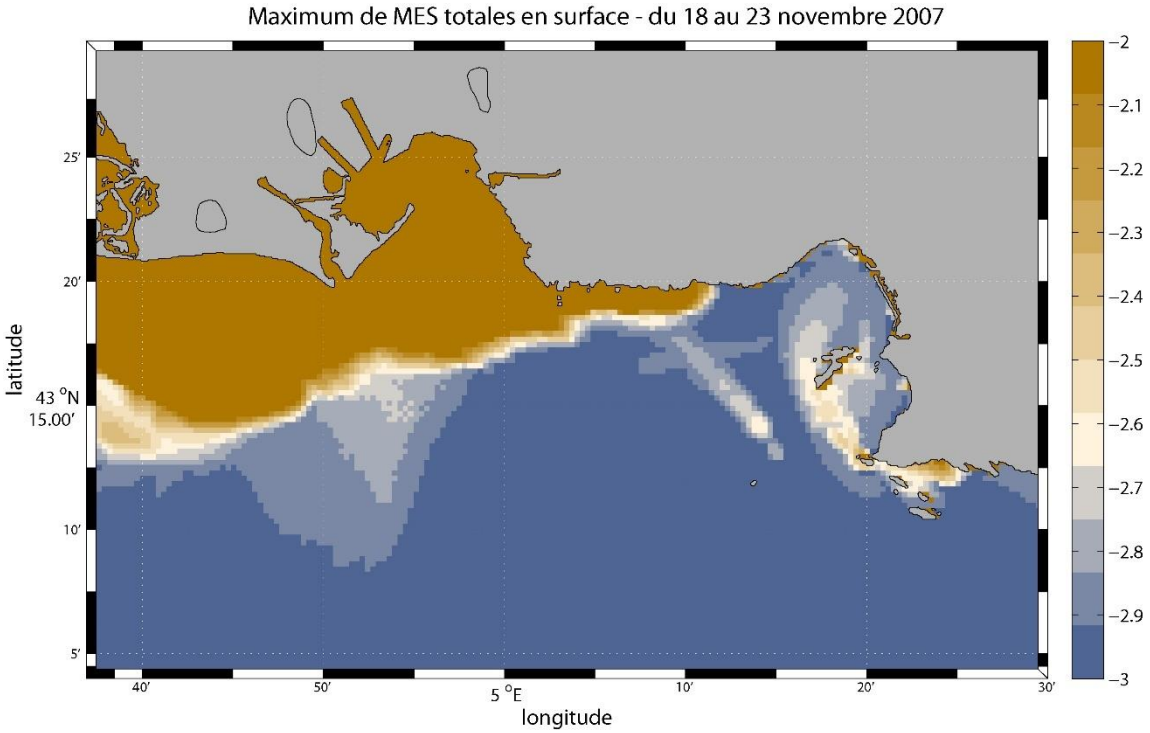

Figure 68: Total suspended matter concentration in the surface layer (g/L, log scale: -2= 10mg/L, -3=1mg/L) between 18-23 Nov.

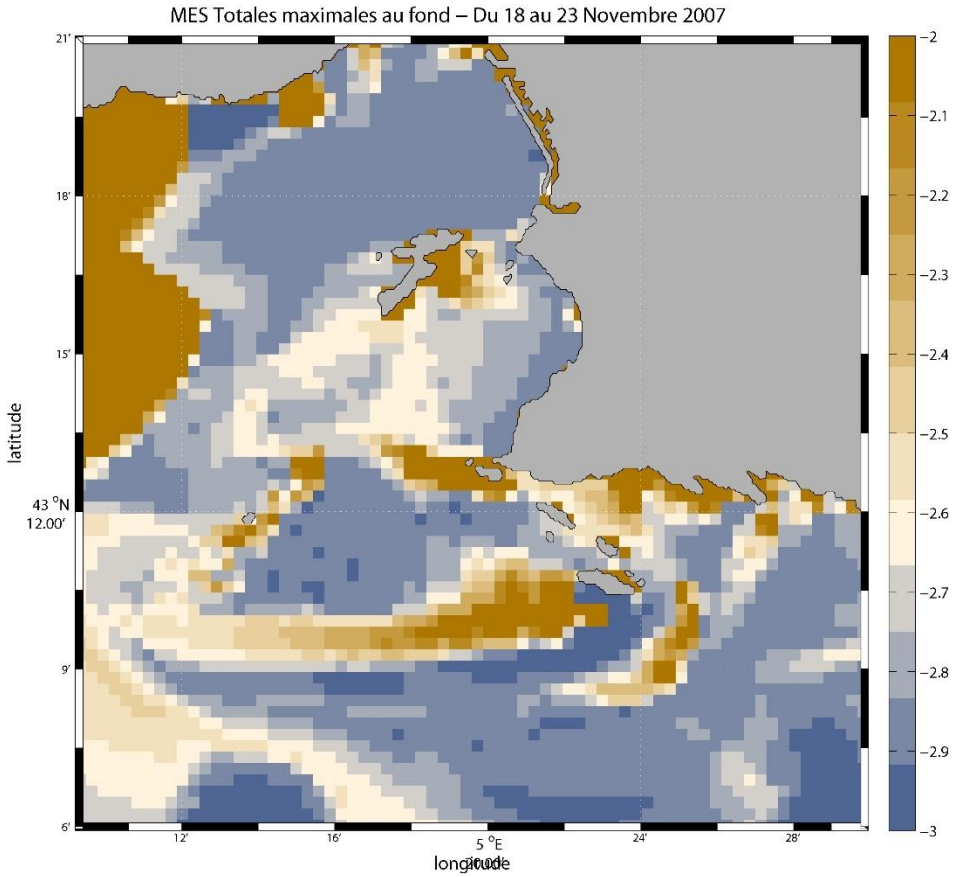

Figure 69: Total suspended matter concentration at the sea bed (g/L, log scale: -2= 10mg/L, -3=1mg/L) between 18-23 Nov in the Bay of Marseille.

Due to the north-westerly currents induced by the wind, the suspended solids that enter via tributary rivers or are being resuspended are mainly transported towards the west, i.e., the northern and southern bays which are protected from the waves and where sedimentation occurs. Sediment resuspended near Cortiou is also partially redeposited further down the slope where wave action is weaker. However, on average erosion prevailed in this area over the study period (Figure 70).

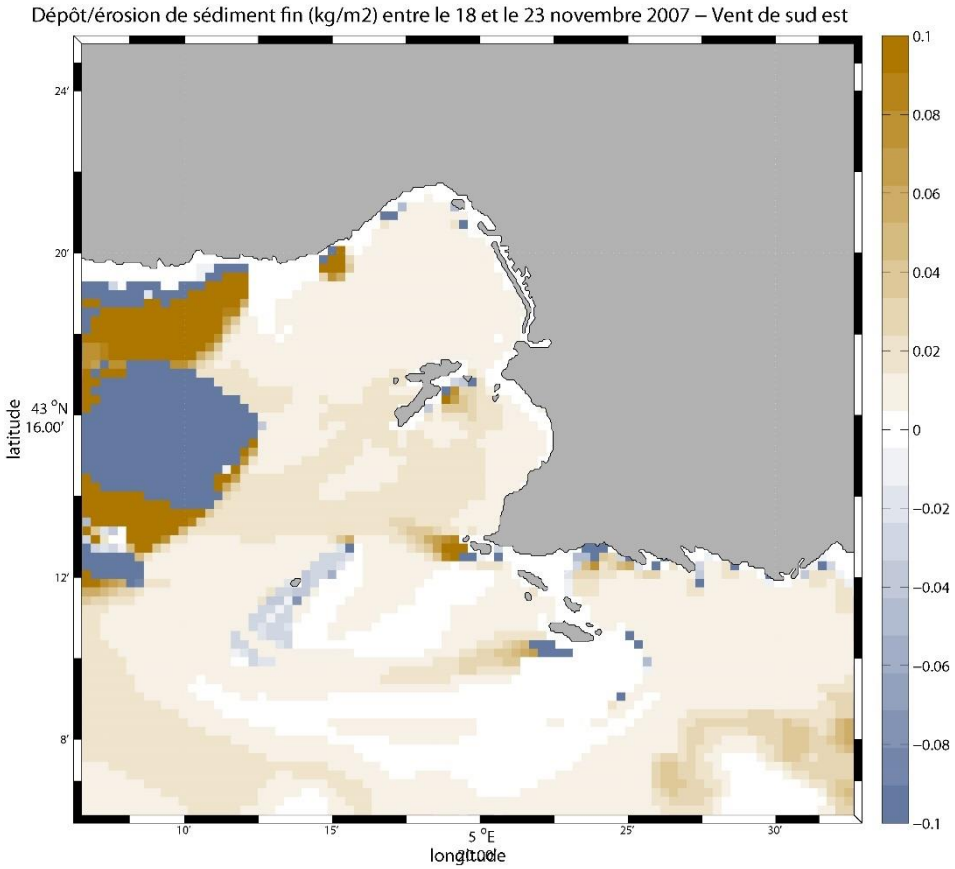

Figure 70: Sedimentation/resuspension of fine sediments between 18-23 Nov.

Contamination with CB153

The south-easterly winds induce a circulation in Marseille harbour which transports the effluents to the southern and northern bays (Figure 71 and Figure 72), particularly the effluents from Cortiou. At the sea bed there are high concentrations near the Cortiou discharge (Figure 72), due to resuspension in the area around 20-21 November. Erosion is weak in the northern and southern parts and whatever material gets eroded is redeposited in the same area within the following days. The amount of CB153 mostly depends on the in-/outflow at the boundaries (Figure 73) which remains small. A small part of the CB153 that arrives from Cortiou is redeposited while the bulk is exported further offshore. There is also erosion occurring in the western part, the result of which is also exported.

(a) Dissolved at the surface (pg/L)

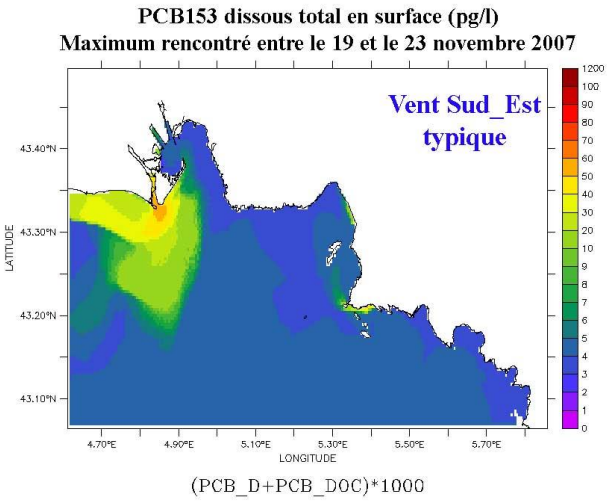

(b) Particulate at the surface (pg/L)

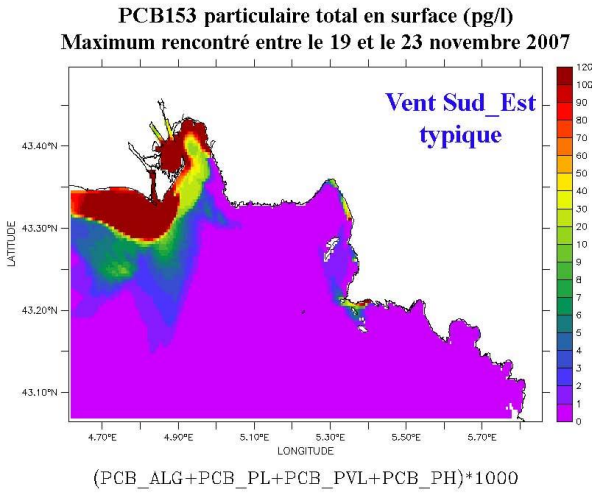

Figure 71 : Maximum surface concentrations (pg/L) between 19 and 23 Nov 2007.

(a) Particulate at the surface (ng/g)

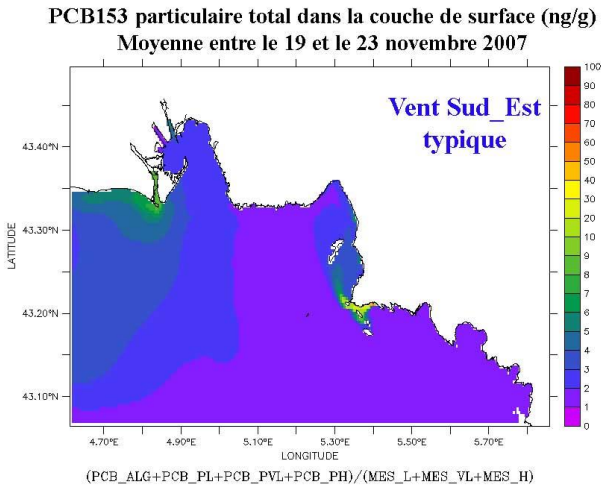

(b) Particulate at the bottom (ng/g)

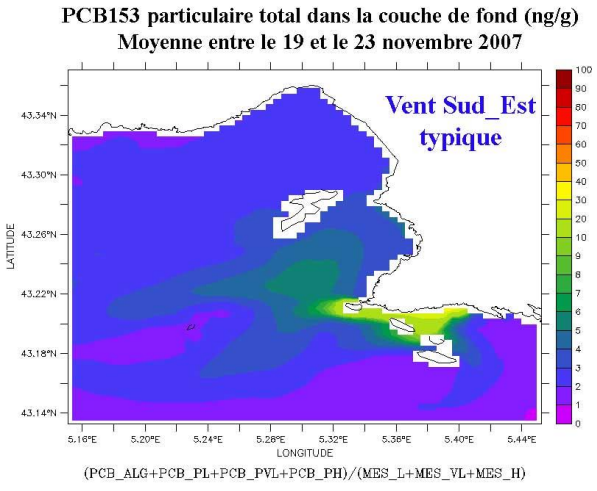

Figure 72 : Average levels of particulate CB153 (ng/g) at the surface and sea bed between 19 and 23 Nov 2007.

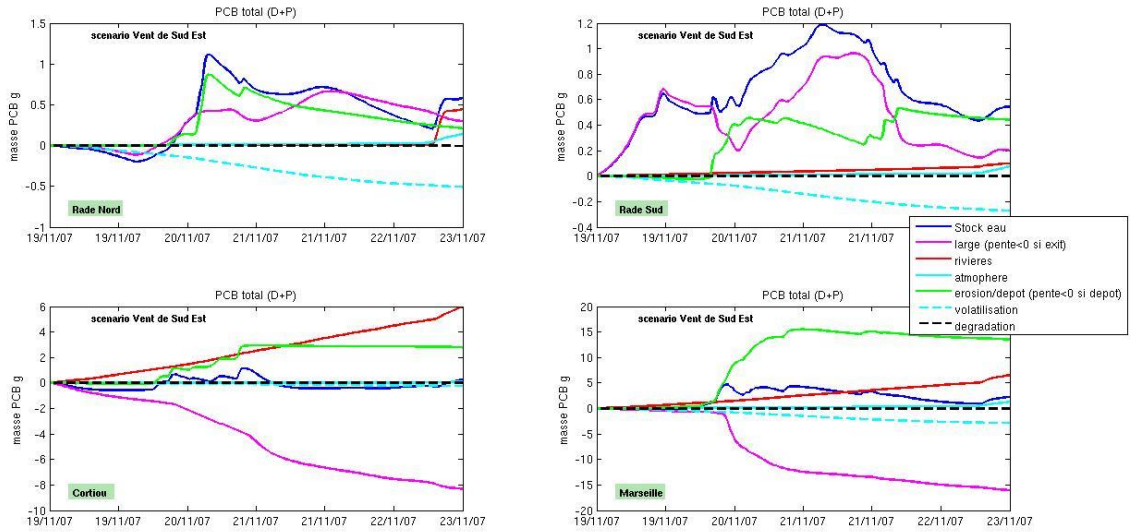

Figure 73 : Variation of total CB153 in the water column during the period and in each zone (described in Figure 15), associated with variations in concentration due to the different processes; "large": in-/outflow at boundaries; "rivières": riverine; "atmosphère": dry deposition and from rain; "érosion/dépôt" = erosion/deposition; "volatilisation" and "dégradation". (if the slope >0 then the concentration increases which is equivalent to an net influx of contaminant, and vice versa)

5.2.2 Extreme storm event with south-easterly winds in January 2008

Note: this extreme situation has been chosen because the MM5 forcing represents December 2008 very poorly while the high-resolution WRF model describes it much better.

5.2.2.1 Météo France data from the Hippodrome station in Marseille

According to the Météo France data, there was a predominantly easterly wind blowing from 2 to 5 January 2008, with a daily average maximum of 14.1 m/s reached on 3 January 2008. This represents a record for the month of January and the maximum south-easterly wind for all months since 2001. The same average maximum was also reached in December 2008, but poorly simulated by MM5.

5.2.2.2 Atmospheric modelling

There were two disturbances present, one on the Iberian Peninsula and the second in the Gulf of Genoa. In the eastern part of the PACA region, we notice the advection of a mass of cold air while warm and humid air moves from the Mediterranean to the Rhône River delta (Figure 74).

The disturbance in the Balearic Islands is progressed eastward on 3 January, contributing to an increase in temperature gradient in the low layer over the Rhône River delta.

Then, a very strong jet at 925 hPa develops in the baroclinic zone, reaching 70 knots (Figure 75).

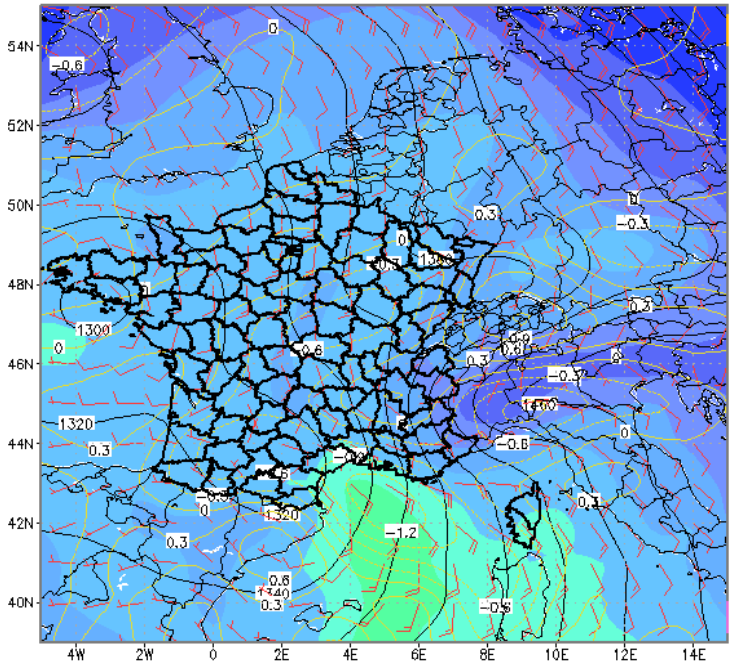

Figure 74 : Θw 850hPa (°C colour) Wind 900hPa (kts red arrows) Vertical speed 700hPa (Pa/s yellow contours) HGT 850hPa (black contours) on 03 Jan 2008 at 12h.

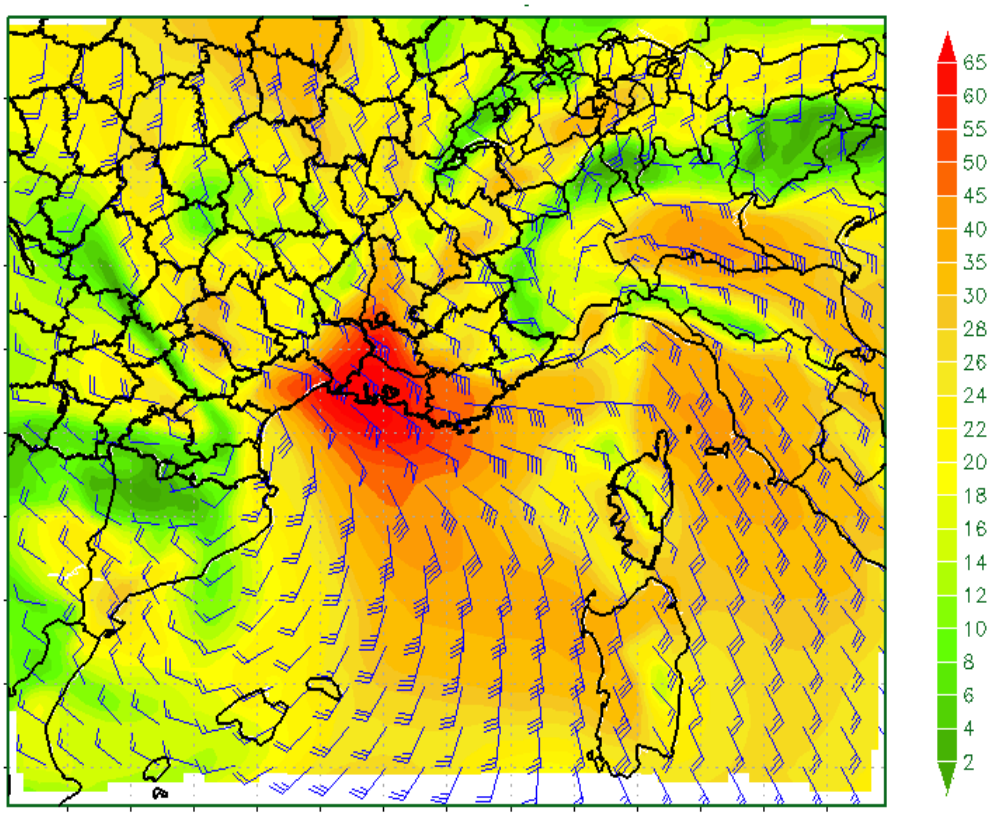

Figure 75 : Wind 925hPa (kts) on 04 Jan 2008 at 00h.

The strong wind zone over the Rhône delta results from the confluence of the wind and the convergence of the air masses. Thus, surface wind velocities reach 45 knots (Figure 76).

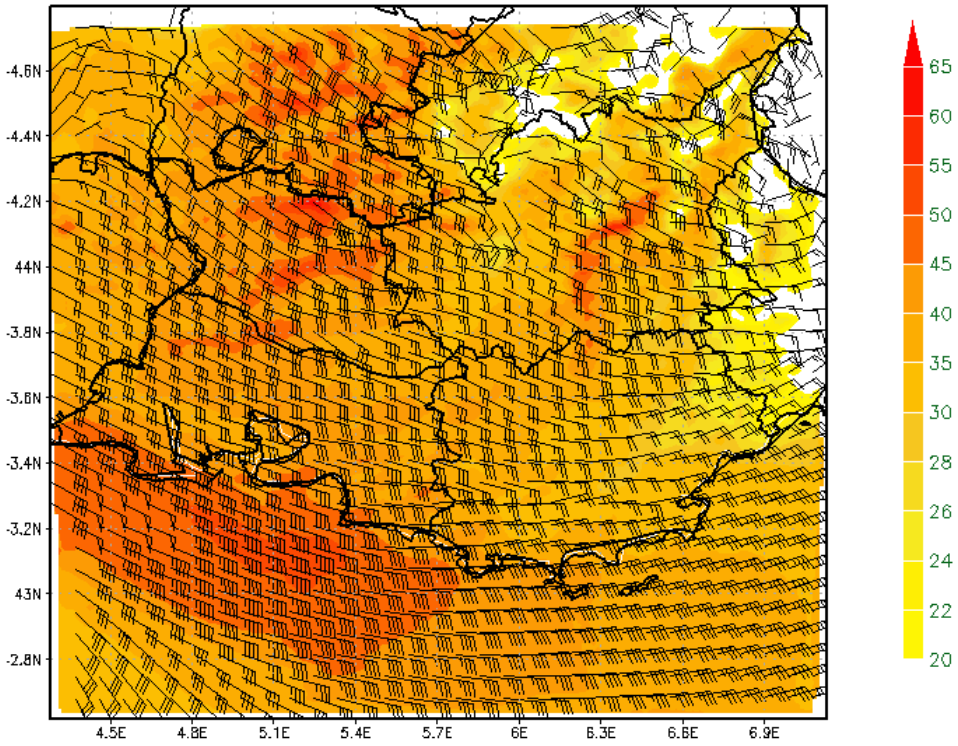

Figure 76 : Wind 10 m and gust speed 10 m (kts) on 04 Jan 2008.

5.2.2.3 Hydrodynamic situation (MARS3D-RHOMA)

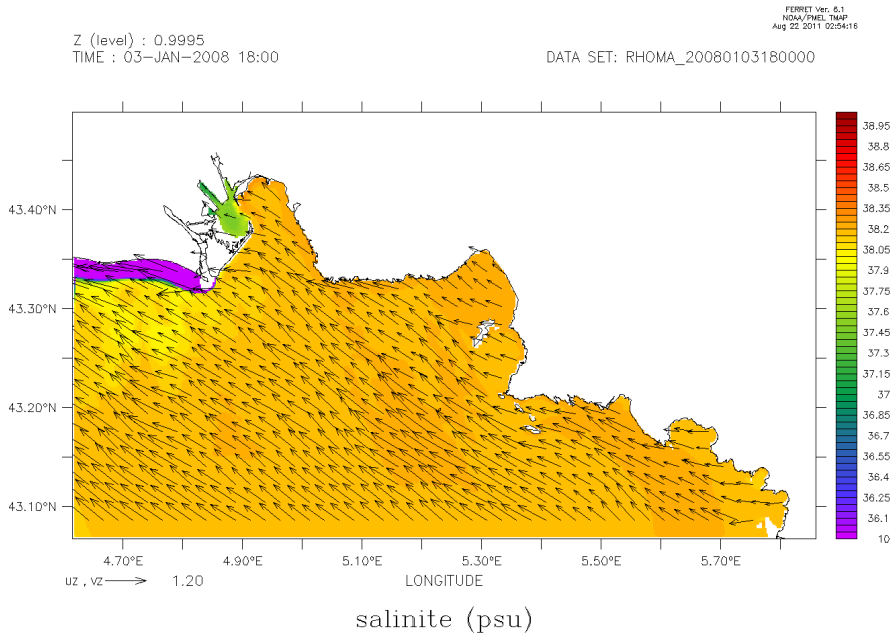

Figure 77 : Modelled surface currents and salinity for 3 Jan 2008 at 18h.

A south-easterly has been blowing for the first 5 days of January 2008 with modelled (MM5) velocities sometimes exceeding 30 m/s on 3 January. This results in surface currents flowing to the north-west (Figure 77 and Figure 78) pushing off-shore water of the same temperature onto the plateau (Figure 78). As a result of this wind, the plume is pushed toward the north-west and flattened against the coast (Figure 77).

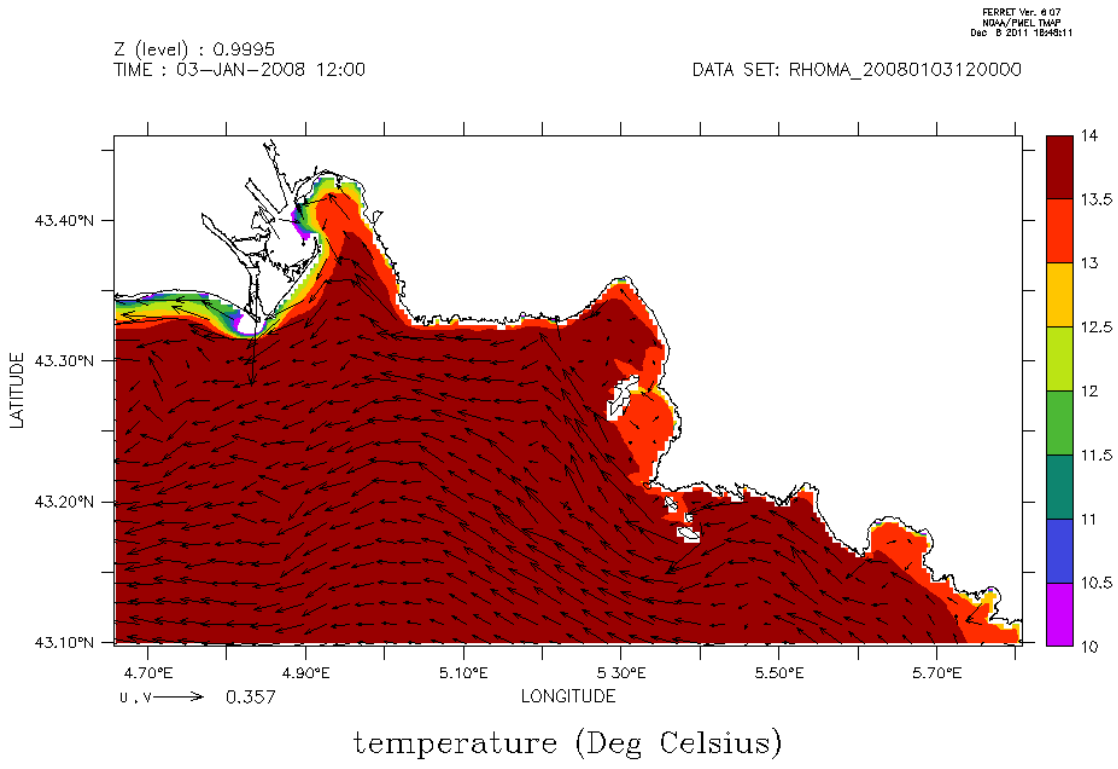

Figure 78: Modelled temperatures and mean currents on 3 Jan 2008 at 18h.

5.2.2.4 Biogeochemical situation (ECO3M-MASSILIA)

We see the same trends as in the typical south-easterly wind situation of November 2007. The offshore waters are pushed towards the coast and induce downwelling. In fact, a typical south-easterly situation seems sufficient for the coastal zone to be impacted over the entire water column (from 0 to 100 m) by the offshore waters in the Bay of Marseille. The same is true in this extreme case. On January 2, the water column is relatively homogeneous at a temperature of 14.5°C as a result of winter mixing. The offshore surface waters have a temperature of around 13.5°C. On 4 January 2008, a homogeneous water column was observed which had the characteristics of offshore surface waters in terms of temperature and nitrate (Figure 79).

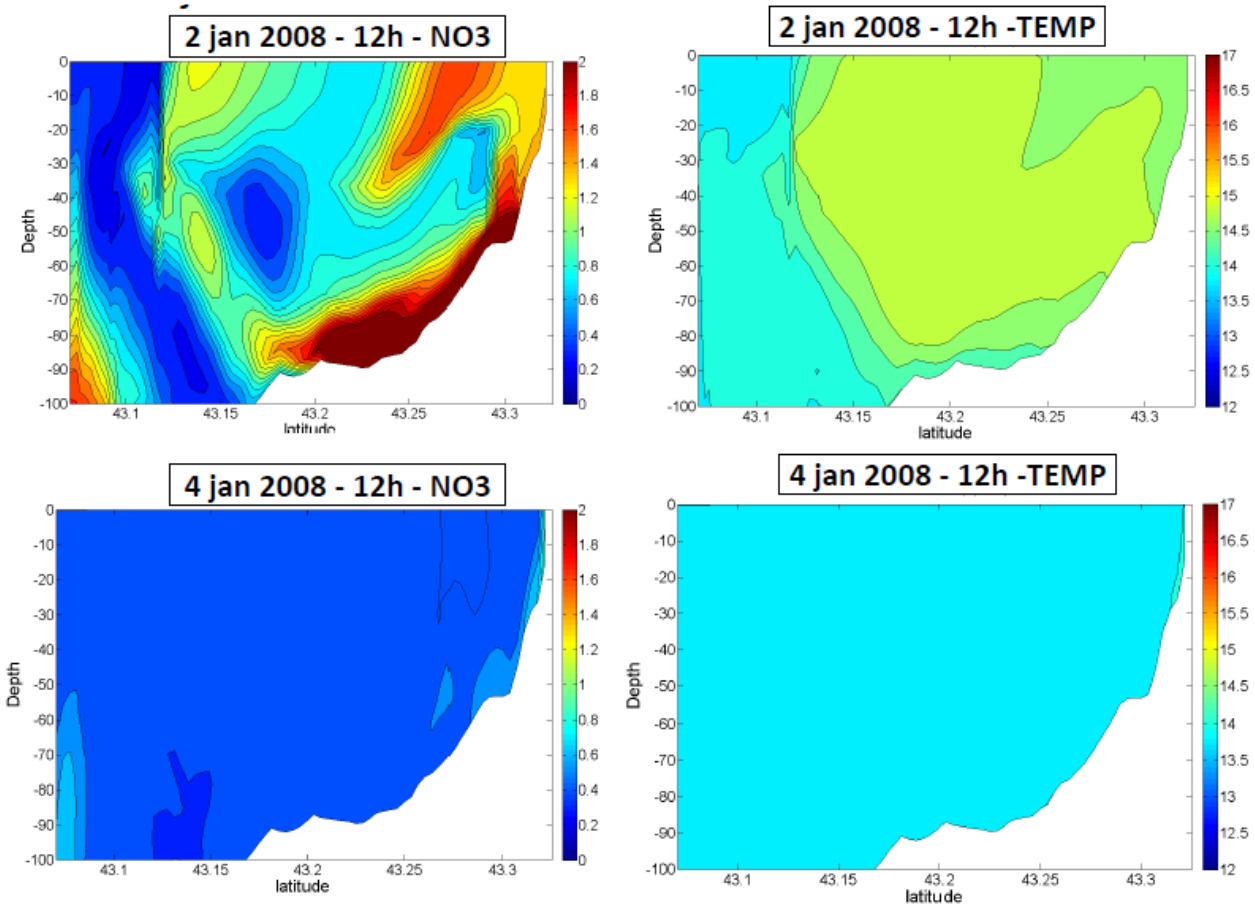

Figure 79: Vertical profiles showing nitrate (µmol/L) and temperature (°C) on 2 and 4 January 2008 as obtained by RHOMA 400m at the latitude of the Côte Bleue.

5.2.2.5 Contamination with CB153

This south-easterly wind in January 2008 produced greater inflows, particularly in the northern harbour. The concentrations are therefore higher overall, especially since more significant resuspensions are also observed in the northern and southern parts of the harbour (Figure 80, Figure 81 et Figure 82).. However, the same scenario occurs with a circulation in the harbour of Marseille which pushes the Cortiou discharge towards the southern and northern parts of the harbour. Basically, the highest concentrations are found around the Cortiou discharge, with no sedimentation in this area. The PCB that gets resuspended in the southern and northern bays is largely redeposited, especially in the southern bay.

(a) Dissolved at the surface (pg/L) (b) Particulate at the surface (pg/L)

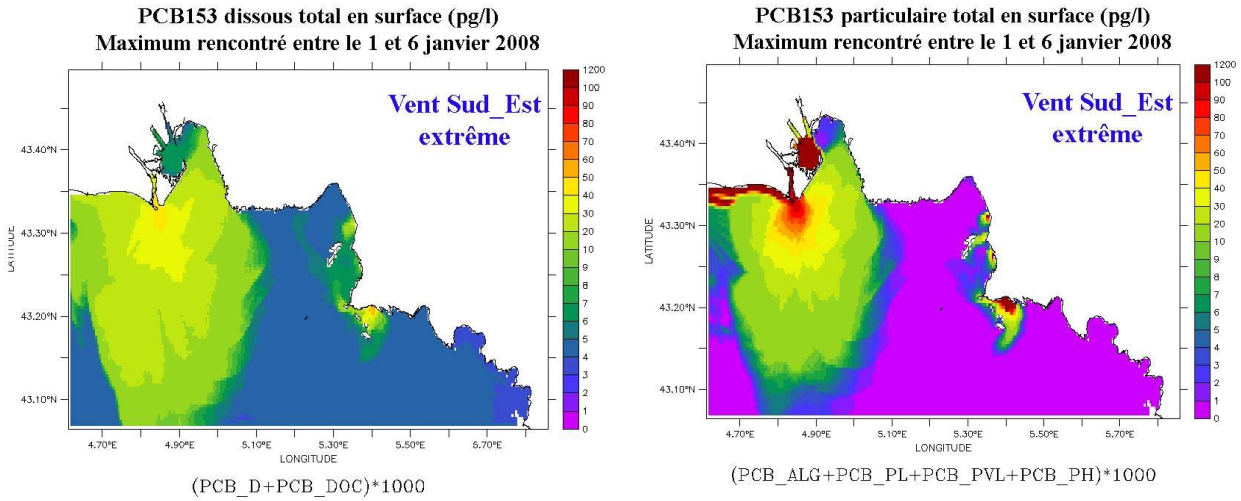

Figure 80: Maximum surface concentrations (pg/L) between 1 and 6 Jan 2008.

(a) Particulate at the surface (ng/g) (b) Particulate at the sea bed (ng/g)

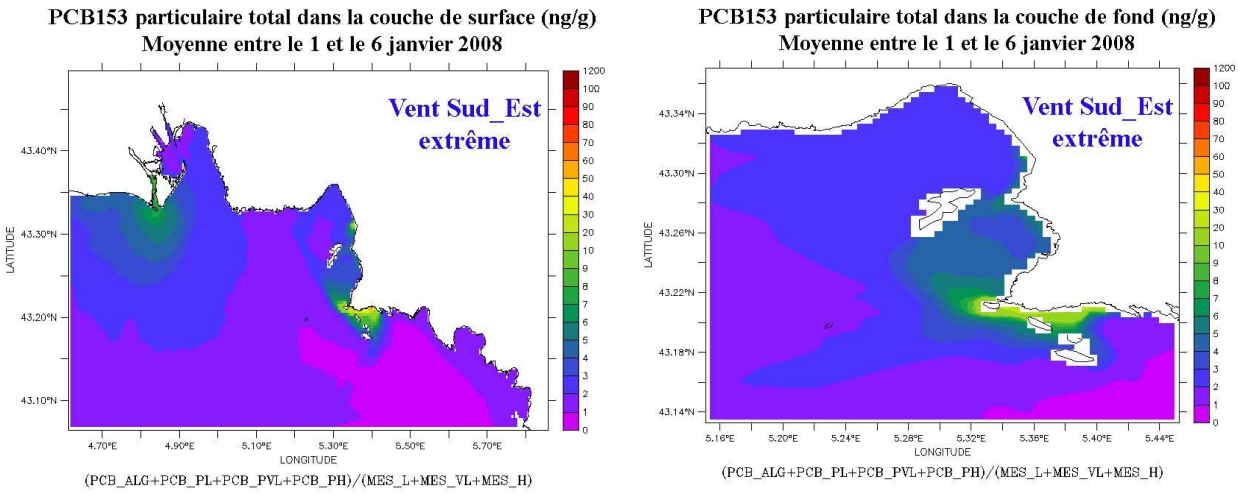

Figure 81: Mean particulate CB153 (ng/g) at the surface and sea bed between 1 and 6 Jan 2008

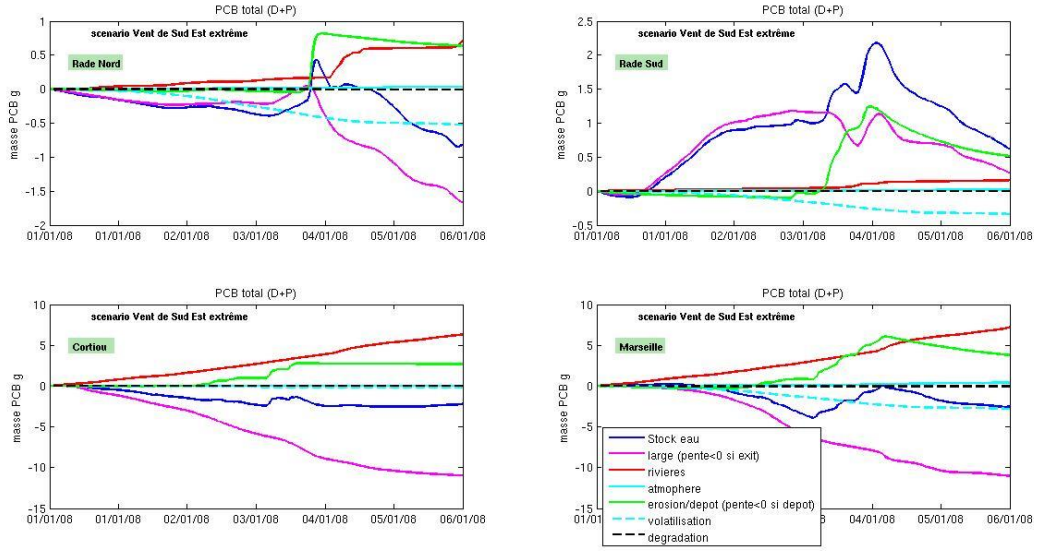

Figure 82: Variation of the total amount of CB153 in the water column during the period and for each zone (described in Figure 15), associated with variations in concentration due to each process; "large": in-/outflow at boundaries; "rivières": riverine; "atmosphère": dry deposition and from rain; "érosion/dépôt" = erosion/deposition; "volatilisation" and "dégradation". (if the slope >0 then the concentration increases which is equivalent to an net influx of contaminant, and vice versa)

5.3 WESTERLY WIND SITUATION

While situations involving westerly winds are present in the weather data, they are too poorly represented by the MM5 model. In fact, when we select the westerly wind events from the intensity data, the selected dates correspond to Mistral episodes with very little westerly wind during the day. As we would like to study events where westerly winds persist for several days, we need to revisit the meteorological data and identify corresponding periods. This could not be carried out during the period of the MASSILIA program.

RAIN

5.4 SITUATIONS INVOLVING RAIN

5.4.1 Typical late summer storm situation on 25 October 2007

5.4.1.1 Météo France data from the Marseille observatory

There was a thunderstorm on August 20, 2007. Then, no rain of more than 5mm/day until October 25, 2007 when 53 mm were recorded at the Observatory station of Météo France. We noted a heavy rain all the night of 25/10/2007. Unfortunately, as it is often the case, there is no usable satellite image before 27/10/2007.

On the MERIS FRS full 300m resolution image, which allows to see even the areas close to the coast, the effect of rain in the Bay of Marseille and at the level of Cortiou is well visible (Figure 83). This image was processed with the algal2 algorithm which tends to overestimate chlorophyll a little.

On the MERIS and MODIS images at 1 km (Figure 84) processed by Francis Gohin (Ifremer, pers. comm.) with the OC5 algorithm, 2 days after the rain it is possible to see an increase in the colour of the water (and in Chl concentration) in the northern and southern parts of the bay in the left zooms, even if it is not possible to see all the way to the coast.

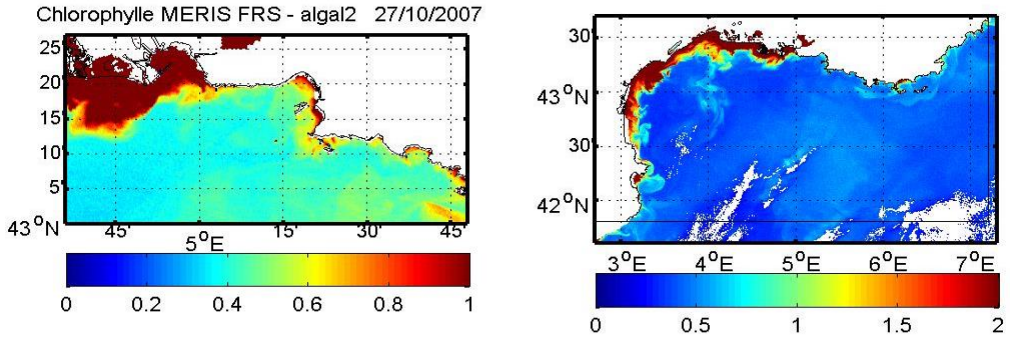

Figure 83 : Chlorophyll concentration (µg/L) from MERIS ocean colour images (full 300m resolution using algal2) for 27 Oct 2007

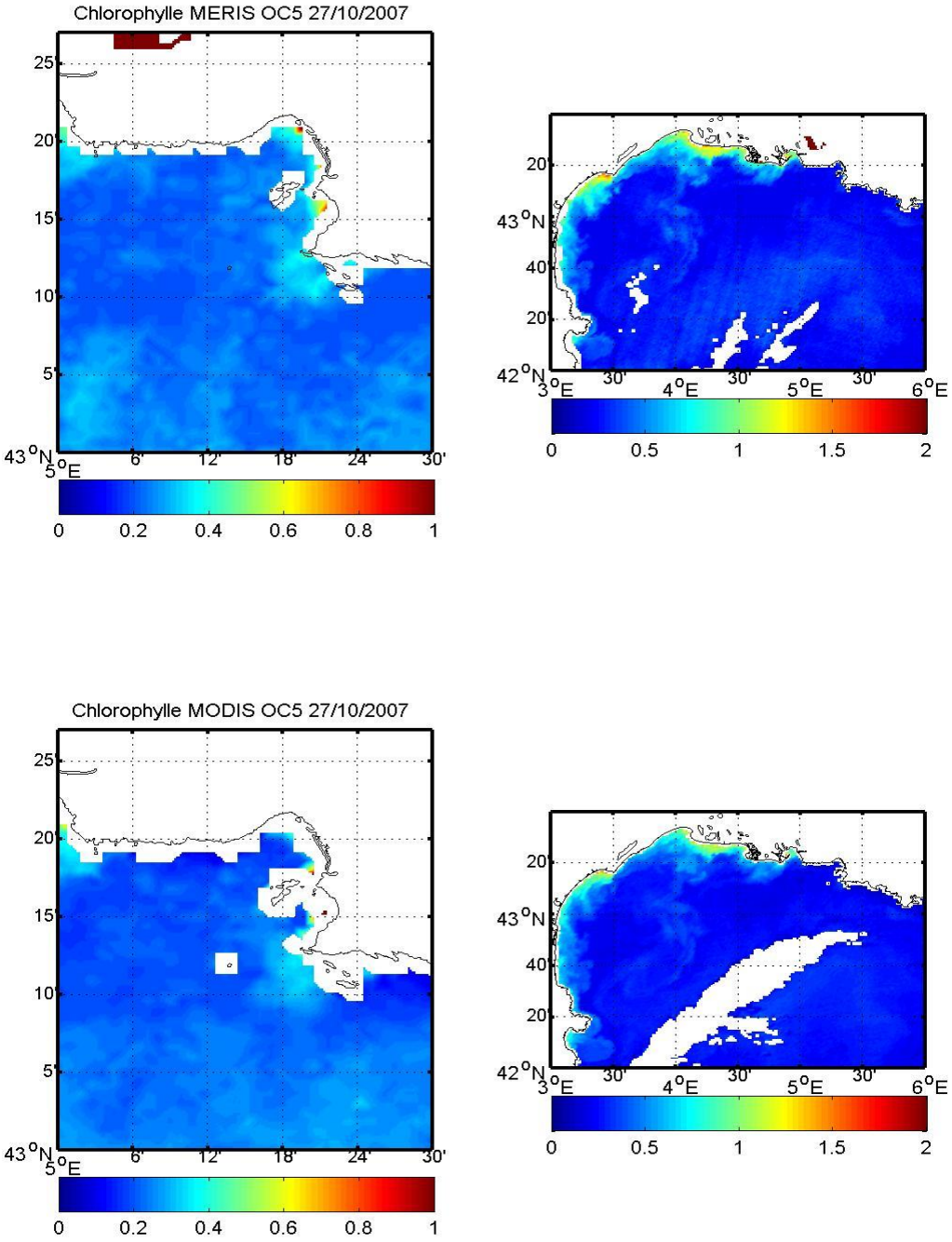

Figure 84 : Chlorophyll concentration (µg/L) from MERIS (upper panels) and MODIS (lower panels) ocean colour images (1km resolution using OC5) for 27 Oct 2007

5.4.1.2 Atmospheric simulation

From October 24, a disturbance moved from east to west over the south of the country. It crossed the region during the day on October 24 and became isolated over Spain on the 26th. This disturbance was marked by a cold anomaly around 500hPa with a core at -25/-27 °C (Figure 85). A ripple in the isohypses field appeared on October 24 at 850hPa over the Balearic Islands. The flow was then

oriented east-northeast along the coast of Provence where a low-level jet developed near the Var coast, reaching 50-55 knots at the end of the day on October 25 (Figure 86).

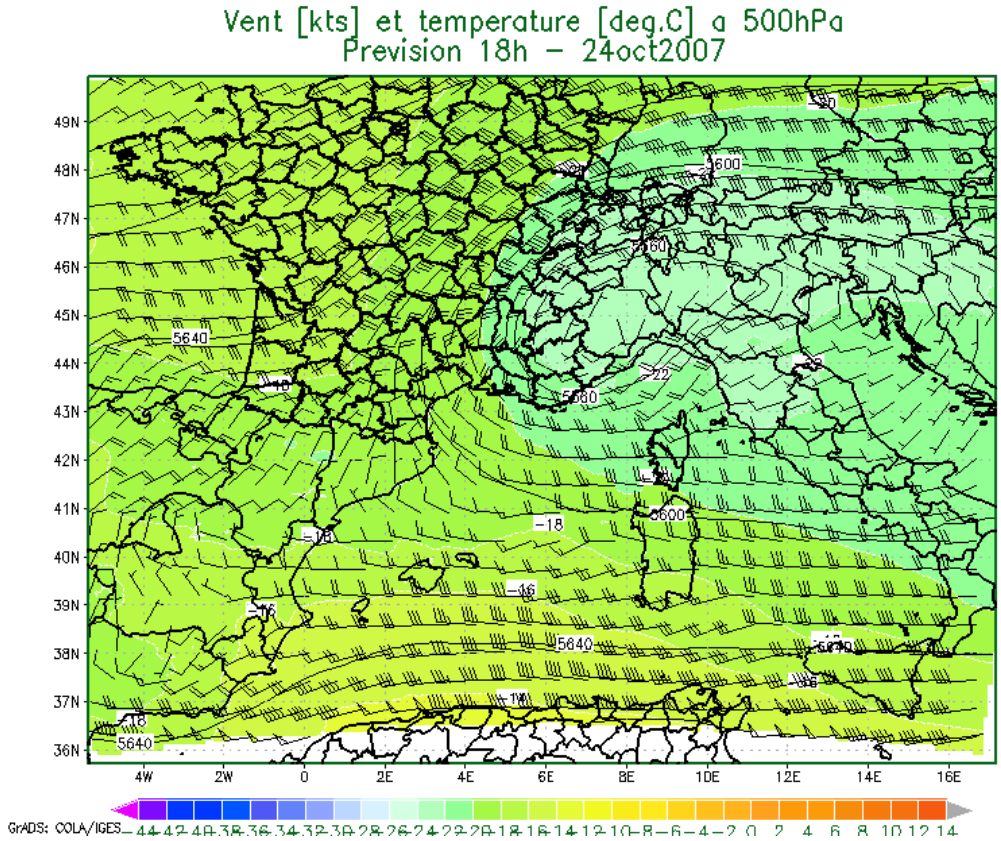

Figure 85: Wind (kts) and temperature (°C, colours) at 500hPa on 24 Oct 2007 at 18h

Initially, humid weather set in over the Var and the Bouches du Rhône and showers occurred during the night of October 24 to 25. As the disturbance deepened, the air mass destabilized at sea in the warm front of the disturbance (Tpw 12/14°C) (Figure 87).

Thunderstorm activity in this sector was reinforced by humidification at 850hPa progressing towards the Bouches du Rhône and the Var. Rain or showers were more numerous during the day on October 25. It was not until the following night, from October 25 to 26, when the Mediterranean disturbance turned northward as it approached the coasts of Provence-Alpes-Côte d'Azur, that the rainfall became more significant (Figure 88). The rain swept across the Bouches du Rhône department from east to west, with more marked activity near the coast. It began to subside by midday before leaving the region in the late afternoon of October 26.

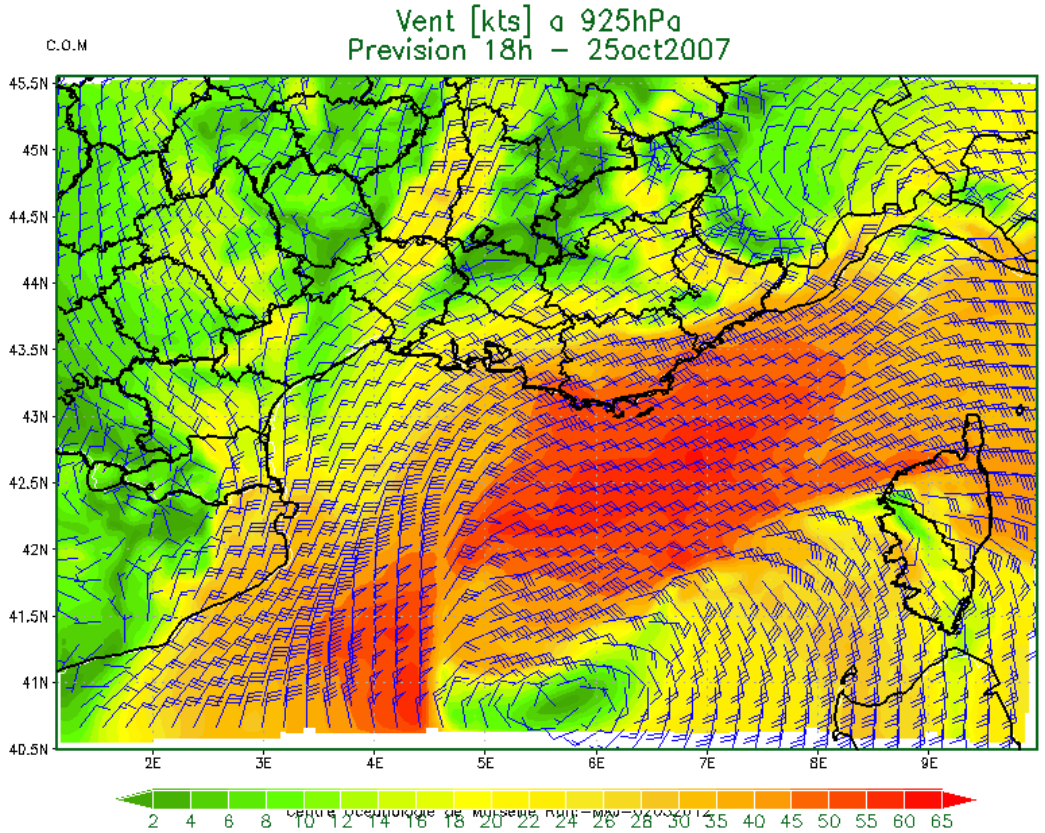

Figure 86: Wind (kts) at 925hPa on 25 Oct 2007 at 18h

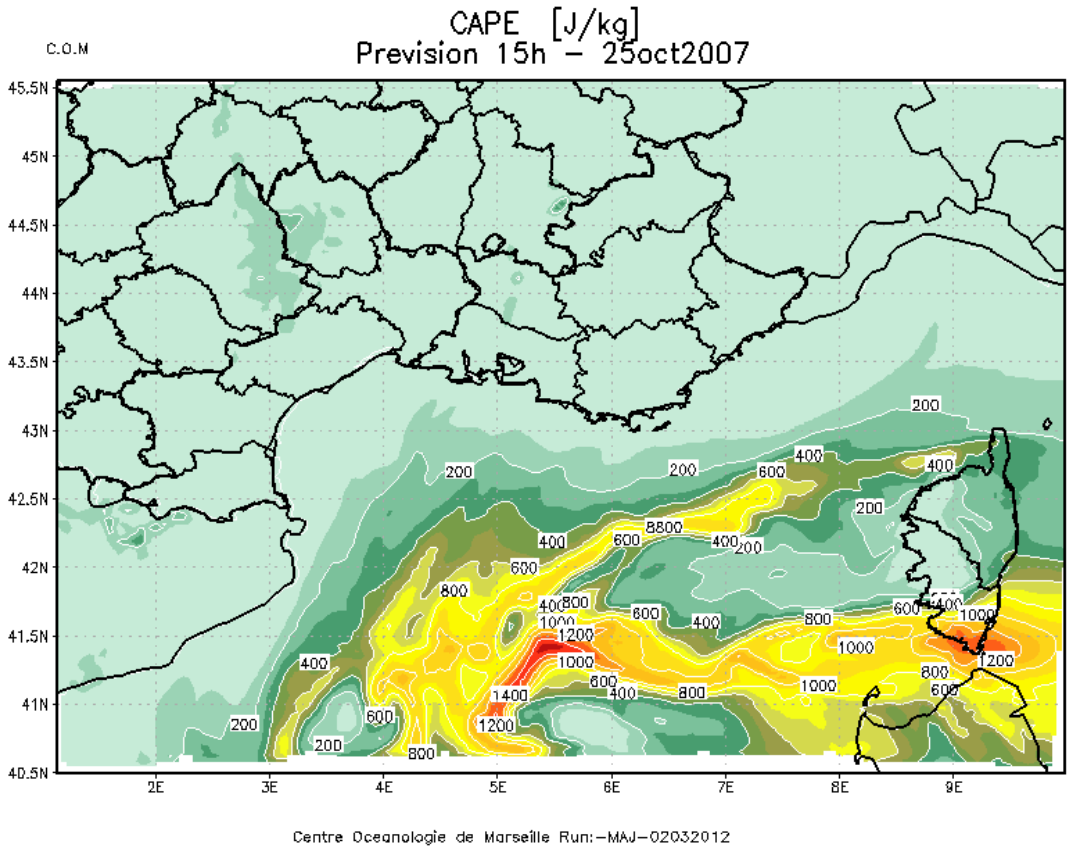

Figure 87: CAPE (Convective Available Potential Energy) (J/Kg) on 25 Oct 2007 at 15h

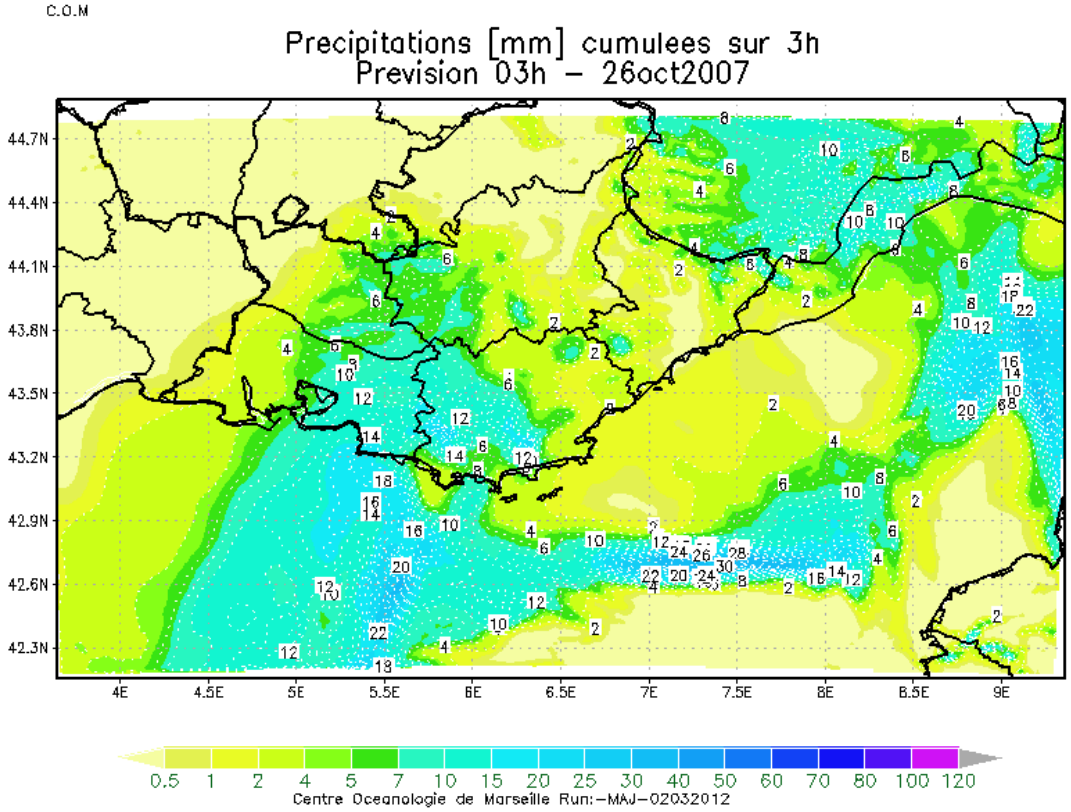

Figure 88: 3h cumulative precipitation (mm) on 26 Oct 2007 at 03h

5.4.1.3 Hydrodynamic (MARS3D-RHOMA) and biogeochemical (ECO3M-MASSILIA) situation

Rain influencing the surface layer has little effect on hydrodynamics. On the other hand, a strong increase in urban river flows occurs during this event (Figure 12). Nitrate discharges are clearly visible (Figure 89). The most important ones are located near Cortiou, and others at the level of the Autonomous Port (Aygalades) and near some storm drains. This corresponds well with the flows measured at different points during the event (Figure 12).

The increase in chlorophyll (relatively small) associated with these nitrate inputs is in agreement with the MERIS 1 km OC5 image of 27 October 2007 (Figure 90). This result suggests that phytoplankton in the environment may be limited by something other than nitrogen, perhaps phosphorus or some contaminants. It is also possible that the low growth in autumn is related to the season (lack of light) because inputs of the same order of magnitude in spring induce much higher simulated phytoplankton growths.

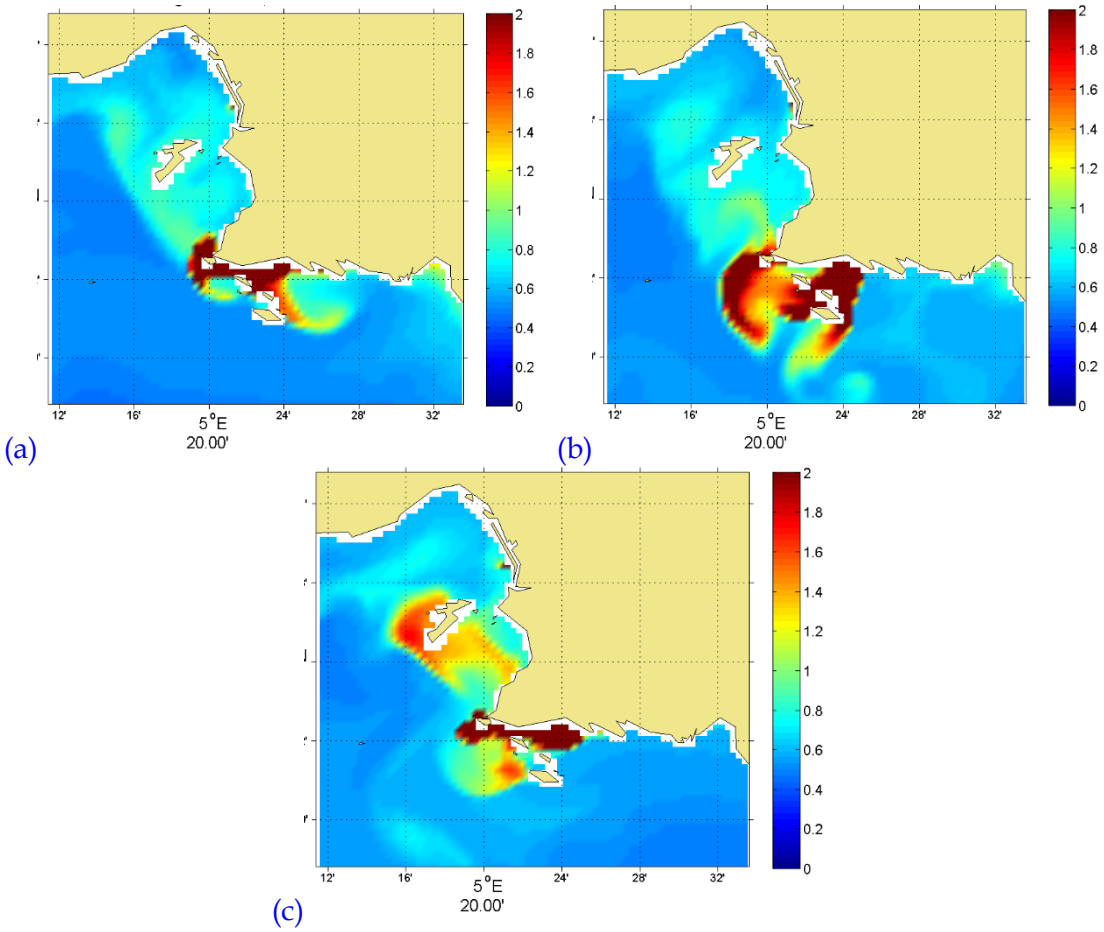

Figure 89: Simulated surface nitrate concentrations (µmol/L) on (a) 25, (b) 26 and (c) 27 October, 2007 after a rain event.

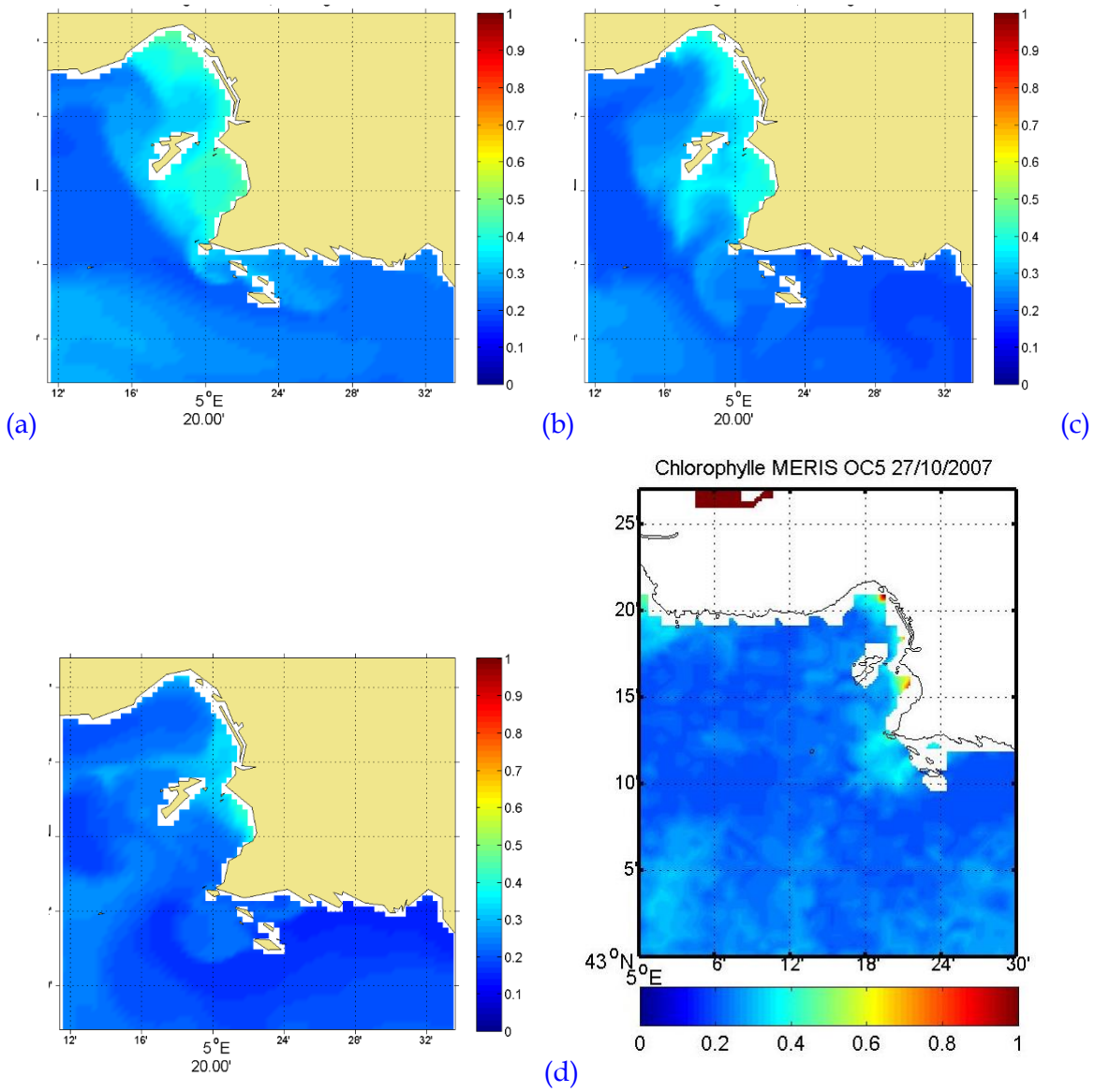

Figure 90: Modelled surface chlorophyll (µg/L) on (a) 25, (b) 26, and (c) 27 October 2007 after a rain event. (d) Comparison with Chl concentrations from the MERIS OC5 image from 27 Oct.

5.4.1.4 Hydrosedimentary situation

The rain event of 25-26 October 2007 was concomitant with the arrival of a short but intense swell episode, with strong action in the Cortiou area on the morning of 26 October (Figure 91). This episode induced erosion very close to the coast, the eroded SS being mainly redeposited further down the slope, in the same area. The end of this episode also impacted the southern harbour later in the night of 26 to 27 October, inducing erosion very close to the coast with very rapid sedimentation. The rain episode induced a clearly visible plume at the surface, with concentrations exceeding 50 mg/L at the height of the discharge (Figures 92 and 93). This plume was oriented along a south-westerly direction on 26 October at midnight, passed south at noon, allowing the plume to spread with significant concentrations of SS (>20 mg/L) beyond Ile Riou. This plume rapidly diluted, with a transfer of the SS towards the west (Figure 94). High concentrations near Cortiou and to a lesser extent in the southern harbour were observed, but due to the swell episode it was difficult to distinguish the part of the sediment that was resuspended from those sediments that were brought by the rain (Figure 94).

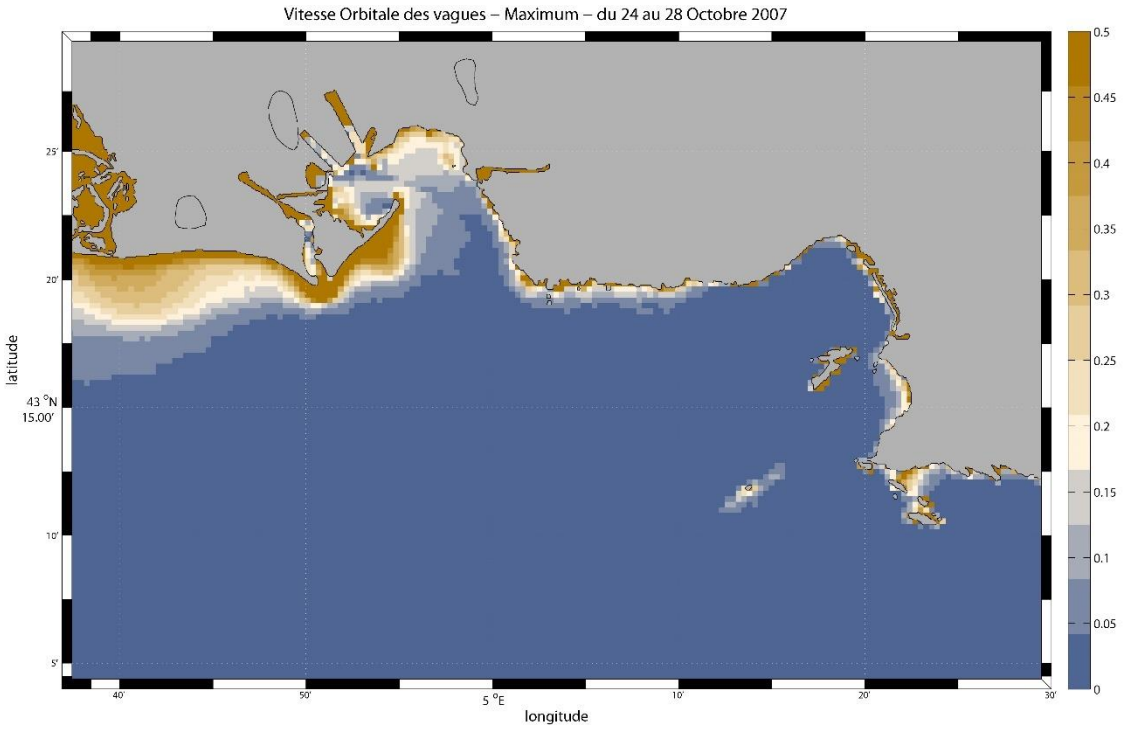

Figure 91: Spatial distribution of maximum orbital wave speeds (m/s) at the sea bed between 24 and 29 Oct 2007

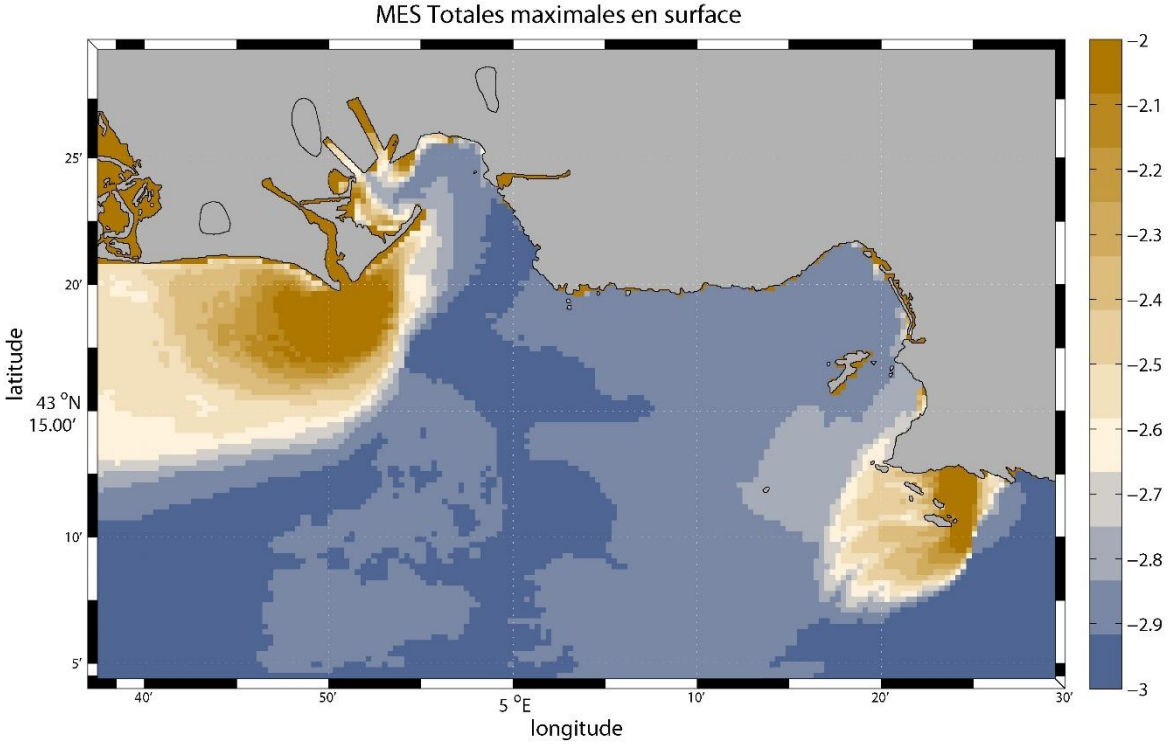

Figure 92: Spatial distribution of maximum surface concentrations of fine sediments between 24 and 29 Oct 2007(g/L, log scale : -2 = 10 mg/L, -3 = 1 mg/L)

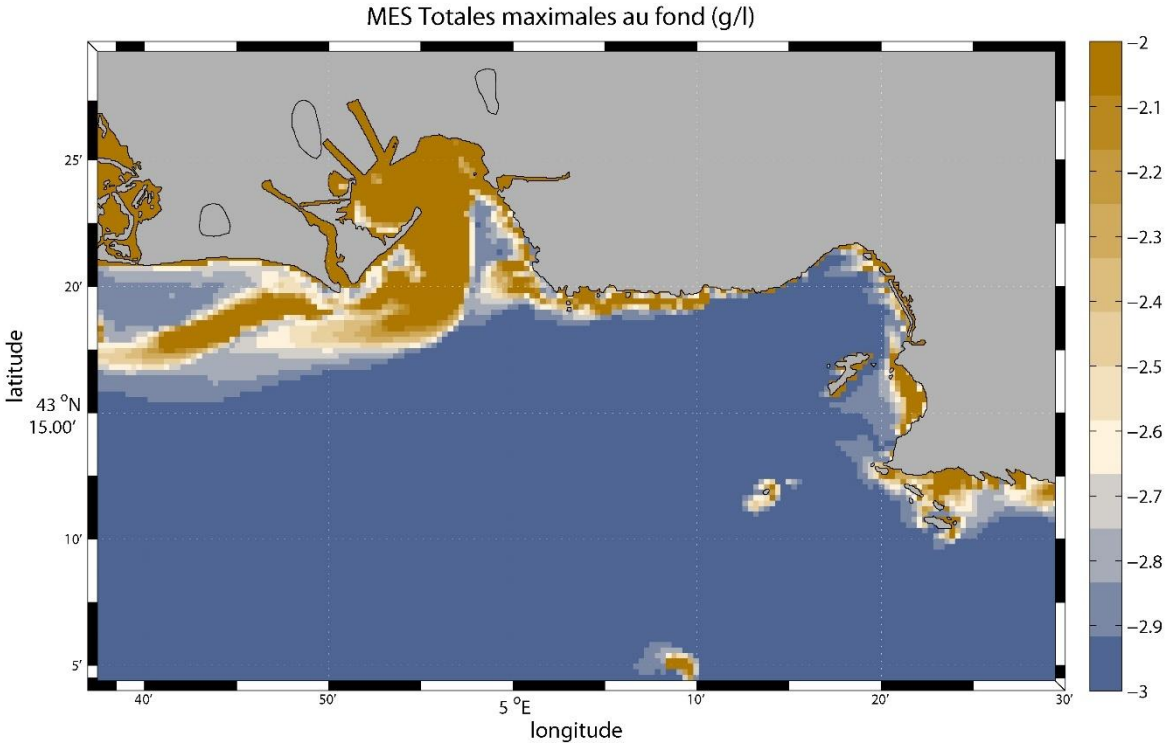

Figure 93: Spatial distribution of maximum fine sediment concentrations at the sea bed between 24 and 29 Oct 2007(g/L, log scale: -2 = 10 mg/L, -3 = 1 mg/L).

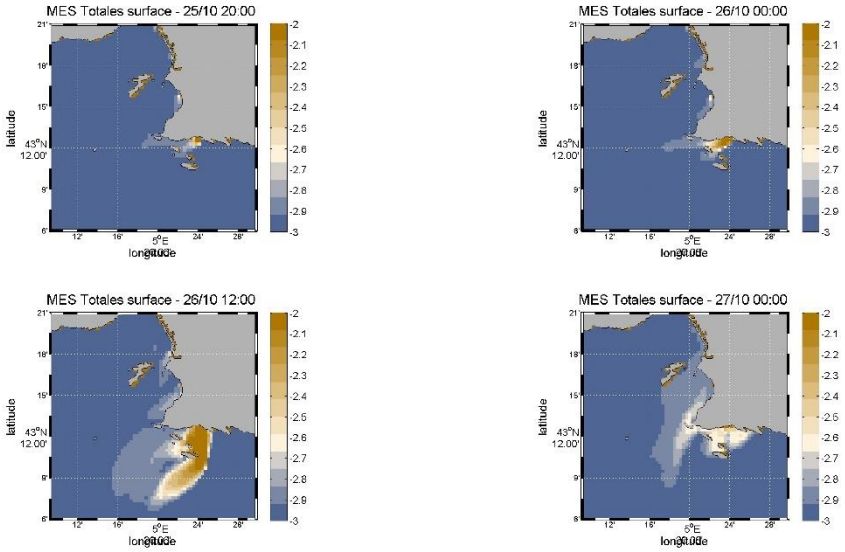

Figure 94: Spatial distribution of surface concentration of fine sediments between 25 Oct and 27 Oct 2007 (g/L, log scale: -2 = 10 mg/L, -3 = 1 mg/L).

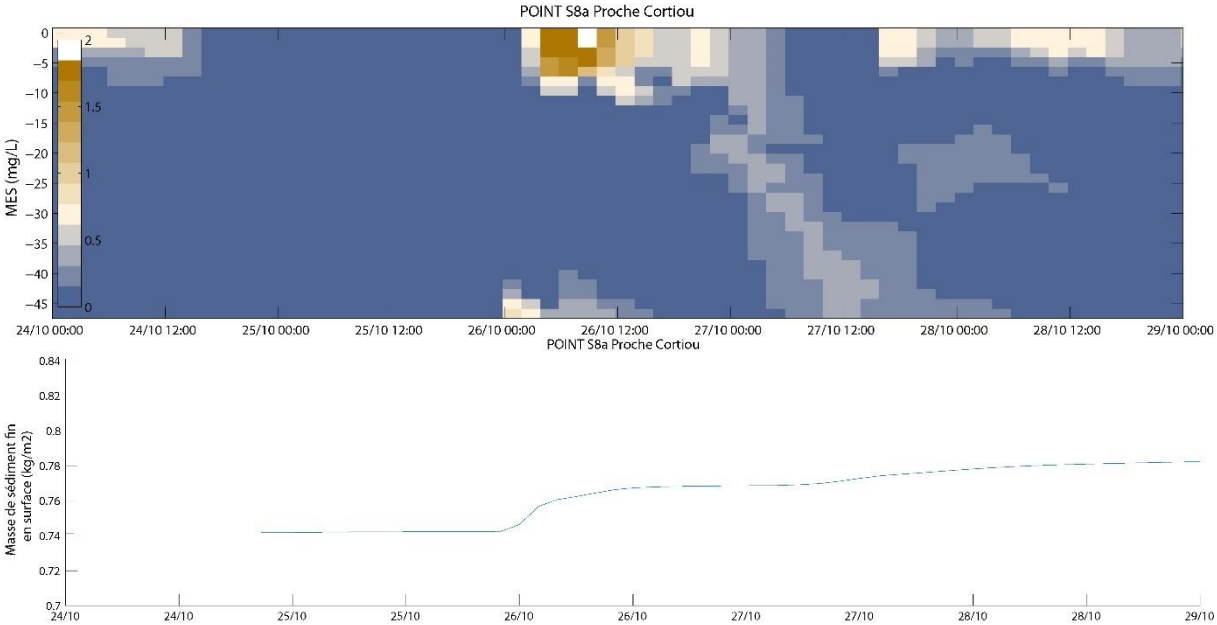

Figure 95: SS dynamics in the water column (upper panel, mg/L, log scale: 1=10 mg/L, 2=100 mg/L) and sediment dynamics (lower panel) at reference point S8a located near the Cortiou outflow between 24 and 29 Nov 2007

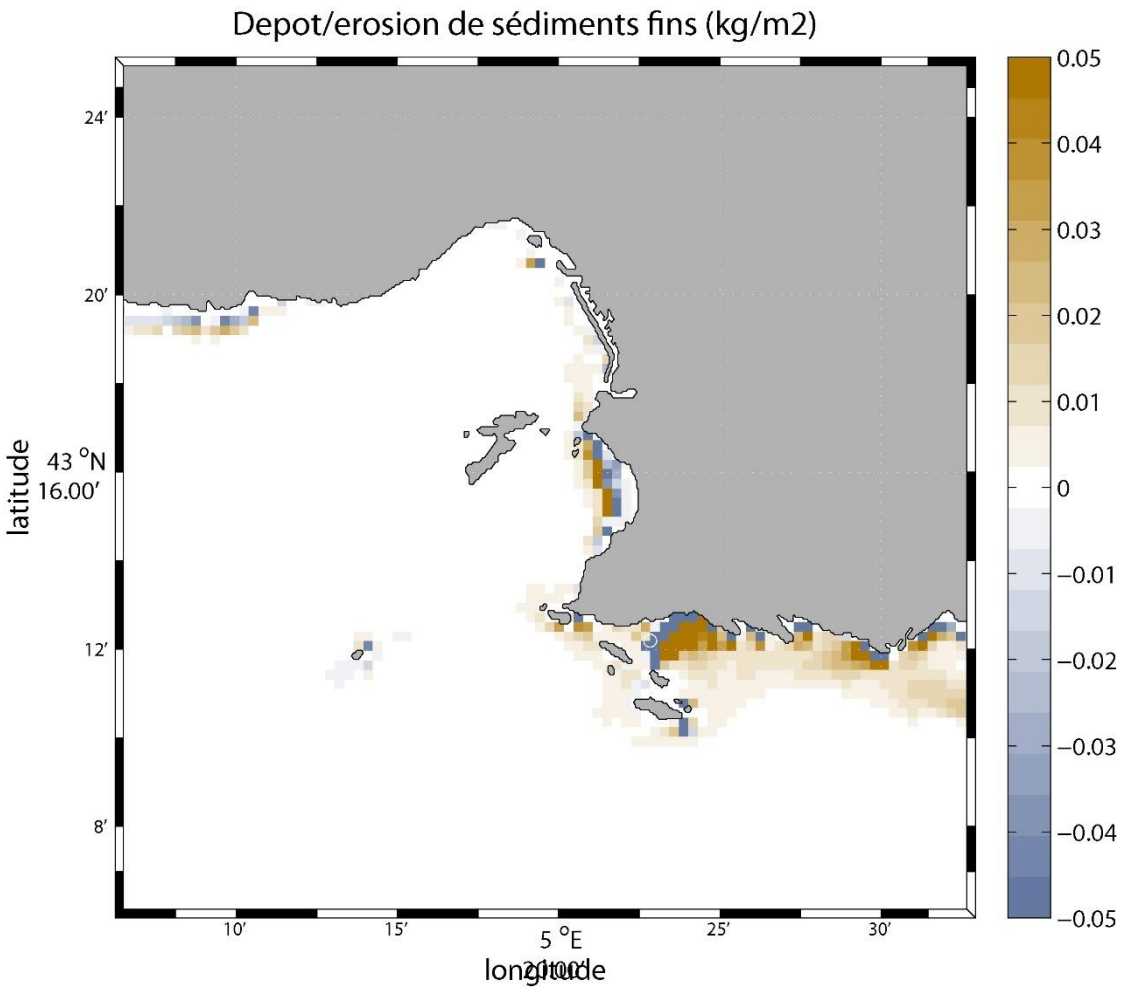

Figure 96: Sedimentation/erosion of fine sediments between 24 and 29 Nov 2007 (kg/m2).

More precisely, Figure 95 allows us to analyse the dynamics of the plume in the area of the discharge. On 26 October at midnight, the swell event involves localised erosion higher up on the slope, and the eroded sediments are advected towards the observation point, involving a well-marked deposition. The rainfall event is marked by two stages: heavy SS, brought by the storm-related rain, deposit near the discharge point and contribute to the accretion of the area (Figures 95 and 96). The lighter SS constitutes as part of a surface plume (5 to 10 m below the surface) which migrates with the surface currents.

5.4.1.5 CB153 contaminant

The situation on 25 October 2007 with a rain event in the afternoon caused an arrival of contaminant in the area and a plume of Cortiou that was more concentrated and extended than at low tide (Figures 97, 98); its life span was short (observed maximum on 26 October, all morning). Discharges in the northern harbour are also visible (Figures 97, 98). At the bottom, high concentrations are observed along the coast (Figure 99), largely due to the inputs with some erosion in the southern harbour and a resuspension episode in the Cortiou area a few hours before the rain that is redeposited during the same day. Most of the mass discharged at Cortiou was deposited in the nearby area, but the model simulated erosion at the coast during the night of 25 to 26 October, followed by progressive deposition a little further offshore (Figures 100 and 101). In the southern harbour, the model simulates erosion on the afternoon of 26 October which is redeposited in the same area. The final balance at the end of the day on 27 October shows a residual deposit (green curves in Figure 100: negative value at the end of the period) in all zones, which means that part of the input was deposited locally. In Marseilles harbour, the input from the rivers, particularly at Cortiou, led to a significant increase in the stock of PCBs in the water which was still present at the end of the period.
The biogeochemical conditions (concerning the enrichment of particles in organic matter) were not greatly modified by the input; they therefore did not impact the speciation of PCBs which continued to be governed mainly by the quantity of particles in suspension. This rainfall event only induced a small phytoplankton bloom (Figure 90) even though the nitrate inputs were substantial (Figure 89). This result suggests that phytoplankton may be limited in their growth by phosphates or light.

(a) : Dissolved at the surface (pg/L)

(b): Particulate at the surface (pg/L)

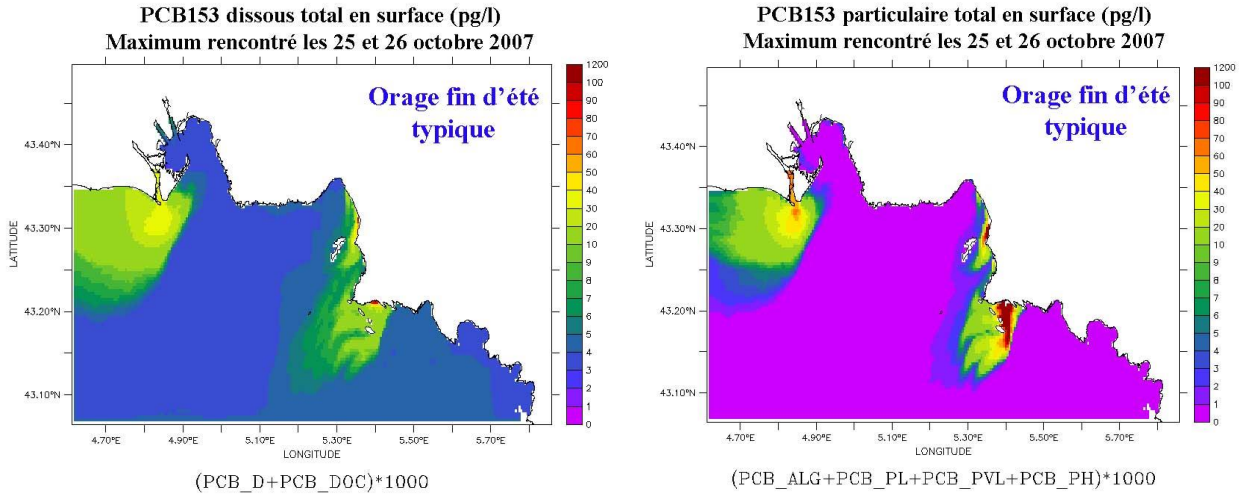

Figure 97: Maximum concentrations at the surface (pg/L) between 25 and 27 Oct 2007

(a) Dissolved at the surface (pg/L)

(b) Particulate at the surface (pg/L)

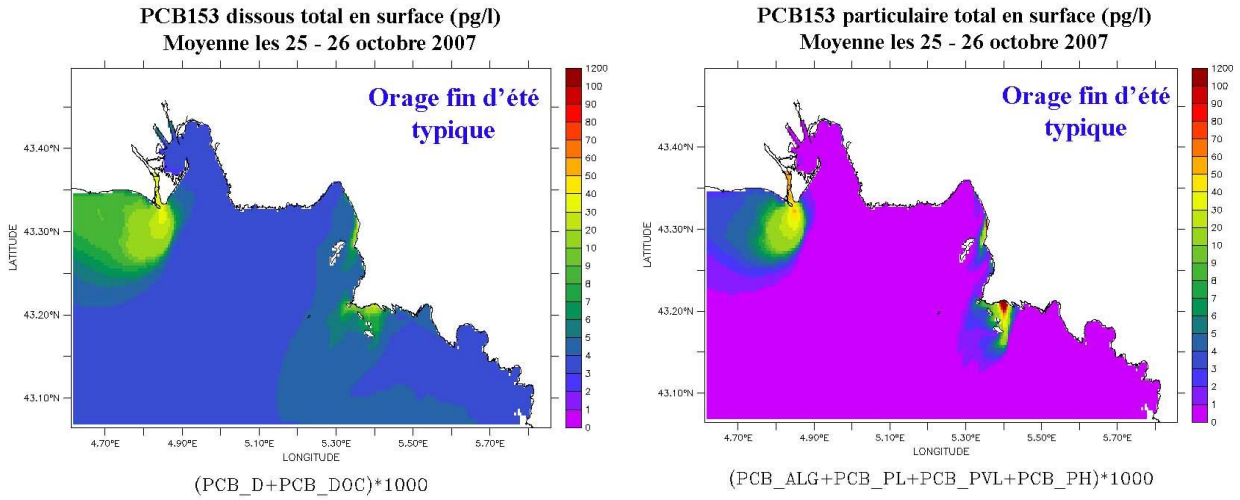

Figure 98: Mean concentrations at the surface (pg/L) between 25 and 27 Oct 2007

Particulate at the surface (ng/g)

Particulate at the sea bed (ng/g)

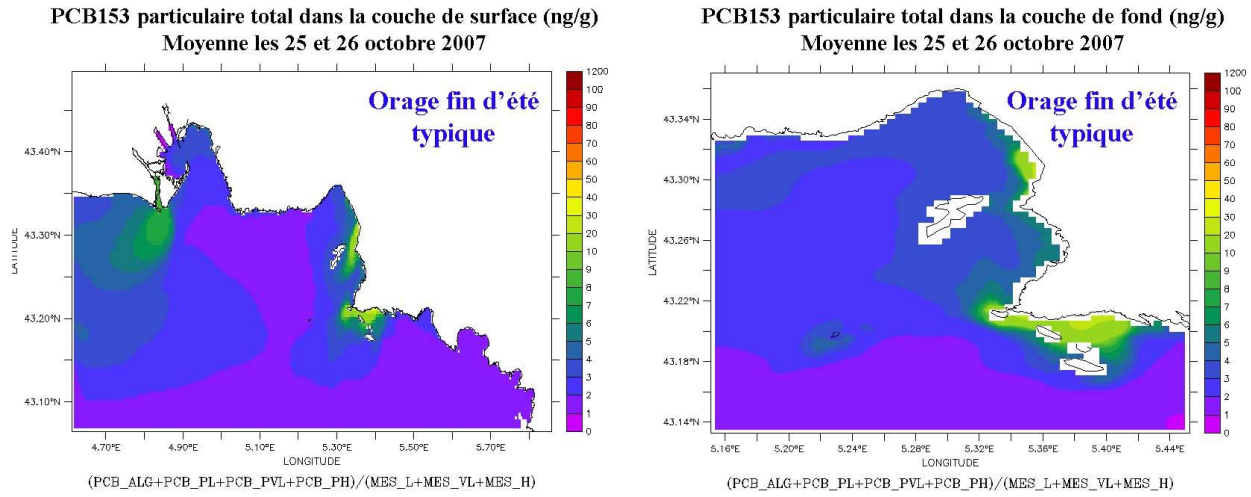

Figure 99: Mean CB153 particulate concentrations (ng/g) at the surface and sea bed between 25 and 27 Oct 2007

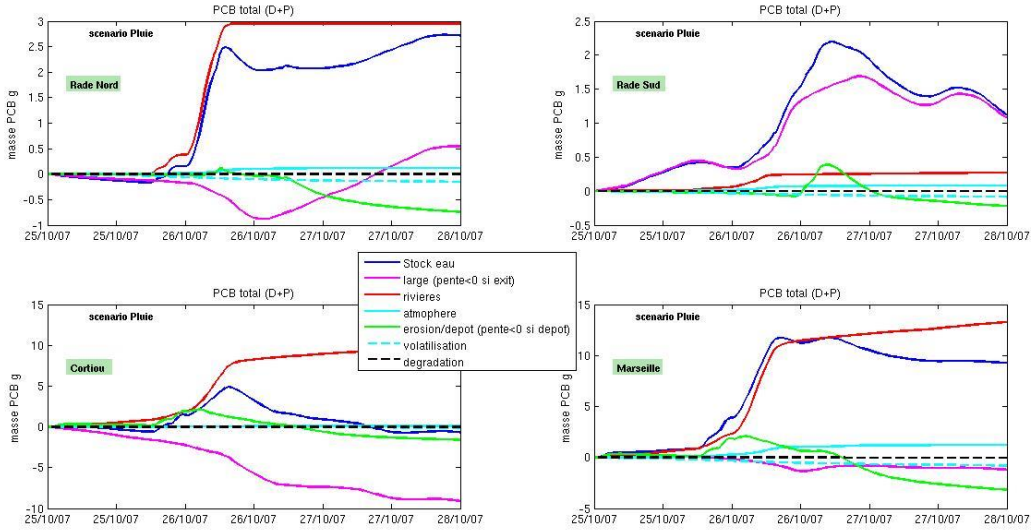

Figure 100: Variation in total CB153 stocks in the water column over the period and in each area (depicted in Figure 15), associated with variations in concentration due to each process: "open sea": input/output at boundaries; "rivers": input at the coast; "atmosphere": dry deposition and rainfall; "erosion/deposition"; "volatilisation" and "degradation". (if slope >0 = positive change in concentration= contaminant input, and vice versa)

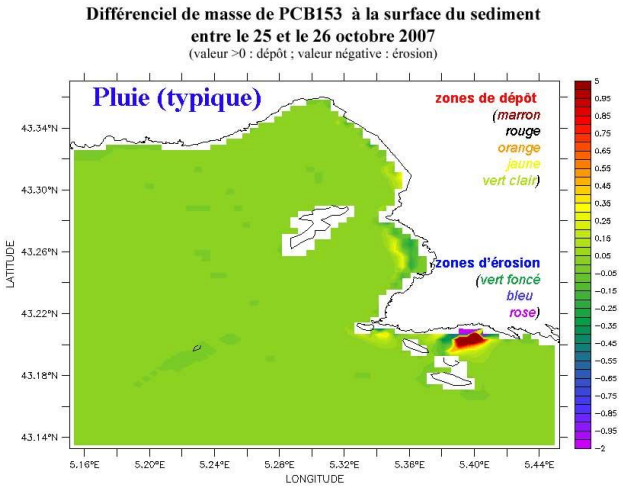

Figure 101: Erosion and deposition zones after the typical rain event on 25 Oct 2007

5.4.2 Autumn rains of 2008

5.4.2.1 Météo France data from the Marseille observatory

After the numerous rains in June 2008, not a drop of water was recorded until September at the Observatory (personal notes: rain on the 19th and 20th of July and light rain during the night of the 11th to the 12th of September <5mm). In September, the rainfall was still very low. The first end-of-summer thunderstorm finally arrived on 7 and 8 October 2008, but rainfall was only around 20 mm/d/m². Rainfall in excess of 30 mm/d/m² then appeared at the end of October and beginning of

November 2008. These rains are not well reproduced in the models, but the mid-December event can be studied.

Table 12

Dates with rainfall >5 mm quantified as mm of rain per day and m²

Date	mm/m²/d
20080918	6
20080926	5
20081007	19.8
20081008	21
20081022	31.,8
20081028	31.4
20081102	36.8
20081103	10
20081104	34
20081123	8
20081127	14.2
20081129	9.4
20081209	36.,6
20081213	7.2
20081214	59
20081215	14.6

5.4.2.2 Atmospheric simulation

A disturbance moved across the North Atlantic from Iceland to the south of the British Isles in the first part of the night on Friday 12 December (Figure 102). It approached the Bay of Biscay and Spain late Friday night. As it moved eastwards, a secondary disturbance developed in its southern part during the night of Saturday to Sunday 14 over the Iberian Peninsula.
Ahead of it, the weak westerly flow will undulate weakly over the western Mediterranean basin and then gradually turn south. The Spanish disturbance will rapidly deepen in the second half of the night over this sector. The cyclogenesis is reinforced by a significant temperature gradient between the air behind and above the disturbance. Air over the sea was at 10 °C (Figure 103) while the air mass over the rest of the country was at around 4/6 °C.

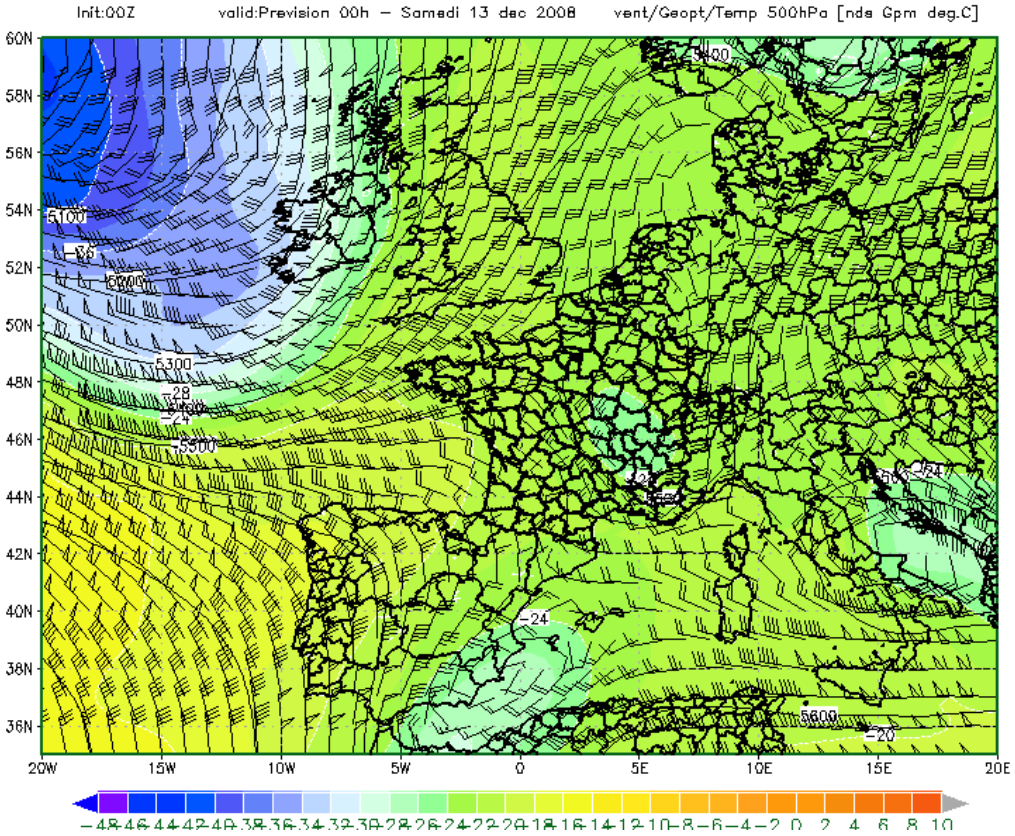

Figure 102: Wind (kts), geopotential (deca gpm), and temperature (°C) at 500hPa on 13 Dec at 00h.

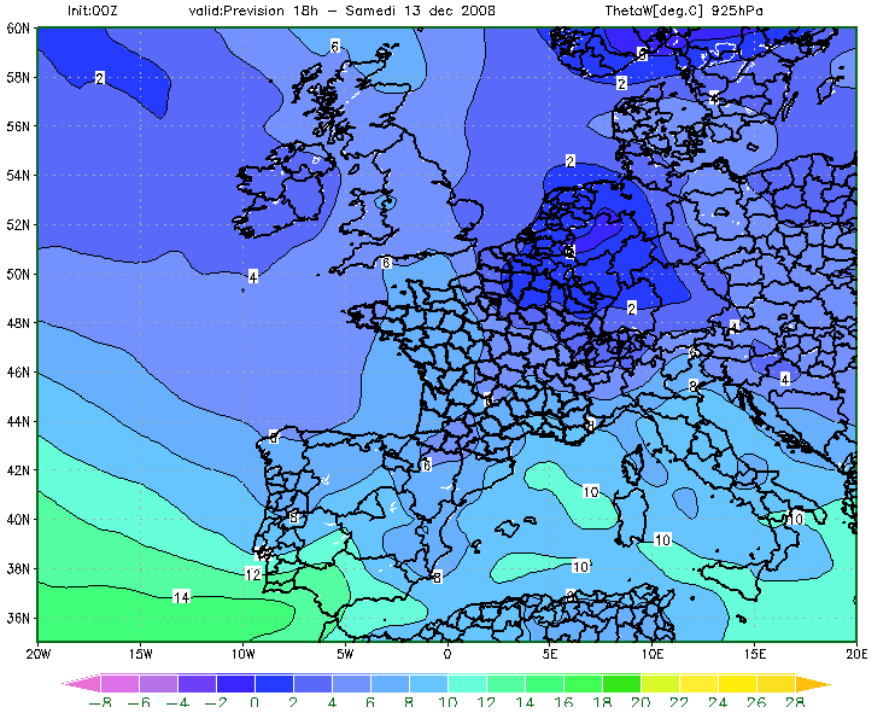

Figure 103: Pseudo-adiabatic potential temperature (°C) at 925hPa on 13 Dec 2008 at 18h.

At the beginning of the day on Sunday, the axis of the disturbance moved into the Gulf of Lion, causing a shift in the wind in the lower layers to the south, contributing to the arrival of humid air over the Rhone valley.
Below the main axis of the air flow, nuclei with vertical velocities developed at sea and over the department (Figure 104). These cores become more intense over the first Provençal mountains.

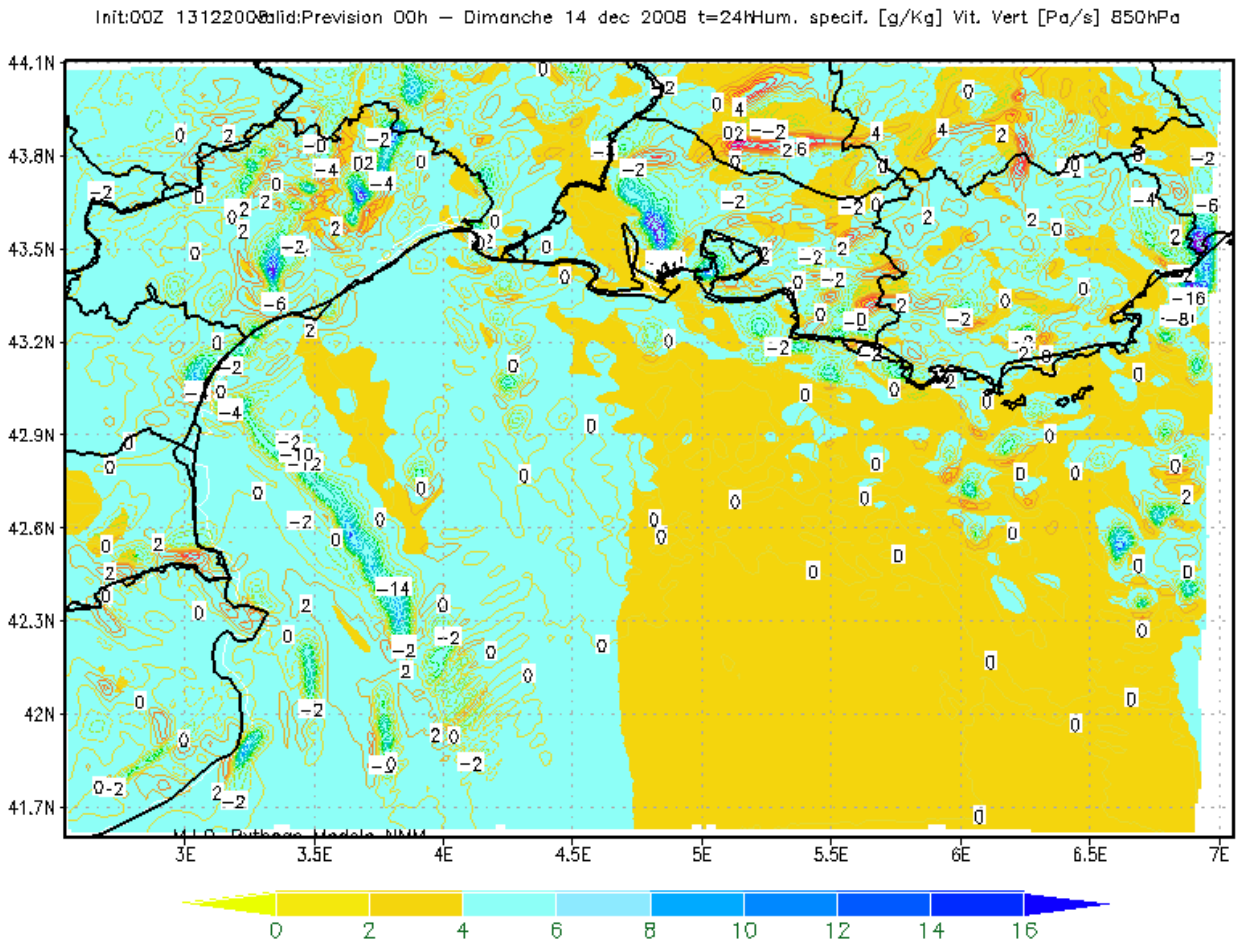

Figure 104: Specific humidity (g/Kg) and vertical velocity (Pa/s) at 850hPa on 14 Dec 2008 at 00h.

In the axis of the front off the Bouches du Rhône, a low-level instability developed on the morning of 14 December and overflowed onto the coast of Marseilles, where thunderstorms sometimes occurred (Figure 105). The most significant accumulations occurred in the baroclinic zone, clearly visible in the Thetaw 850hPa field.
At certain points, the quantities of water exceeded 40 mm over 3h with a more active zone at sea in the southern part of the front.

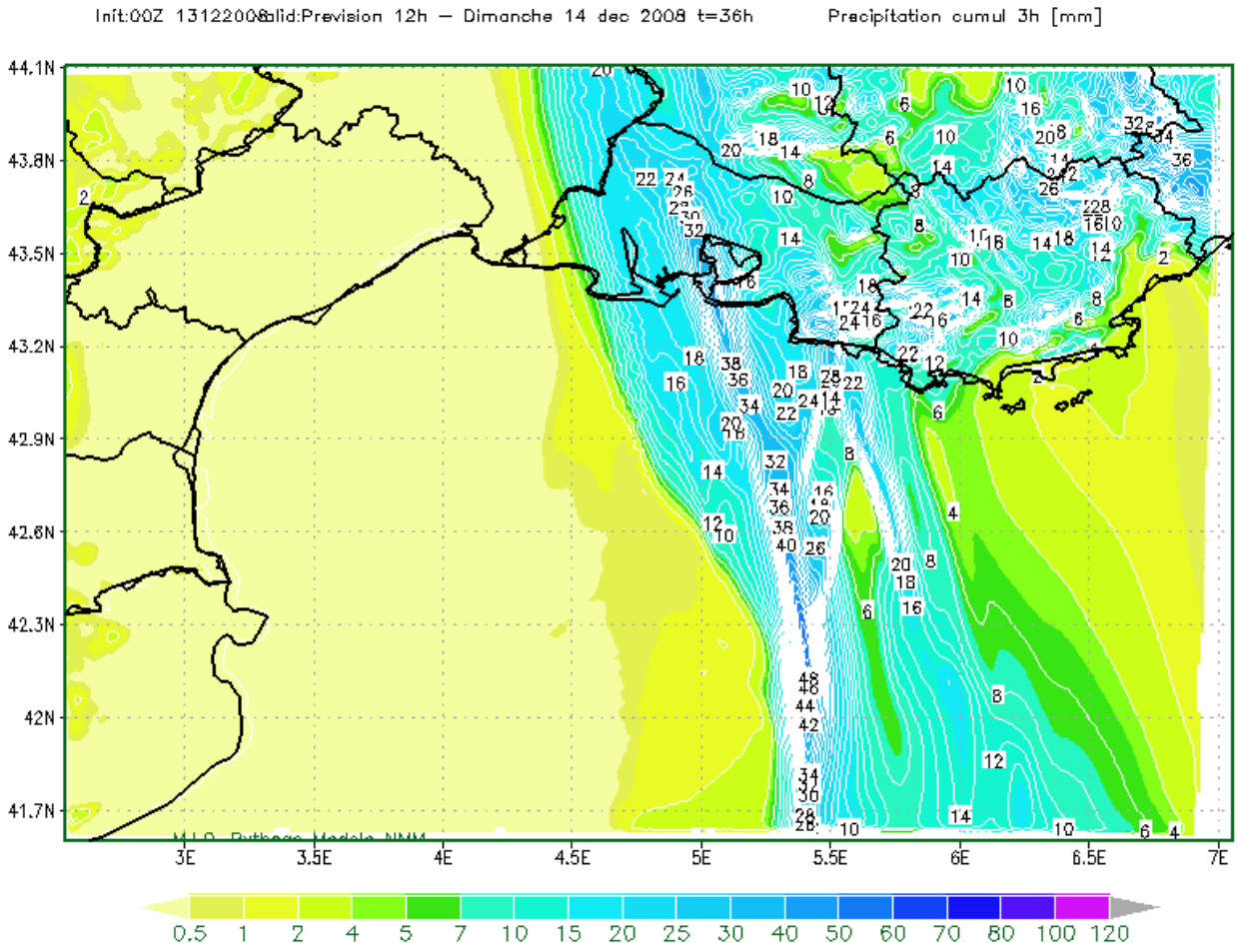

Figure 105: 3h cumulative precipitation (mm) on 14 Dec 2008 at 12h.

During the day on 14 December, the rain front moved eastwards, first affecting the Var and then the Alpes Maritimes. The rainfall in Marseille occurred mainly between 7 am and 4 pm with a maximum intensity around 12 pm (local time).

5.4.2.3 Hydrodynamic (MARS3D-RHOMA) and biogeochemical (ECO3M-MASSILIA) situation

The rainfall that occurred between 9 and 15 December 2008 led to high flow volumes in urban rivers. On 15 December 2008, the salinity signature of these high water discharges via urban rivers is very visible in the Bay of Marseille on the surface salinity map (Figure 106). At SOLEMIO station, the model and *in situ* salinity measurements show a drop in salinity (to about 37.2) in the top 3m (Figure 107). The discharges from the urban rivers of the southern harbour (Huveaune and Bonneveine) therefore seem to have an impact on salinity that extends all the way to the SOLEMIO station. This is also the case in terms of temperature, as these discharges from the rivers seem to be characterised by fairly low temperatures (Figure 108).

From a biogeochemical point of view, the discharges from urban rivers are very rich in nutrients (NO3 and PO4), but they occur at a time of year when nutrient concentrations are already very high (Figure 109 and 110). As winter mixing has already taken place, nutrient concentrations in the water column of the Bay of Marseille are homogeneous and high.

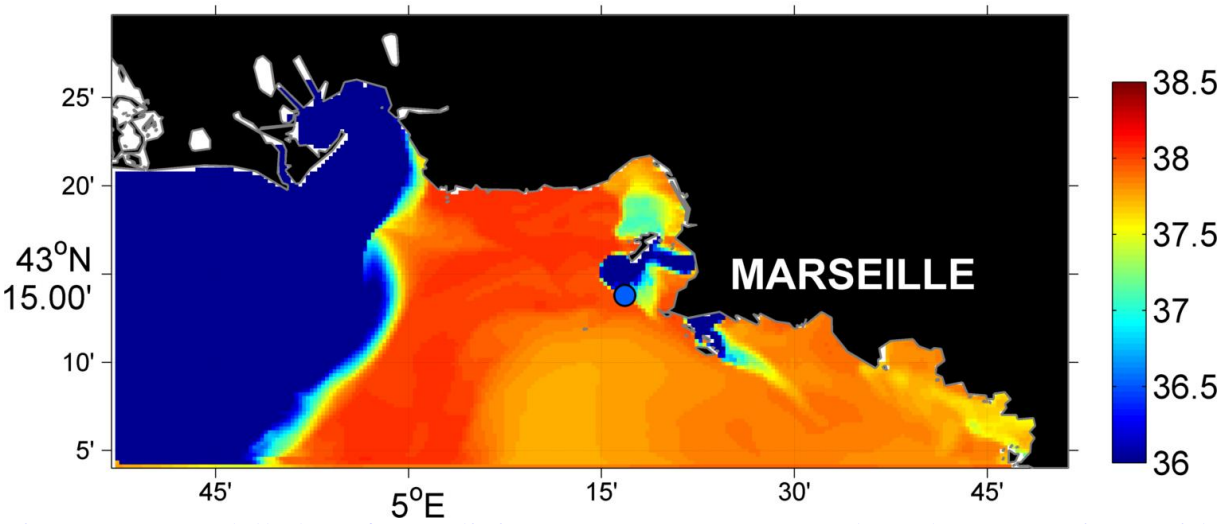

Figure 106: Modelled surface salinity on 15 Dec 2008 at 12h and a comparison with SOMLIT station (shown as a circle with the fill colour corresponding to the *in situ* salinity measured at the station).

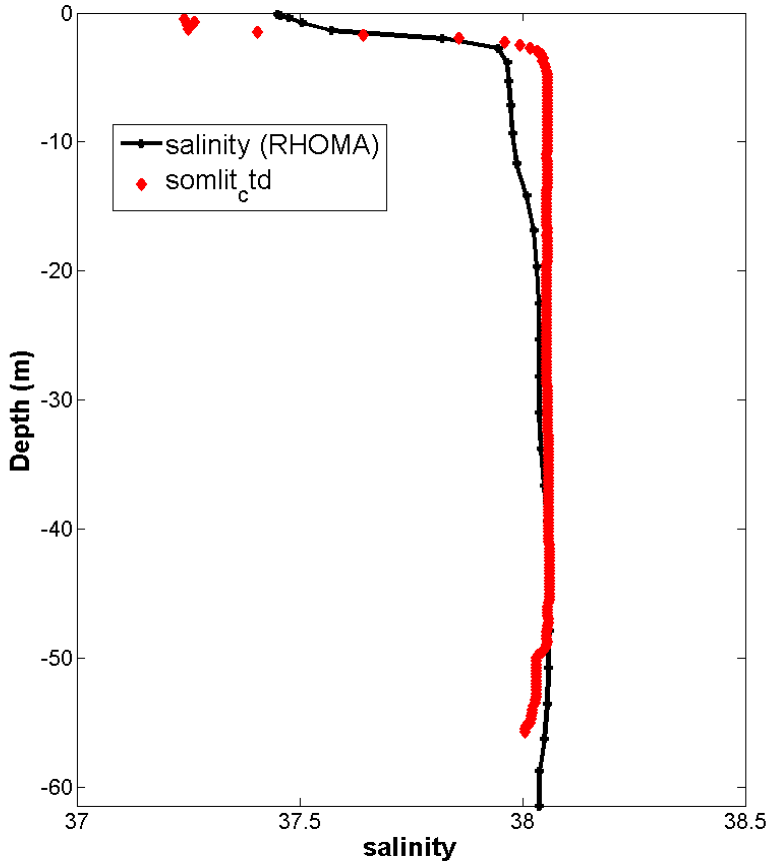

Figure 107: Vertical salinity profile at SOLEMIO on 15 Dec 2008 comparing the model output (black line) to the measured salinity (from a CTD, in red).

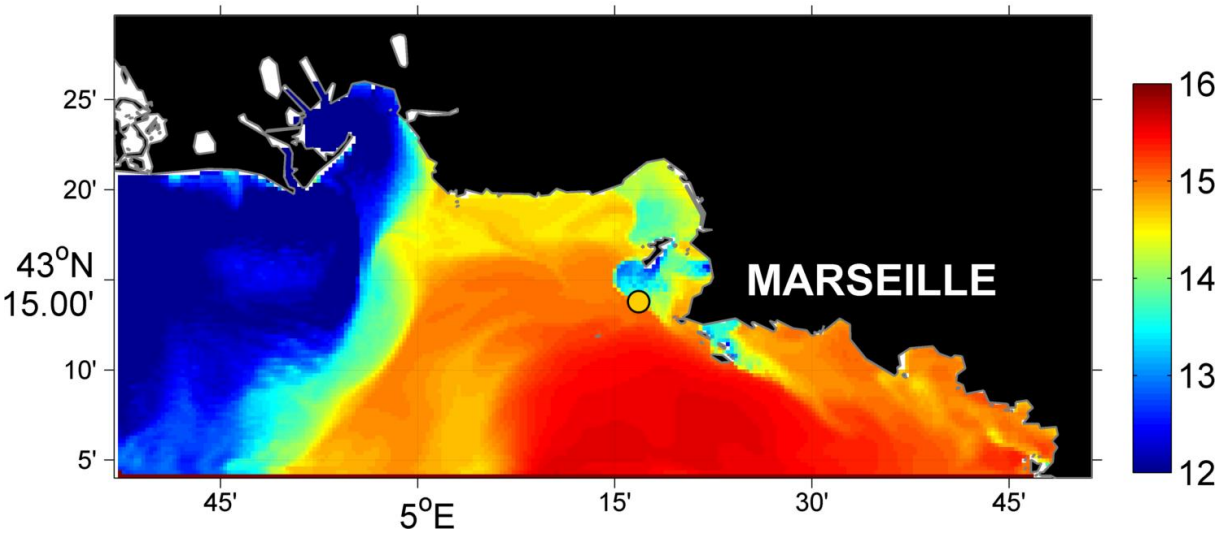

Figure 108: Modelled SST (°C) on 15 Dec 2008 at 12h and the comparison with SOMLIT station (shown as a circle with the fill colour corresponding to the *in situ* temperature measured at the station).

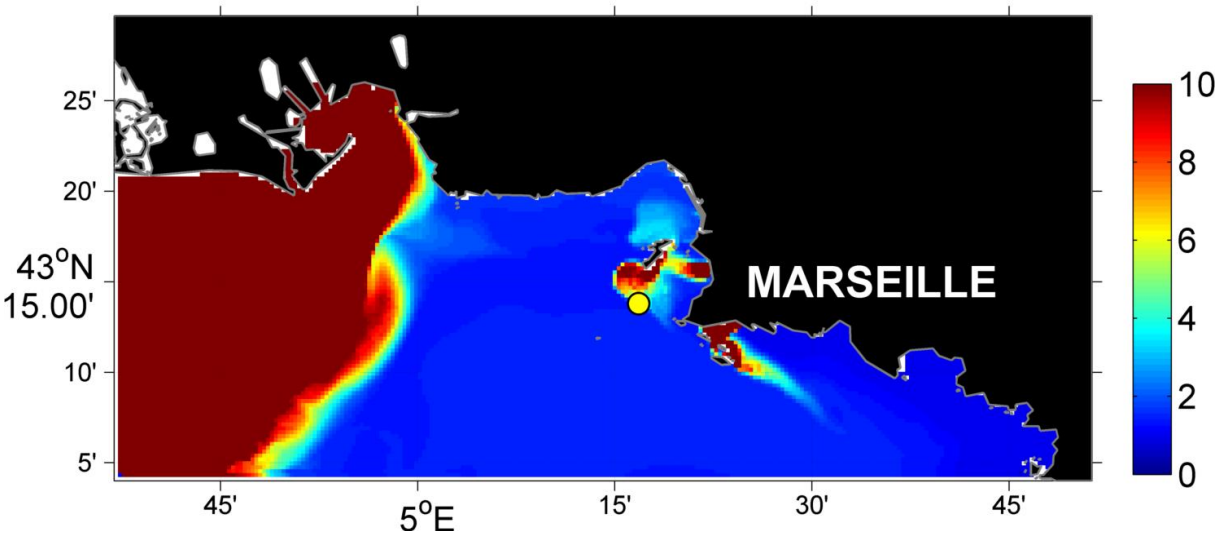

Figure 109: Modelled surface nitrate (µmol/L) on 15 Dec 2008 at 12h and the comparison with SOMLIT station (shown as a circle with the fill colour corresponding to the *in situ* nitrate concentration measured at the station).

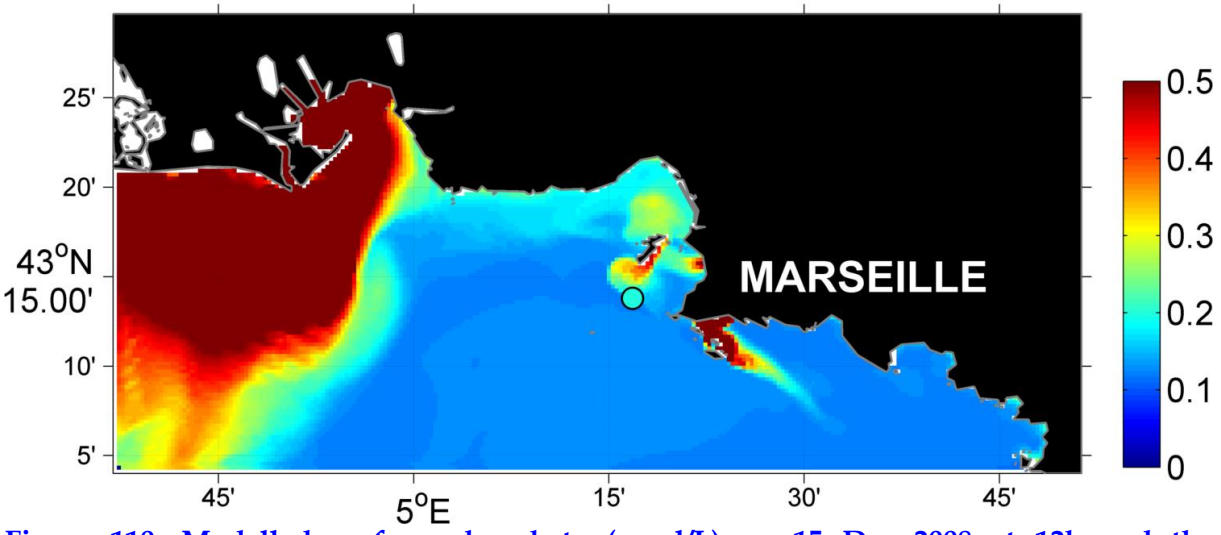

Figure 110: Modelled surface phosphate (µmol/L) on 15 Dec 2008 at 12h and the comparison with SOMLIT station (shown as a circle with the fill colour corresponding to the *in situ* phosphate measured at the station).

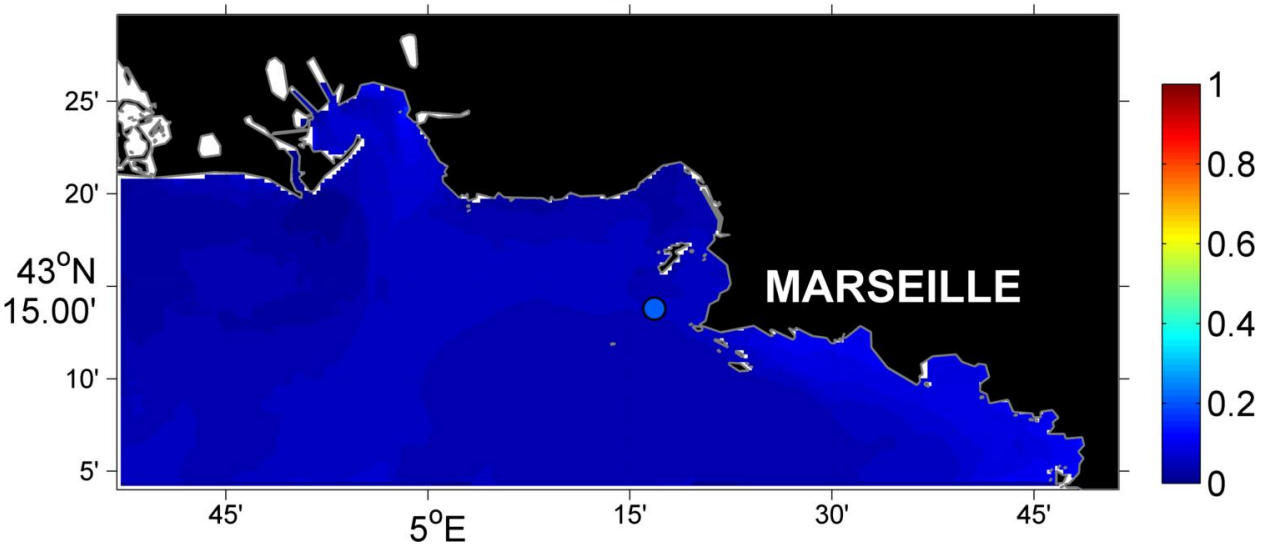

Figure 111: Modelled surface chlorophyll (µg/L) on 15 Dec 2008 at 12h and the comparison with SOMLIT station (shown as a circle with the fill colour corresponding to the *in situ* chlorophyll measured at the station).

Phytoplankton is therefore not limited by nutrients but by light during this winter period, which explains why there is no phytoplankton production associated with these nutrient-rich discharges (Figure 111). On the other hand, high concentrations of particulate organic carbon (POC) were observed at SOMLIT station (Figure 112).

In conclusion, even though at this time of year the high inputs from urban rivers during rainfall events have little impact on the biogeochemical functioning of the bay, significant quantities of particulate organic matter are discharged into the bay.

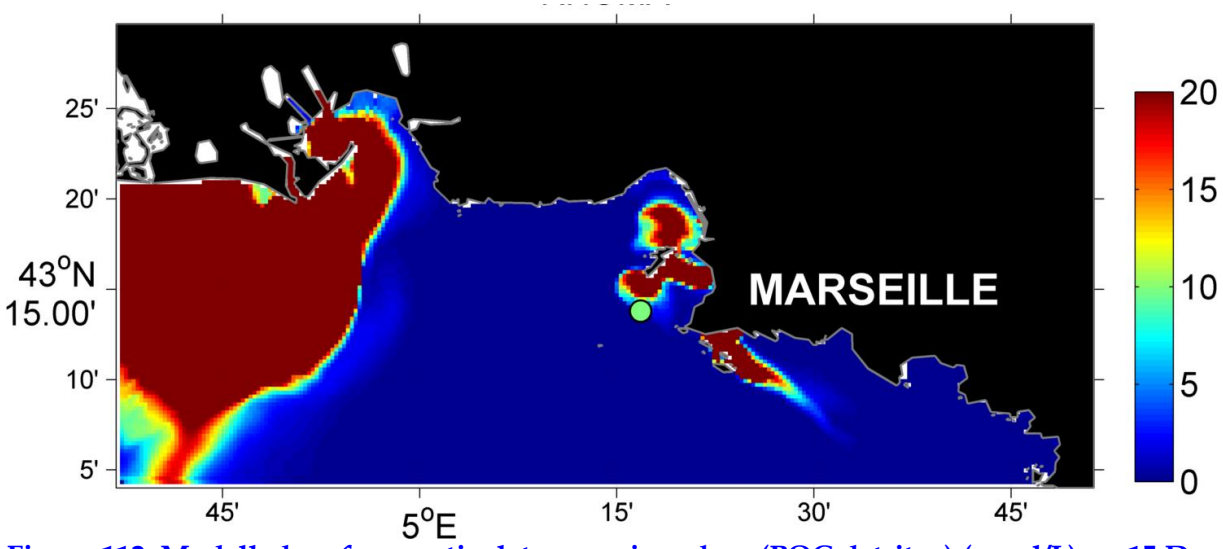

Figure 112: Modelled surface particulate organic carbon (POC detritus) (µmol/L) on 15 Dec 2008 at 12h and the comparison with SOMLIT station (shown as a circle with the fill colour corresponding to the *in situ* measurements).

5.4.2.4 Hydrosedimentary situation (MARS3D-RHOMA)

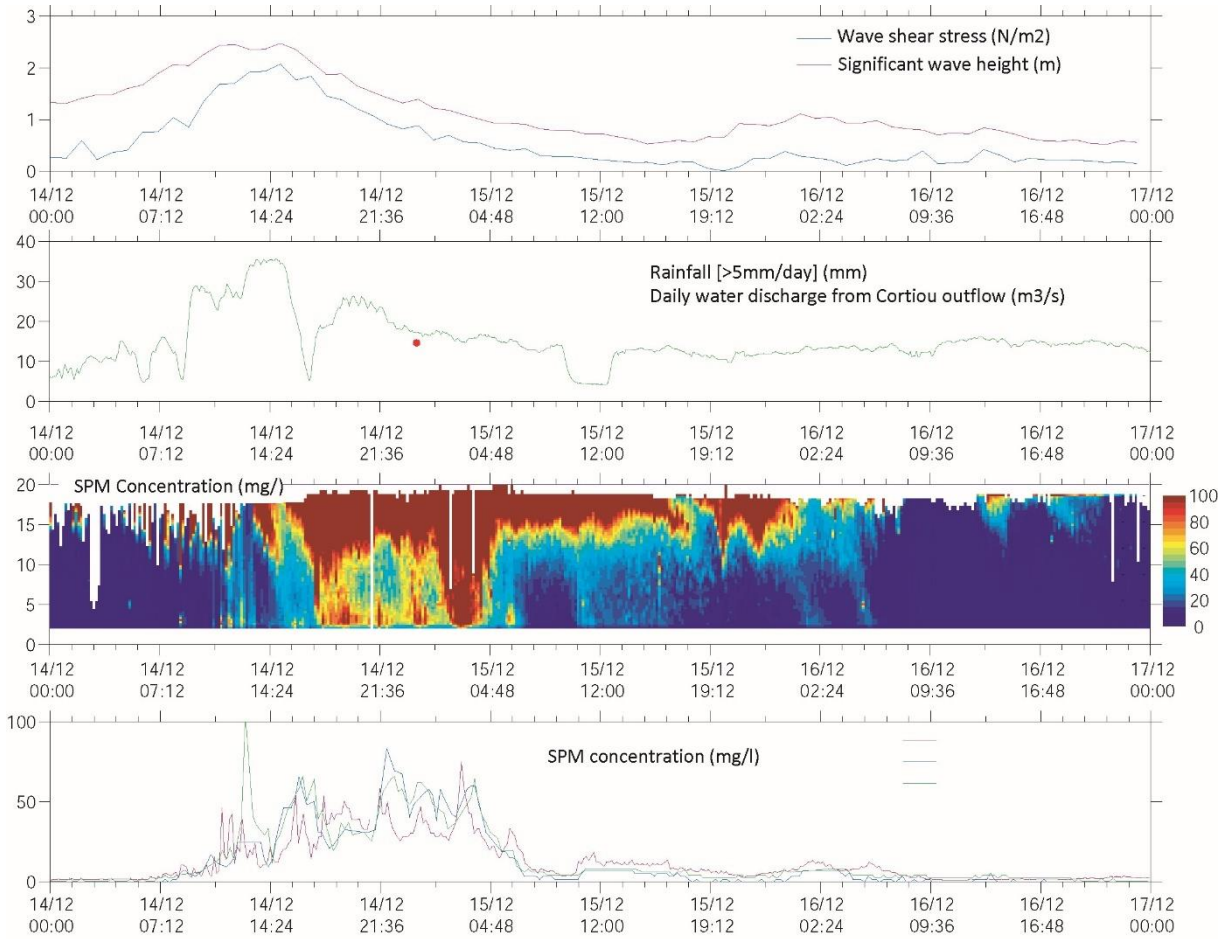

Figure 113: Hydrosedimentary measurements at FRAME station during the rainy episode at the end of December 2008: Waves, inflow from Cortiou, suspended matter estimated from the acoustic backscatter intensity, suspended matter near the bottom measured by the optical turbidimeters.

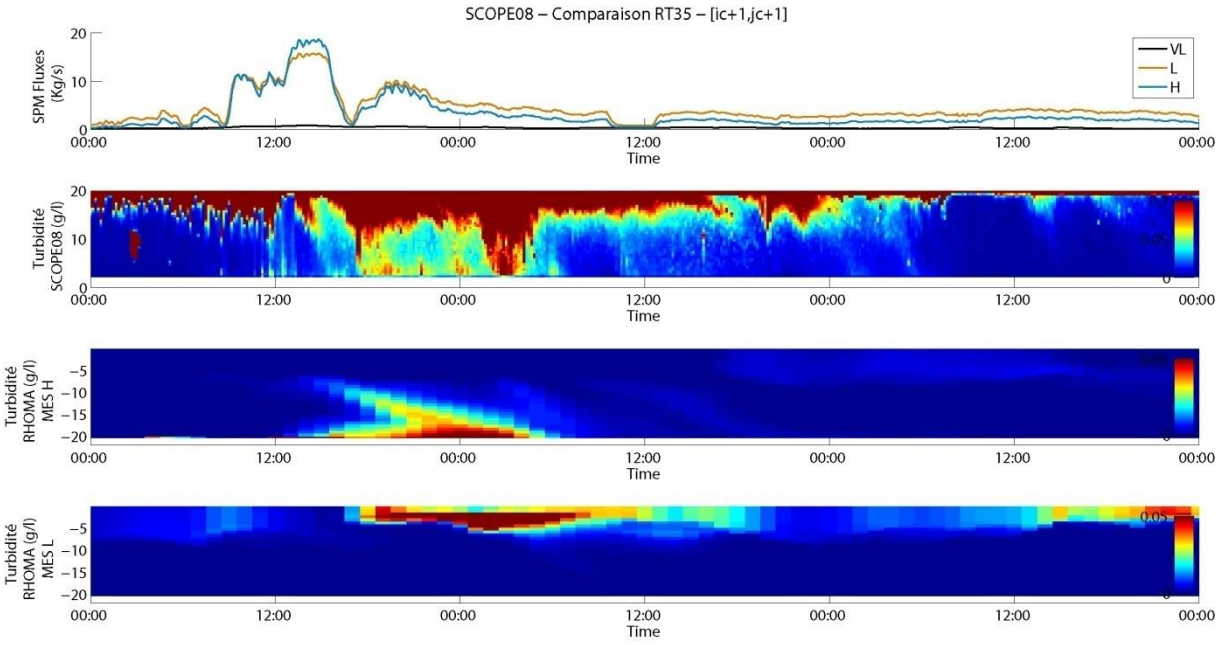

Figure 114: Comparison of the model with measurements taking near FRAME station during the December 2008 rainfall episode (SS flux, measured and simulated SS (TSS H and TSS L), concentration in g/L).

The rain episode at the end of December 2008 was particularly well observed, as the FRAME autonomous measuring station was deployed on the plateau des chèvres to the west of the Cortiou outflow during this period. The ADCP and optical measurements show a rapid and significant input of suspended matter over a few metres of thickness, associated with the plume of turbid (>50 mg/L) and desalinated water created by the sudden input of turbid runoff (Figure 113). In addition to the plume, heavier suspended solids fall through the water column and deposit at the sea bed.

The model correctly reproduces both processes, with a plume supported by the lighter TSS, with similar orders of magnitude in terms of plume thickness and suspended solids concentration (>50 mg/L). The transfer of TSS to the bottom is also simulated, but with potentially lower TSS concentrations (Figure 114). The surface SS concentrations are highly dynamic, with the plume extending far to the south under the effect of a strong mistral on the afternoon of 14 December, which changes to a west/northwesterly extension once the wind changes from mistral to south-easterly (Figure 115). There is also a high turbidity in the southern harbour, induced by the water coming from the catchment area of the old bed of the Huveaune which is discharges in the middle of the southern harbour. Although most of the lighter TSS input leaves the Marseille area quickly, most of the heavier TSSH from Cortiou is deposited i) at the outflow, ii) to the west of the islands, and iii) to a lesser extent in the western part of the southern harbour.

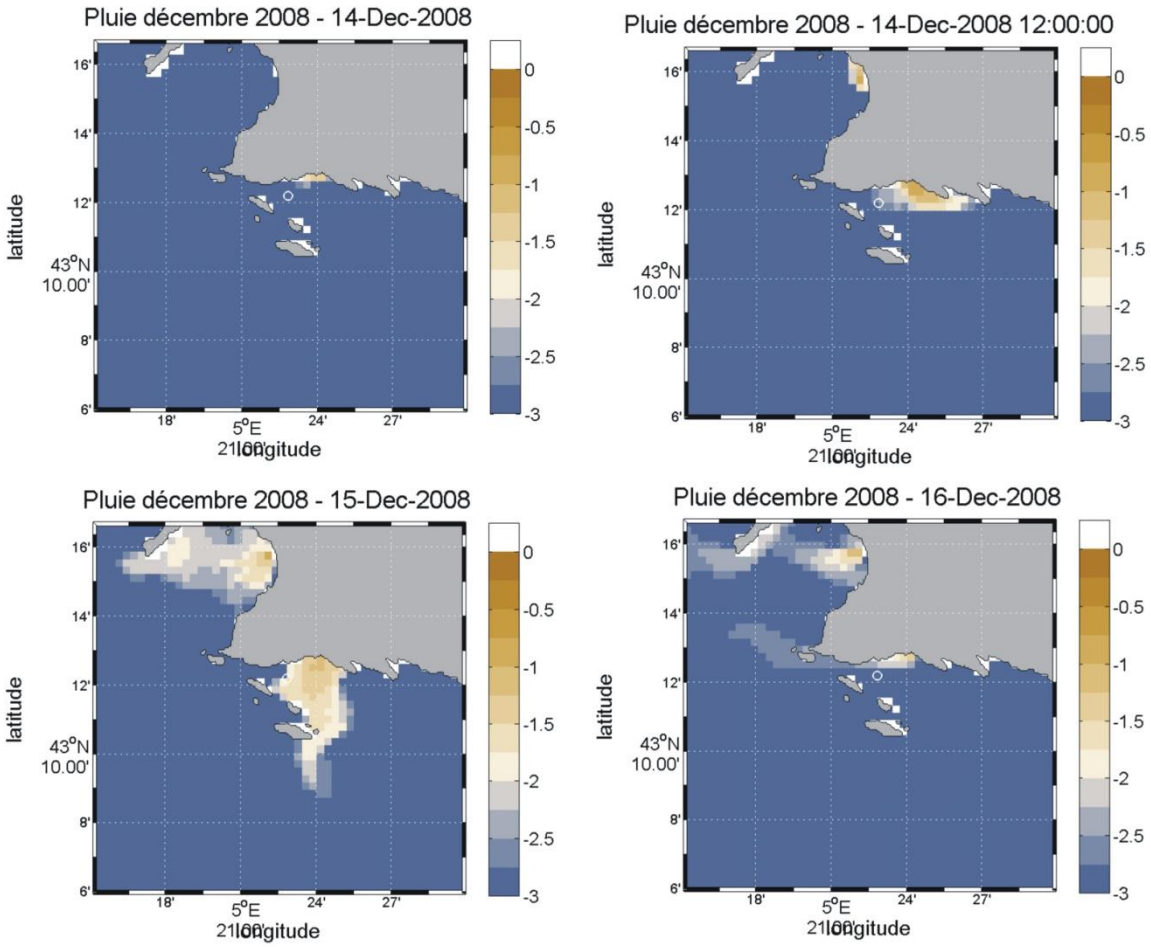

Figure 115: Surface SS dynamics between 14 Dec and 16 Dec. Concentrations (g/l) in log scale: -3=1 mg/L, -2=10 mg, -1=100 mg/L.

5.4.2.5 Contamination with CB153

The intensity of the December 2008 rainfall event caused an increase in the flows entering Marseilles harbour that greatly exceeded the "typical" event in October 2007 (see a comparison in Figure 12). The Huveaune and the Jarret returned to the river bed towards the Prado beaches due to the very high flows during the period. The Rhone outflow also greatly increased. Consequently, the plumes are more intense and more extensive (Figure 116) and CB153 concentrations are high, even if we consider averages (Figure 117). The concentrations on the particles are characteristic of the inputs (Figure 118: around 10-30 ng/g). An erosion episode was added to the inputs on 14 December (Figure 119) at Cortiou and in the southern harour in particular. The model simulates PCB deposits at the end of the period between Cortiou and the islands; in the southern harbour at the open sea limit between the Frioul and Goudes islands; and in the northern harbour (Figure 120). As in the typical situation and probably due to the season, these inputs of nutrients and detrital organic matter do not induce an increase in primary production and therefore do not have any notable consequence on the speciation of CB153 during this period.

Dissolved at the surface (pg/L)

Particulate at the surface (pg/L)

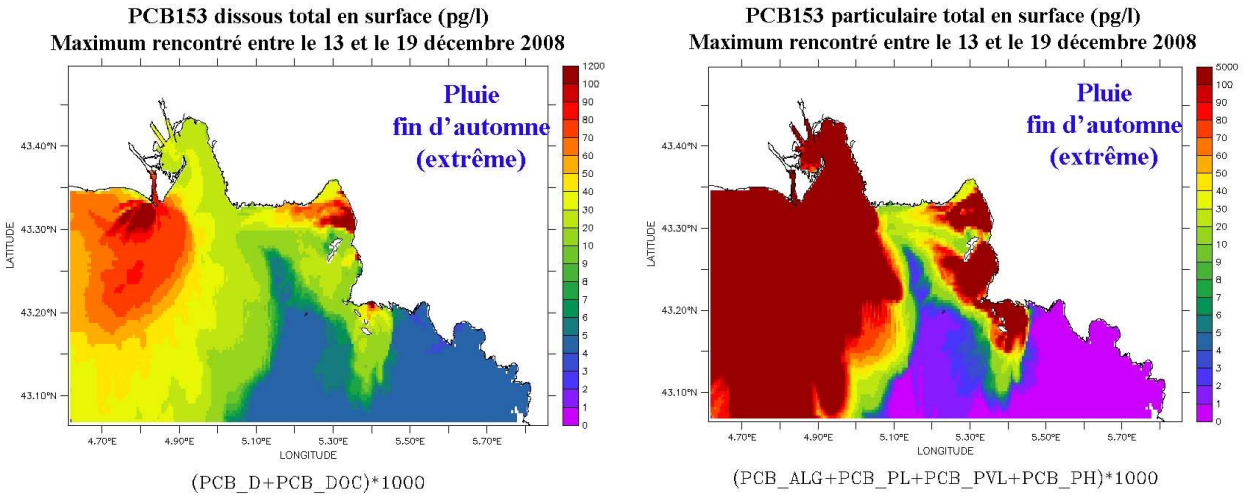

Figure 116: Maximum surface concentrations (pg/L) between 13 and 19 Dec 2008.

Dissolved at the surface (pg/L)

Particulate at the surface (pg/L)

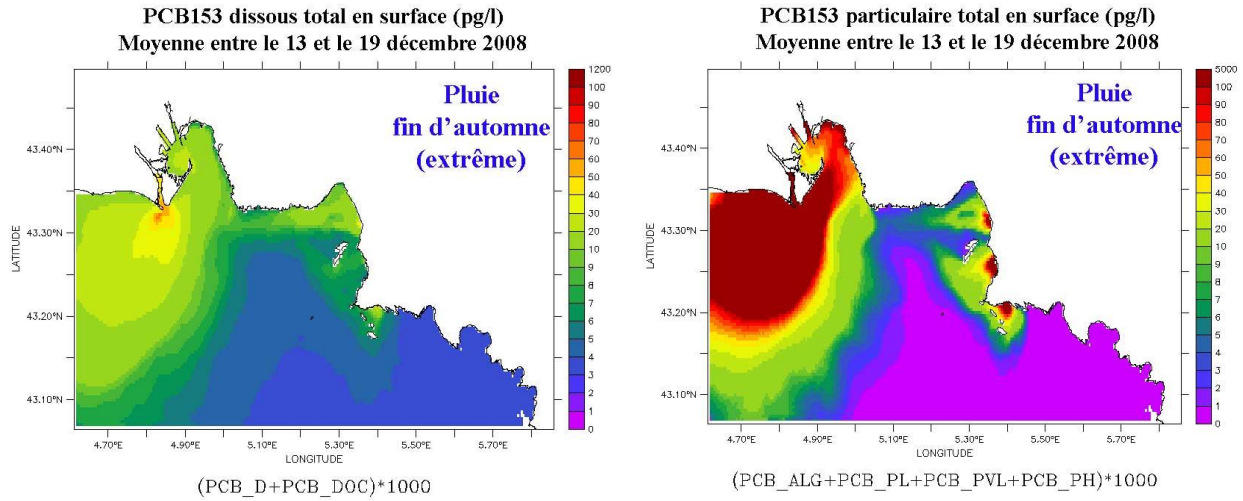

Figure 117: Mean surface concentrations (pg/L) between 13 and 19 Dec 2008.

Particulate at the surface (ng/g)

Particulate at the sea bed (ng/g)

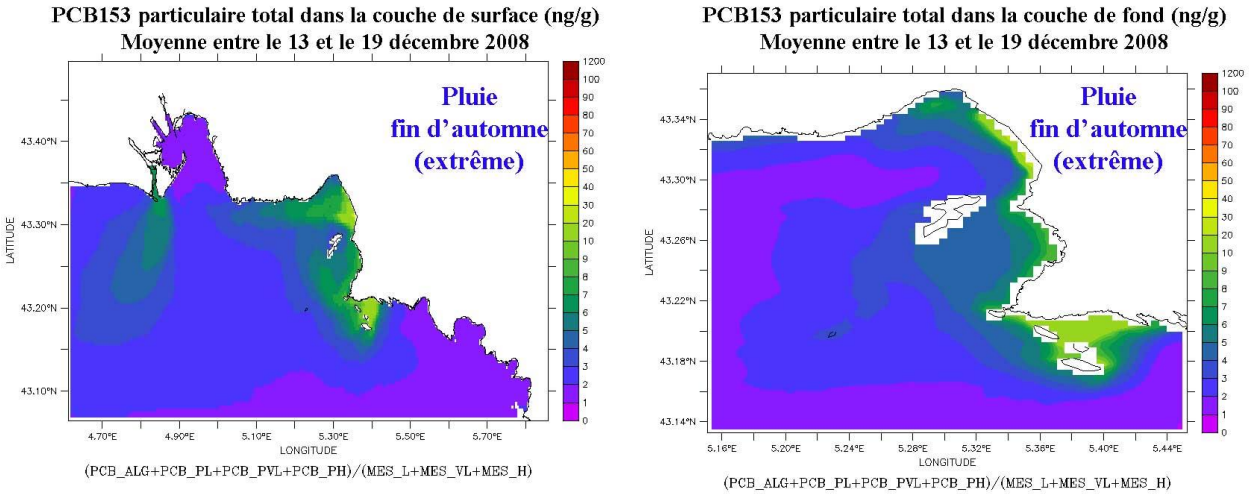

Figure 118: Mean particulate CB153 (ng/g) at the surface and sea bed between 13 and 19 Dec 2008.

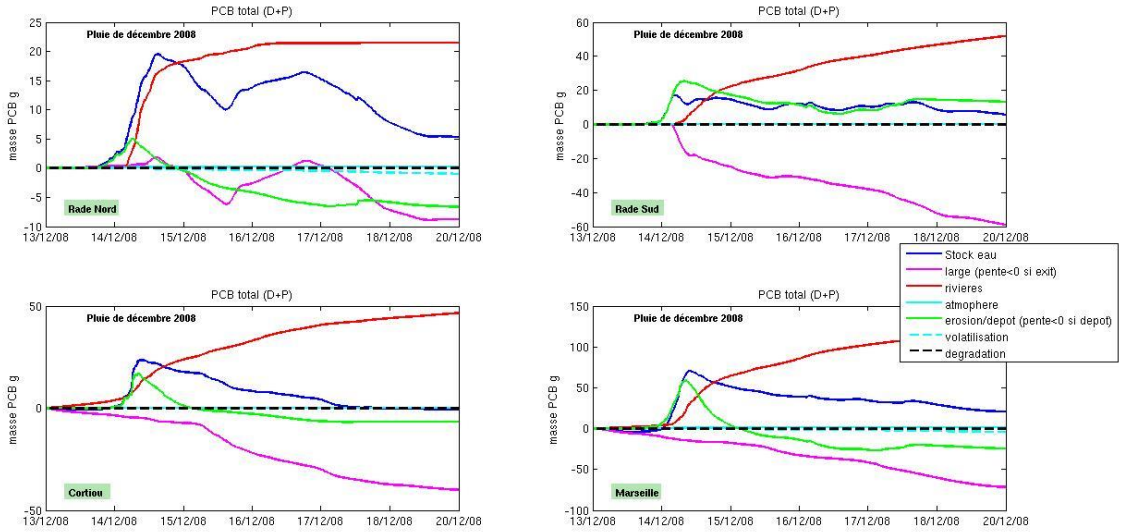

Figure 119: Variation in total CB153 stock in the water column over the period and in each area (depicted in Figure 15), associated with variations in concentrations due to each process: "open sea": input/output at boundaries; "rivers": input at the coast; "atmosphere": dry deposition and rainfall; "erosion/deposition"; "volatilisation" and "degradation". (slope >0 means positive change in concentration= contaminant input, and vice versa)

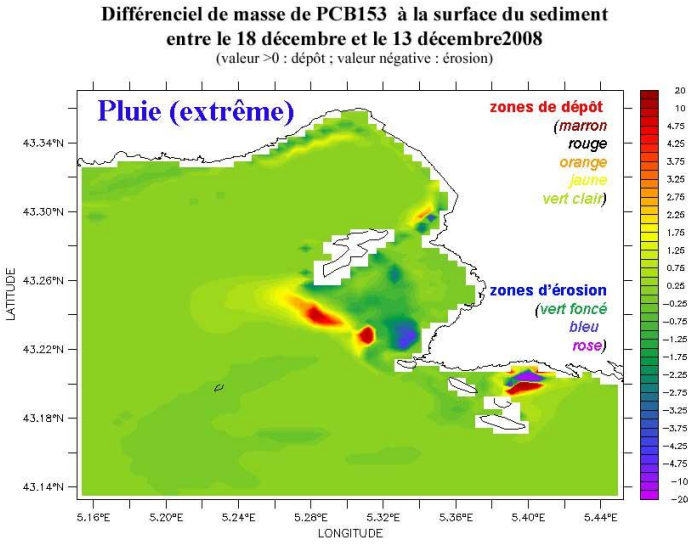

Figure 120: Deposition/erosion areas after an extreme rainfall event.

INTRUSIONS OF THE RHONE RIVER PLUME

5.5 INTRUSIONS BY THE RHONE RIVE PLUME

While the low-salinity water plume from the Rhone typically extends westward due to the Coriolis force, it can also be pushed offshore or eastward toward the coast by Mistral and South-Easterly winds, respectively, the latter causing periodic intrusions of the plume into the Bay of Marseille where it influences the surface waters (Para et al., 2010; Pairaud et al., 2011). These episodes are called Rhone intrusions in the Bay of Marseille, although they are of course intrusion of diluted Rhone river water. Fraysse et al (2014) described this process and gave a precise definition: An intrusion of Rhône waters into the Bay of Marseille is characterised by the transport of low-salinity water (< 37.8) from the Rhône to an area east of longitude 5°17.30'E (SOMLIT SOLEMIO station) into the Bay of Marseille (Figure 121).

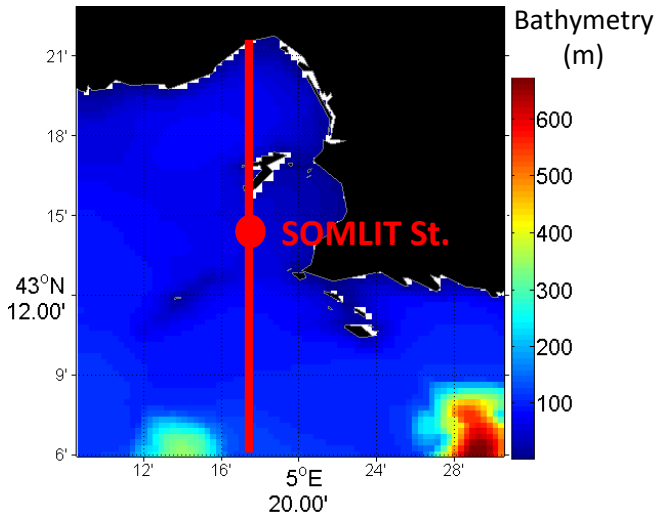

Figure 121: Showing the longitude of SOLEMIO station (in red) used to define Rhône river intrusions in Fraysse et al. (2014).

5.5.1 Typical intrusion event: 1 October 2007

5.5.1.1 Hydrodynamic and biogeochemical situation

An intrusion of the Rhone plume occurred on 1 October 2007 when the Rhone flow volume was rather low, below the 2007 average (Figure 122).

On 27 September, the Rhône plume extended southwards and eastwards under the effect of a strong Mistral wind. From 28 to 29 September, the winds were weak, and a circulation was established which favoured the eastward displacement of Rhone water. On 30 September and 1 October, strong south-easterly winds pushed the plume back toward the coast and diluted water from the Rhône was present in the northern harbour and a filament extended along a north-south axis (Figures 123 and 124).
An increase in chlorophyll was observed on 1 October in the area of the filament of diluted Rhone water, both in the satellite images and in the model.

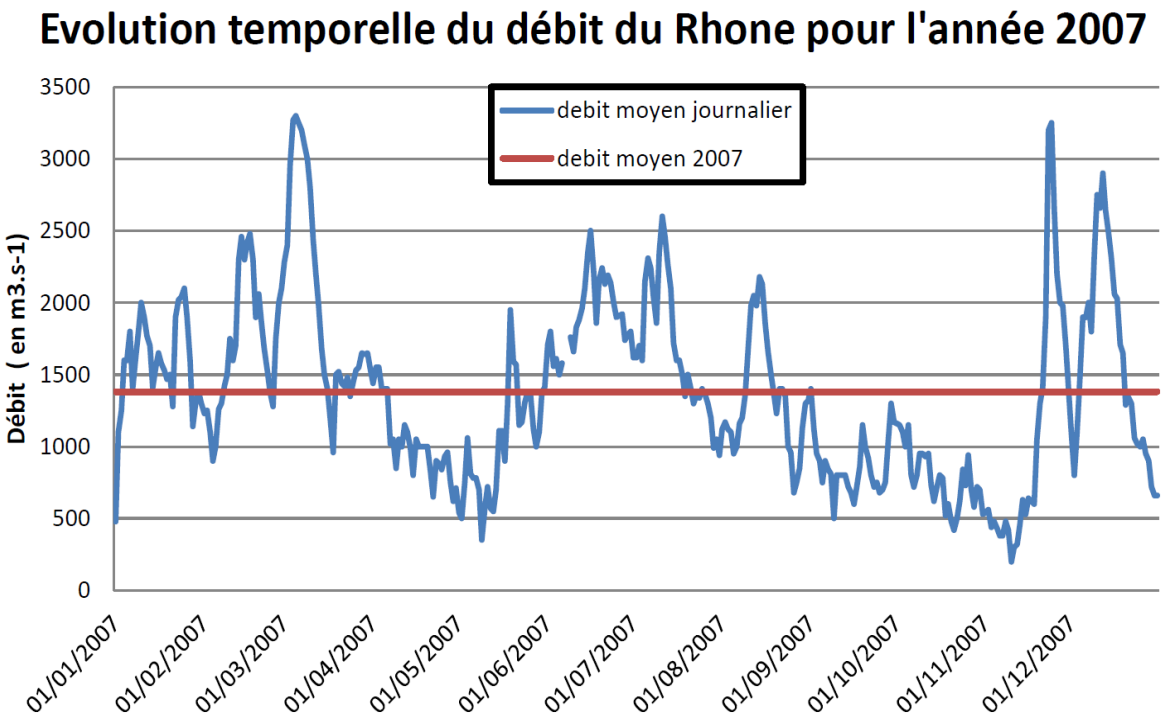

Figure 122: Daily flow volume of the Rhône river during 2007 (in blue) and annual mean (in red).

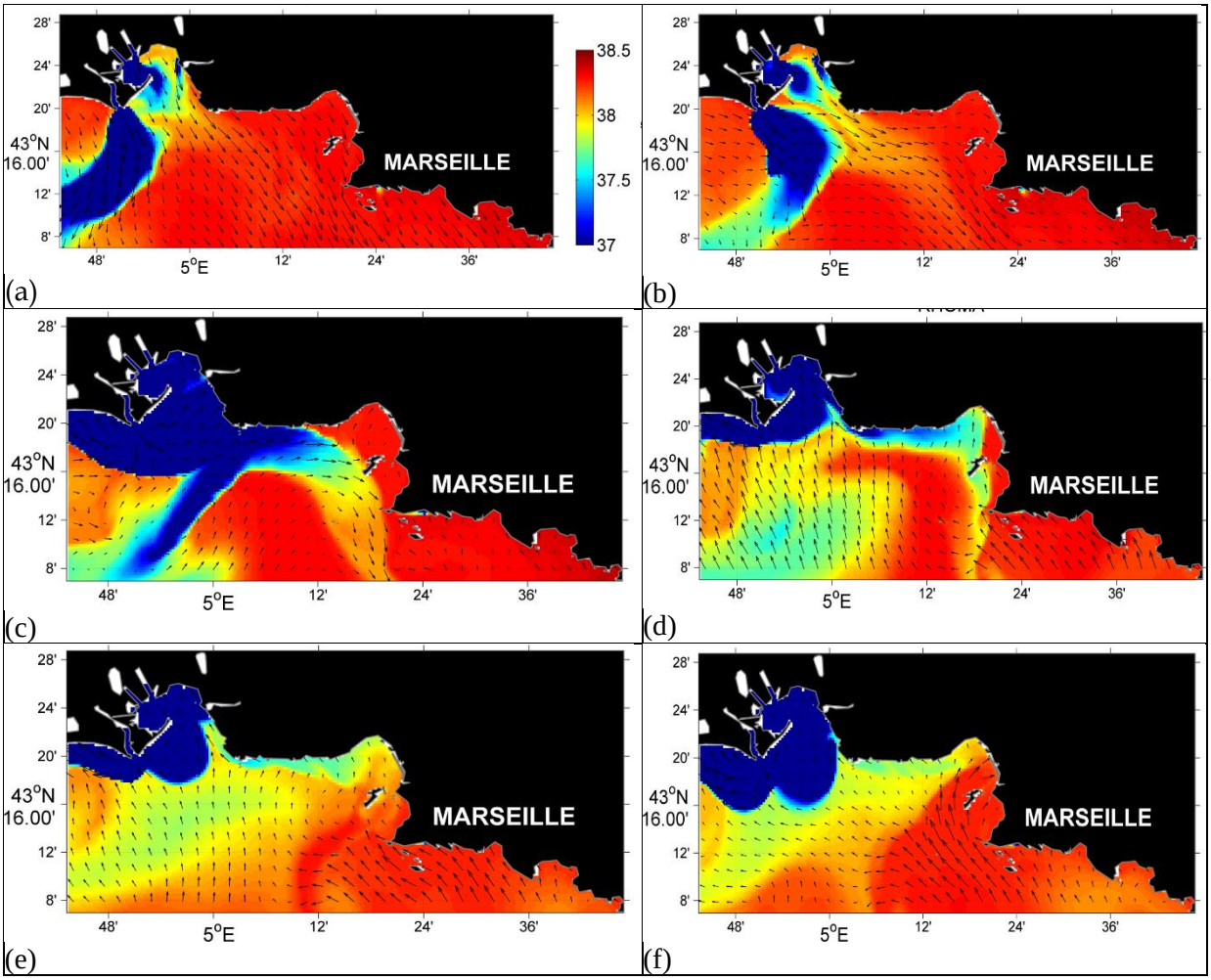

Figure 123: Surface salinity and currents on (a) 27, (b) 28, (c) 29, (d) 30 Sept 2007, and on (e) 1 and (f) 2 Oct 2007.

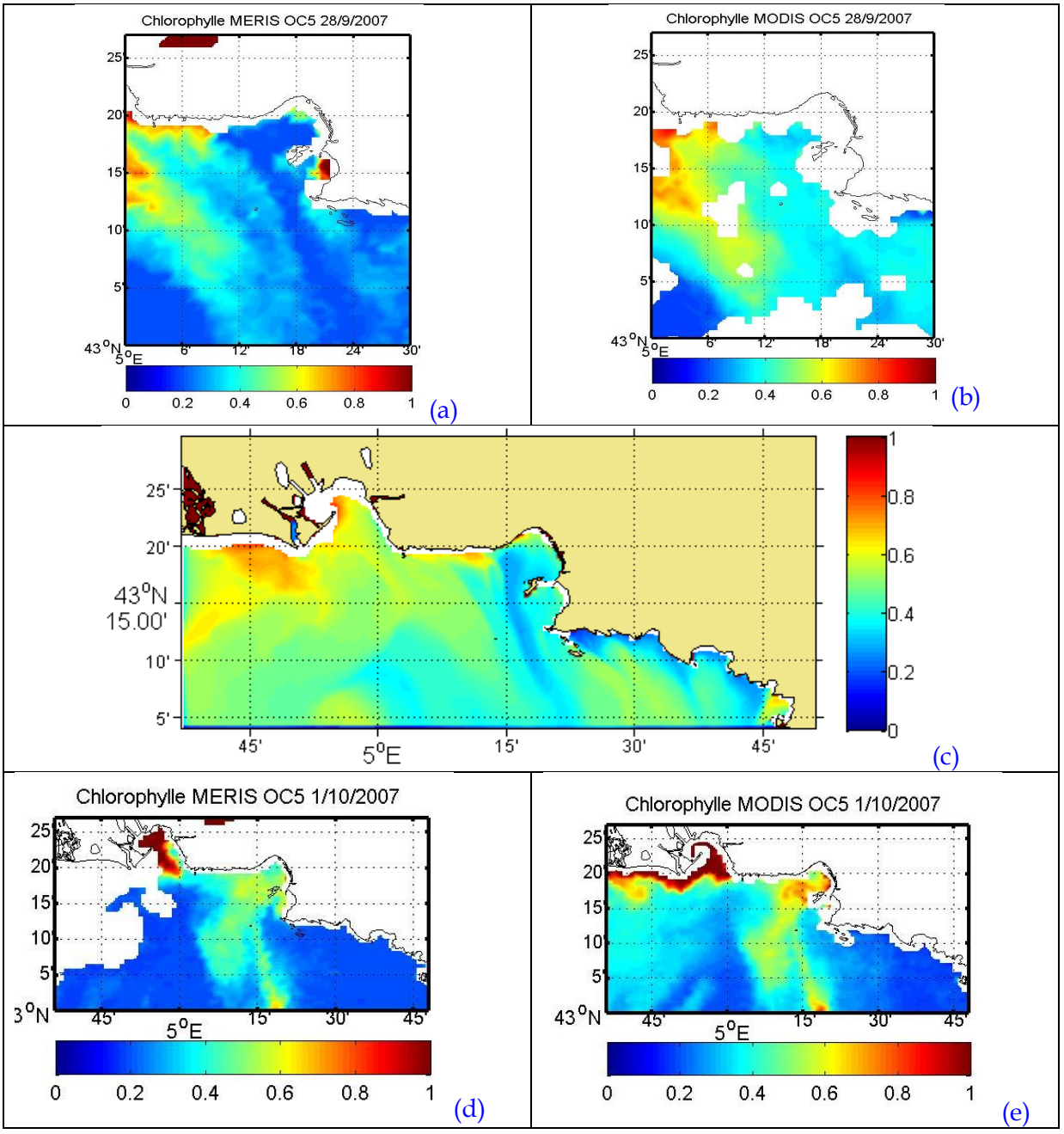

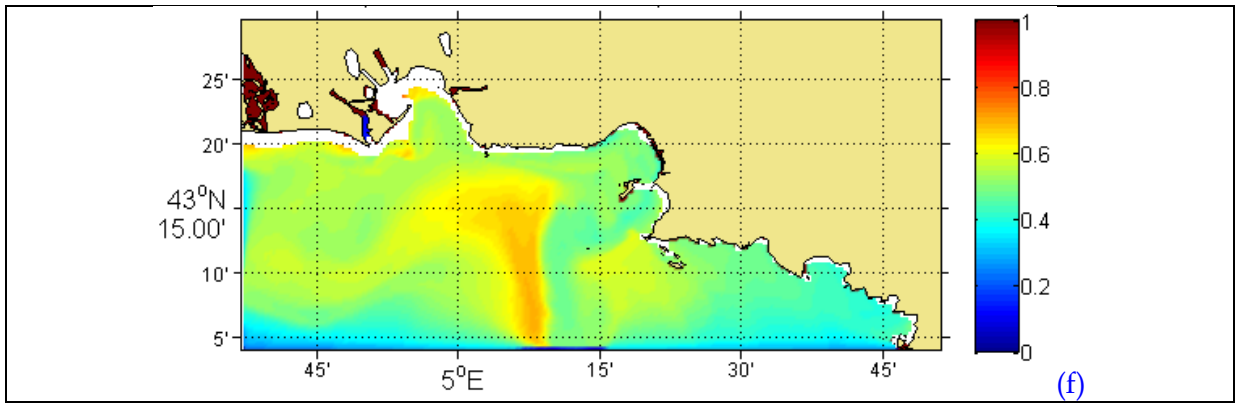

Figure 124: Initial conditions on 28 Sept 2007 as seen by the (a) MERIS and (b) MODIS satellites, as well as (c) a map of modelled surface chlorophyll µg/L. Surface chlorophyll during the Rhône intrusion event on 1 Oct 2007 as seen by (d) MERIS and (e) MODIS and (f) predicted by the model (µg/L).

5.5.1.2 Hydrosedimentary situation

A slight increase in turbidity in the northern harbour was observed during the event, indicating an intrusion of water from the Rhône to depths of about 30 metres below the surface (Figure 125). This intrusion remains minimal, due to the low flow volume of the Rhone at this period, and does not result in a very significant deposition of sediments (Figure 126).

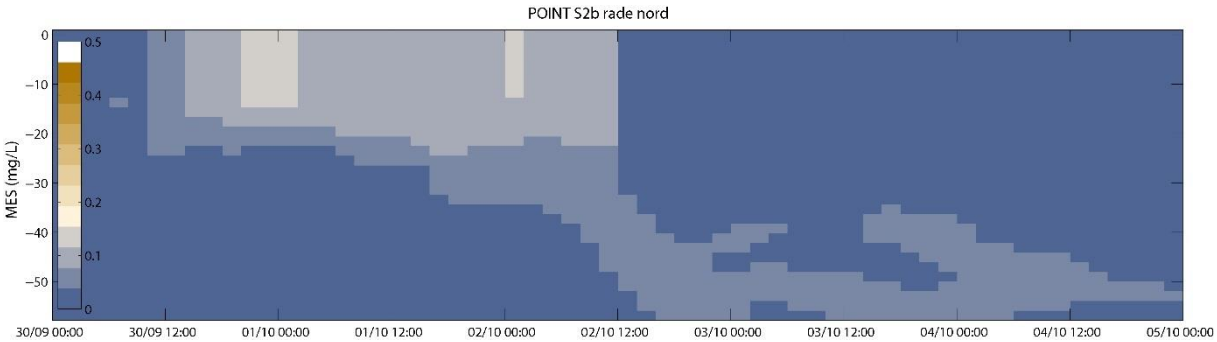

Figure 125: Vertical water column structure near the norther harbour between 30 Sept and 6 Oct (concentrations in mg/l, log scale).

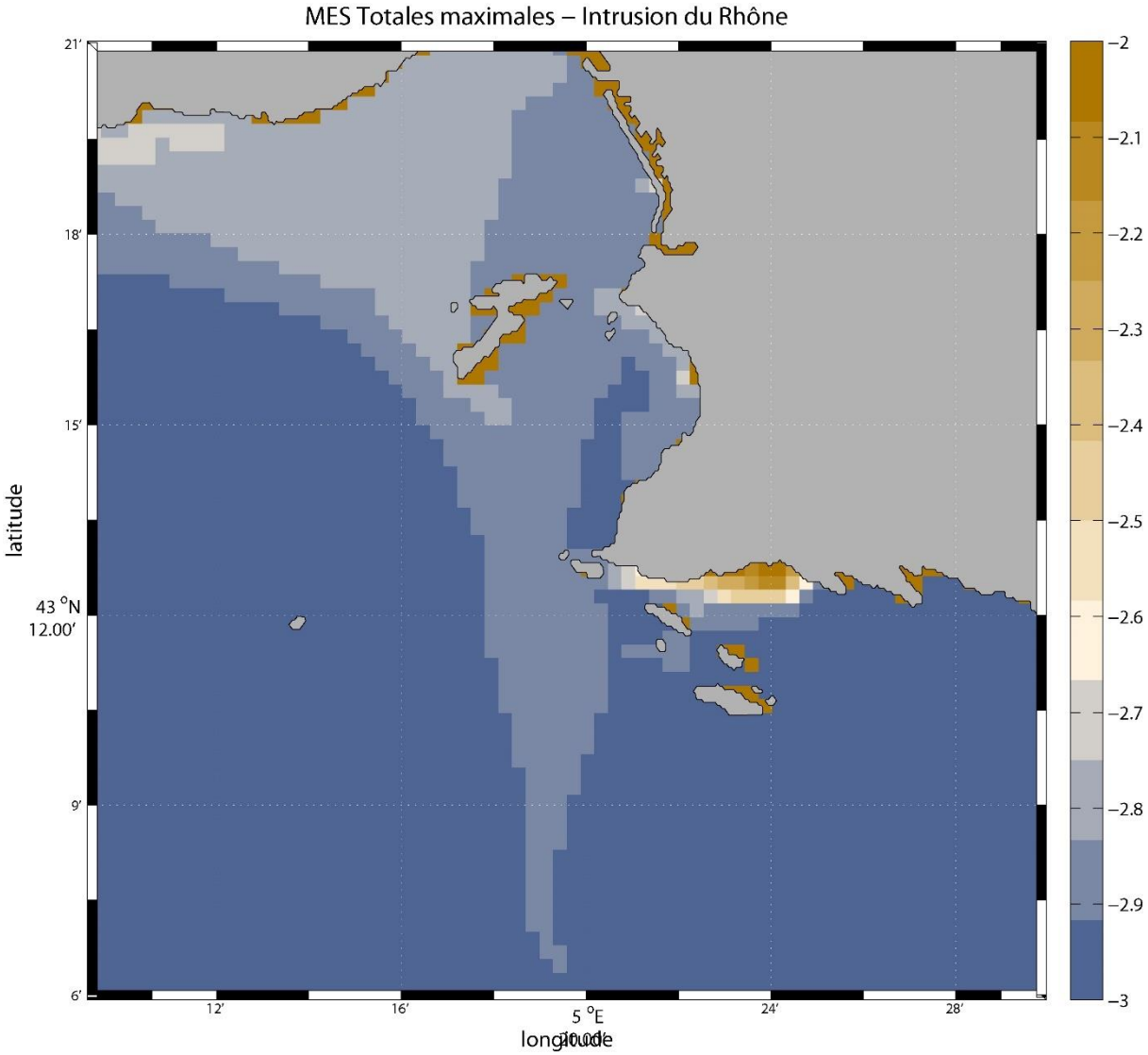

Figure 126: Spatial distribution of maximum SS concentration (in g/L, log scale).

5.5.1.3 Contamination with CB153

Whatever its flow rate, the Rhône plume in the model carries a constant amount of PCB on the suspended particles. The contaminant tends to desorb as the particles disperse in the water mass. During the period of 1 October 2007, the intrusion of the Rhone into the Marseilles harbour occurs mainly in the northern harbour and brings relatively high volumetric concentrations which are not accompanied by high levels of particles (Figures 127 and 128). Instead, the increase in particulate CB153 concentrations to the west and east of the plume are related to higher detrital POC concentrations. CB153 stocks in each zone (Figure 129) increased slightly, except near Cortiou (after a decrease due to a period of Mistral wind at the end of September; see typical Mistral event in Section 5.1.1.6). This intrusion is not accompanied by sedimentation in the harbour. An erosion episode took place at the same time at Cortiou.

(a) : Dissolved at the surface (pg/L)

(b): Particulate at the surface (pg/L)

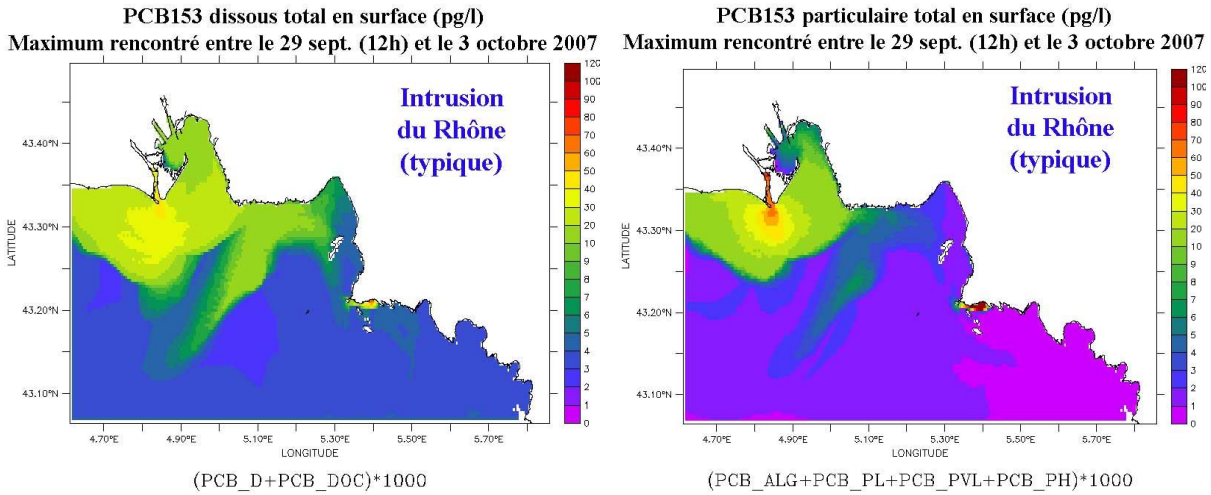

Figure 127: Maximum concentrations at the surface (pg/L) between 29 Sept and 3 Oct 2007

Particulate at the surface (ng/g)

Particulate at sea bed (ng/g)

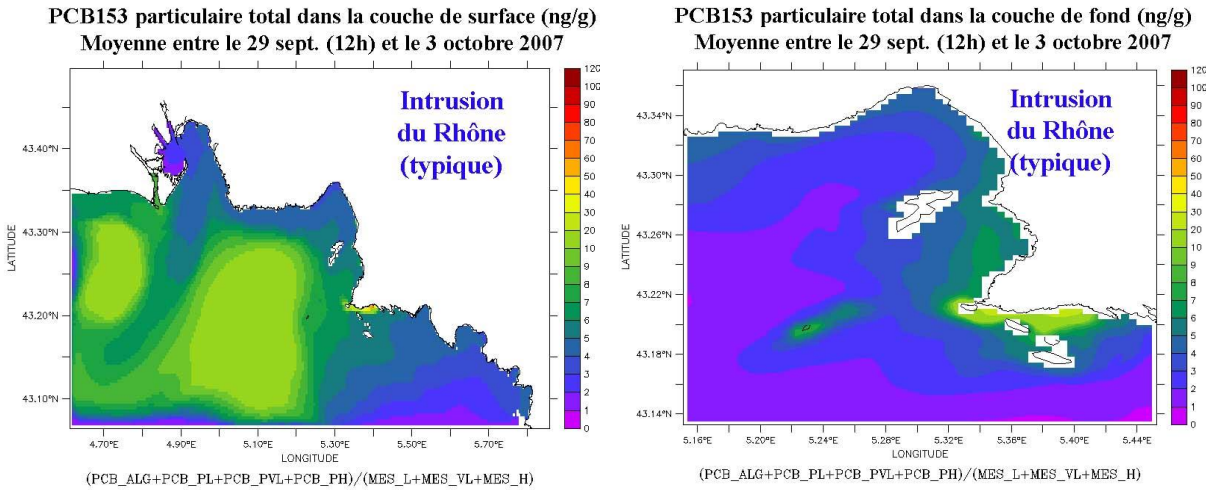

Figure 128: Mean particulate CB153 (ng/g) at the surface and sea bed between 29 Sept and 3 Oct 2007.

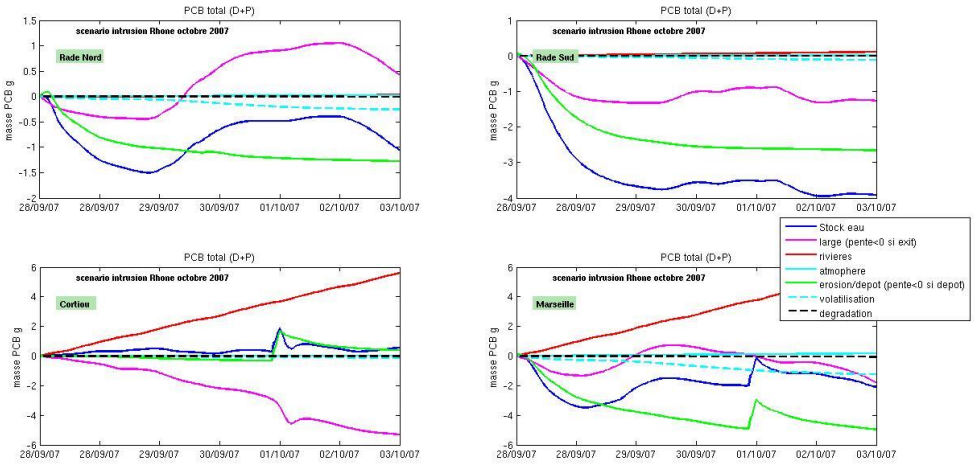

Figure 129: Variability in total CB153 in the water column in each area (see Figure 15), associated with variations in concentrations due to each process "open sea": input/output at boundaries; "rivers": input at the coast; "atmosphere": dry deposition and rainfall; "erosion/deposition"; "volatilisation" and "degradation". (slope >0 means positive change in concentration= contaminant input, and vice versa).

5.5.2 Typical situation with intrusion of plume toward the east: 21 May 2011

Another typical situation was studied by Fraysse (2014) to illustrate typical intrusion events which they characterised as "small" intrusions (see Section 5.5.5).

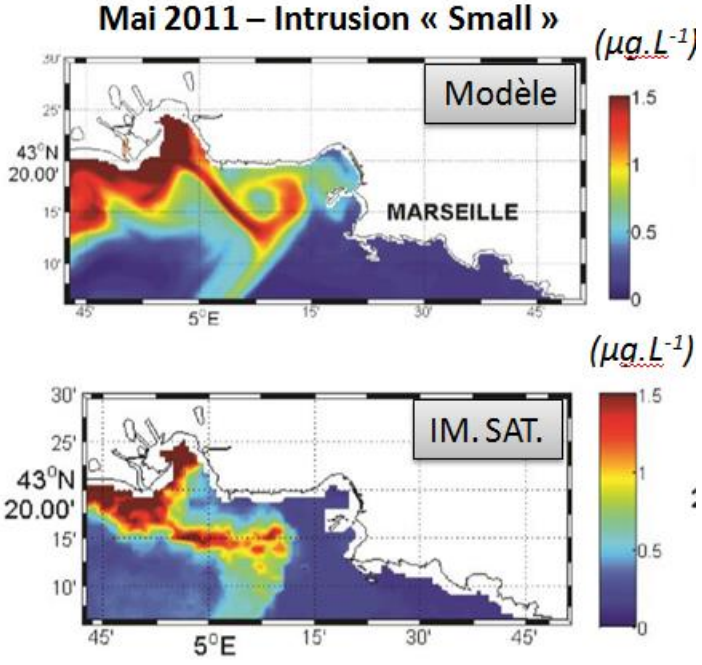

Figure 130: (a) Modelled surface chlorophyll (µg/L) on 21 mai 2011 and (b) MODIS (OC5) image for the same date.

This "small" intrusion occurs when the water column is stratified with a low flow rate (here 560 $m^3 s^{-1}$) leading to a drop in salinity to 37.2 at SOLEMIO, a low nitrate input of the order of 3 µM and a Rhone plume water reaching the Bay of Marseille driven by currents at the edge of the Marseilles Eddy (Fraysse , 2014).

It was possible to distinguish the different sources of the inputs during this episode (Figure 131). By running two simulations, one with inputs from the Rhone and the other with pure freshwater, and subtracting one result from the other we obtain the evolution of the total stock (B^{stock}) solely due to variations at the boundaries (B^{OB}) and the biology (B^{BIO}) as the atmospheric and river inputs cancel each other out since they are equal in both simulations.

When considering the temporal evolution during the May 2011 intrusion, it can be seen that at the beginning of the 19-21 May event, there is an increase in the total nitrate stock (Figure 132) which is due to input at the boundary Rhone plume water (in blue) immediately consumed by phytoplankton (in green), which stabilises after 22 May when all inputs have been consumed. If we look at the evolution of chlorophyll over the same period (Figure 133), we can see that despite the small bloom (due to the consumption of nitrates) (green), the increase in chlorophyll in the bay mostly originates from the frontal zone of the Rhone plume that is transported into the bay (blue). After 22 May, this chlorophyll decreases again, mainly due to the export of Rhone water out of the area, but also due to the consumption of phytoplankton by zooplankton (green).

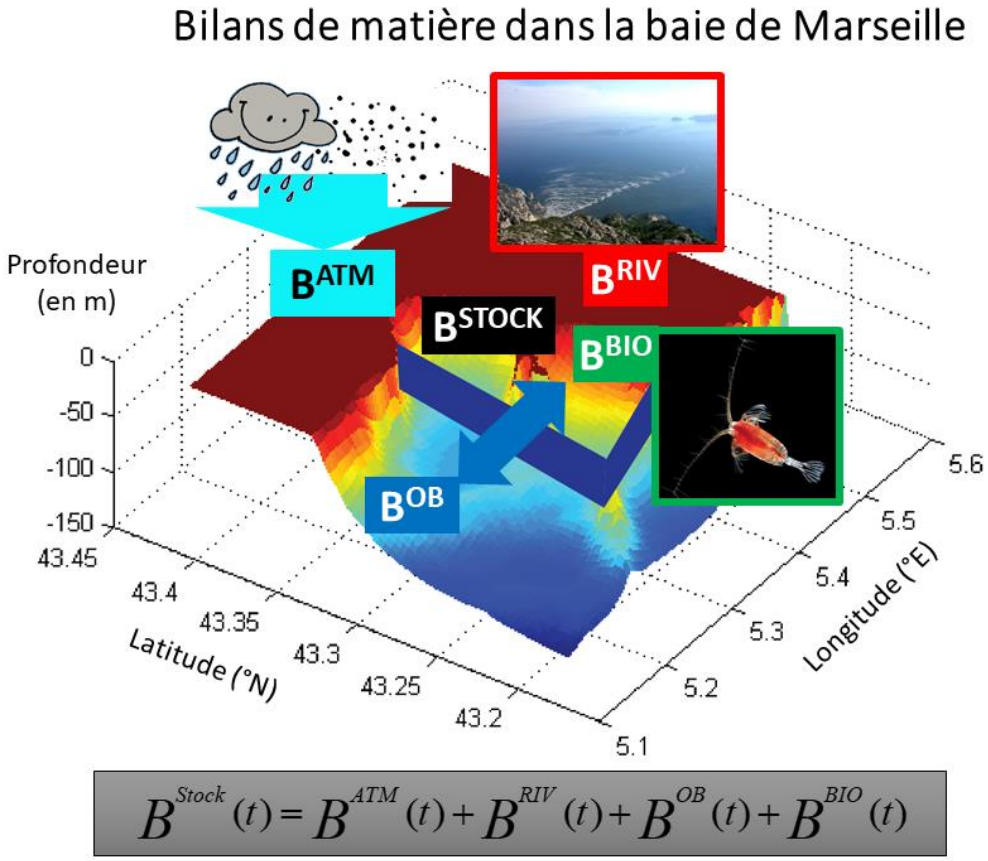

Figure 131: Contributions of different sources (atmosphere, rivers, open boundaries, biology) to changes in total stock in the bay (delimited by the blue vertical boundaries).

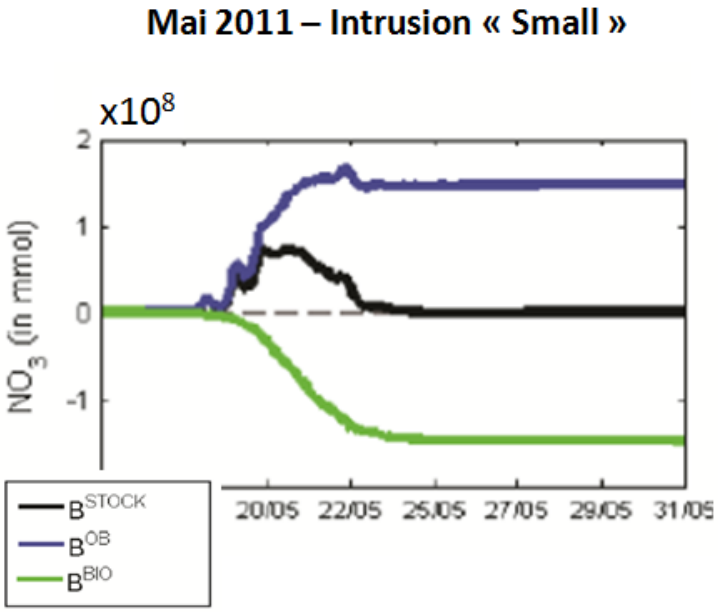

Figure 132: Temporal variation in total nitrate stock (black) in the bay (delimited by the blue vertical walls Figure 131) and contributions by different sources: open boundaries (blue), biology (green) (if slope >0 = positive variation of the concentration = nitrate input, and vice versa).

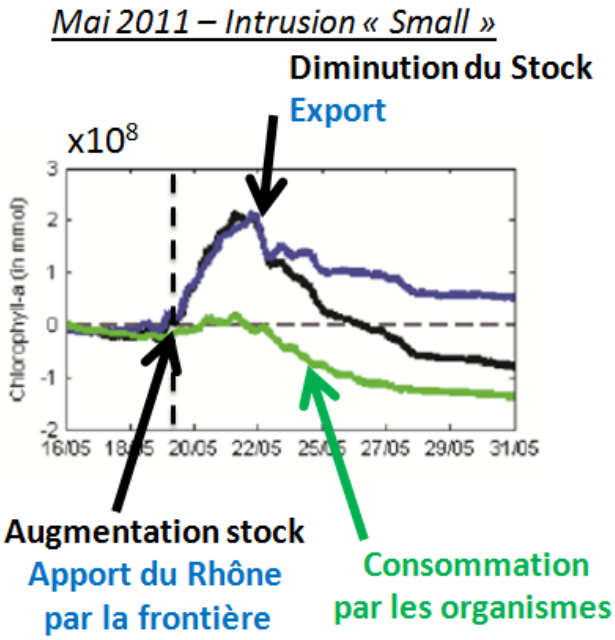

Figure 133: Temporal variation in total chlorophyll stock (black) in the bay (delimited by the blue vertical walls Figure 131) and contributions by different sources: open boundaries (blue), biology (green) (if slope >0 = positive variation of the concentration = Chl input, and vice versa).

5.5.3 Typical situation of an eastward intrusion of the plume: 16 March 2017

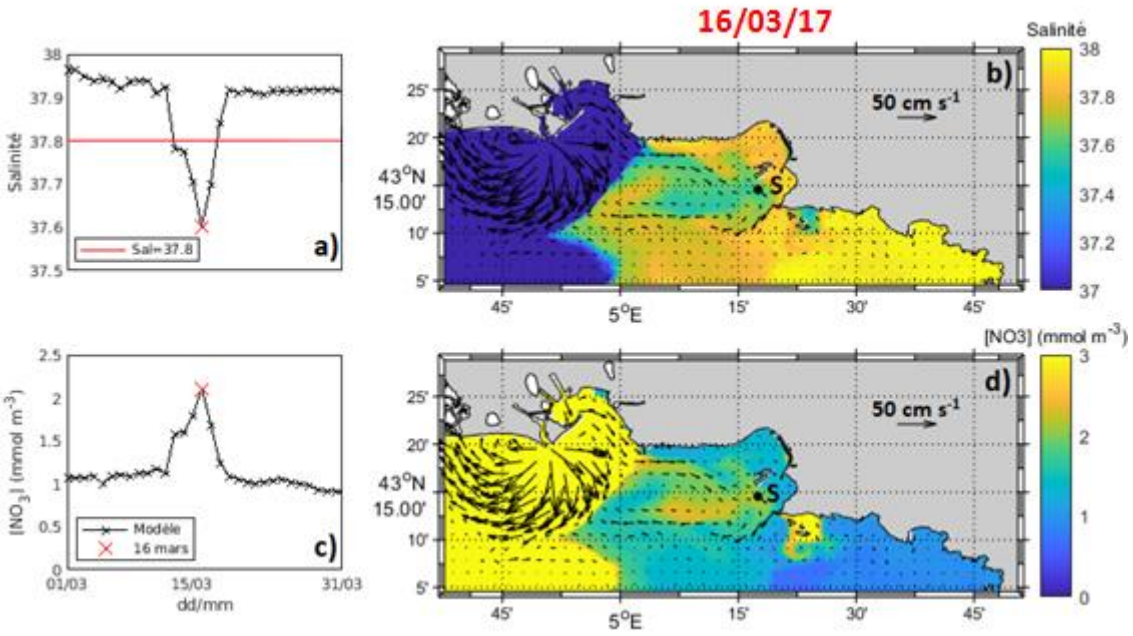

Figure 134: Modelled surface (a) salinity and (c) NO_3 at SOLEMIO and (b,d) corresponding maps for 16/03/17 (Barré, 2020).

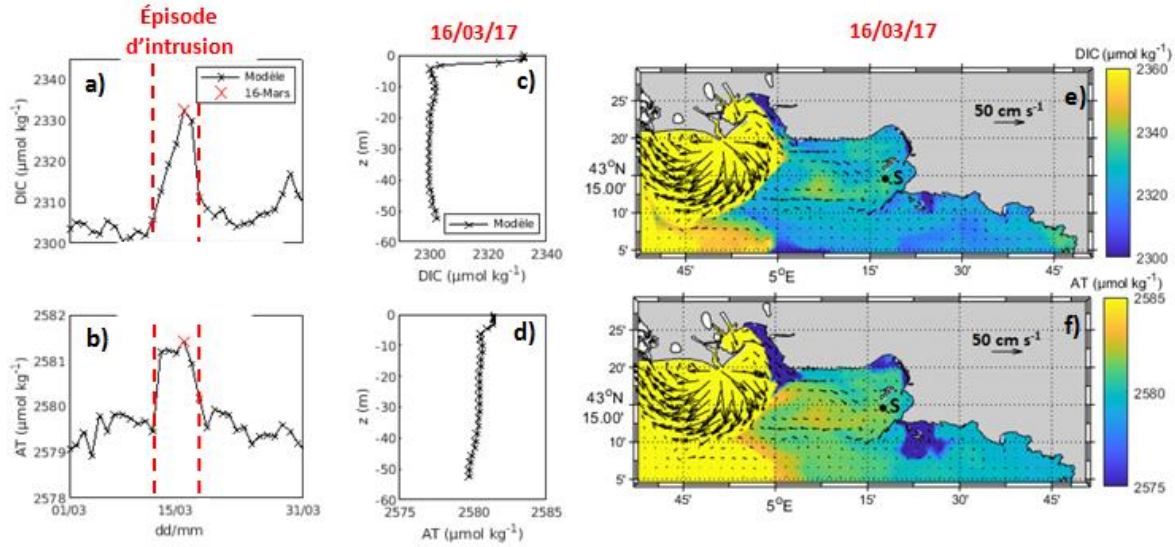

Figure 135 : Modelled surface (a) DIC and (b) TA at SOLEMIO on 16 March 2017. Corresponding (c,d) vertical profiles, (e,f) maps (Barré, 2020).

A typical "small" intrusion took place in March 2017 and was studied with the MARS3D-RHOMA ECO3M-Carbox model to see the impact of these intrusions on the carbonate system. The Rhone intrusion was detected due to a drop in salinity (Wimart-Rousseau et al., 2020) which is well reproduced by the model and is accompanied by an increase in nitrate concentrations (Figure 134). This intrusion of Rhone water that is rich in DIC and TA induces an increase in these variables at SOLEMIO Station (Figure 135). Looking at the temporal variation of all biogeochemical variables, we notice that the water coming from the Rhône causes a certain heterotrophy (Figure 136). If we look at the temporal evolution of the net community production (NCP) throughout 2017, we see that in spring it is positive, indicating an autotrophic ecosystem. During the Rhone water intrusion, the NCP turns negative suggesting that the ecosystem becomes heterotrophic before returning to being autotrophic once the intrusion is over (in green on the right in Figure 137 and Table 13).

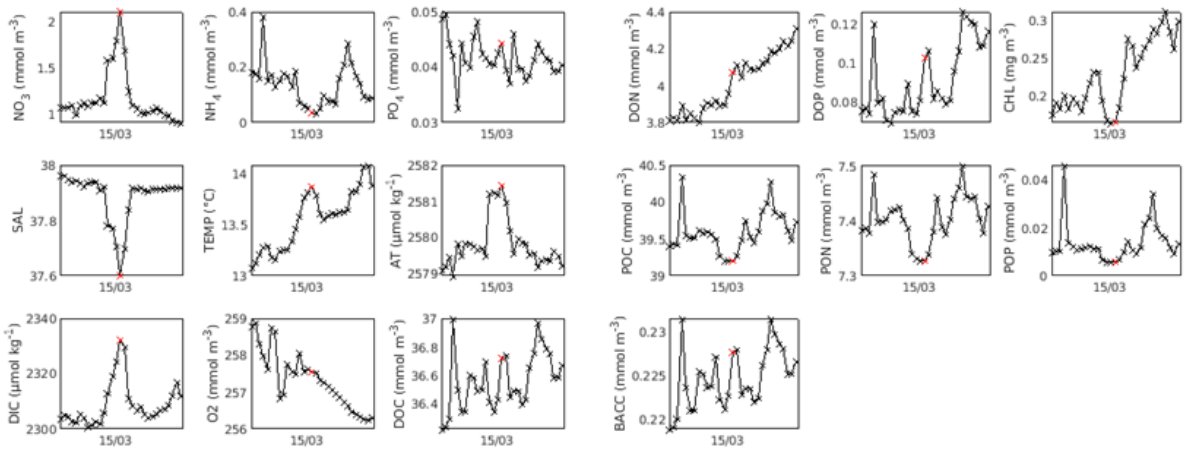

Figure 136: Summary of all modeleld variables for the surface layer at SOLEMIO during the intrusion event from 16/03/17: NO_3, NH_4, PO_4, SAL, TEMP, TA, DIC, O_2, DOC DON, DOP, Chl, POC, PON, POP, BACC (Barré, 2020).

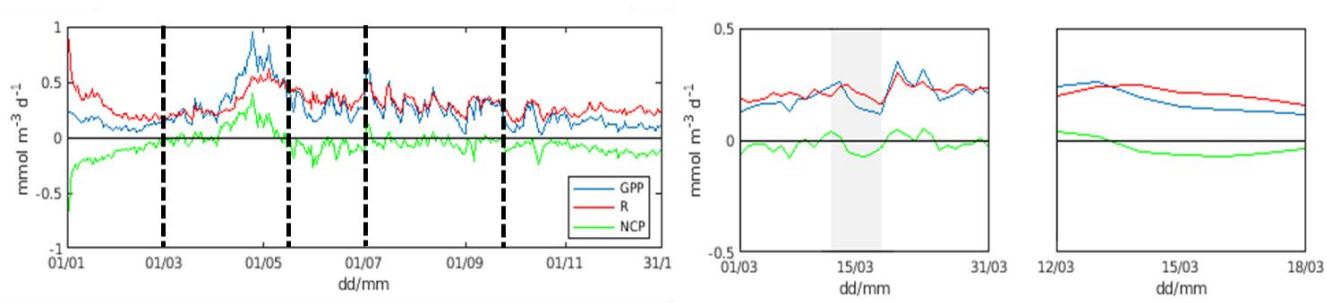

Figure 137: Temporal evolution of NCP (in green), GPP (blue) and total respiration R (red) for 2017, March 2017, and the intrusion event (mmol m^{-3} d^{-1}) (Barré, 2020).

Table 13

NCP, GPP, and respiration (total: R, autotroph: RA, heterotroph: RH) for 2017, March 2017, and the intrusion event (mmol m^{-3} d^{-1})

	NCP	GPP	R	RA	RH
Year 2017	-0.060	0.237	0.297	0.042	0.255
March 2017	-0.017	0.198	0.215	0.042	0.173
Intrusion event	-0.034	0.172	0.206	0.035	0.171

5.5.4 Extreme Rhone intrusion event: June 2008

5.5.4.1 Meteorological situation

On 17 June, a tropopause anomaly is present over the Iberian Peninsula. Ahead of this anomaly, there is a southwesterly regime at 5000m over the southern part of France and the Mediterranean basin. During the morning, the potential vorticity minimum (PV) associated with the anomaly moves eastward and penetrates Languedoc-Roussillon and the Gulf of Lion. It crossed the PACA region during the day on 17 June and moved over Italy during the night of 17 to 18 June. The jet then positioned in the southern part of the anomaly was progressively pushed towards Corsica. In the western part of the potential vorticity core, the wind was north-westerly with an advection of dry air at medium altitude.
At 850hPa, in front of the minimum altitude, a relative minimum over Languedoc-Roussillon evolving over PACA during the day on June 17. The surface wind was light south-easterly over the three coastal departments of the PACA region, then turned west during the day. The westerly wind then remained weak over the period.

At the mesoscale, the initial south-easterly over the Bouches du Rhône becomes a weak westerly wind. The Mistral became established during the night of 17 to 18 June but its spatial extension remained limited to the west of the department, extending as far as Ensues-La-Redonne. It had gust speeds of up to 24/26 knots. It weakened on the morning of 18 June then gradually shifted to the south-west over Camargue turning into a westerly wind from Port Saint Louis du Rhône to La Ciotat while remaining light at 10/15 kts. During the night of 18 to 19 June, the westerly wind became variable and there were onshore breezes with a flow from the continent towards the sea.
In the middle of the morning, the synoptic wind combines with the sea breeze to become a south-westerly to the west of the Etang de Berre, a west-south-westerly elsewhere. During the night, the wind shifts to the north-west over the continent (thermal breeze regime).
During the day, the wind shifts back to being a south-wester on the west coast of the Bouches du Rhône and a west-south-westerly wind over the Marseilles region.
This change in wind direction is linked to breezes. During the day, the synoptic wind combines with the sea breeze, giving directions in the 240/260 degree range, and at night the winds are relatively weak with a dominant north-westerly component near the coast. This situation persists until 23 June.

5.5.4.2 Hydrodynamic situation (MARS3D-RHOMA)

In June 2008, the flow of the Rhône reached 4160 m3/s (Figure 138) and the plume covered a large part of the RHOMA domain and was likely to reach the Bay of Marseille (Figure 139).

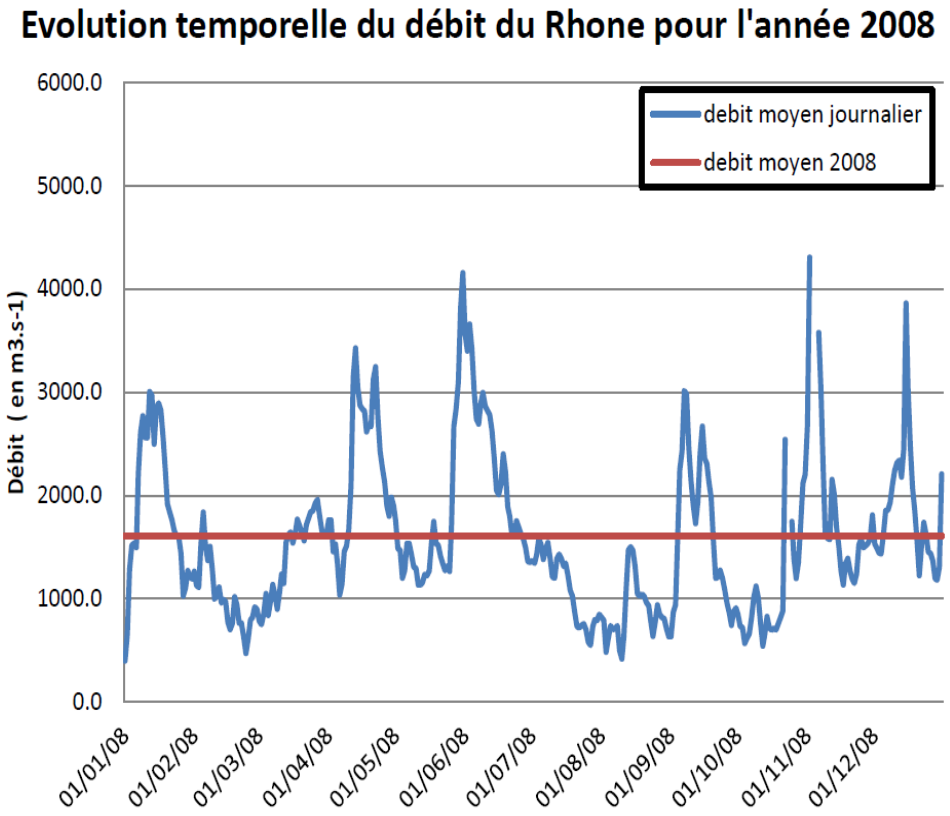

Figure 138: Daily mean flow of the Rhône in 2008 (en bleu) and annual mean flow (in red).

As the Rhone is a major source of nutrients, the plume extension is likely to correspond to areas of high chlorophyll concentrations. Figure 139 shows comparisons between the modelled plume extension, corresponding to salinities below 36.5, and its observed extension estimated using chlorophyll from MODIS satellite images for 3 dates: 17, 19, and 23 June 2008. The plume extension in the model outputs corresponds to the extension of the satellite chlorophyll maxima. Diluted water from the Rhone is present for several days in the Bay of Marseille (Figure 139a, c, and d) during different wind conditions. On the 17th, after two days of southerly winds which pushed the plume towards the coast, the north-westerly winds in the western part moved it towards the open sea, while in the eastern part the westerly winds pushed the diluted Rhone waters towards the east, resulting in two low-salinity zones (Figure 139 a and b). On 18 June, under the influence of the westerly wind, the fresh water that had accumulated on the plateau was advected eastwards and low-salinity water reached the Bay of Marseille. On 19 June (Figure 139c and d), south-westerly winds pushed the low-salinity water towards the bay, which was reinforced by the westerly gale on 20 June. On 23 June (Figure 139e and f), after a day of south-easterly winds, the diluted water from the Rhone is still present throughout the RHOMA domain.

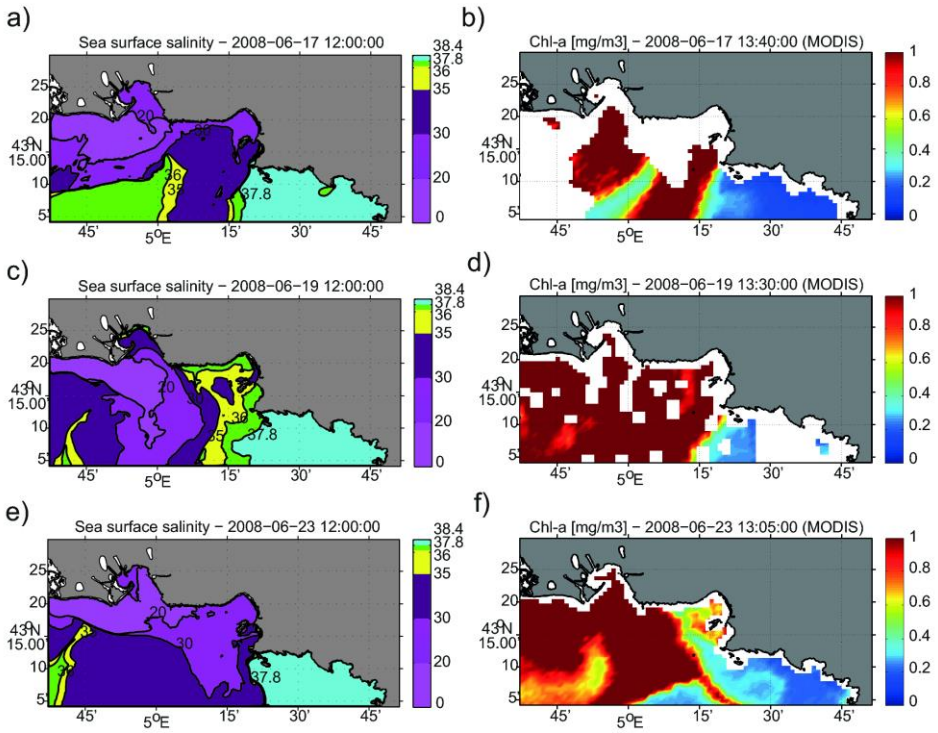

Figure 139: Evolution of the Rhône plume as seen from modelled surface salinities (RHOMA configuration, left) and MODIS chlorophyll maps (in µg/L) (right) for different dates: (a) 17 June 2008, (b) 19 June 2008, and (c) 23 June 2008 (from Pairaud et al., 2011).

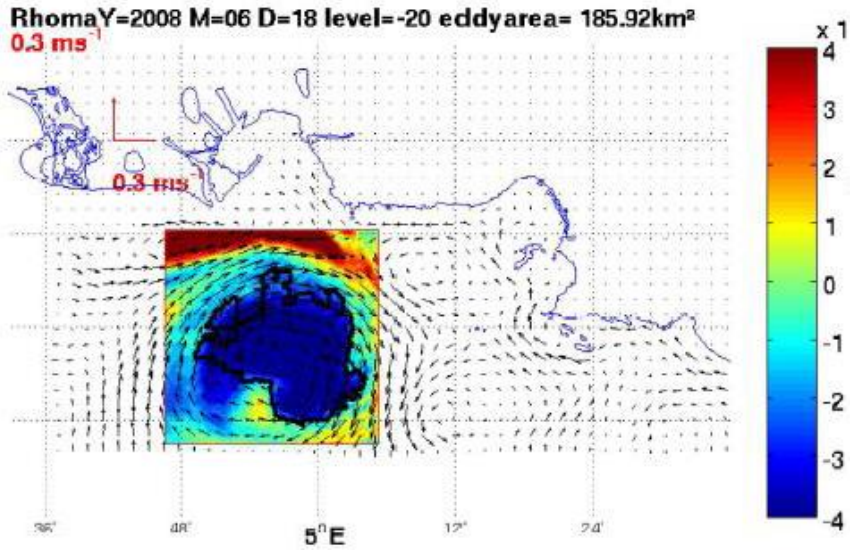

Figure 140: Anticyclonic eddy detected in the model current velocity fields of 18 June 2008 (after Boiron, 2011).

The persistence of Rhone water could be related to the presence of an anticyclonic eddy found by Schaeffer et al. (2011) using HF radar and detectable also in the results of the hydrodynamic model for 18 June 2008 using the wavelet method (Figure 140).

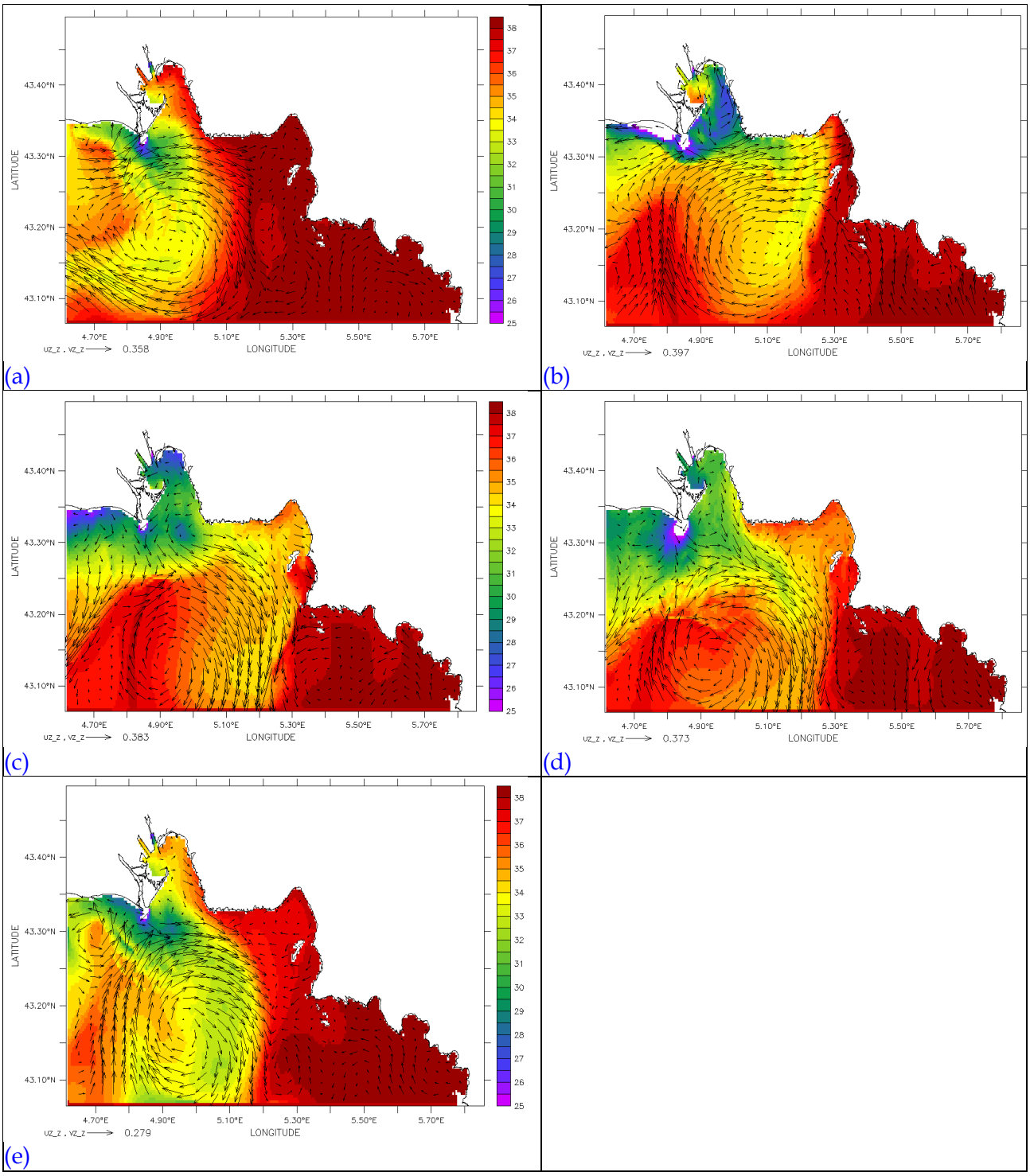

Figure 141: Maps of surface salinities and currents (at 2m) for (a) 15 June 2008 at 6h, (b) 16 June 2008 at 18h, (c) 17 June 2008 at 6h, (d) 17 June 2008 at 18h, and (e) 20 June 2008 at 6h.

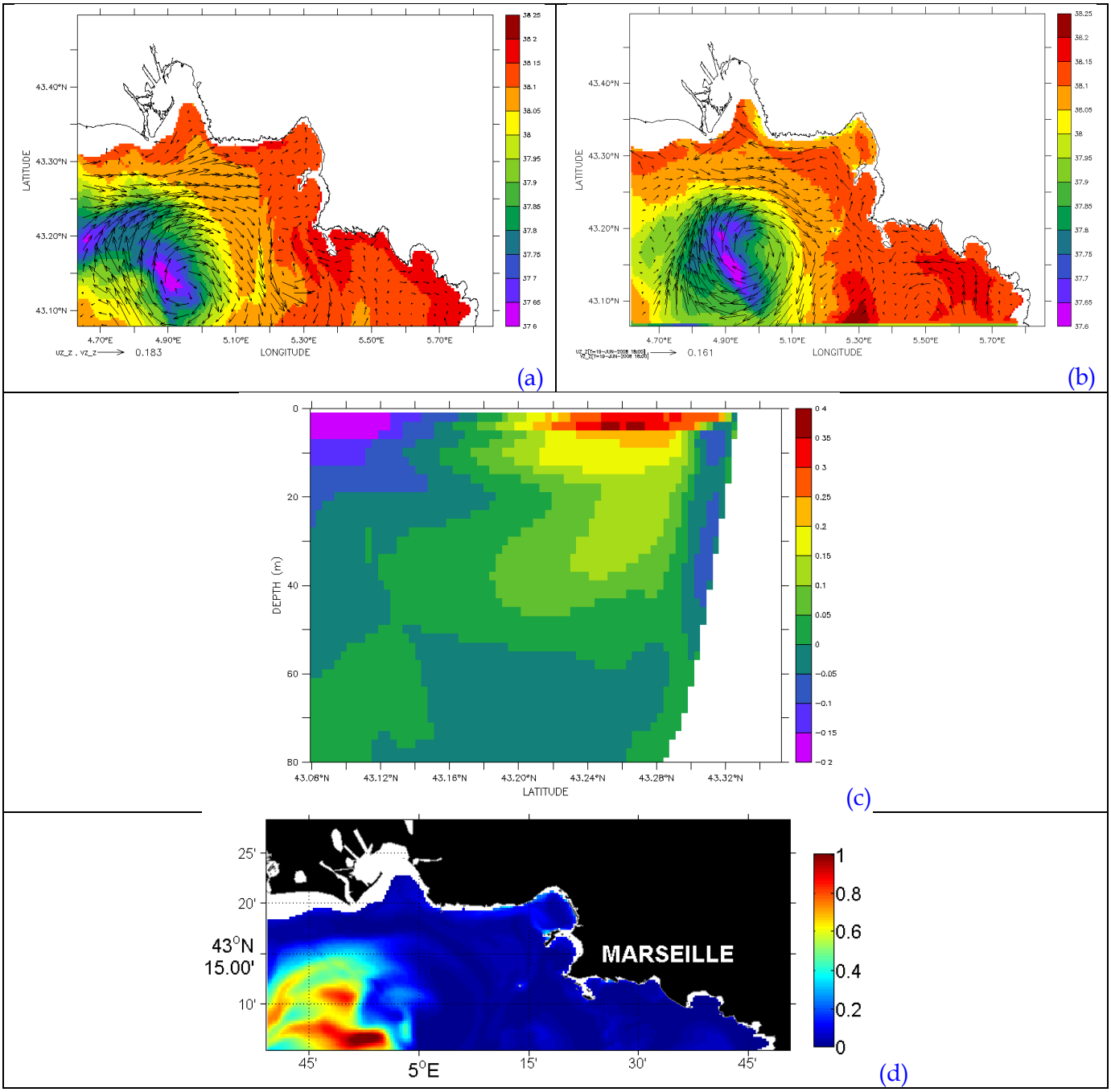

Figure 142: Maps of salinities and currents (at 20m) for (a) 15 June 2008 at 18h and (b) 20 June 2008 at 18h. (c) Vertical cut along 5.1°E showing the zonal velocities (m/s) for 16 June 2008 at 18h. (d) Nitrate concentration at 20 m on 20 June at 18h (µmol/L).

This type of dynamic structure can contribute significantly to horizontal mixing and thus to the redistribution of Rhone plume water in the study area. Similar anticyclonic eddies were also modelled and observed by HF radar in June 2005 and 2006 by Schaeffer et al. (2011) who suggested two formation mechanisms. The first mechanism is related to Mistral wind forcing and topography; the second is related to a strong southerly wind and a buoyancy pulse created by the Rhône waters. In the case of the 2008 eddy, the wind was not particularly intense which makes it difficult to decide which mechanism might have been responsible as they likely acted together.

This eddy remained present for a long period of time (Figure 141a to e). The currents at the edge of the eddy seem to direct the water towards the Bay of Marseille, which leads to a strong intrusion of Rhône water on 17 June (Figure 141c). From the longitudinal section of the zonal velocities passing through the centre of the eddy (Figure 142c), it can be seen that the eddy extends down to 20-30 metres. A downwelling at the centre of the anticyclonic eddy seems to trap and sink the desalinated water from the Rhone. Indeed, desalinated water can be seen at the heart of the eddy at a depth of 20m (Figure 142a and b). Due to the nutrient-rich Rhone waters there is an enrichment of nitrate at the centre of the eddy (Figure 142d) which leads to the development of phytoplankton and high concentrations of chlorophyll.

This eddy therefore seems to interact strongly with the water masses coming from the Rhone, both by transporting them towards the Bay of Marseille, but also by trapping them and exporting them towards greater depths.

5.5.4.3 Biogeochemical situation (ECO3M-MASSILIA)

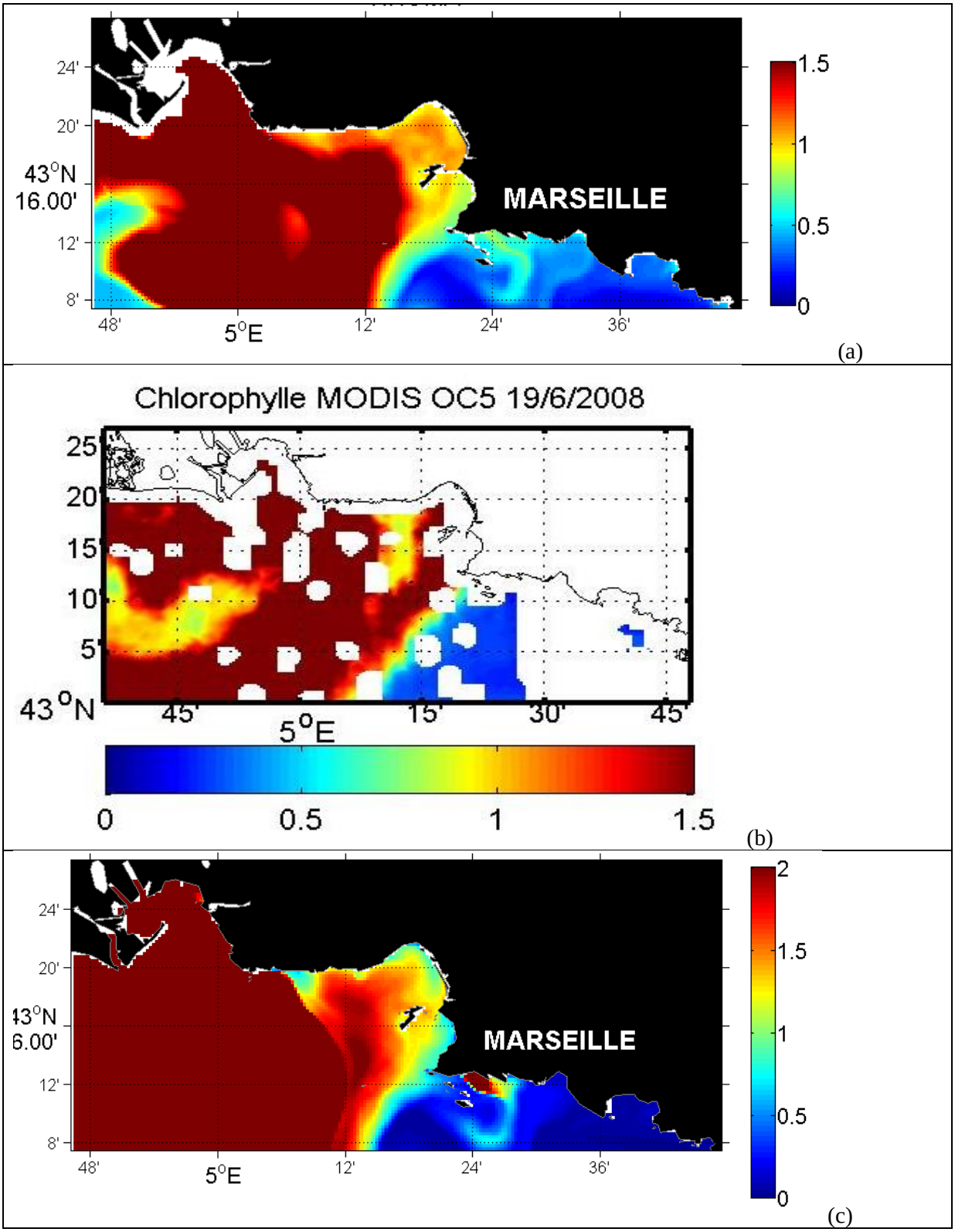

Figure 143: Maps for 19 June 2008 of (a) modelled surface chlorophyll concentrations (µg/L) (integrated over top 10m), (b) observed chlorophyll (µg/L) by MODIS, and (c) modelled surface nitrate (µmol /L).

The coupled biogeochemical model also correctly represents the increase in surface chlorophyll observed on the satellite images on 19 and 21 June 2008 (Figures 143 and 144). This increase in

chlorophyll is due to the high concentrations of nutrients in the water coming from the Rhône. In fact, nitrate concentrations in the Bay of Marseille on 19 and 21 June 2008 are much higher than usual.

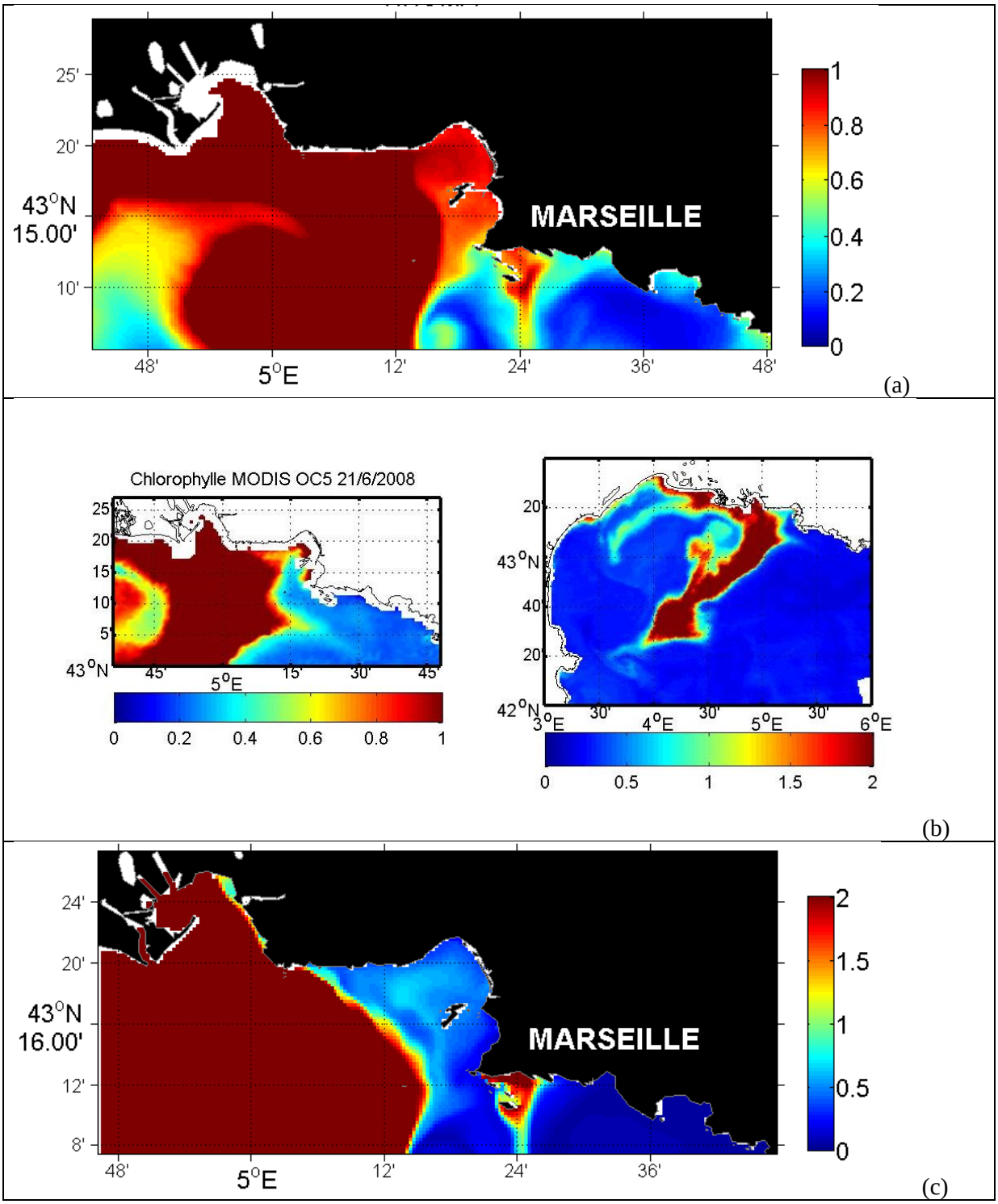

Figure 144: Maps for 21 June 2008 of (a) modelled surface chlorophyll concentrations (µg/L) (integrated over top 10m), (b) observed chlorophyll (µg/L) by MODIS (left: zoon on RHOMA area), and (c) modelled surface nitrate (µmol /L).

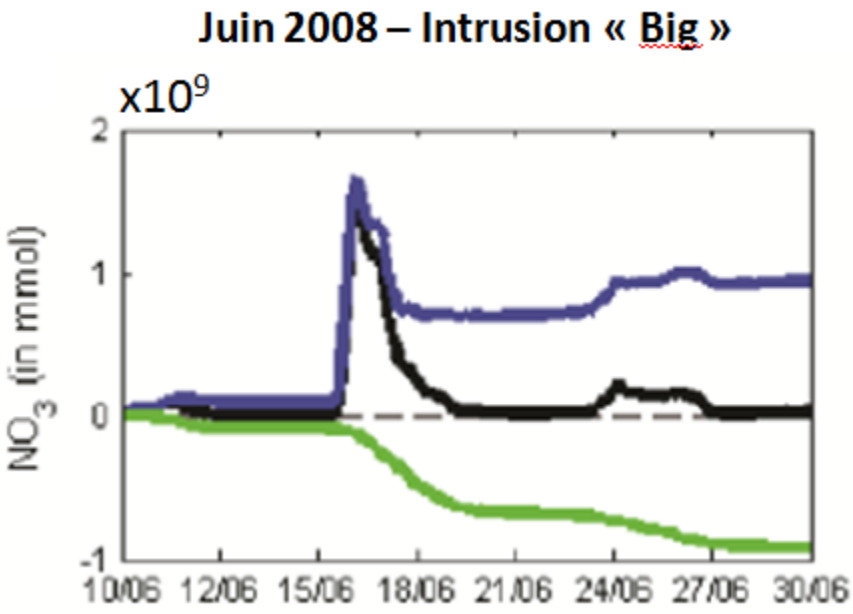

Figure 145: Temporal variation in total nitrate (black) and contributions by different sources: open boundaries (blue), biology (green) (if slope >0 = positive variation of the concentration = nitrate input, and vice versa).

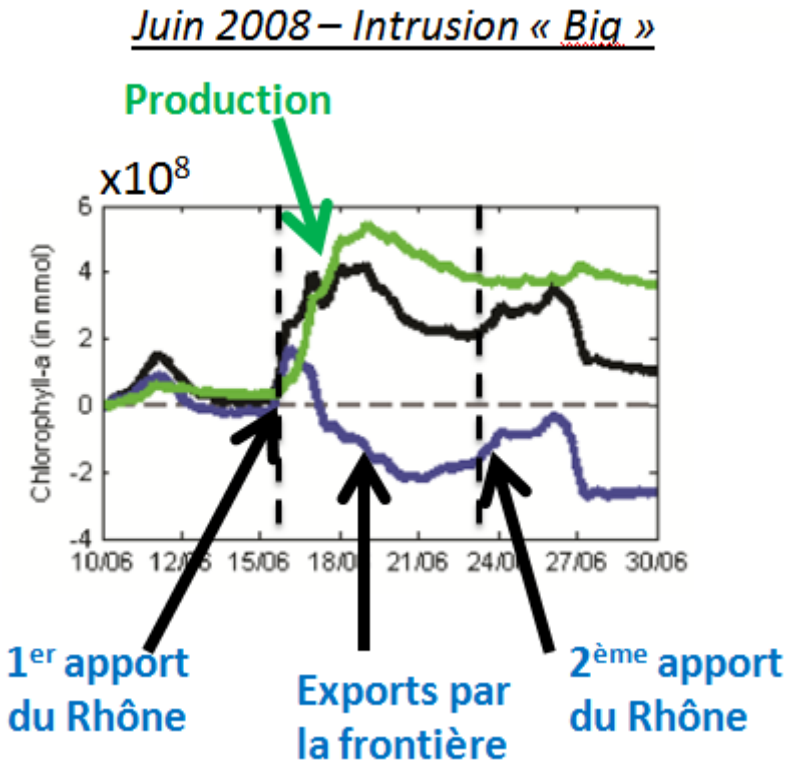

Figure 146: Temporal variation in total chlorophyll (black) and the contribution of the different forcings: open boundaries (blue), biology (green) in the evolution of the total stock in the bay (delimited by the blue vertical walls in Figure 131) (if slope >0 = positive variation in concentration = input of chl, and vice versa)

When considering the temporal evolution of the June 2008 intrusion, it can be seen that at the beginning of the 16-17 June event, there is an increase in total nitrate (Figure 145) which is due to the input of Rhone plume ater through the boundary, some of which is exported outside the domain (blue) and some is immediately consumed by phytoplankton (green), which stabilises after 20 June when all

inputs have been consumed. Then, after 24 June, another intrusion from the Rhone can be observed (in blue). If we look at the evolution of chlorophyll over the same period (Figure 146), we can see that the consumption of nitrate from the 1st input gives rise to a significant increase in chlorophyll (autochthonous) 2 to 3 days later (green). During the 2nd input it is essentially chlorophyll from the frontal zone of the Rhone plume that is transported into the bay (blue), which explains the increase in total chlorophyll in the bay. However, 3 days later (27 June) there is a small autochthonous bloom (green).

5.5.4.4 Hydrosedimentary situation

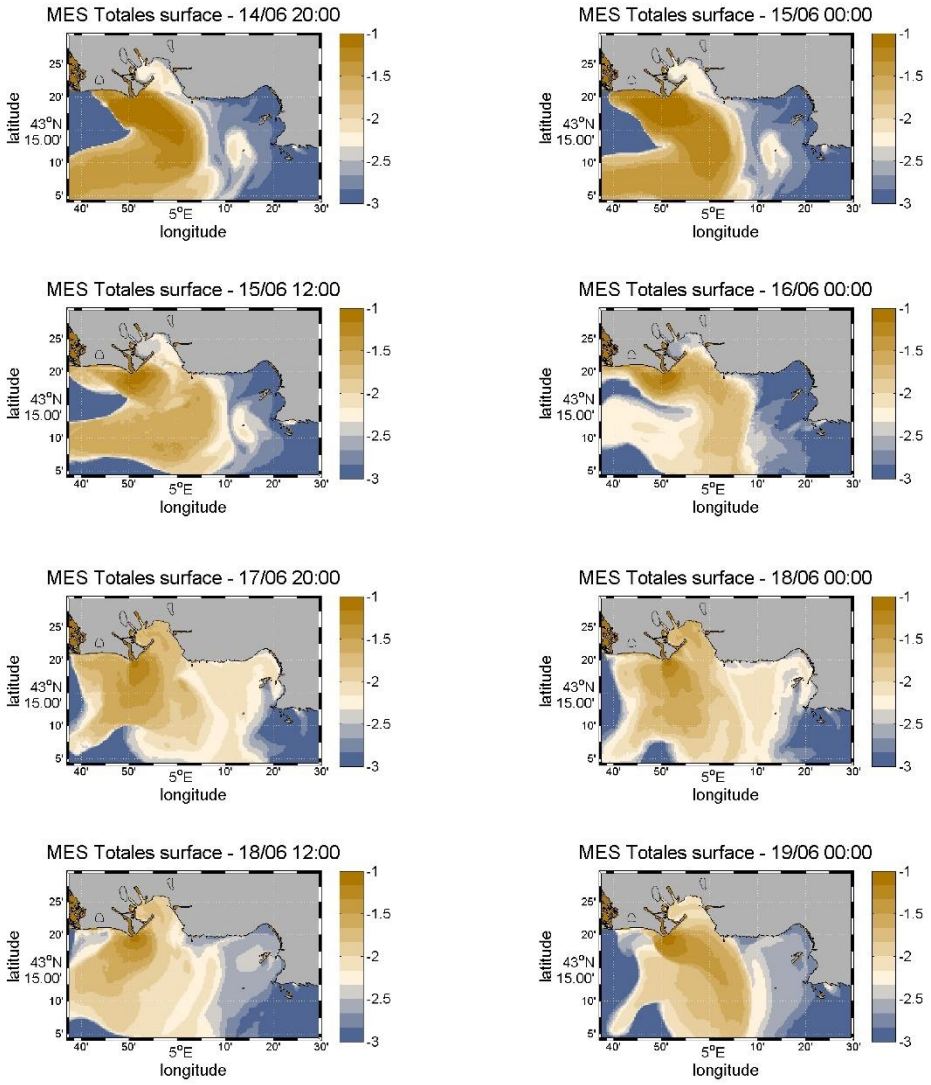

Figure 147: Spatial distribution of SS at the surface (in g/L, log scale) between 14 and 19 June 2008.

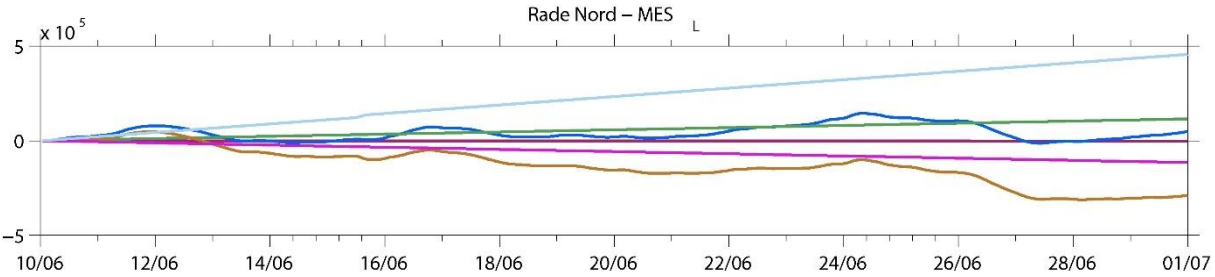

Figure 148: Balance of light SS (brought by the Rhone) into the Northern Harbour (in g/L, log scale)

In contrast to the typical intrusion observed in 2007, the extreme intrusion in 2008 is consistent with a large flow of the Rhone, and therefore a high influx of solids from the river. Figure 147 shows the dynamics of the surface plume during the Rhone intrusion. The concentration of SS is high in the prodelta (over 100 mg/L) on 14 and 15 June. Progressively, the plume shifted eastwards and reached the northern harbour on 17 and 18 June, with concentrations in this zone exceeding 10 mg/L. This intrusion resulted in depositions in the northern harbour over a long period after the start of the intrusion (Figure 148).

5.5.4.5 CB153 contamination

The intrusion of the Rhône during this period causes a very significant increase in concentrations in the Marseilles harbour (Figure 149 to 151). However, the plume is mainly confined to the surface layer (top 10 m) (Figure 151) and the average concentrations in the bottom layer remain of the same order of magnitude as in the other situations examined (Figure 150). The evolution of the CB153 stock in the northern harbour matches exactly the in-/outflow through the boundaries, with only minor sedimentation occurring in the southern harbour (Figure 152). The Cortiou area, on the other hand, is not impacted by this Rhone intrusion. Overall, on the scale of the Marseilles harbour, the Rhone intrusion has a significant but brief impact, especially in the northern and western parts.

Dissous en surface (pg/L)

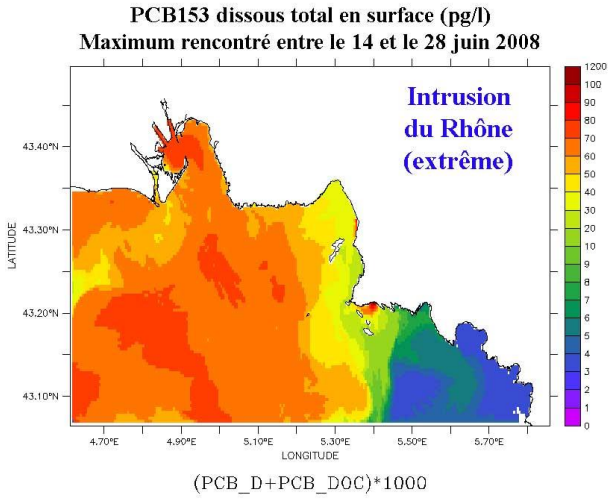

Particulaire en surface (pg/L)

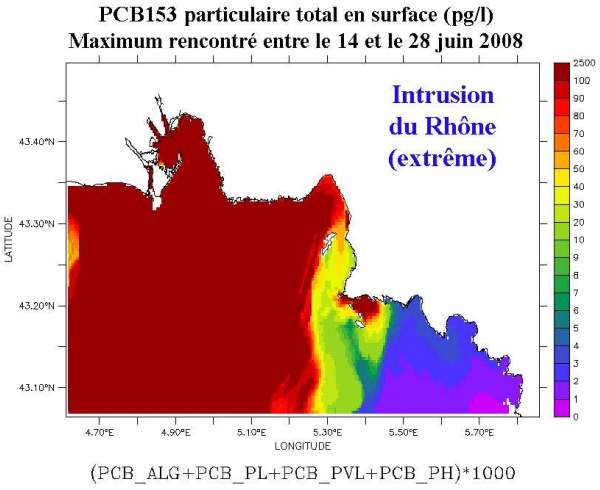

Figure 149: Maximum surface concentrations (pg/L) between 14 and 28 June 2008.

Particulate at the surface (ng/g)

Particulate at the sea bed (ng/g)

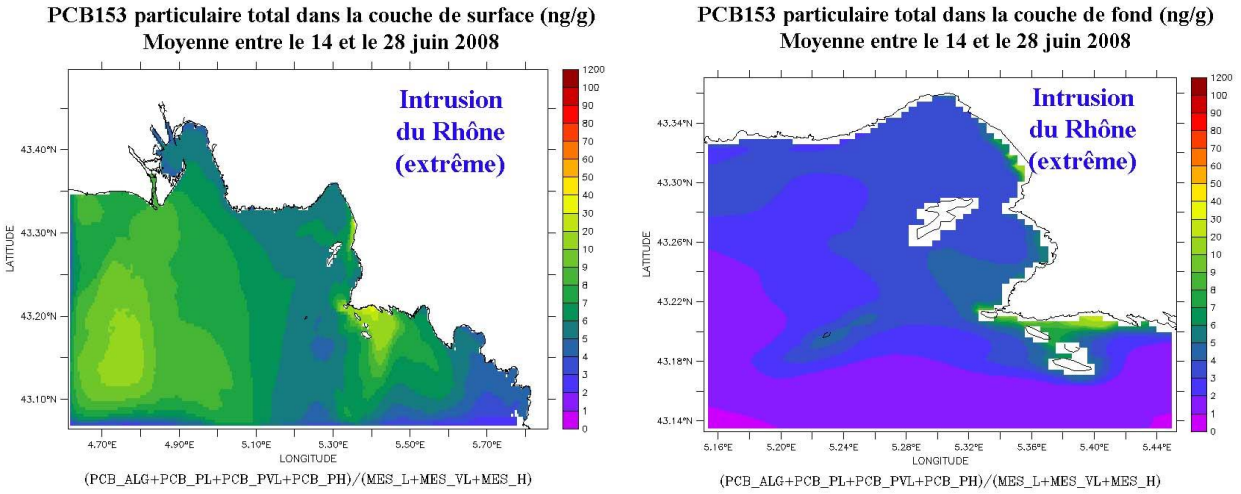

Figure 150: Average levels of particulate CB153 (ng/g) found at the bottom and surface between 14 and 28 June 2008.

Dissolved (pg/L) Particulate (pg/L)

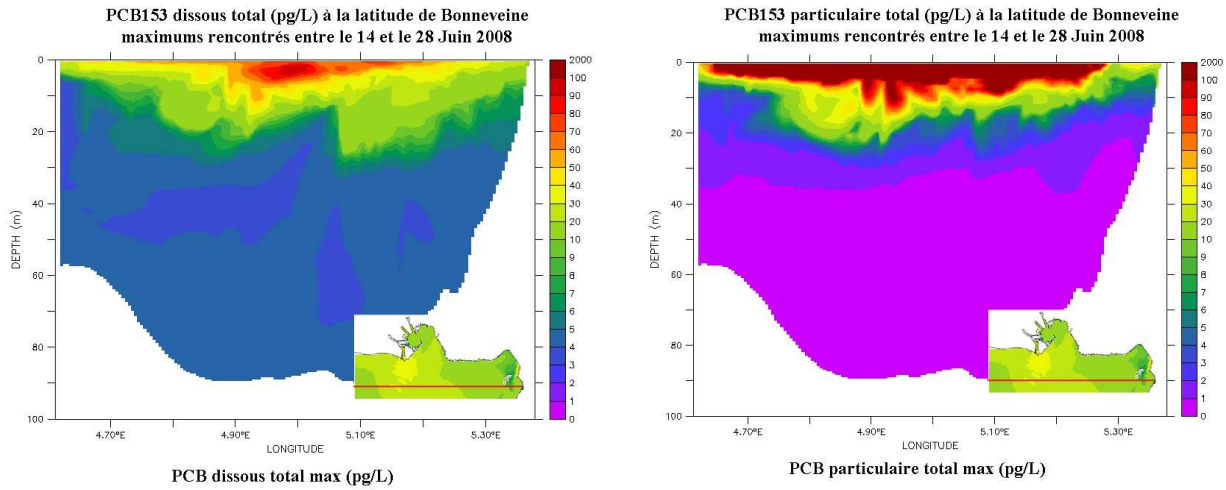

Figure 151: Maximum concentrations between 14 and 28 June 2008 in vertical sections along the latitude of Bonneveine

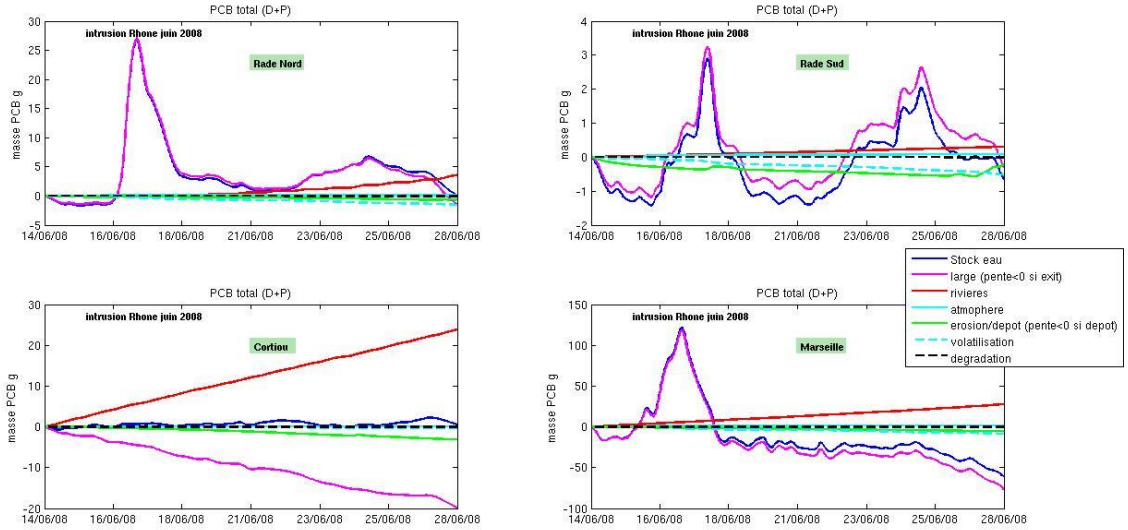

Figure 152: Variability in total CB153 in the water column in each area (see Figure 15), associated with variations in concentrations due to each process "open sea": input/output at boundaries; "rivers": input at the coast; "atmosphere": dry deposition and rainfall; "erosion/deposition"; "volatilisation" and "degradation". (slope >0 means positive change in concentration= contaminant input, and vice versa).

5.5.5 Generation and characterization of this Rhone river intrusions

Subsequently, Fraysse et al. (2014) studied the frequencies and processes of occurrence and destruction of Rhone intrusions in the Bay of Marseille. After studying numerous Rhone intrusions, they highlighted the factors which allowed the Rhone plume to extend into the Bay of Marseille in the surface layer, namely significant river flows (Rhone flows >1700 $m^3 s^{-1}$) and/or a thermal stratification of the water column generated by a thermocline located at a depth < 40 m. This extension is then accompanied by factors allowing the transport of plume water into the bay through currents related to either the presence of the anticyclonic eddy (ME) or the generation by winds, particularly in the event of a wind reversal (NW/SE) linked to a weakening of the wind.

An in-depth analysis of these events and generation factors showed that 50% of intrusions occur with a Rhone flow >1700 $m^3 s^{-1}$, 79% of intrusions occur in the presence of thermal stratification with the a shallow (< 40 m) thermocline, 90% of intrusions occur in the presence of the eddy (ME), and 95% of intrusions in case of wind reversal (NW/SE). Based on these findings, Fraysse (2014) proposed a conceptual scheme to determine whether an intrusion event will occur based on the aforementioned factors, and if so, the type of intrusion and its frequency of occurrence. Based on their spatial coverage and duration, they also divided intrusion events into three different categories: 'big' intrusions that have a large spatial coverage and long duration, 'short' intrusions have a large spatial coverage but a short lifetime, and 'small' intrusions which have a small spatial coverage and short duration (Figure 153).

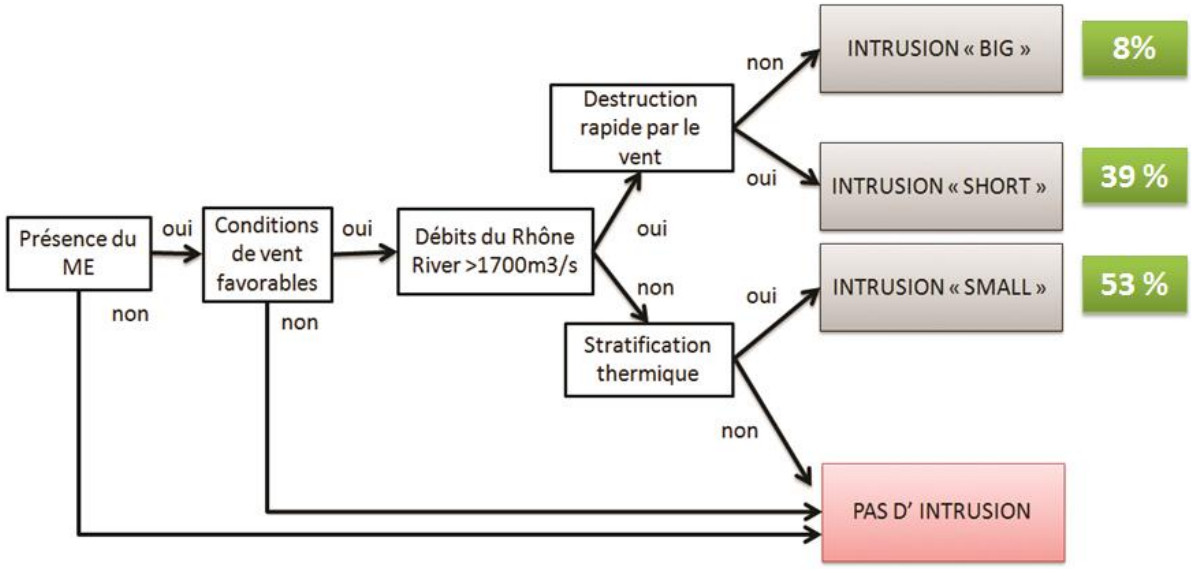

Figure 153: Conceptual diagram of the generation factors that lead to different types of Rhone intrusion events with their relative frequency of occurrence given as percentages.

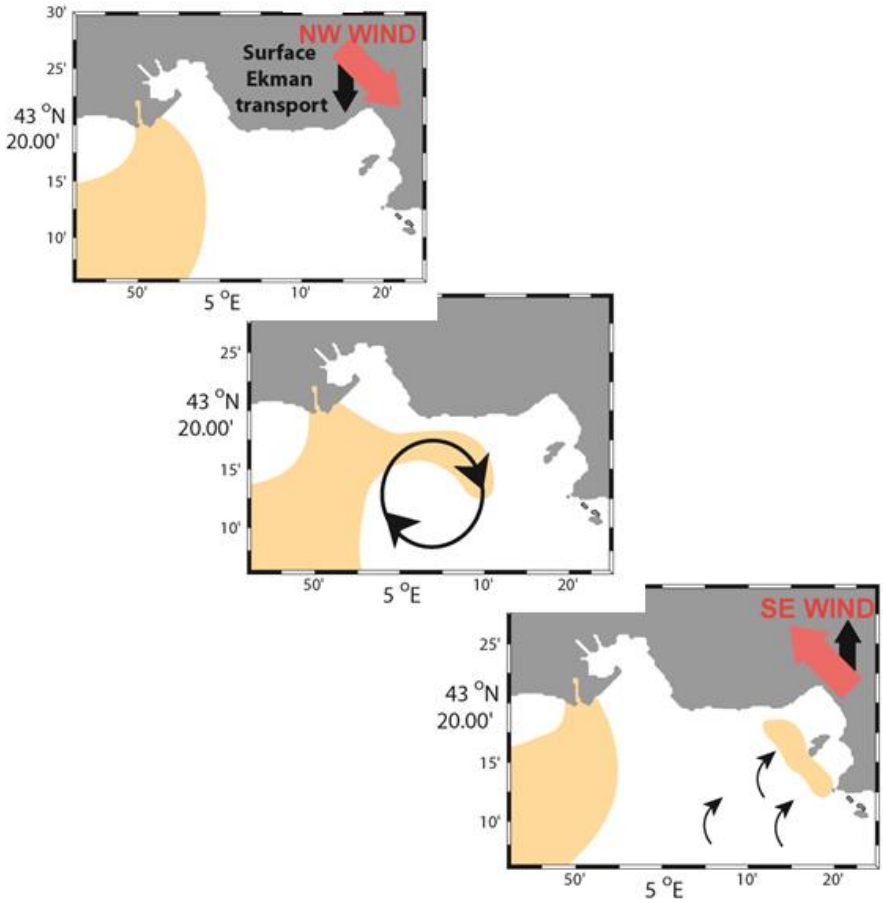

Figure 154 : Graphical representation of a typical situation with the westward displacement of the Rhône plume and the different mechanisms of generation of a "small" Rhône intrusion.

The authors were able to establish different scenarios that could lead to the generation of an intrusion event. Under NW wind conditions (Mistral), the Rhône plume extends offshore in a SW direction with a comma shape. The volume of water in the Rhone and the depth of the thermocline are decisive for bringing the Rhone water into contact with the northern edge of the ME anticyclonic eddy, which pushes the plume water eastward into the Bay of Marseille. This point of contact is achieved either if there is a sufficiently large volume of plume water (independent of stratification) or, of the plume water volume is small and there is a shallow thermocline present allowing the diluted Rhone water to glide along the surface and thus spread far enough south to come into contact with the eddy.

In situations where the Rhone flow is low, a shallow thermocline allows the plume water to come into contact with the ME, which then transports this water towards the Bay of Marseille with SE winds pushing it toward the coast. These SE winds can detach a small tongue of plume water from the eddy. As the plume water only comes into contact with the northern edge of the gyre, only small amounts of water from the Rhone are advected towards the Bay of Marseille, leading to a “small” intrusion event (Figure 154).

In situations where the volume of Rhone water is high, the extent of the plume is sufficiently large and part of it becomes trapped in the ME. If this happens and the wind shifts from NW to SE, the trapped plume water is pushed into the Bay of Marseille, leading to a "big" or "short" intrusion event (depending on the lifetime which is related to the persistence of favourable wind conditions) (Figure 155). When the winds become unfavourable, the intrusion is destroyed either by NW winds (Mistral) pushing the plume water offshore or by persistent SE winds leading to a confinement of the plume water near the coast (Figure 156).

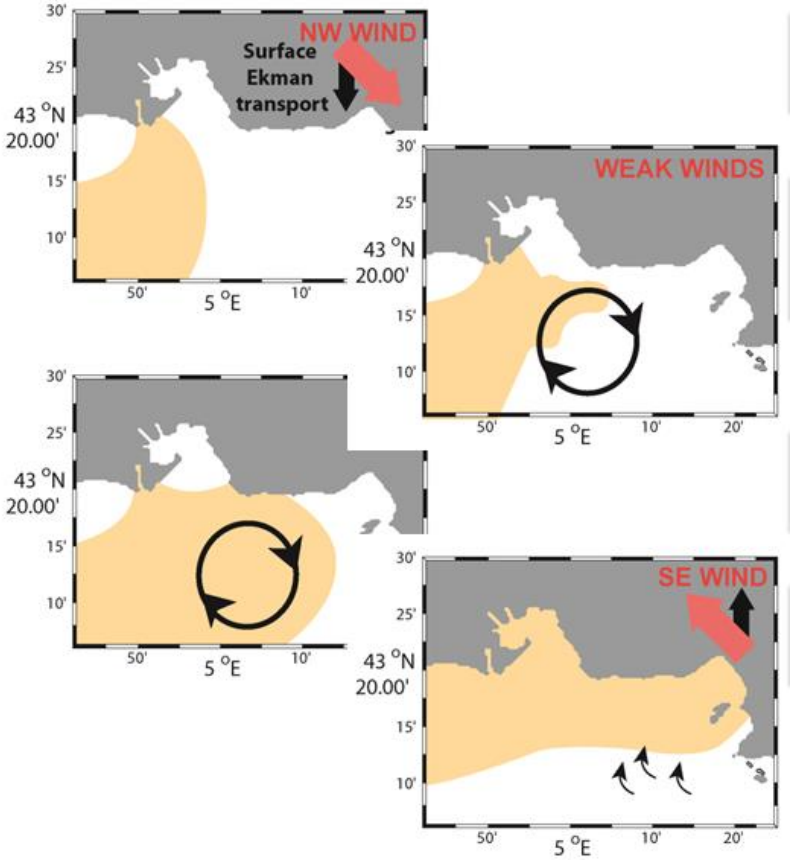

Figure 155: Graphic representation of a typical situation with the westward displacement of the Rhone plume and the different mechanisms of generation of a "big" and "short" intrusion.

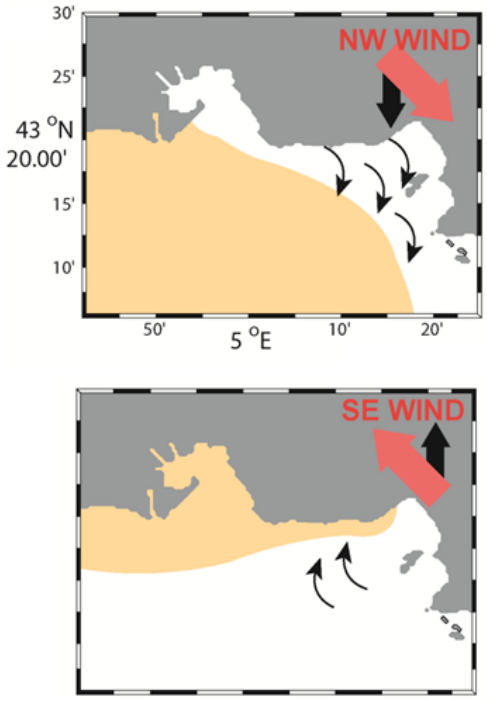

Figure 156: Graphic representation of the two mechanisms leading to the end of an intrusion event.

The impact on the Bay of Marseille is identical for both destruction mechanisms: the water from the Rhône is pushed out of the bay, which leads to a significant export of biogeochemical substances. Finally, the main difference between the different types of intrusions is the amount of water transported into the Bay of Marseille. Due to their different generation mechanisms, the "big" and "short" intrusions impact up to 20 m depth while the "small" ones only affect the surface.

INTRUSIONS BY THE NORTHERN CURRENT

5.6 INTRUSIONS BY THE NORTHERN CURRENT

The main component of the general circulation in the north-western Mediterranean is the North Current (NC) (Figure 157), which runs along the continental slope off the Gulf of Lion, where it delimits and controls the cross-shore circulation, effectively separating the typically nutrient-rich waters of the continental shelf (due to the presence of the Rhone) from the rather oligotrophic open Mediterranean. The Northern Current originates from the confluence of the western and eastern Corsican currents in the Ligurian Sea and flows towards the Balearic Sea constituting the general cyclonic circulation in the north-western Mediterranean.

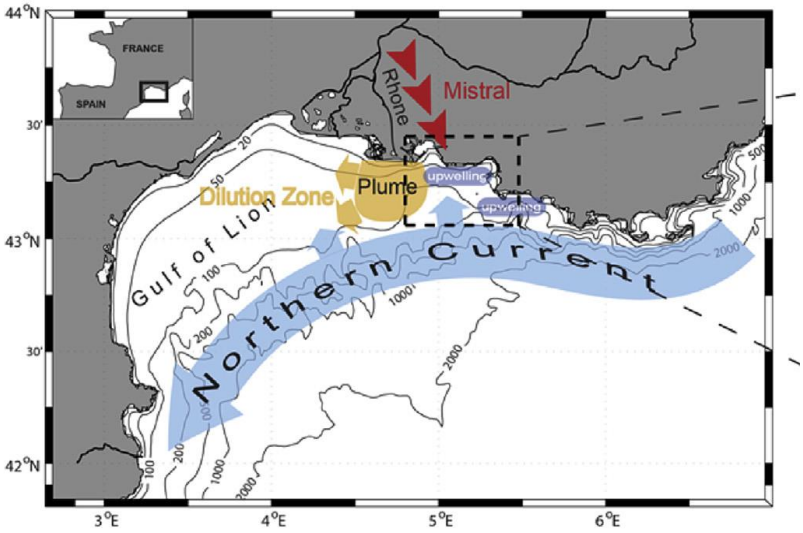

Figure 157: Circulation of the Northern Current (blue) in the north-western Mediterranean and possible intrusions into the Bay of Marseille (dotted black box) from Ross et al. (2016).

The NC exhibits a seasonally variable flux (maximal in winter) between 1 and 2 Sv which is comparable to the fluxes through the Strait of Gibraltar (Alberola et al., 1995). The NC is wider and shallower in summer (50 km and 250m respectively) when it flows further off-shore. In winter, it moves in-shore where it narrows and deepens (ca. 30 km and 450 m) reaching maximal velocities of over 50 cm s^{-1} (Andre et al., 2009). Particularly in winter, the NC also becomes baroclinically unstable and produces important mesoscale meanders which can penetrate onto the GoL shelf (Millot, 1999; Petrenko, 2003; Rubio et al., 2009).

These intrusions of the NC can occur at various places along the shelf. Most frequently, they tend to occur at the eastern entrance to the Gulf (Petrenko et al., 2005) and at the centre (Estournel et al., 2003), with more rare occurrences at the south-western side (Petrenko et al., 2008). Using data from 12 coastal cruises, Gatti et al. (pers. comm.) found that intrusions can occur during any season of the year and that the intrusion flux can amount to 0.37 SV or 30% of the flux of the NC itself. They also carried out numerical realistic simulations which suggest that intrusions can occur as often as three to four times per month with durations of a few days to two weeks. By combining *in situ* observations and high-resolution modelling, Barrier et al. (2015) observed a total of 12 intrusion events during their 12 month study period, although they state that the amount of observational data in particular is not sufficient to capture all intrusion events and they only counted very large intrusions in their analysis.

Three kinds of wind events are likely to generate intrusions: cessations of strong Mistral events (Millot and Wald, 1980), episodes of inhomogeneous Mistral, or periods of easterly winds (Petrenko, 2003; Petrenko et al., 2013). NC intrusions onto the shelf have also been linked to the strength of density stratification and the pycnocline depth with the NC splitting into a main and a northern branch, the latter creating an intrusion if the stratification is strong and shallow (Echevin et al., 2003; Petrenko et al., 2005). However, other studies showed that intrusions at the eastern entrance to the GoL could occur independently of stratification (Petrenko, 2003). These seemingly contradicting results suggest that the real causes of intrusions are still unclear (Petrenko et al., 2005) although the shift in the local wind regime may play a crucial role (Pairaud et al., 2011; Petrenko et al., 2008). Barrier et al. (2015) suggested that intrusions on the eastern part of the gulf are mainly forced by easterly or north-westerly wind events and they found them to be most frequent in the autumn and winter months.

While the Northern Current (NC) and its intrusions onto the continental shelf in the Gulf of Lion have been widely studied from a hydrodynamical point of view (Alberola and Millot, 2003; Petrenko, 2003), including intrusions in the eastern GoL (Pairaud et al., 2011; Petrenko et al., 2008), little is known about the impact of these intrusions on the biogeochemistry.

Ross et al (2016) investigated the impact of intrusions of this oligotrophic current on the biogeochemical functioning of the Bay of Marseille during the October 2011 intrusion. Just before 13 October, there was a week of Mistral generating an upwelling at the coast whose characteristic cold, nutrient-rich waters (and chlorophyll to a lesser extent) are still visible on 12 and 13 October (Figure 158 and 159). Then the Mistral weakened and gave way to an East-South-Easterly wind on 15 October. On 13 October, the NC passed by the entrance to the Bay of Marseille with high velocities of over 0.5 m s^{-1} and warmer waters which progressively replaced the cold nutrient rich upwelled waters (increase in temperature by up to 4°C), clearly visible from October 16th onward. The anticyclonic Marseille Eddy begins to form. The vertical velocity profile clearly shows that the current affects the whole water column down to at least 70 m (Figure 158), which confirms that it is indeed an intrusion of the NC and not only a surface current due to the south-easterly wind. On 18 October, the shelf is covered with warm water of about 20°C and the Marseille Eddy is well formed. The biogeochemical impact of this NC intrusion, which replaced the cold, nutrient and chlorophyll rich water that had been upwelled on 12 October by warm and rather oligotrophic offshore water, is very visible from 15 October onward. Moreover, the arrival of this water with higher N/P ratios will induce a shift in the nutrient limitation of phytoplankton, which were limited by nitrogen during the upwelling period to becoming phosphorus limited as the intrusion takes place (Figure 159).

From a biogeochemical point of view, it is possible to distinguish a different ecosystem functioning during the upwelling (before 12 October), during the NC intrusion period (13-15 October), and once the intrusion is in a steady state (from 16 October onward). The chlorophyll increase associated with the upwelling (in green, input of nutrients from the bottom) is compensated by the input of NC water containing a lower concentration of chlorophyll (in blue, Figure 160), before gradually stabilising after 16 October (no change). In the same way, the phosphates brought in by the upwelling are gradually replaced by poorer water with a lower PO4 concentration (Figure 161).

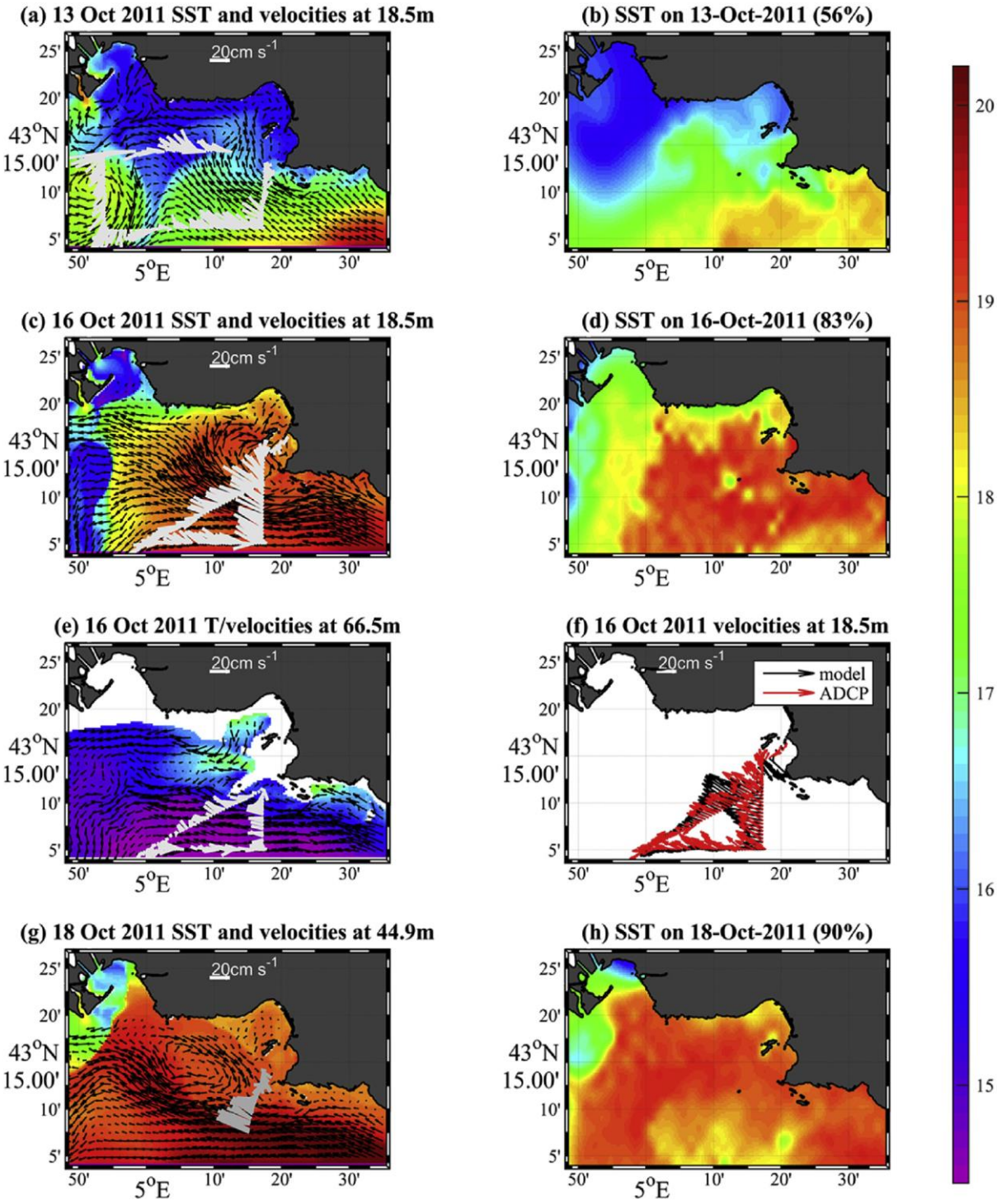

Figure 158: (a) Model velocities (black arrows) with measured ADCP velocities (light grey bars) at a depth of 18.5 m on 13 Oct 2011 superimposed on modelled SST. (b) Remotely sensed SST for 13 Oct 2011 (the percentage in brackets gives the satellite coverage for that day). Corresponding plots for (c-d) 16 Oct 2011 and (g-h) 18 Oct 2011. (e) as in (c) but with both the temperature and velocities at 66.5 m. (f) Comparing modelled with measured velocities along the ship track at 18.5 m depth (from Ross et al. (2016)).

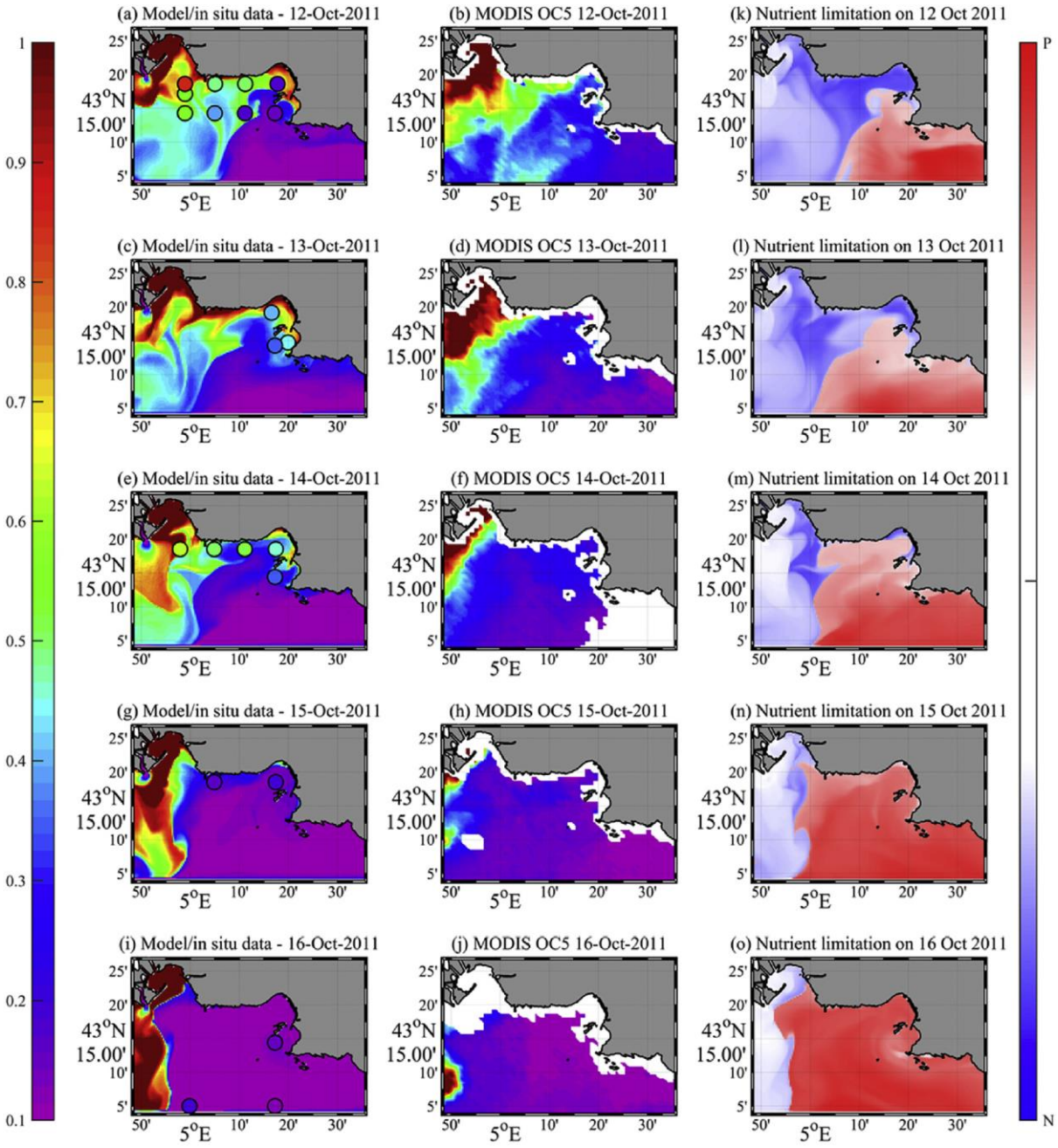

Figure 159: (a) *In situ* observations of surface Chl-a (filled circles, various times of the day) superimposed on the modelled surface Chl-a concentrations (at 12:00 h) for 12 Oct 2011. (b) MODIS image for the same date. Corresponding images for (c-d) 13 Oct 2011, (e-f) 14 Oct 2011, (g-h) 15 Oct 2011 and (i-j) 16 Oct 2011. The colour scale on the left is valid for panels (a) through (j) and is in mg m^{-3}. Panels (k) to (o) have their own colour scale on the right and show the modelled nutrient limitation in the surface layer for the same dates as before. Red colours signify that photosynthesis is phosphorous limited, blue colours indicate limitation by nitrogen and white colours suggest little or no limitation. The colour intensity corresponds to the strength of the limitation (from Ross et al. (2016)).

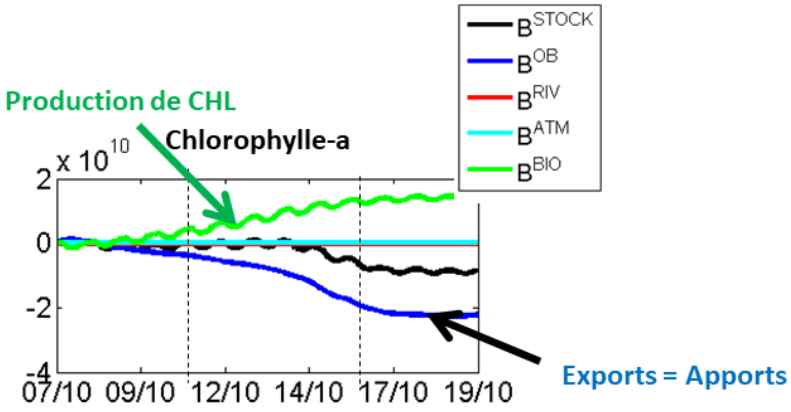

Figure 160: Temporal variation of total chlorophyll and contributions by different forcings: open boundaries (blue), biology (green) in the evolution of the total stock in the bay (delimited by the blue vertical walls in Figure 131) (if slope >0 = positive variation in concentration = input of chl, and vice versa).

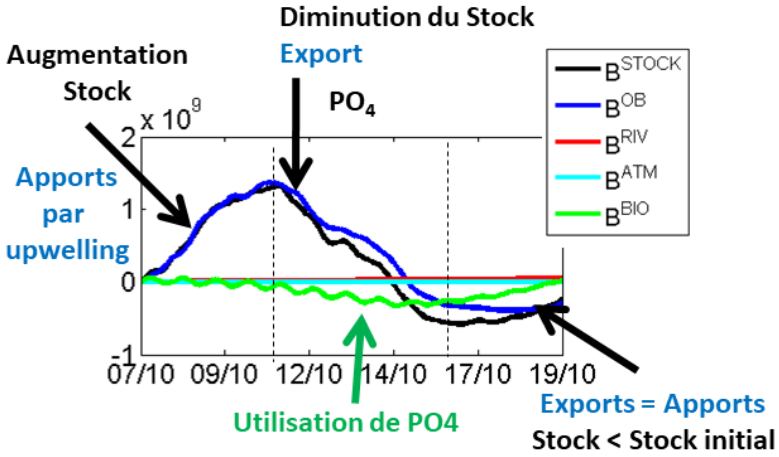

Figure 161: Temporal variation of total phosphate and contributions by different forcings: open boundaries (blue), biology (green) in the evolution of the total stock in the bay (delimited by the blue vertical walls in Figure 131) (if slope >0 = positive variation in concentration = input of PO4, and vice versa).

INTERACTIONS WITH THE MARSEILLE EDDY

5.7 POSSIBLE INTERACTIONS WITH THE MARSEILLE EDDY

In the chapters dedicated to the Mistral-induced upwellings and intrusions by the Rhone plume and Northern Current, we have seen that the anticyclonic Marseille Eddy (ME) interacts with all three processes along its outer edge (points of impact indicated by the crosses in Figure 162).

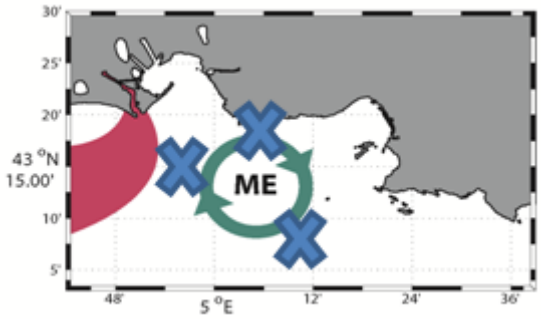

Figure 162: Graphical representation of the position of the anticyclonic eddy Marseille Eddy (ME) and the Rhône plume (pink) and the locations (cross) of interactions with the upwellings (top), the Rhône plume (left) and the Northern Current (bottom)

However, the interior of the eddy is fairly isolated from the eddy's surrounding environment by the dynamic front at the edge and the water inside the eddy will have its own dynamics and evolution. Barré (2020) studied the isolation of these waters and the impact on biogeochemistry, net community production (NCP), and the carbonate system in the eddy's centre during the presence of a ME on 3 June 2017.

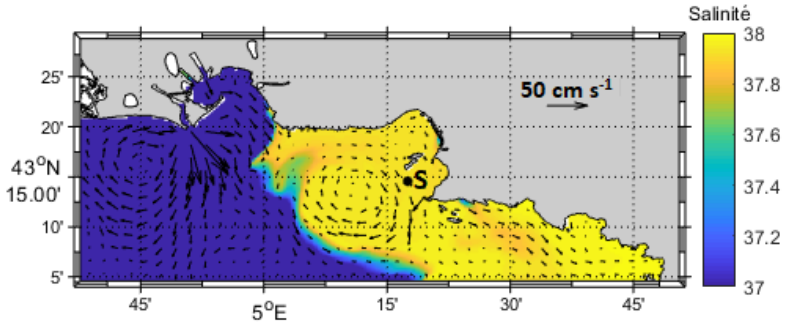

Figure 163: Modelled surface salinity on 3 June 17 at, SOLEMIO station is shown as a black dot with letter S (Barré, 2020).

The presence of the anticyclonic Marseille Eddy can be seen in the simulations from 1 to 4 June 2017. It constitutes a physical barrier to the low-salinity water from the Rhone which remains positioned to the west of the domain, with only a small part being transported along the edge of the ME toward SOLEMIO station (Figure 163). It also represents a physical barrier that traps the water in the eddy's interior which shows a slightly higher chlorophyll concentration due to phytoplankton growth. The anticyclonic current causes the ME to have a slight increase in sea surface height at its centre which can be easily detected and which, along with the velocity field, allows to pinpoint the ME's location (red frame, Figure 164). This convergence of water at the centre causes a downwelling.

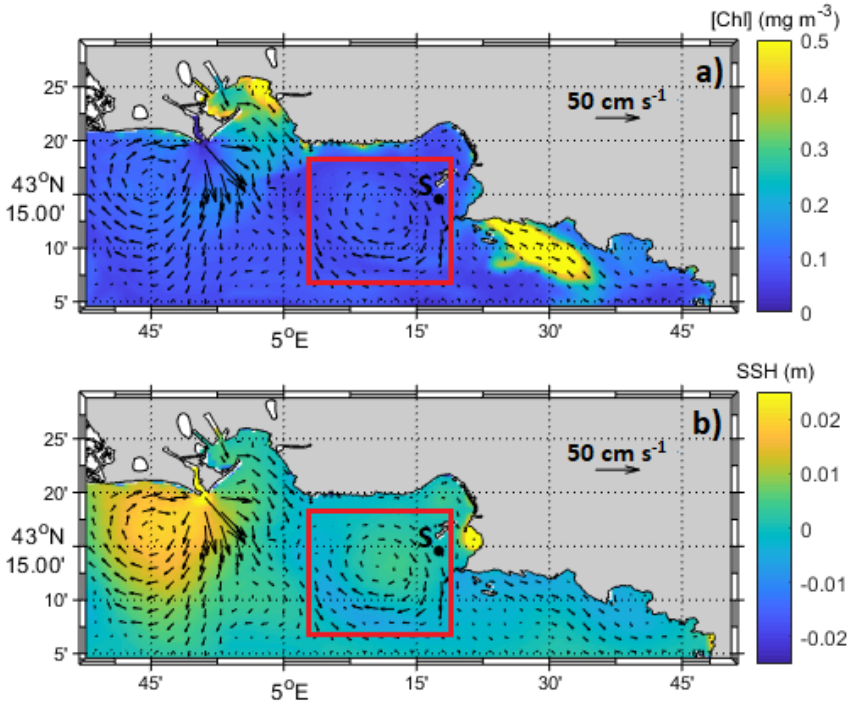

Figure 164: (a) Surface currents and chlorophyll and (b) sea surface height (SSH) modelled for 3 June 2017. The red square marks the location of the Marseille Eddy (Barré, 2020).

A small part of the Rhone plume water will be transported toward SOLEMIO station, located at the outer edge of the eddy, bringing water with higher DIC and TA concentrations, causing a relative increase on 3 June which disappears on 4 June. This increase is small compared to the increase produced by a real Rhone intrusion which takes place on 15 June 2017 (Figure 165).

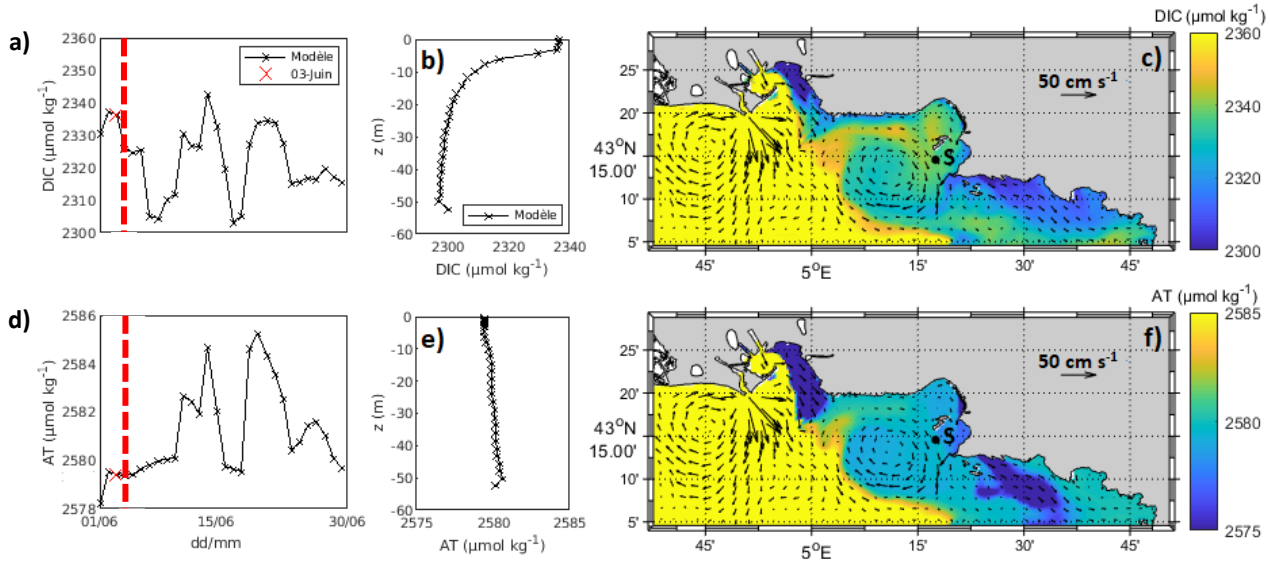

Figure 165 : Modelled (a) DIC and (b) TA surface concentrations at SOLEMIO for 3 June (3 June marked by a cross, 4 June marked by a dashed red line). Vertical profiles of modelled (c) DIC and (d) TA at SOLEMIO (black dot and letter S) on 3 June 2017. Maps of surface (e) DIC and (f) TA concentrations on 3 June 17 (Barré, 2020).

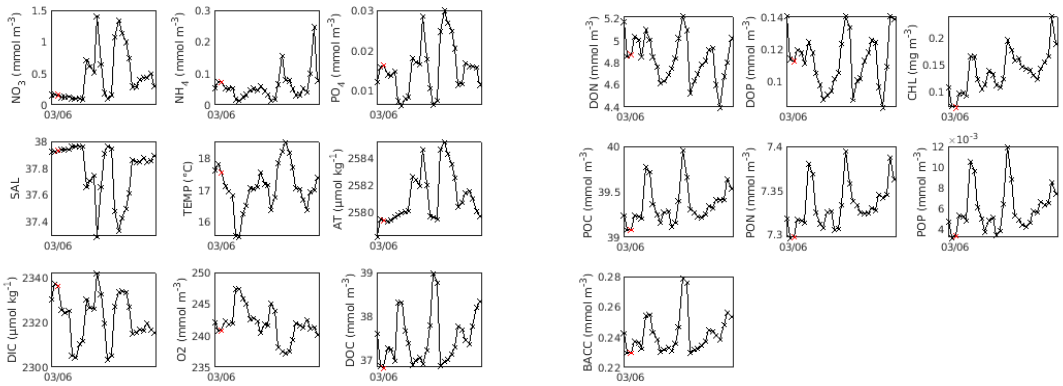

Figure 166: Ensemble modelled variables in the surface layer at SOLEMIO station during the presence of the Marseille Eddy on 3 June 2017: NO_3, NH_4, PO_4, SAL, TEMP, TA, DIC, O_2, DOC DON, DOP, Chl, POC, PON, POP, BACC (Barré, 2020)

The influence of this Rhone water, arriving in small quantities at the beginning of June by the eddy and in larger quantities in mid-June during the Rhone intrusions, is clearly visible in the biogeochemical variables, resulting in an increase in nutrients and organic matter and in a decrease in oxygen due to the heterotrophic processes occurring in these riverine waters, especially during the mid-June intrusion (Figure 166). This results in a drop in phytoplankton production and an increase in heterotrophic respiration (Table 14), which further reduces the NCP, which is already negative at this point (i.e., with mostly heterotrophic processes in June) (Figure 167).

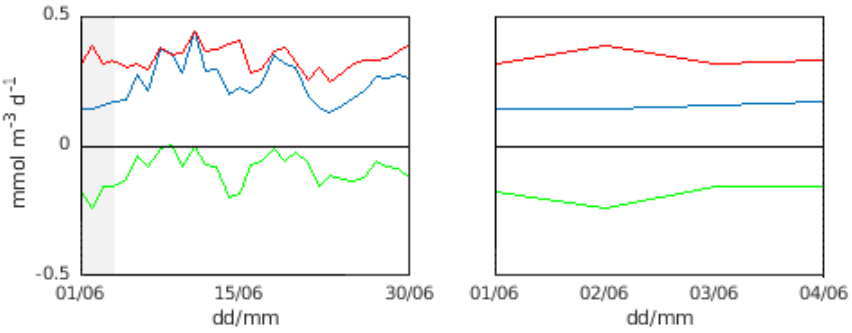

Figure 167: Temporal evolution of NCP (green), GPP (blue), and total respiration R (red) (mmol m^{-3} d^{-1}) in June 2017 with the period from 1 to 4 June shaded in gray. The right panel shows a zoom onto the period when the ME is present (Barré, 2020).

Table 14

NCP, GPP, and respiration (total: R, autotrophic: RA, heterotrophic: RH) for June 2017 and the Marseille Eddy period (mmol m^{-3} d^{-1}).

	NCP	GPP	R	RA	RH
June 2017	-0,096	0,240	0,336	0,035	0,301
Marseille Eddy	-0,182	0,153	0,335	0,022	0,313

6 CONCLUSIONS and PERSPECTIVES

6.1.1 Mistral Events

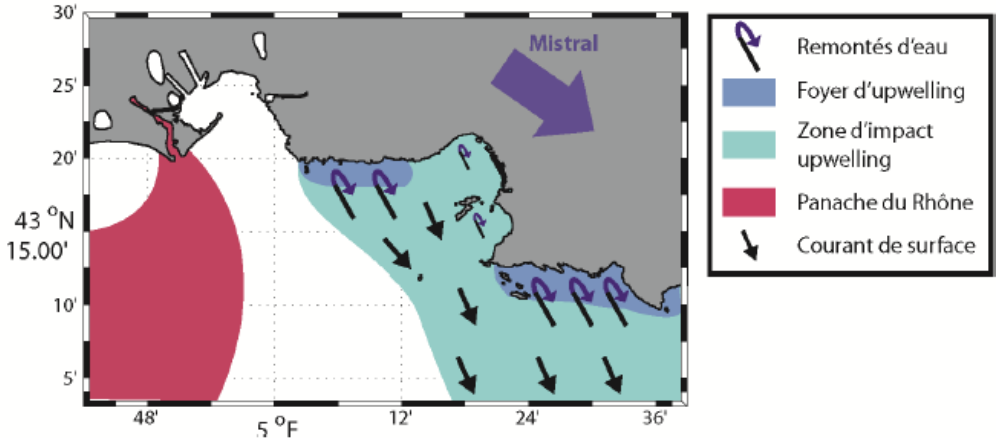

Figure 168: Graphical representation of a typical upwelling situation during a Mistral event according to Fraysse et al. (2014).

The Mistral induces upwelling processes that bring cold, nutrient-rich bottom water to the surface, while the water already present at the surface is exported offshore. The water that rises along the Côte Bleue forms a clear front with the surrounding surface water (Figure 168). There is also resuspension of sediments taking place in the southern harbour which are then carried offshore. The differences between the typical and extreme events lie mainly in the intensity and response time of the cooling of the surface water after the onset of the Mistral, and the maximum depth from which the water is upwelled, as well as in the intensity of the resuspension and the distance from the coast to which the resuspended sediments are transported. Potentially, these events can induce phytoplankton blooms in the frontal zone at the edge of the upwelled water plume and temporary remobilisations of CB153, but with a general tendency to export contaminants offshore. These events constitute CO_2 sinks (Lajaunie-Salla et al., 2021; Barré et al., 2022a; 2022b).

6.1.2 South-Easterly Wind Events

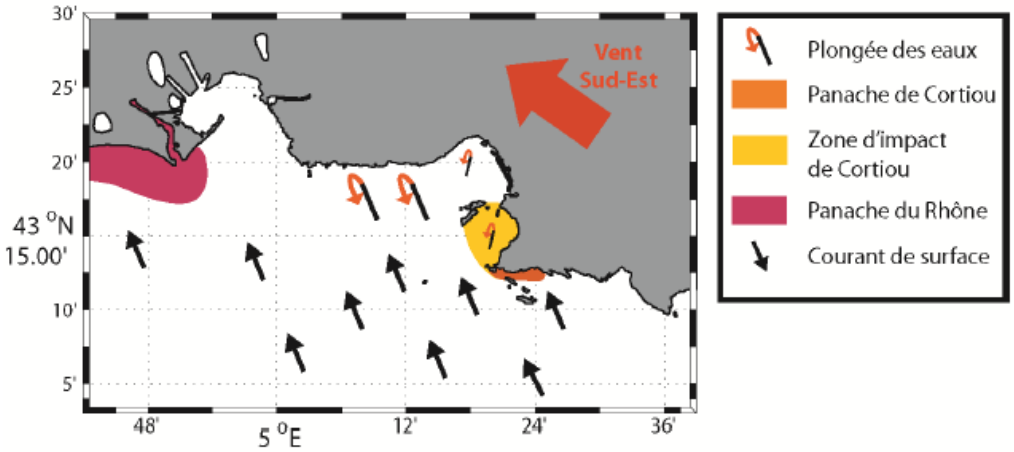

Figure 169: Graphical representation of a typical downwelling situation during a south-easterly wind event according to Fraysse et al. (2014).

South-easterly winds bring in water from the open sea, which is generally warmer and poorer in nutrients and chlorophyll. This water then sinks to the bottom through downwelling processes near the coast (Figure 169). This downwelling process seems to homogenise the whole water column (approximately 0-100 m) leaving the Bay of Marseille with the same characteristics as the open sea. During these events, the southern and northern harbour are protected from the influence of waves and the sediments generally remain in place. On the other hand, erosion events can be observed in the Calanques area in the vicinity of Cortiou, which are likely to mobilise a certain quantity of sediment and CB153. The main difference between typical and extreme events is essentially the intensity of the resuspension. Potentially, these events can therefore induce temporary remobilisation of sediments from contaminant-laden areas such as Cortiou; these particles are then transported by the currents during and redeposited further offshore or in the southern harbour.

6.1.3 Late summer Rain Events

Even if rainfall does not seem to have a significant effect on the hydrodynamics in the area, it adds fresh water loaded with nutrients, suspended matter, and contaminants mostly through the discharge at Cortiou, but also at the Port Autonome and through storm overflows, and occasionally at the Huveaune (Figure 106). In contrast to the spring rains (Fraysse et al., 2014), these inputs do not seem to have any significant impact on phytoplankton at the end of the summer, which suggests that phytoplankton growth is not limited by nitrogen.
On the other hand, the inputs of suspended matter (plumes with concentrations >10mg/L off the discharge area) and CB153 are very significant during these events. The fate of the suspended solids brought in by these rains is strongly dependent on the meteorological situation (wind regime). However, these events are often associated with strong winds and swells which cause erosion on the coast and therefore a resuspension of sediments. On the other hand, these strong particulate inputs due to rain are mostly consist of "heavy" particles which are deposited locally, particularly near the Cortiou outflow. The lighter particles, which make up the surface plume (5 to 10 m below the surface) will move with the surface currents. These events generate the highest variability in concentration, sedimentation, and therefore retention and accumulation of contaminants in the area.

6.1.4 Rhone diluted water Intrusion Events

The Rhone intrusions lead to a decrease in surface salinity and an increase in nutrients, suspended matter, and CB153. These events have a significant impact on the functioning of the ecosystem in the Bay of Marseille. They do not necessarily appear to be directly related to the Rhone flow volume. However, particular wind regimes can induce an intrusion and maintain it over time (Figures 154 and 155). Intrusions can be associated with the presence of an eddy in the area, as in June 2008, which can form in one of two ways (Schaeffer et al., 2011): (1) due to wind (Mistral) and topographic forcing and (2) as a result of strong southerly winds and a buoyancy pulse created by Rhone waters.
This is an important process that must be taken into account, especially if its occurrence is significant during the year. From the point of view of contamination, the Rhone intrusions can cause strong fluctuations in concentrations in the harbour (especially in the northern part), but the impact is transient and does not lead to significant local accumulations; the plume is mainly confined to the surface. These events are a source of dissolved inorganic carbon (DIC) and total alkalinity (TA) (Barré, 2020).

6.1.5 Intrusions by the Northern Current

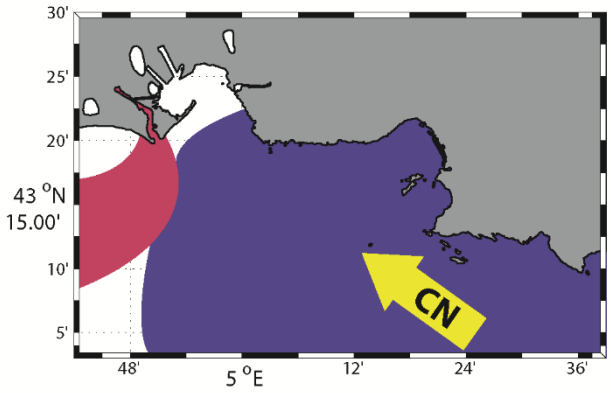

Figure 170: Graphical representation of a typical Northern Current (CN in the figure) Intrusion situation in the Bay of Marseille.

Intrusions of the Northern Current (NC) into the Bay of Marseille transport different water masses into the bay, including at depth, that are characterised by being: warm and low in nutrients and chlorophyll which typically completely changes the biogeochemical characteristics in the bay (Ross et al., 2016). This NC intrusion can initiate the formation of the Marseille Eddy, at least in the upper half of the water column (Figure 158).

6.1.6 Events related to the presence of the Marseille Eddy

We have seen that the anticyclonic Marseille Eddy (ME) interacts with several processes and can transport along its outer edge either upwelled water, or water originating from intrusions of Rhone water or the NC (Figure 162). The water along the outside of the ME will therefore have the same characteristics as those waters, i.e., be nutrient rich if it is upwelled or Rhone water or more oligotrophic if it is NC water. However, at the intereior of the ME, the water masses are isolated from its surroundings and may be downwelled.

6.2 ANSWERS TO QUESTIONS

In the Introduction we posed a number of questions and in this section we will try to answer them. The models, as diagnostic exploration tools, have made it possible to understand and identify the role played by forcings in the functioning of the ecosystem by simulating realistic scenarios (Table 15).

Table 15

Hierarchy of processes studied in the Bay of Marseille and their impacts on the ecosystem (after Fraysse, 2014).

	Intrusions Rhône	Pluies	Vents mistral	Vents SE	Intrusions CN	
Apports Nutriments	+++ (NO_3) + (NH_4)	+ (NO_3) +++ (NH_4)	Apport du fond par *upwelling* +	+ si apport Cortiou (- - si pas d'apport Cortiou)		Quantités décroissantes
Apports allochtones de chlorophylle-*a*	+	0	Variable (MPC)	- - -		Diminution Chl-*a* dans la baie
Production autochtone de chlorophylle-*a*	+++		+	-		Production décroissante
Période de l'année avec impact max observé	Période stratifiée	Printemps > automne	Période stratifiée	Période stratifiée (mais non étudié au printemps)		Impact max en période stratifiée
Impact vertical	Couche de surface		Colonne d'eau			
Export des eaux			Export +++			Diminution de l'impact des apports

Regarding the effect of the the urban Marseille area on the marine ecosystem, we tried to answer the following questions:

- What are the respective roles played by physical (wind: mixing, stratification, upwelling, eddies) and biogeochemical (nutrient inputs, MOP, MOD) forcings in processes that could lead to a possible degradation or restoration of coastal ecosystems subject to strong anthropogenic inputs?

Based on the events we studied, we wanted to describe the processes that can potentially lead to a relative increase in nutrient, phytoplankton, SS, or contaminant concentrations. We knew from the outset that the Bay of Marseille was a very specific environment, since it has a base level that if fairly oligotrophic with typical chlorophyll concentrations < 0.2 µg/L which can increase to > 1 µg/L. The response of the ecosystem (primary production) to the same physical process (upwelling, downwelling, etc.) is very variable and depends on the season. In fact, a net input of nutrients or organic matter does not always lead to and increase in phytoplankton growth as other limitations may be at play such as light or temperature.

The Rhone river intrusions constitute a very high input of nutrients (NO3 > 1 µmol/L), suspended solids (>1 - 15 mg/L), and contaminants (total dissolved CB153: 5-20 pg/L, total particulate CB153: 2 - 50 pg/L; [4 - 5 ng/g]), dissolved inorganic carbon (DIC) and total alkalinity (TA) into the BBay of Marseille. These intrusions also impact on phytoplankton, especially if this process is associated with stratification and/or an anticyclonic eddy. The ME anticyclonic eddy (Schaeffer et al., 2011) seems to play a role in maintaining the Rhone intrusion water in the bay for longer as it can carry Rhone water along its outder edge. The salinity stratification observed during the extreme Rhone intrusion of June 2008, which brought surface salinites of < 35 in the Bay of Marseille, allowed a chlorophyll concentration > 1 µg/L to be reached, which is rather high for this area which normally has concentrations of less than 0.2 µg/L outside the spring bloom or periods of terrigenous inputs.

Water from rainfall is also a major source of nutrients in the Bay of Marseille (NO3: 2 - 5 µmol/L; PO4 > 0.1 µmol/L), suspended matter (> 10 mg/L - 100 mg/L before discharge) and contaminants (CB153 max total dissolved: 20 pg/L - 100 pg/L before discharge, CB153 max total particulate: 50 pg/L - 100 pg/L [> 10 ng/g] before discharge). These inputs concern the Bay of Marseille in the areas near the urban coastal river discharges, but also the Cortiou area. The rain events we studied are associated with south-easterly winds that generate swells allowing the resuspension of sediments (which may be contaminated by PCBs, coliform bacteria, or other contaminants). Once in the water column, the currents induced by the south-easterly wind are likely to transport these sediments into the southern part of Marseille harbour.

The upwelling processes induced by the Mistral wind bring cold, nutrient-rich water to the surface (average temperature variations in summer are of the order of -2 to -3°C at the Côte Bleue and about - 4°C at the Calanques; NO3: 1 - 2 µmol/L at the Côte Bleue and 2 - 3 µmol/L at the Calanques). This input of nutrients can have lead to an increase in phytoplankton if the decrease in temperature and mixing are not too limiting and allow phytoplankton to use the available nutrients.

Based on the studied events, we wanted to examine the processes that can lead to a decrease in residence time due to more rapid renewal of waters, due to advective and mixing processes.

The south-easterly wind, which is generally associated with an intrusion of water from the open sea (Northern Current), leads to a homogenisation of the whole water column (0-100m) in the Bay of Marseille, which constitutes an almost total renewal of the local water by water arriving from outside the bay.

The Mistral wind induces upwelling processes which bring water from the bottom to the surface where the wind then advects it offshore; this leads to a replacement of the surface water and a certain homogenisation.

These advective processes have a major impact on the rapid renewal of the waters in the Bay of Marseille, considerably more important than the impact of wind-induced turbulent mixing.

- How do extreme physical events whose frequency is increasing with climate change (storms, floods, thunderstorms, heat waves) impact on the marine ecosystems?

Based on the results of the hydrodynamic, biogeochemical, and sedimentary models, we were only able to study storms, floods, and autumn storms.

Based on the individual events considered here, Mistral and south-easterly storms appear to lead to an intensification of the typical processes, i.e., more intense upwellings bringing colder water from greater depths to the surface, more significant resuspension events (especially in the southern and northern harbour during a Mistral, and more

towards Cortiou during a south-easterly). However, the differences between the typical and extreme events studied were not visually significant.

Autumn storms have no significant impact on the phytoplankton biomass in October and December due to the season, although the amounts of nutrients, suspended solids, and contaminants brought into the Bay of Marseille near the coast and at Cortiou are significant. SS and contaminants show the most significant variations in concentration during these periods with external inputs constituting the most important forcing component. The December 2008 rainfall event produced such an extreme input (about twice the input of October 2007). The variability of nutrient concentrations near the outflow and discharge channels was 5 times higher during the extreme event of 2008 (NO_3 > 10 µmol/L). SS and contaminant concentrations reached high values near these outlets (SS > 100 mg/L, dissolved CB153 >100 pg/L, particulate CB153 >1000 pg/L). The average concentration of total CB153 (dissolved + particulate) over the entire water column varied 5 to 10 times more during this extreme event compared to a typical rainfall event. The resulting plumes become very visible, but unlike the Rhone plume, they are only present for the duration of the rainfall and play a relatively small role in the overall annual fluxes. The variation in concentrations is rapid but can be strong and contribute to a transfer towards the trophic chain if these inputs are concomitant with an increase in phytoplankton. These rain events are associated with south-easterly winds which can carry a small part of these strong inputs into the southern harbour of Marseille.

There can be intrusions of Rhône plume water eastward into the Bay of Marseille. These waters sometimes remain in the harbour for a long time, as in June 2008. In addition to the quantity of the inflow, which is considerable, the duration of the inflow has an impact on the phytoplankton biomass with chlorophyll concentrations reaching values > 1 µg/L during such events (usually for several days, sometimes even weeks, as in March 2001). In the case of phytoplankton, PCBs can adsorb onto the phytoplankton biomass and be transferred to the food chain via zooplankton grazing on the contaminated detritus and living particles.

- Does a Mediterranean coastal environment, of the scale such as The Bay of Marseille, constitute a transit or retention zone for hydrophobic contaminants? What is the role of PCB speciation in its biogeochemical cycle on the scale of the Bay of Marseille?

By using a modelling approach we could obtain a certain amount of information regarding PCB dispersion and transfer towards the open sea. Like many contaminants, it is present in the environment in several forms (species): some dissolved, others particulate. CB153 is a hydrophobic and persistent compound which means that once it enters the sea it has a strong affinity for organic particles.

On the scale of the Bay of Marseille, it does not degrade and shows a low volatility; atmospheric exchanges are relatively low. The variation in concentrations in the bay is essentially the result of rain that increase the contribution of coastal discharges (streams, storm drains), but it is also the result of intrusions from the Rhone that carry contaminated water from the river, particularly into the northern harbour.

The very high dilution of coastal discharges at sea contributes to the rapid dispersion of particles in the water column, with the heaviest particles precipitating near the discharges. If the water is not very turbid, particulate PCB tends to dissolve and becomes partly associated with dissolved organic matter. If phytoplankton is present in the vicinity of the discharge, the PCB will adsorb onto these living cells and be transferred into the food chain.
Due to the movement of small coastal plumes with currents and strong local gradients, the observation of the variation in concentrations at one point in the area (e.g., SOMLIT) does not provide sufficient

information on the impact of other events. We therefore analysed the average response in each zone for a range of events and processes (input, erosion, deposition, offshore transport).

In its dissolved form, the contaminant transits the bay in a few hours or days depending on the circulation pattern. In its particulate form, it is either dispersed in the same way as the dissolved phase when it is associated with fine, light particles, or deposited on the sea bed when it is associated with heavy (sandy-muddy) particles. There is still a great deal of uncertainty about the level of affinity of CB153 for light or heavy particles and about the characterisation of the inputs. Nevertheless, in dry weather, most of the particles released are fine and very light and they disperse towards the open sea and their concentrations are rapidly attenuated. Only in rainy weather do large inputs lead to large increases in concentration in the area, with a significant proportion associated with heavy particles that will settle locally.

Accumulation of the contaminant in the sediments is most significant in the areas close to a discharge, e.g., in the Cortiou area or in the southern and northern harbour. Resuspension episodes can cause significant increases in concentrations near the bottom. Depending on the situation, the contaminant is then exported towards the open sea where it is redeposited fairly quickly (within a few hours or days depending on the circulation pattern) in nearby areas and particularly in the southern harbour.
Adsorption onto particles that are more or less rich in organic matter introduces a degree of variability into the concentrations of particulate CB153, but given the generally low concentrations, PCB, even if it is very hydrophobic, is found in greater quantities in dissolved form. The small fraction that adsorbs onto detrital or living organic particles resulting from biogeochemical cycles (primary production, lysis, etc.) does not follow a specific local dynamic that can be linked to inputs from the Bay of Marseille.

According to this study, the Bay of Marseille seems to be a transit zone rather than a retention area, even if there are significant deposits in the northern and especially southern harbour and near the Cortiou discharge. These deposits only represent a few % of the total input arriving along the coast. Unfortunately, we do not know the exact percentage since it depends on the underlying hypotheses and chosen parameter values, which are very poorly constrained.

6.3 GENERAL CONCLUSION

In conclusion, the hydrodynamic model appears to be able to deliver a fairly good reproduction of the hydrology of the local area. The main processes such as upwelling, intrusions of low-salinity Rhone water or by the North Current, as well as eddies, which affect the advection and mixing of water masses, are correctly reproduced. In this context, we could demonstrate the utility of a high resolution model for studying discharge events.

Theo coupled biogeochemical modelling yielded some interesting results for the 2007-2008 period. A rigorous validation was carried out using multi-year simulations for the years 2009 to 2011 (Fraysse et al., 2013). This model was then used in several studies (Ross et al., 2016: Millet et al., 2018; Schmidt et al., 2019) and further developed to include the carbonate system (Lajaunie-Salla et al., 2021; Barré et al., 2022a and b).

The project has facilitated the acquisition and analysis of a coherent hydrosedimentary dataset (erodibility, erosion/suspension/deposition/transport), which makes it possible to understand the processes involved and therefore improve their representation in the model. Within the MASSILIA framework, the hydrosedimentary model has been improved by including mixed sand/mud degraded sediments (Vousdoukas et al., 2011).

The model has been set-up and first realistic simulations have been carried out which allowed a first comparison of the models with historical and other complementary data. Particular efforts were devoted to gathering the necessary data to provide realistic forcing to the models, such as the inputs from the Rhône and the atmosphere (in collaboration with the MIO Observational Service) and the inputs from the small coastal rivers and the WWTP (in collaboration with the Marseille Provence Métropole Urban Community and SERAMM).

We studied both typical situations and extreme events. These simulations have been used in numerous training courses for students, in theses, by post-docs, and in presentations at international conferences. The work was published by discipline or process study in peer-reviewed journals. This course has made it possible to collect all the information from these studies and combine them into a single document. The simulations were used to determine the respective roles of physical (wind mixing, stratification, upwelling, eddies) and biogeochemical forcing (nutrient inputs, POM, DOM) in the modulation of the strong anthropogenic inputs to which coastal ecosystems are subjected; we studied the role of extreme physical events whose frequency is increasing with climate change (mainly floods, storms, thunderstorms); we assessed whether a Mediterranean coastal environment such as the Bay of Marseille constitutes a transit or retention zone for contaminants

6.4 PERSPECTIVES

During these studies, we favoured an event-based approach in an attempt to understand the processes at play in the local ecosystem and their interactions. Subsequently, a multi-year modelling approach using the developed models made it possible to place these events within the context of interannual variability from 2007 to the present. Given that the areas of interest appear to be located near the coast at shallow depths, it may be beneficial to develop higher-resolution zooms (50 m) for the Cortiou area,

the southern and northern harbour, and the Côte Bleue. Moreover, the events studied in the MASSILIA project date from before the Geolide biological stage was commissioned in the WWTP. The Perseus project obtained data from the WWTP until 2014. The agreement with Seramm was interrupted at that date and is only recently being considered for renewal. It would therefore be interesting to study new rainfall events since the new treatment systems has been put in place in 2008.
As the renewal of the water in the area seems to have a major impact on the quality of this ecosystem, it would be interesting to complement the study of Jany et al. (2012b) with new calculations of water residence times. Such a study could be complemented by releasing Lagrangian floats in the area in order to compare their *in situ* trajectories to model predictions. This topic would also be very useful for fisheries scientists studying the distribution of larvae in this area, or for studying the dispersion of plastic waste.

It has been shown that the Marseille coastal area is a transit zone for contaminants such as PCBs rather than a retention area. However, a small proportion of these contaminants remain in the study area and in the future it would be interesting to develop smaller-scale studies targeting these retention areas to study the evolution contamination levels. In addition, other contaminations impacting living beings could be studied such as PAHs, phthalates, or soot from forest fires.

To further improve the model, we could envisage to complement the inorganic sedimentary compartment by adding biogeochemical benthic-pelagic coupling while taking into account benthic organisms such as the microphytobenthos or Posidonia.

The modelling tools developed during this study, and in the METROC and GIRAC projects, have been used in other projects such as EC2CO-Massilia, Mermex C3A, Mermex River, FP7 Perseus, the study of the connectivity of the larvae of the Prado artificial reefs, the dispersion of the waters of the Cortiou WWTP, and the acidification of the Bay of Marseille (OT-Med AMC and AERMC IAMM projects).

7 REFERENCES

Alberola, C., and C. Millot. 2003. Circulation in the French mediterranean coastal zone near Marseilles: the influence of wind and the Northern Current. Continental Shelf Research 23 (6):587-610.

Alberola, C., Millot, C., Font, J., 1995. On the seasonal and mesoscale variabilities of the Northern Current during the Primo-O experiment in the Western Mediterranean-sea. Oceanol. Acta 18 (2), 163e192.

Andral B. & Pairaud I., 2010. Metroc : les apports par les grandes métropoles. Evaluation des apports et modélisation hydrosédimentaire de la Baie de Marseille. RST.DOPLER/PAC/10-13, AERM&C/Ifremer n° 2007 1745, 83p.

Andre, G., Garreau, P., Fraunie, P., 2009. Mesoscale slope current variability in the Gulf of Lions. Interpretation of in-situ measurements using a three-dimensional model. Cont. Shelf Res. 29 (2), 407e423.

Arfi R., A. A., Bellan-Santini D., Bellan G., Laubier L., Pergent-Martini C., Bourcier M., Dukan S., Durbec J-P., Marinopoulos J., Millot C., Moutin T., Patriti G., Petrenko A. 2000. Impact du grand emissaire de Marseille et de l'Huveaune détournée sur l'environnement marin de Cortiou - Etude bibliographique raisonnée 1960-2000. Rapport de la ville de Marseille:137 pp.

Barré L., 2020. Dynamique du système des carbonates et production communautaire nette en baie de Marseille. Approche par modélisation couplée 3D physique biogéochimie. Rapport de stage Master 2 Recherche d'Océanographie, Aix-Marseille Université, Marseille: 1-25.

Barré L., F. Diaz, C. Pinazo, France Van Wambeke, C. Mazoyer, C. Yohia and T. Wagener, 2023a. Implementation and assessment of model including mixotrophs and carbonate cycle (Eco3M_MIX-CarbOx v1.0) in a highly dynamic Mediterranean coastal environment (Bay of Marseille, France) (Part I): Evolution of ecosystem composition under limited light and nutrient conditions. Geoscientific Model Development

Barré L., F. Diaz, T. Wagener, C. Mazoyer, C. Yohia and C. Pinazo, 2023b. Implementation and assessment of model including mixotrophs and carbonate cycle (Eco3M_MIX-CarbOx v1.0) in a highly dynamic Mediterranean coastal environment (Bay of Marseille, France) (Part. II): Towards a better representation of total alkalinity when modelling the carbonate system and air-sea CO2 fluxes. Geoscientific Model Development

Barrier, N., Petrenko, A.A., Ourmières, Y., 2016. Strong intrusions of the Northern Mediterranean Current on the eastern Gulf of Lion: insights from in-situ observations and high resolution numerical modelling. Ocean. Dyn., 66 (3) : 313-327.

Boiron A., 2011. Comparaison de l'activité mésoéchelle entre différents modèles numériques 3D de circulation. Rapport de stage, Ecole normale supérieure de Lyon, http://www.com.univ-mrs.fr/~doglioli/report_master1_Antoine_Boyron.pdf.

Conan P., 1996. Variabilité et bilan de la production primaire en zone côtière (Méditerranée Nord occidentale, entrée du golfe du Lion) en relation avec les systèmes biologique, chimique et hydrodynamique (Courant Nord Méditerranéen). Thèse, Université de la Méditerranée, (T. I 185 p. et T. II 102 p.).

Dencausse G. J., M. Arhan, and S. Speich, 2010. Routes of agulhas rings in the south eastern cape basin, Deep-Sea Res. I, 57, 1406–1421, doi:10.1016/j.dsr.2010.07.008.

Doglioli A. M., Blanke B., Speich S., and Lapeyre G., 2007. Tracking coherent structures in a regional ocean model with wavelet analysis: Application to Cape Basin eddies. J. Geophys. Res., 112, C05043, doi:10.1029/2006JC003952.

Dufois F., P. Garreau, P. Le Hir, Ph. Forget, 2008. Wave- and current-induced bottom shear stress distribution in the Gulf of Lions. Continental Shelf Research, 28 (15) : 1920-1934.

Echevin, V., Crepon, M., Mortier, L., 2003. Interaction of a coastal current with a gulf: application to the shelf circulation of the Gulf of Lions in the Mediterranean Sea. J. Phys. Oceanogr. 33 (1), 188e206.

Estournel, C., de Madron, X.D., Marsaleix, P., Auclair, F., Julliand, C., Vehil, R., 2003. Observation and modeling of the winter coastal oceanic circulation in the Gulf of Lion under wind conditions influenced by the continental orography (FETCH experiment). J. Geophys Res-Oceans 108 (C3).

Fraysse M., 2010. Modélisation couplée physique-biogéochimie de la baie de Marseille, Rapport de stage Master 2 Recherche d'Océanographie, Université de la méditerranée, Marseille: 1-45.

Fraysse M., 2014. Rôle du forçage physique sur l'écosystème à l'est du Golfe du Lion : modulation de l'impact des apports anthropiques en sels nutritifs et matière organique étudiée par modélisation 3D couplée physique et biogéochimique. Thèse de doctorat d'Aix-Marseille Université, 1-350.

Fraysse M., C. Pinazo, V. Faure, R. Fuchs, P. Lazzari, P. Raimbault, I. Pairaud, 2013. 3D coupled physical-biogeochemical model development around Marseille's coastal area (NW Mediterranean Sea): What complexity is required in coastal zone? PLoS One, 8(12), 1–18, doi:10.1371/journal.pone.0080012.

Fraysse M., Pairaud I., Ross O. N., Faure V. and Pinazo C., 2014. Intrusion of Rhone River diluted water into the Bay of Marseille: Generation processes and impacts on ecosystem functioning, J. Geophys. Res. Ocean., 119(10), 6535–6556, doi:10.1002/2014JC010022.

Faure, V., C. Pinazo, J.-P. Torréton, and P. Douillet. 2010b. Modelling the spatial and temporal variability of the SW lagoon of New Caledonia II: Realistic 3D simulations compared with in situ data. Marine Pollution Bulletin 61 (7-12):480-502.

Faure, V., C. Pinazo, J.-P. Torréton, and S. Jacquet. 2010a. Modelling the spatial and temporal variability of the SW lagoon of New Caledonia I: A new biogeochemical model based on microbial loop recycling. Marine Pollution Bulletin 61 (7-12):465-479.

Gatti, J., A. Petrenko, J.-L. Devenon, Y. Leredde, and C. Ulses. 2006. The Rhone river dilution zone present in the northeastern shelf of the Gulf of Lion in December 2003. Continental Shelf Research 26 (15):1794-1805.

Harrmelin-Vivien M., Bodiguel X., Charmasson S., Loizeau V., Mellon-Duval C., Tronczynski J., Cossa D., 2012. Differential biomagnification of PCB, PBDE, Hg and Radiocesium in the food web of the European hake from the NW Mediterranean. Marine Pollution Bulletin 64. pp974-983

Jany C., Zebracki M., Sauzade Didier, Cossa Daniel, Thouvenin Benedicte, Pairaud Ivane, Djellali Z., Mounier Stephane, Garnier C., Andral Bruno 2012a. METROC : Evaluation des apports de containants chimiques de la métropole marseillaise au milieu marin. Rapport Ifremer DOP/LER-PAC/12-02 Convention AERM&C / Ifremer n° 2009-0351. 140pp

Jany C., Pairaud I., Thouvenin B., Verney R., 2012b. METROC : modélisation idéalisée de substances dissoutes et particulaires rejetées en rade de Marseille. RST.ODE/LER/PAC/12-21. https://archimer.ifremer.fr/doc/00090/20088/

Jany, C., & Thouvenin, B., 2012. Récapitulatif des hypothèses utilisées pour les rejets de MES dans les simulations pour METROC. Rapport Ifremer, RST.ODE/LER/PAC/12-19: 33pp.

Lajaunie-Salla, K., Diaz, F., Wimart-Rousseau, C., Wagener, T., Lefevre, D., Yohia, C., Xueref-Remy, I., Nathan, B., Armengaud, A., and Pinazo, C., 2021. Implementation and assessment of a carbonate system model (Eco3m-CarbOx v1.1) in a highly dynamic Mediterranean coastal site (Bay of Marseille, France), Geoscience Model Developpment, 14, 295–321, https://doi.org/10.5194/gmd-14-295-2021

Le Hir P., Bassoullet P. and H. Jestin, 2001. Application of the continuous modelling concept to simulate high-concentration suspended sediment in a macrotidal estuary. In Proceedings in Marine Science Vol.3, Elsevier, 229-247.

Le Masson J. 1995 . Mesures de pollution par temps de pluie à Marseille. Rapport SERAM. 20pp.

Le Masson J. 1997. Mesures de pollution par temps de pluie à Marseille entre 1992 et 1996 -- Synthèse -- Rapport SERAM. 34pp

Le Masson J. 1998. Mesures de pollution par temps de pluie à Marseille. Rapport SERAM. 17pp

Millet B., C. Pinazo, D. Banaru, R. Pagès, P. Guiart, I. Pairaud, 2018. Unexpected spatial impact of treatment plant discharges induced by episodic hydrodynamic events: modelling Lagrangian transport of fine particles by Northern Current intrusions in the bays of Marseille (France). Plos ONE 13(4): e0195257. https:/doi.org/10.1371/journal.pone.0195257.

Millot, C., 1990. The gulf of Lions hydrodynamics. Cont. Shelf Res. 10 (9e11), 885e894.

Millot, C., 1999. Circulation in the western mediterranean sea. J. Mar. Syst. 20 (1e4), 423e442.

Millot, C., Wald, L., 1980. The effect of mistral wind on the ligurian current near Provence. Oceanol. Acta 3 (4), 399e402.

Pairaud, I.L., J. Gatti, N. Bensoussan, R. Verney and P. Garreau, 2011. Hydrology and circulation in a coastal area off Marseille: Validation of a nested 3D model with observations, Journal of Marine Systems, 88, 20-33.

Para J., P. G. Coble, B. Charrière, M. Tedetti, C. Fontana, and R. Sempéré, 2010. Fluorescence and absorption properties of chromophoric dissolved organic matter (CDOM) in coastal surface waters of the northwestern Mediterranean Sea, influence of the Rhône River. Biogeosciences, 7, 4083-4103

Petrenko, A., 2003. Variability of circulation features in the gulf of lion NW Mediterranean Sea. Importance of inertial currents. Oceanol. Acta 26 (4), 323e338.

Petrenko, A., Y. Leredde, and P. Marsaleix. 2005. Circulation in a stratified and wind-forced Gulf of Lions, NW Mediterranean Sea: in situ and modeling data. Continental Shelf Research 25 (1):7-27.

Petrenko, A., Dufau, C., Estournel, C., 2008. Barotropic eastward currents in the western Gulf of Lion, north-western Mediterranean Sea, during stratified conditions. J. Mar. Syst. 74 (1e2), 406e428.

Pont D., Bombled B., Coste B., Moutin T., Raimbault P., Thomas A.J., Huang W.W., Noel H., Tronczynski J., Chiffoleau J.F., Cossa D., Auger D., Chartier E., Sanjuan S., Moizan T., Sicre M.A., Ferandes M.B., Cauwet G., 1996. Evaluation des charges polluantes du Rhône à la Méditerranée. Rapport pour le compte de l'Agence de l'Eau Rhône-Mediterranée-Corse et l'Agence Régionale pour l'Envronnement Provence-Alpes-Côtes d'Azur.

Ross O.N., M. Fraysse, C. Pinazo, I. Pairaud, 2016. Impact of an intrusion by the Northern Current on the biogeochemistry in the eastern Gulf of Lion, NW Mediterranean. Estuarine and Continental Shelf Research,170 :1-9. doi: 10.1016/j.ecss.2015.12.022

Rubio A., Blanke B., Speich S., Grima N. and Roy, C., 2009. Mesoscale eddy activity in the southern Benguela upwelling system from satellite altimetry and model data, Prog. Oceanogr., 83, 288–295.

Sauzade D., Andral B., Gonzalez J.L., Galgani F., Grenz C., Budzinski H., Togola A., Lardy S. (2007). Synthèse de l'état de la contamination chimique du golfe de Marseille. Rapport Ifremer DOP/LER-PAC/07-05 – Agence de l'eau RM&C- Vol 1 : 118p. Vol 2, 86p.

Schaeffer A. Molcard A., Forget P., Fraunie P. and P. Garreau, 2011. Generation mechanisms of mesoscale eddy in the Gulf of Lions: radar observations and modelling. Ocean Dynamics, 61 (10) 1587-1609.

Souza J.M. A. C., C. de BoyerMontégut, and P. Y. Le Traon, 2011. Comparison between three implementations of automatic identification algorithms for the quantification and characterization of mesoscale eddies in the South Atlantic Ocean, Ocean Sc., 7, 317–334, doi:10.5194/os-7-317-2011.

Tett P., 1990. A three-layer vertical and microbiological processes model for shelf seas, Report No. 14. Proudman Oceanographic Laboratory, Birkenhead, UK, 85 pp., 1990. http://nora.nerc.ac.uk/id/eprint/3877/

Tronczynski J., Tixier C., Cadiou J.F., Belly N., Heas-Moisan K., Castelle S., Migon C., Dufour A., Merieau R., 2012. Apports rhodaniens et suivi atmosphérique des contaminants organiques persistants (PCB, PBDE, HAP, PCDD/F) dans le Golfe du Lion (2009 – 2010). ARC-MED. Rapport Ifremer RST-RBE/BE/LBCO/2012-04 pour l'Agence de l'Eau Rhône Méditerranée-Corse. 68pp

Tronczynski J., Munschy C., Héas-Moisan K., Guiot N., Truquet I., 2005a. Analyse de contaminants organiques (herbicides, PCB, OCP, HAP) dans les eaux estuariennes et marines côtières. Ed. Ifremer, méthodes d'analyse en milieu marin, 52p

Tronczynski J., Munschy C., Héas-Moisan K., Guiot N., Truquet I., 2005b. Analyse de contaminants organiques (PCB, OCP, HAP) dans les sédiments marins. Ed. Ifremer, méthodes d'analyse en milieu marin, 44p

Vousdoukas M.I., , R. Verney, F. Dufois, C. Pinazo, S. Meulé, D. Sauzade, Ph. Cann, T. Plomaritis, 2011. Sediment dynamics in the Bay of Marseille: hydrodynamic forcing versus bed erodibility. Journal of Coastal Research, doi: 10.2112/JCOASTRES-D-10-00122.1, 27 (5): 942-958.

Waeles B., Le Hir P., Lesueur P, Delsinne N, 2007. Modelling sand/mud transport and morphodynamics in the Seine river mouth (France): an attempt using a process-based approach. Hydrobiologia, 588(1), 69-82.

Waeles B., Le Hir P., Lesueur P., 2008. A 3D morphodynamic process-based modelling of a mixed sand/mud coastal environment: the Seine estuary, France. Sediment and Ecohydraulics: INTERCOH 2005, T. Kusuda, H. Yamanishi, J. Spearman and J.Z. Gailani (Eds), Proceedings in Marine Science 9, Elsevier, 477-498.

Wimart-Rousseau, C., Lajaunie-Salla, K., Marrec, P., Wagener, T., Raimbault, P., Lagadec, V., Lafont, M., Garcia, N., Diaz, F., Pinazo, C., Yohia, C., Garcia, F., Xueref-Remy, I., Blanc, P. E., Armengaud, A., and Lefèvre, D., 2020. Temporal variability of the carbonate system and air–sea CO2 exchanges in a Mediterranean human-impacted coastal site, Estuar. Coast. Shelf S., 236, https://doi.org/10.1016/j.ecss.2020.106641.

Yohia, C., 2017. Genèse du mistral par interaction barocline et advection du tourbillon potentiel, Climatologie, 13, 24–37 [online] https://doi.org/10.4267/climatologie.

Zebracki M, 2011. Evaluation des flux bruts de contaminants chimiques par la métropole marseillaise à la mer. Rapport final. Contrat n°10/3211467